UNIVERSITAT POLITÈCNICA DE CATALUNYA BARCELONATECH

Effect of microstructural and chemical cues on the *in vitro* cell response to calcium phosphates

Joanna Maria Sadowska

PhD Thesis

EFFECT OF MICROSTRUCTURAL AND CHEMICAL CUES ON THE *IN VITRO* CELL RESPONSE TO CALCIUM PHOSPHATES

Doctoral Program of Material Science and Engineering

Joanna Maria Sadowska

Supervisors:

Dr. Jordi Guillem Marti

Prof. Maria-Pau Ginebra Molins

Biomaterials, Biomechanics and Tissue Engineering Group

Department of Material Science and Metallurgical Engineering

Universitat Politècnica de Catalunya

Barcelona, 2018

Moim Rodzicom i Babci

Table of contents

ABSTRACT

Bone has a natural ability to regenerate. However, it cannot bridge large defects without the additional help of a supporting material. Among the different synthetic bone grafts, calcium phosphates are excellent candidates for bone regeneration due to their close resemblance to the mineral phase of bone, as well as the bioactive and osteoinductive potential. The present thesis explores the effect of the physicochemical features of calcium phosphates on the interaction with the cells involved in the different stages of the bone healing process, *i.e.* inflammation, angiogenesis and osteogenesis, paying special attention to biomimetic calcium deficient hydroxyapatite (CDHA). This is analysed through *in vitro* cell cultures with immune, endothelial and bone forming cells, respectively.

An overview of bone biology and bone healing process is presented in **Chapter 1**. Moreover, the **Chapter 1** describes synthetic bone grafts based on calcium phosphates and the impact of their physicochemical features on cellular behaviour *in vitro*. **Chapter 2** and **Chapter 3** study the response of immune cells to calcium phosphates and its outcome on osteogenic differentiation of bone forming cells. Specifically, **Chapter 2** explores the link between nanotopography, specific surface area (SSA) and porosity of biomimetic CDHA and its immunomodulatory, osteoimmunomodulatory and antinflammatory features, demonstrating that neddle-like topography of CDHA stimulated the osteogenic activity of bone forming cells, whilst a reduction of porosity to CDHA substrates decreased the inflammatory state. **Chapter 3** is devoted to study the interaction of two chemically and texturally different calcium phosphates *i.e.* biomimetic CDHA and sintered β-tricalcium phosphate (β-TCP) with macrophages under inflammatory environment and its further impact on osteogenic differentiation of mesenchymal (MSCs) and osteoblastic cells. Whilst the incubation with β-TCP resulted in greater downregulation of released pro-inflammatory molecules from immune cells, the interaction between macrophages and CDHA led to a more favourable environment for osteogenic differentiation of bone forming cells.

Angiogenesis ensures the availability of oxygen and nutrients and controls the recruitment and osteogenic differentiation of bone forming cells, being one of the crucial processes during bone healing. **Chapter 4** explores the interaction of two texturally different CDHA, *i.e.* needle-like and plate-like structured surfaces, as well as β-TCP with endothelial progenitor cells (EPCs). Moreover, the cellular crosstalk between endothelial and mesenchymal stem cells is investigated by performing co-culture studies. Overall, the upregulation of angiogenic gene expression was more pronounced for needle-like CDHA in monocultured EPCs. Furthermore, the cellular crosstalk was demonstrated through the upregulation of osteogenesis-related genes being this scenario especially pronounced for needle-like CDHA.

Finally, the independent effect of surface chemistry and ionic exchange of sintered and biomimetic calcium phosphates on osteogenesis are explored in **Chapter 5** and **Chapter 6**. **Chapter 5** describes the response of MSCs and osteoblastic cells to biomimetic CDHA and three sintered ceramics *i.e.* β-TCP, α-tricalcium phosphate (α-TCP) and hydroxyapatite (HA). The cells were cultured either directly on the biomaterials or indirectly on glass coverslip placed on top of the substrates to expose the cells to exclusive effects of CaP-induced ionic changes without additional effect of surface topography. The results showed that the direct contact with substrate is required to induce the osteogenic differentiation of both MSCs and osteoblasts. Moreover, the culture with the CDHA resulted in greater upregulation of ALP secretion for both cell types suggesting osteoinductive capacity of this substrate. Nonetheless, MSCs proliferation was impaired both in direct and indirect cultures on CDHA, suggesting that the increased ionic fluctuations, triggered by high SSA and calcium deficiency of the substrate, were responsible for this scenario. The results demonstrated that cellular death was induced through apoptotic pathway. Hence **Chapter 5** revealed the complexity to assess the cell-material interactions of highly reactive substrates in static *in vitro* cultures. This is further explored in **Chapter 6,** where a strategy is proposed to analyse the parameters affecting the response of MSCs to CDHA. The approach consisted of adjusting the volume ratio between the cell culture medium and CaP substrate, which allowed mitigating the drastic ionic changes. The results demonstrated that the alterations of calcium and phosphate concentrations impaired cell adhesion by reducing the number of focal adhesions, this leading to cell shrinkage and apoptosis. On the contrary, when the ionic fluctuations were attenuated, MCSs spread, proliferated and differentiated over time. The contact with CDHA led to earlier expression of osteogenesis-related genes like alkaline phosphatase (ALP), bone morphogenetic protein 2 (BMP-2) and osteopontin (OPN) compared to sintered β-TCP suggesting greater osteogenic potential of biomimetic CDHA.

RESUMEN

El hueso tiene una capacidad natural para regenerarse. Sin embargo, no puede restaurar grandes defectos sin la ayuda adicional de un material de soporte. Entre los distintos injertos óseos sintéticos, los fosfatos de calcio son excelentes candidatos para la regeneración ósea debido a su gran parecido con la fase mineral del hueso, así como también a su potencial bioactivo y osteoinductor. La presente tesis explora el efecto de las características fisicoquímicas de los fosfatos de calcio en la interacción con las células involucradas en las diferentes etapas del proceso de regeneración ósea, es decir, inflamación, angiogénesis y osteogénesis, prestando atención especial a la hidroxiapatita biomimética deficiente en calcio (CDHA). Dicho efecto se analiza mediante el cultivo celular *in vitro* de células inmunológicas, endoteliales y formadoras del hueso, respectivamente.

En el **Capítulo 1** se presenta una descripción general de la biología ósea y el proceso de regeneración ósea. Además, el **Capítulo 1** describe el estado del arte respecto a los injertos óseos basados en fosfatos de calcio y el impacto de sus características fisicoquímicas en el comportamiento celular *in vitro*. En el **Capítulo 2** y el **Capítulo 3** se estudia la respuesta de las células inmunológicas a los fosfatos de calcio y su implicación en la diferenciación osteogénica de las células formadoras de hueso. Específicamente, el **Capítulo 2** explora el vínculo entre la nanotopografía, la superficie específica (SSA) y la porosidad de la CDHA biomimética y sus características inmunomoduladoras, osteoinmunomoduladoras y antiinflamatorias, demostrando que la CDHA con topografía en forma de aguja estimuló la actividad osteogénica de las células formadoras de hueso, mientras que una reducción en la porosidad de los sustratos CDHA resultó en una disminución del estado inflamatorio. El **Capítulo 3** está dedicado a estudiar la interacción de dos fosfatos de calcio químicamente y texturalmente diferentes, es decir, la CDHA biomimética y el fosfato tricálcico beta (β-TCP), con macrófagos bajo un ambiente inflamatorio y su repercusión en la diferenciación osteogénica de las células mesenquimales (MSC) y osteoblásticas. La incubación con β-TCP dio como resultado una disminución en la liberación de moléculas proinflamatorias en las células inmunológicas, mientras que la interacción entre los macrófagos y la CDHA llevó a un entorno más favorable para la diferenciación osteogénica de las células formadoras de hueso.

La angiogénesis asegura la disponibilidad de oxígeno y nutrientes y controla el reclutamiento y la diferenciación osteogénica de las células formadoras del hueso, siendo uno de los procesos cruciales durante la regeneración ósea. El **Capítulo 4** explora la interacción de dos CDHA texturalmente diferentes, es decir, con superficie en forma de aguja o placa, además del β-TCP con células endoteliales progenitoras (EPCs). Asimismo, se investiga la interacción celular entre células endoteliales progenitoras y

células mesenquimales realizando estudios de cocultivo. En general, la expresión de genes relacionados con procesos de angiogénesis en el monocultivo de ECPs fue más pronunciada para la CDHA con topografía en forma de aguja. Además, se demostró la comunicación celular mediante la regulación positiva de los genes relacionados con la osteogénesis, siendo este comportamiento especialmente pronunciado para la CDHA con microestructura en forma de aguja.

Finalmente, el efecto independiente de la química y del intercambio iónico de los fosfatos de calcio, tanto sinterizados como biomiméticos, sobre la osteogénesis se explora en el **Capítulo 5** y **Capítulo 6**. El **Capítulo 5** describe la respuesta de las MSCs y las células osteoblásticas a la CDHA biomimética y a tres cerámicas sinterizadas, es decir, β-TCP, fosfato tricálcico alfa (α-TCP) e hidroxiapatita (HA). Las células se cultivaron directamente sobre los biomateriales o indirectamente sobre un cubreobjetos de vidrio colocado sobre los sustratos, para exponer las células a los efectos exclusivos de los cambios iónicos inducidos por los CaPs sin el efecto adicional de la topografía. Los resultados mostraron que se requiere el contacto directo con el sustrato para inducir la diferenciación osteogénica de las MSCs y los osteoblastos. Además, el cultivo con la CDHA dio como resultado una mayor secreción de ALP para ambos tipos de células, lo que sugiere una gran capacidad osteoinductora de este sustrato. De todos modos, la proliferación de MSCs se vio afectada tanto en el cultivo directo como indirecto en la CDHA, lo que sugiere que las fluctuaciones iónicas, causadas por la elevada superficie específica y la deficiencia de calcio del sustrato, provocaron este comportamiento. Los resultados demostraron que la muerte celular fue inducida a través de la vía apoptótica. Por lo tanto, el **Capítulo 5** reveló la complejidad de la evaluación de las interacciones célula-sustrato en cultivos estáticos *in vitro* en los biomateriales que presentan una alta reactividad iónica. Esa complejidad se explora más a fondo en el **Capítulo 6**, donde se propone una estrategia para analizar los parámetros que afectan la respuesta de las MSCs a la CDHA separadamente. El enfoque consistió en ajustar la relación de volumen entre el medio de cultivo celular y el volumen del sustrato de CaP permitiendo, de esa manera, mitigar los cambios iónicos drásticos. Los resultados demostraron que las alteraciones en las concentraciones de calcio y fosfato afectaron la adhesión celular reduciendo el número de adhesiones focales y el área celular, llevando finalmente a la muerte celular por apoptosis. En cambio, cuando las fluctuaciones iónicas fueron atenuadas, se observó como las MSCs se extendieron, proliferaron y diferenciaron a lo largo del tiempo. Además, el contacto con la CDHA dio lugar a una expresión más temprana de genes relacionados con la osteogénesis como la fosfatasa alcalina (ALP), la proteína morfogenética ósea 2 (BMP-2) y la osteopontina (OPN) en comparación con el β-TCP, lo que sugiere un mayor potencial osteogénico de la CDHA biomimética.

Acknowledgments

En primer lloc voldria donar les gràcies als meus directors: Pau, moltes gràcies per donar-me l'oportunitat de desenvolupar aquesta tesi en el grup BBT. M'has fet créixer com a investigadora, m'has ensenyat que no només és important fer ciència, sinó que cal fer ciència de bona qualitat, sent rigorosa a nivell de disseny i anàlisi dels resultats. Jordi, t'agraeixo la teva paciència i la transferència de coneixement. Moltes gràcies per ser la meva viquipèdia privada quan, al principi de la tesi, els temes biològics eren un nou món que em tocava descobrir.

Quería dar las gracias a los miembros del BBT que me acompañaron durante estos cuatro años en mi gran aventura. Muchas gracias a los profesores: Elisa, Daniel, José María, Marta, Xavier y a los Postdoc del grupo: Anna, Carles, Clara, Edgar, Giuseppe y Juan. Quería dar las gracias, muy especialmente, a Montse y Cristina. Montse, has sido mi guía científica durante todo mi doctorado. Estoy muy agradecida por tu infinita paciencia y el tiempo que has dedicado a resolver mis dudas. Cristina, gracias por ayudarme con la escritura de los proyectos y las becas que he pedido durante estos últimos años. Muchas gracias a todos los doctorandos con los que he compartido mi tiempo en los laboratorios y despachos, así mismo por el tiempo que hemos pasado juntos fuera del horario laboral: Albert, David, Diego, Elia, Inés, Joanna Junior, Joaquim, Kanupriya, Lluís, Mar, María, María Isabel, Miguel, Mireia, Roberta, Romain, Sara, Yago y Yassine. Sobre todo, gracias a los nuevos *minions* del grupo: Inés, Joanna, Lluís, Mar, Miguel y Yago por intentar arreglar un poco mi vida social durante los últimos meses, cuando dedicaba (casi) todo mi tiempo a la escritura de la tesis. Os deseo mucha suerte para los siguientes años del doctorado. No os engañéis, será DURO, DURO, DURO, pero merecerá la pena. Gracias también a la gente de empresas: Mònica, Marc, Sergi, Miquel y, especialmente, a Txell, por hacer que en los laboratorios se trabaje a gusto, siempre con bata y de forma segura.

Finalmente, quería dar las gracias a las glandes del grupo: Dra. Xula, Dra. KochANNA, mini Mar y Noe. Vuestra presencia ha añadido mucho rosa, mucha purpurina y muchos arcoíris a mi doctorado. Habéis sido mis unicornios y T-Rexs del BBT. Gràcies Judit per la teva bondat, les bones paraules i pels anys que hem passat convivint juntes, i per fer-me sentir com a casa al nostre pis. Anna, gracias por hacerme mucho de reír. Gracias por tu apoyo, tanto profesional como personal. Eres una persona extraordinaria y agradezco mucho que la vida te haya puesto en mi camino. Mar, gracias por darme la oportunidad de estrenarme en el papel de tutora. Y gracias por haber sido una proyectista fácil de llevar y por ser una chica muy guapa como Anna. No has desgravado mucho, y trabajar contigo era un placer. Noe, gracia miga por los cafés mañaneros y por las charlas que hacen que los días comiencen de buena mañana. Gracias por siempre encontrar el tiempo cuando necesitaba tu ayuda

A Cédric, por estar a mi lado, siempre.

También quiero dar las gracias a las personas del CMEM con las que he compartido despacho, por crear buen ambiente de trabajo: Anna, Eric, Erica, las Danielas, Hossein, José María, Miquel, Quentin y Violeta.

Quiero dar gracias a mi nueva family del Centro Multiescala: Angélica, Carla, Jordi, Michela, Montse, Trifon y Sandra. Especialmente a ti, Trifon, por todas las charlas, risas y comidas que hemos compartido. Quería agradecer también a Carla y Montse por crear buen ambiente y risas en el despacho.

I would like to thank Prof. Cecila Persson to give me the opportunity to make my internship at Uppsala University at the Materials and Medicine group. Thanks to MiM group members for sharing your knowledge with me. Specially, I would like to acknowledge Gry, whose extraordinary work makes the cell lab a great place for doing research. Thanks to Sara for giving me your Italian warmth in this cold unsunny Swedish city- you were my ray of sunshine. Thank you, Victoria, for all your help during my stay at Uppsala and for make me feel welcome. Finally, thank you, Theresa and Dominique, for sharing fika time with me.

I would like to thank Prof. Yin Xiao for hosting me at Institute of Health and Biomedical Innovation at Queensland University of Technology. I would like to acknowledge this great opportunity to discover the interesting world of osteoimmunology. Thank you for sharing your point of view and for all the valuable remarks that allowed me to obtain such interesting results. Special thanks to Michelle for your infinite patience and for resolving absolutely all administrative issues I ever had, always with a big smile. Without your help, my internship in Australia wouldn't have been possible. Thanks to all the group members who delighted, with their presence, the hours that I spent in the laboratory, especially to: Jia, Menchao, Simon and Ying. Thank you, Long, for making me laugh and for being my teacher of Chinese. My Gurrurrrs: Jayanti and Greeshma, thank you for the immense hospitality and love that you shared with me. Thanks to you, I brought unforgettable memories from Australia. Both of you are very special people for me and I hope that my karma or your Gods will make it possible to see each other soon. Muchas gracias a Nati y Álvaro por formar la mini república independiente de España en el territorio australiano. Gracias por todas las fiestas locas, los litros de calimocho y los días playeros. Nati, gracias por compartir las alegrías y tristezas de cada día. Álvaro, te agradezco los sitios asombrosos y paisajes inolvidables de ese precioso país que he descubierto gracias a ti.

Chciałam również podziękować Magdzie, Dominice, Helenie oraz Michalinie za to, że zawsze znajdujecie dla mnie czas na spotkanie, gdy jestem w Polsce. Świadomość, że ma się bliskie osoby, które Ci kibicują i wspierają mimo odległości, pomogła mi przez te ostanie lata jakie spędziłam poza krajem.

Dziewczynom Marcinkowskim: Halino - dziękuję za ciepłe słowa, nalewki oraz wysłuchanie mnie i rady, zawsze, gdy ich potrzebowałam. Gosiu dziękuję za bycie „my person". Dziękuję za zaufanie i wspólne rozpoczęcie barcelońskiej przygody która, w

moim przypadku, trochę się przedłużyła. Spędziłam wspaniałe chwile z Tobą podczas studiów inżynierskich i magisterskich oraz wyniosłam mnóstwo pięknych wspomnień. Mam cichą nadzieję, że jeszcze wiele wspólnych przygód i nowych wspomnień przed nami.

Moim Rodzicom: Renacie i Tadeuszowi oraz Babci Helenie za wsparcie i wiarę we mnie. Dziękuję za wszelkie poświęcenia jakich dokonaliście, bym mogła znaleźć się w punkcie, zarówno personalnym jak i profesjonalnym, w którym się znalazłam.

Dziękuję

Scope and aim of the thesis

Synthetic bone grafts are biomaterials implanted in bone defects in order to support the growth and the regeneration of bone tissue. Bone healing requires proper-in-time cooperation of various cell types underlining the complexity of the process. Among them, immune cells, endothelial cells and bone forming cells are involved in particular phases of bone regeneration. Therefore, the function of a bone graft is not merely mechanical or structural. Overall, it must stimulate and orchestrate the bone regeneration process. In this regard, the interaction of the material with the different cells involved in the bone healing process is of paramount importance and it is a crucial aspect for the design of more efficient synthetic bone grafts.

Among synthetic grafts, the calcium phosphates are widely used as a bone substitutes. The most commonly used CaP-based substrates like sintered hydroxyapatite (HA), tricalcium phosphate (TCP) or biphasic materials (usually composed of HA and TCP) have been traditionally obtained through high temperature sintering routes. Recently, the potential of calcium phosphate prepared through biomimetic routes, that is through cementitious reactions that occurs at body temperature, has been revealed. Those routes allowed the synthesis of nanostructured calcium deficient hydroxyapatite which is texturally and chemically more similar to mineral phase of bone compared to sintered CaPs. Moreover, the simplicity of tailoring the physicochemical properties of CDHA during synthesis process make this biomaterial very advantageous. Thus, this modulation of particular parameters of CDHA might be an interesting strategy for triggering specific response of cells involved in bone healing process.

The present thesis aims at analysing the effect of different physicochemical properties of biomimetic calcium deficient hydroxyapatite on the material-mediated bone regeneration process, focusing on the material-cell interactions. Specifically, the effect of chemistry, specific surface area and surface topography on the response of immune, endothelial and bone forming cells has been investigated.

The specific objectives to achieve the aforementioned goal are as follows:

Objective I To investigate the effect of the textural and chemical features of biomimetic calcium deficient hydroxyapatite on the *in vitro* immunomodulatory and osteoimmunomodulatory properties, focusing on:

- The assessment of the effect of different topographies and porosities of CDHA on stimulating the polarization of macrophages under standard and inflammatory environment.
- The study of osteogenic and osteoclastogenic activities of immune cells cultured on CDHA substrates.

- The evaluation of the interaction of macrophages cultured on CDHA with bone forming cells in terms of stimulation of osteogenesis process.
- The comparison of the effect of two chemically different CaPs *i.e.* biomimetic CDHA and sintered β-tricalcium phosphate (β-TCP) on activities of immune cells under inflammatory conditions.

Objective II To analyse the effect of chemistry and surface topography of biomimetic CDHA on the interaction with endothelial progenitor cells *in vitro*. Special attention will be paid to:

- The study of endothelial cell behaviour in terms of adhesion, proliferation, endothelial-specific molecule production and angiogenic gene expression on various CDHA substrates with different textural properties.
- The investigation of the crosstalk between endothelial and mesenchymal stem cells on CaPs and its repercussions on angiogenic and osteogenic process.

Objective III To unravel the independent effects of surface chemistry and ionic exchange of CDHA on stimulating osteogenesis of MSCs and osteoblastic cells *in vitro*. Specifically:

- To study of the impact of individual features of various CaPs on osteoblastic and mesenchymal stem cell behaviour.
- To elucidate the effect of cell culture conditions for highly reactive CaPs and their output on mesenchymal stem cells response focusing on unrevealing the cellular pathways involved in death and osteogenic differentiation of MSCs.

Abbreviations

ACP	Amorphous calcium phosphate
ACTB	Actin beta
ALP	Alkaline phosphatase
ARS	Alizarin red staining
ATR	Attenuated total reflectance
α-TCP	Alpha-tricalcium phosphate
BCP	Biphasic calcium phosphates
BG	Bioglass
BMP-2	Bone morphogenic protein 2
BMP-4	Bone morphogenic protein 4
BMP-7	Bone morphogenic protein 7
BMSCs	Bone marrow stromal cells
BMU	Basic multicellular unit
BSA	Bovine serum albumin
BSP	Bone sialoprotien
β-TCP	Beta-tricalcium phosphate
CaPs	Calcium phosphates
CAR2	Carbonic anhydrase 2
CCR7	C-C chemokine receptor type 7
CDHA	Calcium deficient hydroxyapatite
CD11c (ITGAX)	Integrin subunit alpha X
CD163	Cluster of differentiation 163
CD206	Cluster of differentiation 206
CLSM	Confocal laser scanning microscopy
CM	Substrate-conditioned medium
COLL I	Collagen type I
CPC	Calcium phosphate cements
CTSK	Cathepsin K
DAPI	4, 6-diamidino-2-phenylindole
DCPD	Dicalcium phosphate dehydrate
DCPA	Dicalcium phosphate anhydrous
dd H_2O	Double destilled water
DMEM	Dulbecco's Modified Eagle Medium
DMSO	Dimethyl sulfoxide
DNA	Deoxyribonucleic acid
ECs	Endothelial cells
ECM	Extracellular matrix
EDH 1	Endothelin 1
EDTA	Ethylenediaminetetraacetic acid
EGM-2 MV	Microvascular Endothelial Cell Growth Medium-2
ELISA	Enzyme-linked immunosorbent assay
FACS	Fluorescence-activated cell sorting
EPCs	Endothelial progenitor cells
FAK	Focal adhesion kinase
FBGCs	Foreign body giant cells
FBS	Foetal bovine serum
FCS	Foetal calf serum
FGF	Fibroblast growth factor
FITC	Fluorescein isothiocyanate
FN	Fibronectin
FTIR	Fourier transform infrared spectroscopy
HA	Hydroxyapatite
HEPES	4-(2-hydroxyethyl)-1-piperazineethanesulfonic acid
HFs	Human fibroblasts
HIFs	Hypoxia inducible factors
HMDS	Hexamethyldisilazane
HUVEC	Human umbilical vein endothelial cell
ICP-MS	Inductive coupled plasma-mass spectroscopy
ICP-OES	Inductive coupled plasma-optical emission spectrometry
IFNγ	Interferon gamma
IGF	Insulin-like growth factors
IgG	Immunoglobin G
IL-1β	Interleukin 1 beta
IL-4	Interleukin 4
IL-6	Interleukin 6
IL-10	Interleukin 10
IL-13	Interleukin 13
IL-17	Interleukin 17
IL-23	Interleukin 23
LDH	Lactate dehydrogenase
iNOS	Nitric oxide synthase
LPS	Lipopolysaccharide
L/P	Liquid-to-powder ratio
M-CSF	Macrophage-colony stimulating factor
MCPA	Monocalcium phosphate anhydrous
MCPM	Monocalcium phosphate monohydrate
MG63	*Homo sapiens bone osteosarcoma cell line*

MMP9	Matrix metalloproteinase 9
M-PER	Mammalian Protein Extraction Reagent
MSCs	Mesenchymal stem cells
MTT	3-(4,5- dimethylthiazol-2-yl)-2,5-diphenyl tetrazolium bromide
Mϕ	Macrophage
M1	Macrophage type 1
M2	Macrophage type 2
NCP	Non-collagenous proteins
OCN	Osteocalcin
OCP	Octacalcium phosphate
OECs	Ongrowth endothelial cells
ONN	Osteonectin
OSM	Oncostatin M
OPG	Osteoprotegerin
OPN	Osteopontin
Osx	Osterix
PBS	Phosphate-buffered saline
PDGF	Platelet-derived growth factor
PECAM-1	Platelet and endothelial cell adhesion molecule 1
PFA	Paraformaldehyde
pFAK	Phosphorylated focal adhesion kinase
pHA	Precipitated hydroxyapatite
PI	Propidium iodide
PMNs	Polymorphonuclear leukocytes
PTH	Parathyroid hormone
qPCR	Quantitative polymerase chain reaction
RANK	Receptor activator of nuclear factor kappa-B
RANKL	Receptor activator of nuclear factor kappa-B ligand
RAW 264.7	*Murine macrophage cell line*
RGD	Arginylglycylaspartic acid
RIPA	Radioimmunoprecipitation assay buffer
RNA	Ribonucleic acid
ROS	Reactive oxygen species
RT-qPCR	Real time quantitative polymerase chain reaction
Runx2	Runt-related transcription factor 2
SaOS-2	*Homo sapiens bone osteosarcoma cell line*
SDS-PAGE	Sodium dodecyl sulfate polyacrylamide gel electrophoresis
SEM	Scanning electron microscope
SSA	Specific surface area
TBS	Tris-buffered saline
TCPS	Tissue culture polystyrene
TGFβ	Transforming growth factor beta
TGFβ1	Transforming growth factor beta 1
TGFβ3	Transforming growth factor beta 3
TNFα	Tumour necrosis factor alpha
TRAP	Tartrate-resistant acid phosphatase
TTCP	Tetracalcium phosphate
VEGF	Vascular endothelial growth factor
VEGF R1	Vascular endothelial growth factor receptor 1
VEGF R2	Vascular endothelial growth factor receptor 2
XPS	X-ray photoelectron spectroscopy
XRD	X-ray diffraction

Chapter 1

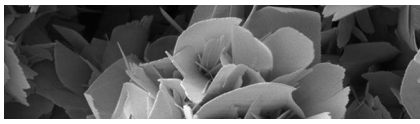

Introduction

INTRODUCTION

Bone is a complex and dynamic organ whose main functions include providing biomechanical support and protection for body's soft tissues, haematopoiesis and ion regulation.[1] Moreover, the bone is reported to be the second most frequently transplanted tissue. According to US Health and Cost Utilization Project (HCUP) bone injuries accounts for more than 500 000 grafting procedures annually, exceeding the healthcare costs of $26 billion.[2,3] These data, paired with the reduced availability of autografts, highlights the need to design synthetic substitutes that are able not only to replace damaged tissue but also to stimulate the bone healing process.

The following sections briefly describe the composition, structure of bone tissue as well as the bone remodelling and bone healing processes, in order to better understand the dynamic environment in which synthetic bone grafts will be placed.

1.1 Bone composition

Bone is a mineralized connective tissue that possesses a complex structure composed of inorganic component, an organic matrix and water, which proportions vary depending on the type and function of bone. The mineral part, that accounts approximately 70 wt.% (49 % in volume) and consists of poorly crystalline carbonated hydroxyapatite (HA) described by general chemical formula: $Ca_{8.3}\square_{1.7}(PO_4)_{4.3}(HPO_4$ and $CO_3)_{1.7}$(OH and $0.5CO_3)0.3\square 1.7$) where □ represents a vacant. The carbonate substitution in bone apatite accounts 6 wt.% and correlates positively with its solubility.[4,5] This and other ionic substitutions (magnesium, sodium, potassium, fluorides and chlorides) makes a bone an important storage depot of ions and explains the lower Ca/P ratio of biological apatites compared to stoichiometric hydroxyapatite that presents Ca/P ratio of 1.67. The crystals of biological apatites have plate-like structure of 27-127 nm of width and 43-226 nm of length providing high surface to volume ratio and increased dissolution rates of bone.[4] The hydroxyapatite contributes to the high density and strength of bone. The remaining 30wt % (38 % in volume) is constituted by the organic component, mainly collagen (90-95 %) that serves as a support for hydroxyapatite crystals and provides flexibility to bone. The 5 % to 10 % of organic fraction consist of non-collagenous proteins (NCP) such as osteocalcin, osteonectin, bone morphogenetic proteins, proteolipids, phosphoproteins and proteoglycans, in addition to bone forming cells, such as osteoblasts, osteoclasts and osteocytes.[6] Moreover, the bone environment is enriched with growth factors and cytokines such as insulin-like growth factors (IGF), tumour necrosis factor-α (TNFα), transforming growth factor-β (TGFβ) and bone morphogenetic proteins (BMP).[7]

1.2 Bone structure

The human skeleton contains 213 bones which are categorised in four main groups: long bones, short bones, flat bones and irregular bones. All of them are composed of an external layer of compact (also known as cortical) bone and a central medullar cavity filled with bone marrow. This cavity located at the extremities of long bones is interrupted by the trabecular (cancellous or spongy) bone. Cortical and trabecular bones possess different structure and composition as well as differ in functions to fulfil.

Compact bone represents approximately 80 wt.% of the skeletal system. Since the major part of cortical bone is calcified, it possesses high rigidity and resistance to bending and torsion. Furthermore, compact bone provides mechanical strength and protection for skeletal system. On the other hand, the trabecular bone comprises 20 wt.% of skeletal system. Spongy bone, due to the large amount of marrow cavities, is less stiff and dense compared with cortical bone. Its major function is to maintain the homeostasis, mainly through the incorporation and release of large amounts of ions.[8]

Bone exhibit highly hierarchical structure that covers levels from nano to microscale (Figure 1.1.). The smaller, nano level corresponds to tropocollagen molecules that align into triple helices that bundle into collagen fibrils of 50-70 nm diameter.[4,6] These collagen fibrils incorporate bioapatite units and form larger arrangements of mineralised collagen - so called lamellae, which, in turn, constructs concentring rings around the osteon or Haversian system. Osteons are around 200 μm of diameter and connect between them by Volkmann canals creating the network that enables the circulation of blood and nutrients. The Haversian canals are organised parallel to long axis of bone making bone highly anisotropic material.[6,8]

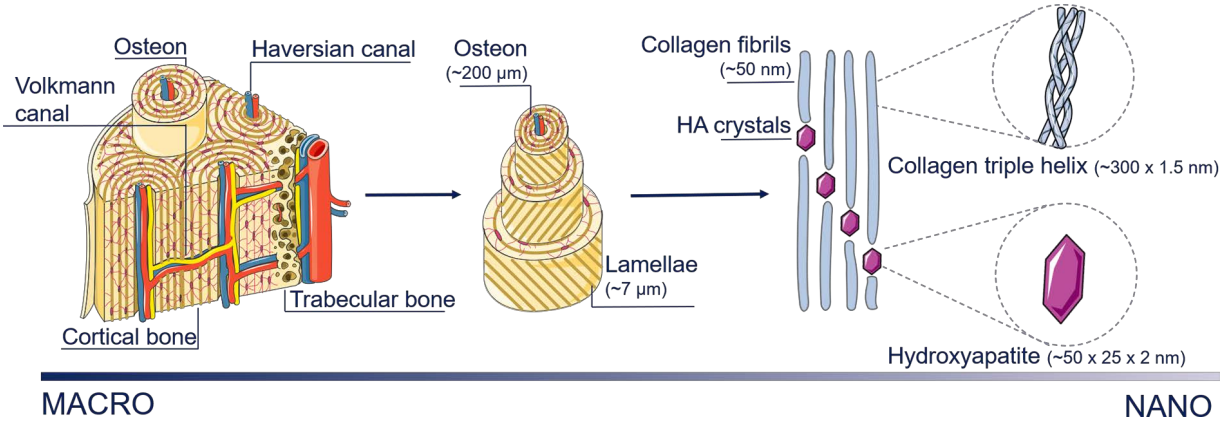

Figure 1.1. Hierarchical structure of bone. Adapted from.[9]

1.3 Bone biology

Bone is an active tissue that host various cell types; three main groups can be distinguished: osteoblasts, osteocytes and osteoclasts.[6]

Osteoblasts are mononucleated cells that synthesise the bone tissue. They derive from pluripotent stem cells, which are of mesenchymal origin.[6] Briefly, mesenchymal cells show the capacity to differentiate into various cell lineages giving rise to cartilage, fat, fibrous connective tissue as well as bone. Therefore, mature osteoblasts proceed from osteoprogenitor cells that have been stimulated to differentiate during the process of osteogenesis. The basic role of osteoblasts includes the secretion of components of bone extracellular matrix (ECM), mainly collagen I, osteocalcin, bone sialoproteins, proteoglycans and phosphoproteins.[6,7] During bone formation, some osteoblasts become trapped inside the matrix they secrete and then mature into osteocytes.

Osteocytes are the most abundant cells in mature bone. They are enclosed and spaced regularly in the mineralized matrix in small cavities called osteocytic lacunae. The gap junctional network that they establish with neighbouring cells allows cell-to-cell communication as well as transport of inorganic ions and small water-soluble molecules such as amino acids, sugars, nucleotides and vitamins.[6,7] Moreover, the particular distribution of osteocytes in the bone matrix allows them to sense the biochemical and mechanical stimuli making them active participants in bone remodelling.

Osteoclasts are terminally differentiated multinucleated cells, which originate from cells of the hematopoietic lineage. Briefly, the hematopoietic cells give rise to monocyte-macrophage precursor cells, which subsequently differentiate into osteoclasts.[6,7] The differentiation into fully functional osteoclasts is achieved do to the influence of several factors released by osteoprogenitor mesenchymal stem cells, osteoblasts and osteocytes.[10] Briefly, the bone forming cells secrete the macrophage colony- stimulating factor (M-CSF) and receptor activator of nuclear factor kappa-B ligand (RANKL) activating in that manner the osteoclastogenesis. The main function of osteoclastic cells is resorption of bone. This process occurs through two mechanisms. The osteoclasts, that are located on bone surface, release H^+ ions leading to the acidification of environment and dissolution of hydroxyapatite crystals. After degradation of mineral phase, osteoclastic cells secretes enzymes such as matrix metalloproteinase 9 (MMP9) or tartrate-resistant acid phosphatase (TRAP) that degrades organic matrix. The osteoclastic activity leaves characteristic depressions on bone surface known as Howship's lacunae.[10]

Although endothelial cells are not considered bone cells their role is crucial in bone development. These cells participate in angiogenesis (blood vessel formation from pre-existing ones) and vasculogenesis (blood vessel formation *de novo*) processes whose main goal is to provide oxygen and nutrients to bone tissue. Both monocyte/macrophage lineage and endothelial cells derive from the same precursor cell - the hemangioblast which transforms into an intermediate pre-endothelial cell. In addition to angiogenesis and vasculogenesis, endothelial cells carry out various metabolic and synthetic functions

such as regulation of haemostasis, vasomotor tone, immune and inflammatory responses.[11,12]

1.3.1 Bone remodelling and bone healing processes

During lifetime healthy bone is constantly renewed. The old bone from the skeleton is being reabsorbed giving the space for new bone formation. The replacement of old bone by new bone is called bone remodelling or bone turnover. This process gives bone the ability to continuously adapt its structure to loading circumstances. Precisely, bone is deposited or removed in locations where size and/or shape modifications are required. The rate of cortical bone turnover is approximately 5 % per year, whereas the remodelling of spongy bone could reach 15 % per year.[4] Remodelling occurs in discrete, focal areas involving both osteoclasts and osteoblasts. These two types of cells have synergistic activity during bone turnover, giving rise to what is called the basic multicellular unit (BMU).[8] The remodelling process is a highly complex system that involves regulation of a wide range of growth factors, proteins, hormones and cells.[6] The bone turnover consists of five phases which are depicted in Figure 1.2.: resting, resorption, reversal, bone formation and mineralization.

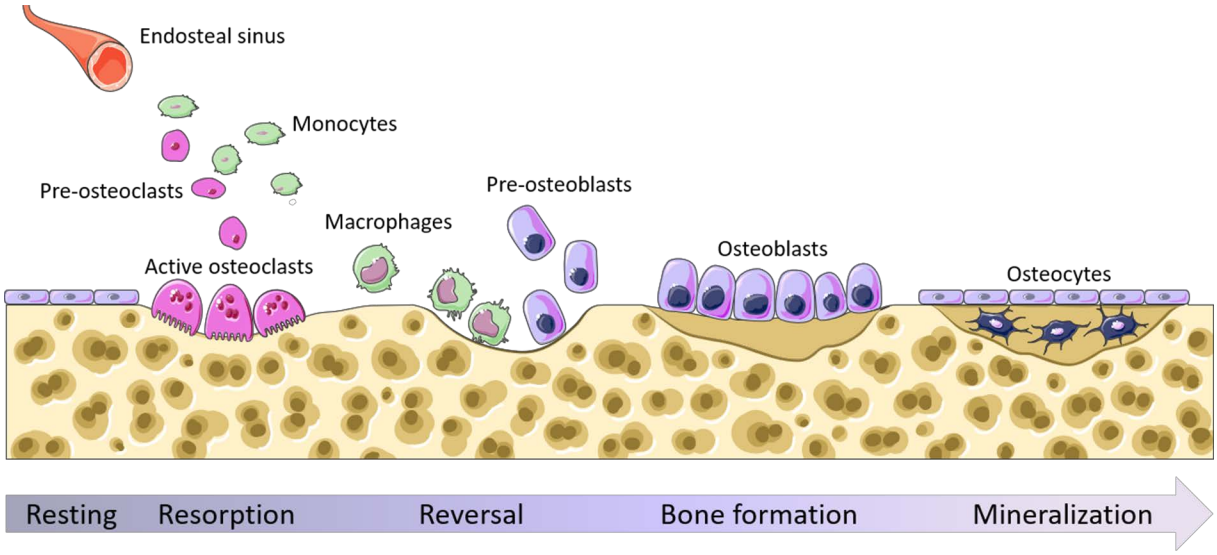

Figure 1.2. Schematic representation of bone remodelling process. Adapted from.[13]

The bone remodelling starts in BMU which become activated through the paracrine signals such as parathyroid hormone (PTH) derived from apoptotic osteocytes. The osteoblast and osteoclast precursors, in the form of MSCs and monocytes respectively, circulate and arrive at the site of interest through endosteal sinus previously created by endothelial cells. In resorption stage, the pre-osteoclasts bind to bone matrix by the interaction between integrin receptors and ECM proteins and form sealing zones around bone-resorbing compartments.[10] The process is followed by the elimination of demineralized and undigested collagen and the resorption lacuna is created in a site where bone has been removed (reversal stage). Then, osteoblastic cells orchestrate the

deposition of osteoid that afterwards undergo primary and secondary mineralization. Likewise, osteoblasts secrete higher amounts of osteoprotegerin (OPG) and reduce the production of RANKL (receptor activator of nuclear factor kappa-B ligand), which generate the inhibition of osteoclasts activity allowing osteoblasts to reconquer the resorption lacuna (formation stage). Finally, osteoblastic cells either undergo apoptosis or become trapped into the ECM transforming into osteocytes (mineralization stage).[6,8]

Despite the remarkable self-regenerative capacity of bone, it requires the help of bone graft to regenerate large bone defects created due to trauma, tumour removal or other clinical situations. The biomaterial placement makes that the remodelling process, which naturally occurs in bone, becomes distorted as the implant is recognised as foreign body causing the inflammatory host response. The graft implantation entails the biological events similar to those observed in process of bone healing. Bone healing is a complex process that involves multiple and overlapping-in-time regulations and its main goal is to rebuild the integrity of bone and restore its functions. Fracture healing cascade can be divided into four major phases that include: inflammatory phase, fibrocartilaginous callus formation, bony callus formation and bone remodelling. Nonetheless, each of them consist of subphases that require the crosstalk of various cell types (among others: immune cells, endothelial progenitor cells and mesenchymal cells) and their signalling molecules (cytokines, growth factors and chemokines).[14]

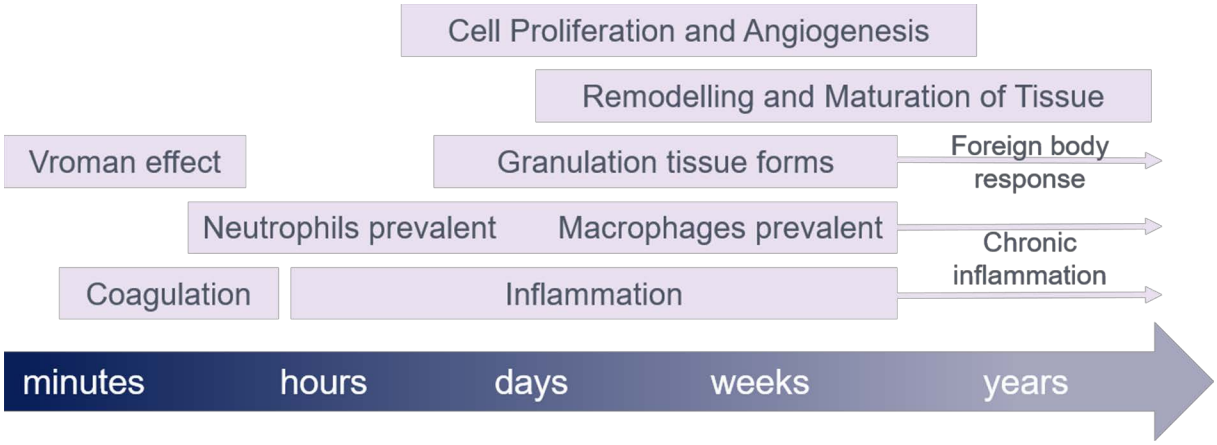

Figure 1.3. Timeline of the host response after graft implantation. Adapted from.[15]

Similar events occurs with grafts placement. As depicted in Figure 1.3., immediately following its implantation, the biomaterial induce a complex host response including protein adsorption, blood clot formation and inflammation process.[15] The extent to which bone implant will be capable to regenerate bone tissue is strictly related to its physicochemical cues and how these properties stimulate the cellular behaviour over particular phases of host response. In the following sections the key stages of the bone healing process are described.

1.3.1.1 Inflammation

The inflammation process is an immediate localized protective response to injury whose main goal is to prepare the tissue for its repair and healing. The disruption of integrity of bone triggers the process of blood clotting and subsequent formation of hematoma. The coagulation cascade, activated by endothelial cells and platelets, is followed by the inflammatory stage mediated by the cytokines and chemokines released from damaged cells. The process involves various cell types mostly neutrophils, granulocytes, macrophages and lymphocytes.[14,15] The acute inflammation phase is marked by the influx of neutrophils and polymorphonuclear leukocytes (PMNs), which upon activation fulfil the phagocytic role through releasing proteolytic enzymes and reactive oxygen species (ROS) that degrade the ECM and damaged cells. Before undergoing apoptosis, PMNs release chemoattractant and activation cytokines whose main function is the recruitment of monocytes which can differentiate into macrophages.[16]

Macrophages (MΦ) have a high plasticity, exhibiting the phenomenon of polarization either to pro-inflammatory M1 or anti-inflammatory M2 type depending on microenviromental cues.[16] Under the activation, M1 or M2 macrophages release factors and cytokines that interact and stimulate endothelial cells, osteoclasts and osteoblasts, among others. For instance, activated M1 macrophages secrete many pro-inflammatory cytokines such as: tumour necrosis factor alpha (TNFα), interleukin 6 (IL-6) and interleukin 1 beta (IL-1β) which induce osteoclastic activity leading to osteoclastogenesis. On the other hand, M2 are known to participate in new bone formation and angiogenesis through secretion of osteogenic/angiogenic molecules: interleukin 10 (IL-10), transforming growth factor beta (TGFβ), BMP-2 and vascular endothelial growth factor (VEGF). Nonetheless, prolonged M2 polarization might result in overexpression of pro-fibrotic molecules (TNFα, TGFβ1, TGFβ3) favouring the formation of fibrous tissue.[17] Figure 1.4. summarises the macrophage polarization phenomenon detailing the inducers, surface markers and functions of M1 and M2 phenotype.

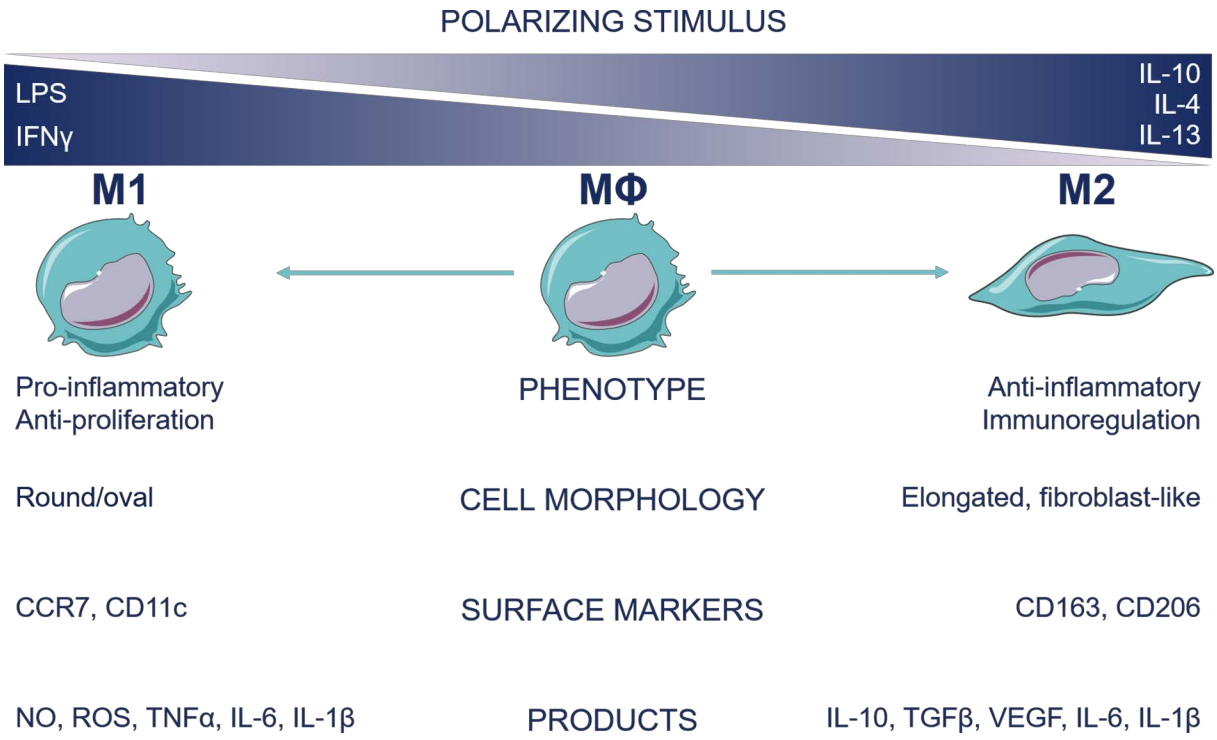

Figure 1.4. Polarizing inducers, surface markers and main functions of macrophage phenotype. Under the stimuli of different inducers, macrophages can switch into pro-inflammatory M1 type or anti-inflammatory M2 type. Adapted from.[17-19]

The bone healing process compromise proper-in-time and dosage pro- and anti-inflammatory cytokine release. Understanding the interplay between inflammatory cytokines, osteogenic and osteoclastogenic factors as well as fibrosis factors will favour designing materials that presents positive outcome on bone repair.

1.3.1.2 Osteoimmunomodulation

The immune and skeletal systems are found to be closely related. The immune cells are demonstrated to play indispensable role in bone remodelling process.[20-22] This led to the creation of the concepts *osteoimmunology* and *osteoimmunomodulation*. Whilst osteoimmunology is a research field which main purpose is to study the intimate relation between immune and bone cells, the osteoimmunomodulation is defined as a capacity of biomaterial to induce proper immune environment that gives the balance between osteogenesis and osteoclastogenesis.[17,19,23] The way in which a biomaterial stimulates the immune system response will either define its success or will lead to chronic inflammation and the formation of a fibrous capsule. The following section describes the close relation between macrophages and bone cells and their paracrine signalling for stimulating osteoclasto- and osteoblastogenesis.

The bone marrow stromal cells and osteoblastic cells secrete proteins thereby stimulating macrophages/monocytes to differentiate into osteoclasts *i.e.* cells responsible for bone resorption. Specifically, this osteoclastic maturation of immune

cells is achieved through macrophage-colony stimulating factor (M-CSF) and receptor activator of NF-kB/receptor activator of NF-kB ligand/osteoprotegerin system (RANKL/RANK/OPG system) released from bone forming cells. Briefly, the RANK-RANKL interaction lead to osteoclasts maturation whilst the OPG, a decoy receptor derived from osteoblastic cells, suppresses this process binding to RANKL.[24,25] Moreover, the immune cells not only undergo osteoclastic differentiation but they also participate osteoclastogenesis through release of cytokine- related signals. The macrophages release inflammatory cytokines such as IL-6, interleukin-23 (IL-23) and oncostatin M (OSM) regulating, in that way, the expression of RANKL. Furthermore, the secretion of TNFα and IL-1 also induces the osteoclast formation.[26,27]

From the other hand, the macrophages regulate osteogenesis-related events. The anti-inflammatory M2 phenotype produce osteoinductive molecules such as BMP-2 and VEGF[28,29] whilst M1 phenotype induce MSCs differentiation via pro-inflammatory signals. For instance, the pro-inflammatory agents such as TNFα were reported to control alkaline phosphatase activity and mineralisation of mesenchymal stem cells (MSCs) and their subsequent differentiation towards osteoblastic phenotype.[30] Moreover, the secretion of pro-inflammatory cytokines *i.e.* TNFα, TGFβ, interferon γ (IFNγ), and interleukin 17 (IL-17) from immune cells can activate the autologous differentiation factor- BMP-2 from MSCs inducing their differentiation into osteoblastic lineage. This reciprocal and related pathways between macrophages and bone forming cells underline the tight relation between immune and skeletal system.[31]

1.3.1.3 Angiogenesis and vasculogenesis

The proper vasculature is also essential during bone-related processes such as development, growth, remodelling and repair. The blood vessels support osteogenesis process through a supply of nutrients, oxygen, growth factors as well as osteoblast and osteoclast precursors.[32] The formation of new blood vessels occurs through one of two well-known routes: the microcapillary structures are either formed from pre-existing ones (angiogenesis) or they are formed *de novo* (vasculogenesis).

The bone trauma coupled with reduced blood supply and local necrosis creates a hypoxic environment that induces bone cells to release Hypoxia Inducible Factors (HIF). Subsequently, the HIF pathway contributes to the upregulation of a wide range of pro-angiogenic factors, released by osteoblastic cells, such as the vascular endothelial growth factor (VEGF), platelet-derived growth factor (PDGF), Transforming Growth Factor-β (TGFβ), Fibroblast Growth factors (FGF), Endothelin 1 (EDH 1) and Bone Morphogenetic Proteins (BMP).[33] Among them, VEGF is recognised as a key player in rebuilding proper vasculature. VEGF interacts with two cell surface receptor tyrosine kinases, VEGF R1 and VEGF R2 thus controlling the recruitment of endothelial

progenitor cells (EPCs) as well as proliferation and differentiation into endothelial cells (ECs).[34]

The newly formed endothelium, either through angiogenesis or vasculogenesis process, secretes the growth factors that recruit hematopoietic cells to the bone site allowing the maintenance of bone homeostasis. Hence, the role of ECs is not limited to the formation of blood vessels. Endothelial cells subjected to hypoxic environment release potent osteogenic enhancers such as BMP-2 and BMP-4 stimulating the differentiation of bone forming cells.[35] Figure 1.5. presents simplified events that occurs during hypoxia conditions.

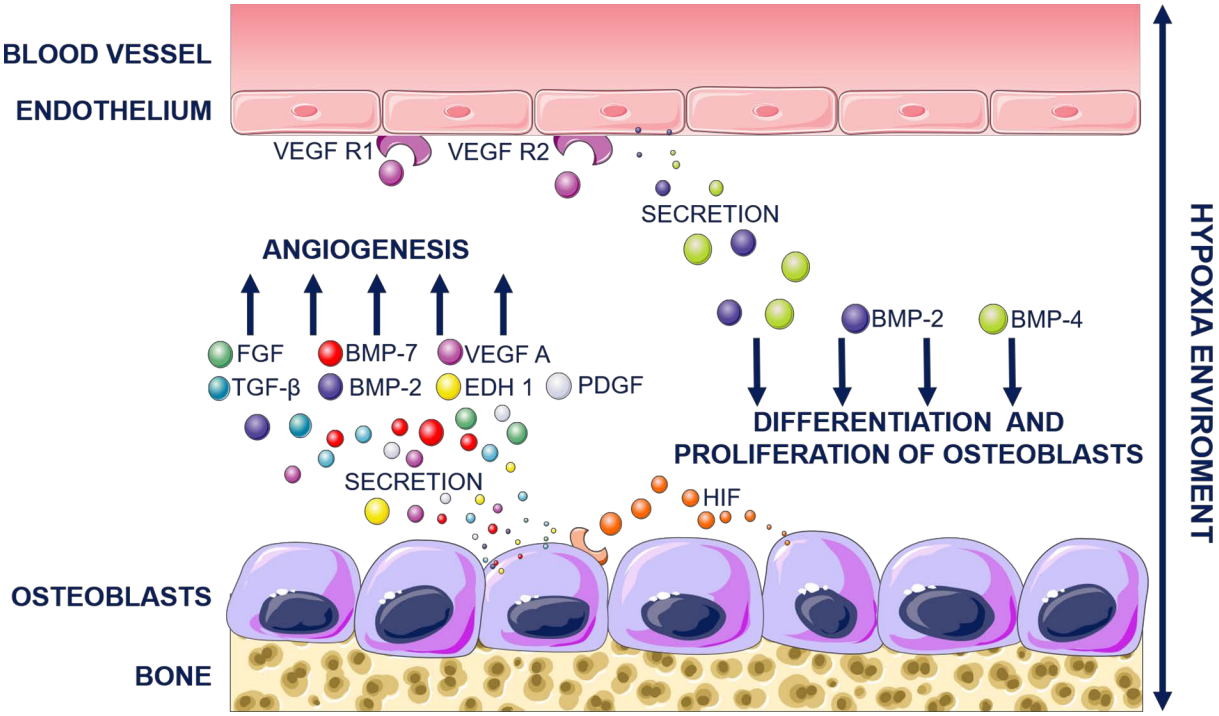

Figure 1.5. Microenvironment during bone fracture repair. Adapted from.[32]

Overall, the presence of molecular crosstalk between endothelial and osteoblastic cells underlines the tight relation between angiogenesis and osteogenesis during fracture repair. Hence, the effect of physicochemical cues of bone graft on angiogenesis and vasculogenesis cannot be neglected and should be also studied when evaluating the suitability of a synthetic bone graft. In like manner, biomaterial should stimulate ECs behaviour and their interaction with bone forming cells.

1.3.1.4 Osteogenesis

There are two routes of bone formation both involving the transformation of pre-existing mesenchymal tissue into bone tissue. Whilst intramembranous ossification consists of direct conversion of mesenchymal tissue into bone, the endochondral ossification differentiates mesenchymal tissue into cartilage which is later replaced by bone.

The main players involved in osteogenesis are osteoblastic cells whose principal function is to secrete and to mineralize bone extracellular matrix. Osteoblasts are developed from mesenchymal precursors which previously differentiated under BMPs pathways[36] involving various transcription factors such as Runx2[37] or Osterix (Osx).[38] Osteoblastic differentiation can be characterised in three stages: cell proliferation, early differentiation and matrix maturation. Each phase is accompanied with the expression of specific osteogenic markers (Figure 1.6.). The early stage usually involves the expression of early osteogenic genes such as alkaline phosphatase (ALP), BMPs and transcription factors. The matrix maturation phase is paired with the maximal expression of ALP and slowing down of proliferation rate. Finally, at the beginning of mineralization of matrix takes place the downregulation of early osteogenic markers such as collagen type I (COLL I) or ALP. The process is followed by the upregulation of genes for proteins such as bone sialoprotein (BSP) or Osteopontin (OPN) as well as the entrapment of osteoblasts into the bone matrix. In that way osteoblastic cells become osteocytes.

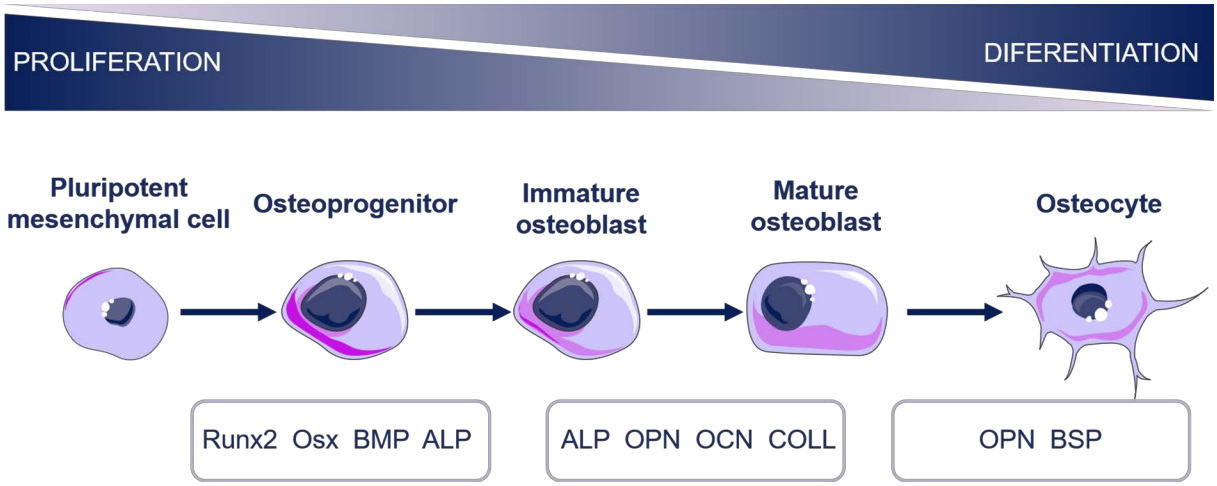

Figure 1.6. Schematic representation of osteogenic commitment of pluripotent mesenchymal stem cells with specific differentiation markers. Adapted from.[39-41]

1.4 Synthetic bone grafts

Despite the great capacity of bone to self-regenerate, the critical sized defects or non-union fractures require the implantation of bone graft to support and stimulate bone healing process. These can be grouped in to main categories: either natural (autografts, allografts and xenografts) or synthetic. Autografts, harvested from the patient became a gold standard since they contain viable osteogenic cells and bone matrix proteins which enhance its osteoconductive and osteoinductive properties. Nonetheless, they accounts with limited availability, high morbidity at the donor site and they require the second surgery intervention.[42,43] An alternative solution such as allogenic (obtained from the same species) and xenogenic (from different species) bone grafts carry the risk of immunogenicity and disease transmission.[44]

In order to meet the growing demand of bone grafting, regenerative medicine focuses its efforts in designing synthetic materials. Ideally, synthetic bone substitute should not only be structurally similar to bone tissue but also should boost the process of osteogenesis. In this field, calcium phosphates (CaPs) have become materials of interest due to their close resemblance to the mineral phase of bone and osteoconductive/ osteoinductive properties.[45,46] In addition, several studies have reported that the physicochemical features of CaPs may be responsible for their osteoconductive/ osteoinductive potential. Nontheless, the underlying cellular mechanisms are still unclear, hence the approach proposed in this thesis.

1.4.1 Calcium phosphate bioceramics

As previously described, CaPs are common bone substitutes due to their bioactivity, ability to reabsorb and osteoconductive/osteoinductive properties. CaPs are salts of orthophosphoric obtained either through precipitation from aqueous solution or through solid state reaction, which requires high temperature sintering processes. Table 1.1. compiles the eleven compounds calcium orthophosphates, with Ca/P ratios varying between 0.5 and 2.0.

Table 1.1. Calcium orthophosphates.[47]

Ca/P ratio	Compound	Chemical formula	Solubility at 25_oC, g/L
0.5	Monocalcium phosphate monohydrate (MCPM)	$Ca(H_2PO_4)_2 \cdot 2H_2O$	~18
0.5	Monocalcium phosphate anhydrous (MCPA)	$Ca(H_2PO_4)_2$	~17
1.0	Dicalcium phosphate dehydrate (DCPD)	$CaHPO_4 \cdot 2H_2O$	~0.088
1.0	Dicalcium phosphate anhydrous (DCPA)	$CaHPO_4$	~0.048
1.33	Octacalcium phosphate (OCP)	$Ca_8(HPO_4)_2 (PO_4)_4 \cdot 5H_2O$	~0.0081
1.5	α-Tricalcium phosphate (α-TCP)	$\alpha\text{-}Ca_3(PO4)_2$	~0.0025
1.5	β-Tricalcium phosphate (β-TCP)	$\beta\text{-}Ca_3(PO4)_2$	~0.0005
1.2-2.2	Amorphous calcium phosphate (ACP)	$Ca_XH_Y(PO_4)_Z \cdot nH_2O$	N.A.
1.5-1.67	Calcium-deficient hydroxyapatite (CDHA)	$Ca_{10-X}(HPO_4)_X (PO_4)_{6-X}(OH)_{2-X}$	~0.0094
1.67	Hydroxyapatite (HA)	$Ca_{10}(PO_4)_6(OH)_2$	~0.0003
2.0	Tetracalcium phosphate (TTCP)	$Ca_4(PO_4)_2O$	~0.0007

The solubility of CaPs is considered to be one of the most important properties of CaP insomuch as it controls its dissolution/precipitation in vitro or in vivo conditions.[48] The following sections focus on giving a brief description of relevance for bone grafting of high-T and low-T CaPs.

1.4.1.1 Calcium orthophosphates obtained by solid-state reactions at high temperature

β-tricalcium phosphate (β-TCP), α-tricalcium phosphate (α-TCP), tetracalcium phosphate (TTCP) and hydroxyapatite (HA) are four of the eleven CaP that are obtained by solid state reaction at high temperatures. All high-T CaPs are used in regenerative medicine. Whilst α-TCP and TTCP are used as starting materials for calcium phosphate cements (CPC), β-TCP and HA (alone or together, forming biphasic calcium phosphates (BCP)) are directly applied as bone substitutes in the field of regenerative medicine.

β-TCP can be obtained at temperatures above 800 ºC either by solid-state reaction of calcium phosphate and carbonate salts or by thermal decomposition of CDHA. At higher temperatures, i.e. ~1125 ºC, it transforms into its allotropic form α-TCP. Both β-TCP and α-TCP present a Ca/P ratio of 1.50. Nonetheless, β-TCP is less soluble compared to its allotropic form. Once exposed to aqueous conditions, α-TCP rapidly hydrolyses to hydroxyapatite (pHA; precipitated hydroxyapatite).[47,49] Similarly, TTCP shows low stability in aqueous solutions, hydrolysing to HA and calcium hydroxide. TTCP is the most basic and soluble of CaPs obtained at ~1300 ºC upon controlled dry air atmosphere.

Stoichiometric HA with Ca/P ratio of 1.67 is the less soluble CaP. The solid-state method of HA formation usually consists on sintering above 1200 ºC the mixture of other CaPs with CaO, $Ca(OH)_2$ or $CaCO_3$. It is worth mentioning that, in contrast to the previously mentioned compounds in this section, HA can also be obtained by precipitation in aqueous solutions.[50]

1.4.1.2 Calcium orthophosphates obtained by precipitation at low temperature

Monocalcium phosphate monohydrate (MCPM), monocalcium phosphate anhydrous (MCPA), octacalcium phosphate (OCP), dicalcium phosphate dihydrate (DCPD), dicalcium phosphate anhydrous (DCPA), amorphous calcium phosphate (ACP), calcium deficient hydroxyapatite (CDHA) and hydroxyapatite (HA) are CaPs that can be obtained at low temperature by precipitation reactions. The majority of low-T CaPs naturally occur in human tissues.

MCPM and its anhydrous form MCPA are the most acidic and the most soluble in almost all pH values. Neither MCPM nor MCPA are naturally found in the body, however, they are used as bone substitute once combined with basic CaP compounds. DCPD has been reported to be biocompatible and biodegradable.[49] Since DCPD is metastable, it is usually converted to DCPA (pH < 6), OCP (pH = 6-7) or precipitated HA (pHA) (pH > 7). OCP is believed to be a precursor in *in vivo* formation of apatitic CaPs.[51] Nonetheless, its metastable nature impedes its precipitation through cementitious reaction. Thereby, OCP may occur as a transient phase during precipitation of HA.[51]

Similarly, ACP is a transitory compound during the formation of CaPs in aqueous systems. The chemical composition of ACP and further, more stable phase strongly depends on pH and concentration of mixing solution. For instance, the gentle agitation of ACP at elevated temperatures usually results in precipitation of CDHA.[51]

Precipitated hydroxyapatite (pHA) is in fact a solid solution, with chemical formula $Ca_{10-x}(HPO_4)_x(PO_4)_{6-x}(OH)_{2-x}$ with x ranging from 0 to 1. Hence, the Ca/P varies from 1.5 up to 1.67. The pHA with Ca/P is known as CDHA and can be easily obtained by hydrolysis of α-TCP. CDHA is particularly interesting as a bone substitute due to its similarity in chemistry and structure to mineral phase of bone. Its elevated specific surface area (SSA) and low crystallinity enhance CDHA' solubility and thus bioactivity compared to stoichiometric HA.

Various methods of CaPs preparation lead to biomaterials for bone regeneration with different physicochemical features. The chemistry of CaPs define the solubility and thus their intrinsic ionic reactivity in aqueous solutions. Similarly, the thermal treatment has repercussions in CaPs' microstructure, SSA and porosity. All properties together define further interaction of CaPs- based graft with bone cells contributing to either its success or fail.

1.5 *In vitro* performance of calcium phosphates

Research on how and which particular properties of CaPs affect cell behaviour is of great importance. Hence, better understanding of CaPs-cells interplay will contribute to design bone grafts that trigger expected response. There is a wide range of parameters that could possibly modulate cellular behaviour *in vitro*. Figure 1.7. points the key role of chemical composition, surface topography and bioactive properties of calcium phosphates in stimulating some of cellular events.[52-60]

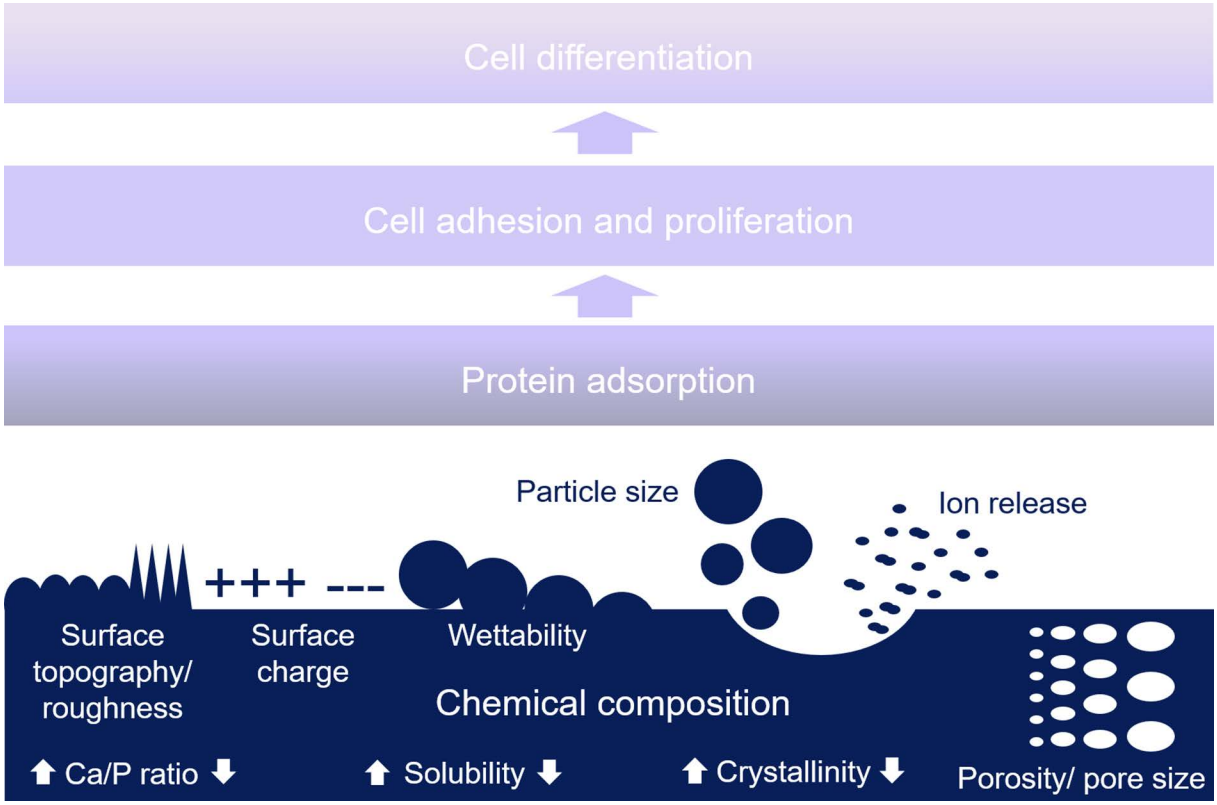

Figure 1.7. Possible properties of calcium phosphates that can modulate *in vitro* cell behaviour. Adapted from.[17,60]

It is important to highlight that the direct correlation between a particular parameter of CaPs and cell response is not straightforward. On the one hand, the modulation of a singular feature of CaPs could potentially affect the others, being very difficult to isolate the effect of individual properties like composition, SSA or surface topography. Moreover, unlike bioinert materials, the CaP release/uptake soluble spices when immersed in aqueous solutions.[53,61] Hence, the *in vitro* assessment of CaP-cell interaction is far more complex as CaPs modulate the cellular behaviour not only through direct biomaterial effects but also indirectly through soluble spices that are released or adsorbed from cell culture medium. On the other hand, the cellular responses are also tightly linked between them. For instance, cell differentiation is guided by how cells are well attached to a surface and this, in turn, depends on previous protein adsorption to biomaterial.

The following sections summarise current knowledge of biological *in vitro* performance of bioceramics and the influence of their cues on cellular processes.

1.5.1 The effect of CaPs features on cellular adhesion

Cellular adhesion is a critical step toward positive cellular response to the material. The biological processes such as cell spreading, proliferation and repair pathways have been reported to be influenced by various biomechanical adhesion factors on the surface of

the calcium phosphate substrates.[62] Furthermore, cell adhesion has been described to be an essential initial step towards creating a mechanically stable interface between the material and the bone tissue.[63] Consequently, the improvement of cell adhesion to a scaffold still remains one of the top challenges in regenerative medicine. Cellular adhesion is modulated through proteins from the media that have been adsorbed to surface of calcium phosphates substrates. For instance, Sawyer *et al.*, showed that proteins adsorbed to the surface of hydroxyapatite regulates attachment and spreading of MSCs through interaction with integrins (membrane cellular receptors).[64] In fact, several authors demonstrated that both protein adsorption and subsequent cell adhesion strictly depend on calcium phosphates properties such as surface roughness, crystallinity and solubility.[53,57,65-70]

The roughness of calcium phosphates is pointed as one of the principal cues in controlling cellular adhesion. In that field, Campoccia *et al.* and Rosa *et al.* demonstrated that initial cell events were affected by roughness of fluorohydroxyapatite or hydroxyapatite, respectively.[71,72] Dos Santos *et al.* showed that nano topography of β-TCP and HA strongly affects protein adsorption but no effect of nano topography on cell attachment was observed.[73,74] On contrary, Deligianni *et al.* proved that human bone marrow cells adhere better to hydroxyapatite with higher surface roughness.[57]

Furthermore, the solubility and crystallinity of calcium phosphates also have impact on cellular adhesion. Fundamentally, both solubility and crystallinity influence the pH and ion concentration in medium likely affecting the adsorption of proteins.[60] For instance, Berube *et al.* showed that highly crystalline HA surface stimulate to greater extent rat calvarial osteoblast adhesion compared to low crystalline HA or ACP.[69] Likewise, Hu *et al.* demonstrated an improvement of rabbit bone marrow stromal cells (BMSCs) attachment when they were cultured on HA (higher crystallinity) compared to ACP (lower crystallinity).[75]

1.5.2 The effect of CaPs features on immunomodulation

The bone graft upon implantation is recognized by host's immune system as a foreign body. This triggers the cascade of immune responses which decide of either encapsulation process or pro-healing and proper implant integration. The interaction of CaPs-based materials and immune cell has been studied highlighting the regulatory effect of some physicochemical properties such as biomaterial' particle size, microstructure, chemistry and ion exchange. Especially, the effect of HA and β-TCP particles and granules on macrophage and monocyte behaviour was extensively investigated.[76-82] That is why particles, in comparison to bulk biomaterial, usually exhibit greater specific surface and reactivity, strengthening the response of targeting cells.[17] Previous studies underlined the effect of particle size on modulating immune cells response. Hence, smaller particles are usually phagocytised whiles larger particles

stimulate macrophages to form foreign body giant cells (FBGCs).[83] Moreover, the smaller particle size is frequently coupled with enhanced pro-inflammatory cytokine release[81] In like manner, bulk CaPs like β-TCP were shown to favour the fusion of macrophages into FBGCs as well as stimulate their osteoclastic activity.[84,85]

The influence of textural properties of bulk biomaterials, including both topography and roughness, on immune cells was also studied. So far, the research was rather focused on investigating the response of macrophages to metallic and polymeric surfaces. In general, the greater roughness of titanium or polyvinylidene fluoride substrarte activates macrophages to a more pronounced release of pro-inflammatory cytokines and chemokines compared to smooth surfaces.[86,87] In the field of CaPs, Mestres *et al*. observed similar trend; the CDHA with micrometric sized crystals activated macrophages to more inflammatory state due to greater ROS release compared to CDHA with needle-like nanosized crystals.[88]

There is little knowledge regarding the response of macrophages to the chemistry and ionic products of CaPs. Only recently, Chen *et al.* shed light on the effect of substitution of CaPs with magnesium or cobalt ions on inflammatory cells behaviour.[19,89] The incorporation of specific ions to CaPs structure resulted in triggering specific immune response. The authors showed that magnesium-doped β-TCP scaffolds stimulated to greater extent the polarization of macrophages to anti-inflammatory M2 phenotype than β-TCP alone.[19] On the contrary, the incorporation of cobalt ions resulted in pro-inflammatory associated gene expression of macrophages.[89]

1.5.3 The effect of CaPs features on angiogenesis

The high vascular supply to bone is pivotal for its proper growth, homeostasis and remodelling. Prompt post-implanting neovascularization/angiogenesis improves subsequent integration with tissue enhancing the success rate of graft.[90-92]

With regards to soluble ions, the importance of calcium[93,94], magnesium[95,96] and phosphate[97] on EC behaviour has been widely described. For instance, certain concentrations of Ca^{2+} could be associated with vascular calcifications whilst Mg^{2+} and P_i have been shown to have an effect on proliferation and death rate of EC, respectively. CaPs are known to alter ionic concentrations when subjected to aqueous environment. Although there is no much information regarding the effect of degradation/reprecipitation products of CaPs on angiogenesis, Aguirre *et al.* showed that calcium phosphate glass/polylactic acid composite (BG/PLA) might stimulate differentiation of endothelial progenitor cells (EPCs), specifically upregulation of VEGF and VEGF R2, through pathways that involve extracellular calcium and mechanotransduction.[98]

Porosity as well as chemical composition has also great influence on angiogenesis process. Hence, the appropriate pore size and interconnectivity leads to better new vessel formation.[99,100] Xiao *et al.* showed that β-TCP scaffolds with high interconnected porosity favour the adhesion, migration and proliferation of human umbilical vein endothelial cells (HUVEC) and upregulates the expression of platelet and endothelial cell adhesion molecule 1 (PECAM-1) and VEGF. The effect of chemistry of ceramics on human fibroblasts (HF) and HUVEC was studied by Chen *et al.* demonstrating that that the higher content of β-TCP (*i.e.* 2/98 HA/ β-TCP or pure β-TCP) in CaPs resulted in greater upregulation of the expression of angiogenic genes compared to pure HA substrate.[100]

1.5.4 The effect of CaPs features on osteogenic differentiation

The modification of the properties of synthetic bone grafts in view of improving its osteoconductive/osteoinductive potential was widely studied in the field of bone substitutes. The surface topography, solubility and porosity (especially in micro- and nanoscale) of CaPs were pointed out as key properties in influencing osteogenic differentiation of cells.

The importance of surface topography was demonstrated by Cairns *et al.* who showed that HA-like thin films with higher nanometric surface roughness stimulated to greater extent the focal adhesion assembly, OCN expression and ALP activity compared to HA-like films with more smooth microstructure.[101] Zhang *et al.* also underlined the importance of microstructure proving that osteogenic differentiation of human BMSCs was enhanced when cultured on TCP ceramic granules with smaller grain size and micropore size.[102]

The great effect of ions, especially Ca^{2+} and P_i, on differentiation into osteoblastic lineage was also pointed in literature.[103-105] In fact, the dissolution/precipitation of CaPs in aqueous media and subsequent ionic alterations account for their bioactive character. Hence, the solubility of CaPs was investigated as potential factor affecting osteogenic differentiation. Nonetheless, the intrinsic ion release/uptake from CaPs is tightly linked to other physicochemical features. Thus, the effect of solubility is frequently studied simultaneously with the effect of surface topography. On the contrary, the influence of surface morphology on osteogenic behaviour can be investigated separately employing the inverse replica of CaPs, through embossing in non-reactive elastomer, or sputtering them with noble metals. The work of Danoux *et al.* demonstrated great impact of solubility and chemistry of CaPs on osteogenic gene expression. The expression of Ca^{2+}-responsive genes such as BMP-2 and OPN was significantly higher for hMSCs cultured on brushite and monetite substrates rather than cells cultured on their inverse replicas.[106] Similarly, dos Santos *et al.* observed higher ALP activity of SaOS-2 osteoblast-like cells

cultured on uncoated HA and TCP surfaces where the cells were directly exposed to biomaterial' chemistry.[74]

Likewise, the role of crystallinity of CaPs was also studied. Hu *et al.* demonstrated that rabbit BMSCs expressed higher levels of osteocalcin, osteopontin and COLLI in contact with HA than in contact with ACP.[75] In a similar way, Brugge *et al.* showed that amorphous CaPs coatings inhibit mineralization of rabbit BMSCs compared to amorphous-crystalline films.[107]

1.5.5 Cellular crosstalk on CaPs substrates

As previously mentioned, the bone healing process involves multiple and overlapping-in-time regulation and thus requires participation of various cell types. Current research particularly emphasises the reciprocal regulation between macrophages or endothelial[108] cells with bone forming cells. Hence, the design of bone graft requires comprehending the impact of its physicochemical features on all stages of bone healing. The successful bone substitute, apart from interacting exclusively with bone forming cells, should also stimulate the proper crosstalk between those and cells from former phases *i.e.* from inflammation and angiogenesis stage. Therefore, the ideal bone graft should possess osteoimmunomodulatory, angiogenic and osteogenic properties.

The effect of immune cells on osteogenesis and osteoclastogenesis was studied by several authors. The importance of cytokines and other factors released by macrophages on bone cell behaviour was emphasized by Chen *et al*. To study the osteoimmunomodulation, the authors firstly cultured immune cells on β-TCP allowing the release of both the inflammatory cytokines from macrophages and the ionic products from the substrate to cell culture medium. Secondly, BMSCs were exposed to the supernatants from either macrophage-β-TCP or β-TCP culture. The authors observed that the osteogenic effect on BMSCs was more pronounced when mesenchymal cells were cultured with macrophage and β-TCP conditioned medium rather than with extracts from β-TCP without cells cultured on it.[19] The positive effect on osteogenesis is frequently paired with the polarization of macrophages to anti-inflammatory M2 phenotype. The activation of macrophages is coupled with expression of anti-inflammatory cytokines as well as angiogenic and osteogenic factors such as VEGF and BMPs.[23] A pro-inflammatory M1 phenotype, instead, presents opposite effects. In like manner, Chen *et al.* showed that osteogenic differentiation of BMSCs was inhibited when cultured with macrophage and cobalt-doped β-TCP conditioned media.[89]

The studies on endothelial and osteoblastic cells underlines the importance of cell-to-cell communication towards angiogenesis and neo-bone formation.[108] This, in turn, can be established either through gap junctional proteins[109] or through diffusible factors. For instance, Bulnheim *et al*. demonstrated the requirement of direct contact of ECs and

MSCs for osteogenic gene induction. The expression of gap junctional protein connexin 43 as well as enhanced ALP activity was found when ECs and MSCs were cocultured on commercial CaPs scaffolds.[110] Similarly, Thein-Han *et al.* reported greater osteogenic gene expression for cocultured HUVEC and osteoblast cells on macroporous CPC composite compared to monocultures.[111] The coculture of ECs and bone cells systems reflects also on the assembly of microcapillary-like structures. The formation of capillarities was rarely observed when ECs are cultured alone on CPC composites or sintered HA or β-TCP.[111,112]

The present PhD thesis focuses on investigating the effect of physicochemical cues of CaPs on regulation processes related to bone healing. For better comprehending the impact of biomaterial on particular phases of host response, the current thesis investigates the *in vitro* interaction of CaPs, mainly biomimetic CDHA, with various cell types including immune, endothelial and bone forming cells. The work also seeks to widen the knowledge of cellular crosstalk on CaPs biomaterials through investigating macrophages and endothelial cell interaction with cells of skeletal system.

1.6 Bibliography

1. Robling, A. G., Castillo, A. B. & Turner, C. H. Biomechanical and Molecular Regulation of Bone Remodeling. *Annu. Rev. Biomed. Eng.* **8**, 455–498 (2006).
2. HCUP Healthcare Cost and Utilization Project. Rockville, MD: Agency for Healthcare Research and Quality. 2006.
3. Rao, R. R. & Stegemann, J. P. Cell-based approaches to the engineering of vascularized bone tissue. *Cytotherapy* **15**, 1309–22 (2013).
4. Pasteris, J. D., Wopenka, B. & Valsami-Jones, E. Bone and Tooth Mineralization: Why Apatite? *Elements* **4**, 97–104 (2008).
5. Elliott, J. C. Calcium Phosphates Biominerals in *Phosphates: Geochemical, Geobiological, and Material Importance. Reviews in Mineralogy & Geochemistry* (eds. Kohn, M. L., Rakovan, J. & Hughes, J. M.) 427–454 (Mineralogical Society of America, 2002).
6. Nanci, A. Bone in *Ten Cate's Oral Histology: Development, Structure, and Function* (ed. Nanci, A.) 95–121 (Elsevier, 2014).
7. Marks, S. C. J. & Odgren, P. R. Structure and Development of the Skeleton in *Principles of Bone Biology, 3rd Edition* (eds. Bilezikian, J. P., Raisz, Lawrence, G. & Martin, T. J.) 3–17 (Elsevier, 2008).
8. Clarke, B. Normal bone anatomy and physiology. *Clin. J. Am. Soc. Nephrol.* **3 Suppl 3**, 131–139 (2008).
9. Nalla, R. K. *et al.* Role of microstructure in the aging-related deterioration of the toughness of human cortical bone. *Mater. Sci. Eng. C* **26**, 1251–1260 (2006).
10. Takahashi, N., Udagawa, N., Takami, M. & Suda, T. Cells of Bone: Osteoclast Generation in *Principles of Bone Biology, 3rd Edition* (eds. Bilezikian, J. P., Raisz, Lawrence, G. & Martin, T. J.) 109–127 (Elsevier, 2008).
11. Sumpio, B. E., Riley, J. T. & Dardik, A. Cells in focus: endothelial cell. *Int. J. Biochem. Cell Biol.* **34**, 1508–1512 (2002).
12. Cines, B. D. B. *et al.* Endothelial Cells in Physiology and in the Pathophysiology of Vascular Disorders. *Blood* **91**, 3527–3561 (1998).
13. Garg, A. K. Bone Biology, Osseointegration, and Bone Grafting in *Implant dentistry : a practical approach* (ed. Dolan, J.) 193–212 (Mosby/Elsevier, 2010).
14. Bucher, C. H., Lei, H., Duda, G. N., Volk, H.-D. & Schmidt-Bleek, K. The Role of Immune Reactivity in Bone Regeneration in *Advanced Techniques in Bone Regeneration* (ed. Zorzi A.) **3**, 169–194 (InTech, 2016).
15. Schmidt-Bleek, K., Kwee, B. J., Mooney, D. J. & Duda, G. N. Boon and Bane of Inflammation in Bone Tissue Regeneration and Its Link with Angiogenesis. *Tissue Eng. Part B Rev.* **21**, 354–364 (2015).
16. Mokarram, N. & Bellamkonda, R. V. A Perspective on Immunomodulation and Tissue Repair. *Ann. Biomed. Eng*. **42**, 338–351 (2014).
17. Chen, Z. *et al.* Osteoimmunomodulation for the development of advanced bone biomaterials. *Mater. Today* **19**, 304–321 (2016).
18. Isidro, R. A. & Appleyard, C. B. Colonic macrophage polarization in homeostasis, inflammation, and cancer. *Am. J. Physiol. - Gastrointest. Liver Physiol.* **311**, G59–G73 (2016).
19. Chen, Z. *et al.* Osteogenic differentiation of bone marrow MSCs by β-tricalcium phosphate stimulating macrophages via BMP2 signalling pathway. *Biomaterials* **35**, 1507–18 (2014).
20. Franz, S., Rammelt, S., Scharnweber, D. & Simon, J. C. Immune responses to implants e A review of the implications for the design of immunomodulatory biomaterials. *Biomaterials* **32**, 6692–6709 (2011).
21. Nakashima, T. & Takayanagi, H. Osteoimmunology: Crosstalk Between the Immune and Bone Systems. *J. Clin. Immunol.* **29**, 555–567 (2009).
22. Takayanagi, H. Inflammatory bone destruction and osteoimmunology. *J. Periodontal Res.* **40**, 287–293 (2005).
23. Chen, Z. *et al.* Osteoimmunomodulatory properties of magnesium scaffolds coated with β-tricalcium phosphate. *Biomaterials* **35**, 8553–8565 (2014).

24. Wright, H. L., McCarthy, H. S., Middleton, J. & Marshall, M. J. RANK, RANKL and osteoprotegerin in bone biology and disease. *Curr. Rev. Musculoskelet. Med.* **2**, 56–64 (2009).
25. Boyce, B. F. & Xing, L. Biology of RANK, RANKL, and osteoprotegerin. *Arthritis Res. Ther.* **9**, S1 (2007).
26. Devlin, R. D., Reddy, S. V, Savino, R., Ciliberto, G. & Roodman, G. D. IL-6 mediates the effects of IL-1 or TNF, but not PTHrP or 1,25(OH) 2 D 3 , on osteoclast-like cell formation in normal human bone marrow cultures. *J. Bone Miner. Res.* **13**, 393–399 (1998).
27. Adamopoulos, I. E. *et al.* IL-23 Is Critical for Induction of Arthritis, Osteoclast Formation, and Maintenance of Bone Mass. *J. Immunol.* **187**, 951–959 (2011).
28. Champagne, C. M., Takebe, J., Offenbacher, S. & Cooper, L. F. Macrophage cell lines produce osteoinductive signals that include bone morphogenetic protein-2. *Bone* **30**, 26–31 (2002).
29. Freytes, D. O., Kang, J. W., Marcos-Campos, I. & Vunjak-Novakovic, G. Macrophages modulate the viability and growth of human mesenchymal stem cells. *J. Cell. Biochem*. **114**, 220–229 (2013).
30. Ding, J. *et al.* TNFα and IL-1β inhibit RUNX2 and collagen expression but increase alkaline phosphatase activity and mineralization in human mesenchymal stem cells. *Life Sci.* **84**, 499–504 (2009).
31. Rifas, L. T-cell cytokine induction of BMP-2 regulates human mesenchymal stromal cell differentiation and mineralization. *J. Cell. Biochem.* **98**, 706–714 (2006).
32. Saran, U., Piperni, S. G., Chatterjee, S., Gemini Piperni, S. & Chatterjee, S. Role of angiogenesis in bone repair. *Arch. Biochem. Biophys.* **561**, 109–117 (2014).
33. Salani, D. *et al.* Endothelin-1 Induces an Angiogenic Phenotype in Cultured Endothelial Cells and Stimulates Neovascularization In Vivo. *Am. J. Pathol.* **157**, 1703–1711 (2000).
34. Ferrara, N., Gerber, H.-P. & LeCouter, J. The biology of VEGF and its receptors. *Nat. Med.* **9**, 669–676 (2003).
35. Peng, H. *et al.* VEGF Improves, Whereas sFlt1 Inhibits, BMP2-Induced Bone Formation and Bone Healing Through Modulation of Angiogenesis. *J. Bone Miner. Res.* **20**, 2017–2027 (2005).
36. Wozney, J. M. *et al.* Novel regulators of bone formation: molecular clones and activities. *Science* (80-.). **242**, 1528–1534 (1988).
37. Banerjee, C. *et al.* Runx2 / Cbfa1 N-Terminal Isoforms in Response to Bone Morphogenetic Protein-2 during Development of the Osteoblast Phenotype. *Situ* **142**, 4026–4039 (2001).
38. Cao, Y. *et al.* Osterix, a Transcription Factor for Osteoblast Differentiation, Mediates Antitumor Activity in Murine Osteosarcoma. *Cancer Res* **65**, 1124–8 (2005).
39. Miron, R. J. & Zhang, Y. F. Osteoinduction. *J. Dent. Res.* **91**, 736–744 (2012).
40. Beederman, M. *et al.* BMP signaling in mesenchymal stem cell differentiation and bone formation *. *J. Biomed. Sci. Eng.* **6**, 32–52 (2013).
41. Arboleya, L. & Castañeda, S. Osteoimmunology: the study of the relationship between the immune system and bone tissue. *Reumatol. Clin.* **9**, 303–15 (2013).
42. Cowley, S. P. & Anderson, L. D. Hernias through donor sites for iliac-bone grafts. *J. Bone Jt. Surg.* **65**, 1023–1025 (1983).
43. Summers, B. N. & Eisenstein, S. M. Donor site pain from the ilium. A complication of lumbar spine fusion. *J. Bone Joint Surg. Br.* **71**, 677–80 (1989).
44. Friedlaender, G. E. Immune responses to osteochondral allografts. Current knowledge and future directions. *Clin. Orthop. Relat. Res.* **174**, 58–68 (1983).
45. J De Bruijn, K Shankar, H Yuan, P. H. in Osteoinduction and its evaluation *Bioceramics and their clinical applications* (ed. T. Kokubo) 199–219 (Wodhead Publishing Ltd.-CRC Press, 2008).
46. Yuan, H. *et al.* Osteoinductive ceramics as a synthetic alternative to autologous bone grafting. *Proc. Natl. Acad. Sci. U. S. A.* **107**, 13614–9 (2010).
47. Dorozhkin, S. V. Calcium Orthophosphates in Nature, Biology and Medicine. *Materials (Basel).* **2**, 399–498 (2009).
48. Ducheyne, P., Radin, S. & King, L. The effect of calcium phosphate ceramic composition and structure on in vitro behavior. I. Dissolution. *J. Biomed. Mater. Res.* **27**, 25–34 (1993).

49. Bohner, M. Calcium orthophosphates in medicine: From ceramics to calcium phosphate cements. *Injury* **31**, 37–47 (2000).
50. El Briak-BenAbdeslam, H., Ginebra, M. P., Vert, M. & Boudeville, P. Wet or dry mechanochemical synthesis of calcium phosphates? Influence of the water content on DCPD–CaO reaction kinetics. *Acta Biomater.* **4**, 378–386 (2008).
51. Tung, M. S. & Brown, W. E. Calcified Tissue International The Role of Octacalcium Phosphate in Subcutaneous Heterotopic Calcification. *Calcif Tissue lnt* **37**, 329–331 (1985).
52. Engel, E. *et al.* Discerning the role of topography and ion exchange in cell response of bioactive tissue engineering scaffolds. *Tissue Eng. Part A* **14**, 1341–51 (2008).
53. Gustavsson, J., Ginebra, M. P., Planell, J. & Engel, E. Osteoblast-like cellular response to dynamic changes in the ionic extracellular environment produced by calcium-deficient hydroxyapatite. *J. Mater. Sci. Mater. Med.* **23**, 2509–20 (2012).
54. Hesaraki, S., Nazarian, H., Pourbaghi-Masouleh, M. & Borhan, S. Comparative study of mesenchymal stem cells osteogenic differentiation on low-temperature biomineralized nanocrystalline carbonated hydroxyapatite and sintered hydroxyapatite. *J. Biomed. Mater. Res. B. Appl. Biomater.* **102**, 108–18 (2014).
55. Pieters, I. Y., Van den Vreken, N. M. F., Declercq, H. A., Cornelissen, M. J. & Verbeeck, R. M. H. Carbonated apatites obtained by the hydrolysis of monetite: influence of carbonate content on adhesion and proliferation of MC3T3-E1 osteoblastic cells. *Acta Biomater.* **6**, 1561–8 (2010).
56. Marchi, J., Ribeiro, C., Bressiani, A. H. D. A. & Marques, M. M. Cell response of calcium phosphate based ceramics, a bone substitute material. *Mater. Res.* **16**, 703–712 (2013).
57. Deligianni, D. D., Katsala, N. D., Koutsoukos, P. G. & Missirlis, Y. F. Effect of surface roughness of hydroxyapatite on human bone marrow cell adhesion, proliferation, differentiation and detachment strength. *Biomaterials* **22**, 87–96 (2001).
58. Chou, Y.-F., Huang, W., Dunn, J. C. Y., Miller, T. A. & Wu, B. M. The effect of biomimetic apatite structure on osteoblast viability, proliferation, and gene expression. *Biomaterials* **26**, 285–95 (2005).
59. Klammert, U. *et al.* Cytocompatibility of brushite and monetite cell culture scaffolds made by three-dimensional powder printing. *Acta Biomater.* **5**, 727–34 (2009).
60. Samavedi, S., Whittington, A. R. & Goldstein, A. S. Calcium phosphate ceramics in bone tissue engineering: a review of properties and their influence on cell behavior. *Acta Biomater.* **9**, 8037–45 (2013).
61. Gustavsson, J., Ginebra, M. P. P., Engel, E. & Planell, J. Ion reactivity of calcium-deficient hydroxyapatite in standard cell culture media. *Acta Biomater.* **7**, 4242–52 (2011).
62. Hidalgo-Bastida, L. A. & Cartmell, S. H. Mesenchymal Stem Cells, Osteoblasts and Extracellular Matrix Proteins : Enhancing Cell Adhesion and Differentiation for Bone Tissue Engineering. *Tissue Eng. Part B* **16**, (2010).
63. Anselme, K. Osteoblast adhesion on biomaterials. *Biomaterials* **21**, 667–81 (2000).
64. Sawyer, A. A., Hennessy, K. M. & Bellis, S. L. Regulation of mesenchymal stem cell attachment and spreading on hydroxyapatite by RGD peptides and adsorbed serum proteins. *Biomaterials* **26**, 1467–75 (2005).
65. Fujii, E. *et al.* Selective protein adsorption property and characterization of nano-crystalline zinc-containing hydroxyapatite. *Acta Biomater.* **2**, 69–74 (2006).
66. Tsapikouni, T. S. & Missirlis, Y. F. Protein–material interactions: From micro-to-nano scale. *Mater. Sci. Eng. B* **152**, 2–7 (2008).
67. Zhou, G. S. *et al.* Different effects of nanophase and conventional hydroxyapatite thin films on attachment, proliferation and osteogenic differentiation of bone marrow derived mesenchymal stem cells. *Biomed. Mater. Eng.* **17**, 387–95 (2007).
68. Dulgar-Tulloch, A. J., Bizios, R. & Siegel, R. W. Human mesenchymal stem cell adhesion and proliferation in response to ceramic chemistry and nanoscale topography. *J. Biomed. Mater. Res. A* **90**, 586–94 (2009).
69. Berube, P. *et al.* The effect of sputtered calcium phosphate coatings of different crystallinity on osteoblast differentiation. *J. Periodontol.* **76**, 1697–709 (2005).

70. Knabe, C. *et al.* Evaluation of calcium phosphates and experimental calcium phosphate bone cements using osteogenic cultures. *J. Biomed. Mater. Res.* **52**, 498–508 (2000).
71. Rosa, A. L., Beloti, M. M. & van Noort, R. Osteoblastic differentiation of cultured rat bone marrow cells on hydroxyapatite with different surface topography. *Dent. Mater.* **19**, 768–772 (2003).
72. Campoccia, D. In vitro behaviour of bone marrow-derived mesenchymal cells cultured on fluorohydroxyapatite-coated substrata with different roughness. *Biomaterials* **24**, 587–596 (2003).
73. dos Santos, E. A., Farina, M., Soares, G. a & Anselme, K. Surface energy of hydroxyapatite and beta-tricalcium phosphate ceramics driving serum protein adsorption and osteoblast adhesion. *J. Mater. Sci. Mater. Med.* **19**, 2307–16 (2008).
74. dos Santos, E. A., Farina, M., Soares, G. a & Anselme, K. Chemical and topographical influence of hydroxyapatite and beta-tricalcium phosphate surfaces on human osteoblastic cell behavior. *J. Biomed. Mater. Res. A* **89**, 510–20 (2009).
75. Hu, Q. *et al.* Effect of crystallinity of calcium phosphate nanoparticles on adhesion, proliferation, and differentiation of bone marrow mesenchymal stem cells. *J. Mater. Chem.* **17**, 4690 (2007).
76. Tai, S. *et al.* Effects of beta-tricalcium phosphate particles on primary cultured murine dendritic cells and macrophages. *Int. Immunopharmacol.* **40**, 419–427 (2016).
77. Sokolova, V. *et al.* Delivery of the TLR ligand poly(I:C) to liver cells in vitro and in vivo by calcium phosphate nanoparticles leads to a pronounced immunostimulation. *Acta Biomater*. **64**, 401–410 (2017).
78. Silva, S. N., Pereira, M. M., Goes, a M. & Leite, M. F. Effect of biphasic calcium phosphate on human macrophage functions in vitro. *J. Biomed. Mater. Res. A* **65**, 475–481 (2003).
79. Nadra, I. *et al.* Effect of particle size on hydroxyapatite crystal-induced tumor necrosis factor alpha secretion by macrophages. *Atherosclerosis* **196**, 98–105 (2008).
80. Lebre, F. *et al.* The shape and size of hydroxyapatite particles dictate inflammatory responses following implantation. *Sci. Rep.* **7**, 1–13 (2017).
81. Laquerriere, P. *et al.* Importance of hydroxyapatite particles characteristics on cytokines production by human monocytes in vitro. *Biomaterials* **24**, 2739–2747 (2003).
82. Lange, T. *et al.* Proinflammatory and osteoclastogenic effects of beta-tricalciumphosphate and hydroxyapatite particles on human mononuclear cells in vitro. *Biomaterials* **30**, 5312–5318 (2009).
83. Xia, Z. & Triffitt, J. T. A review on macrophage responses to biomaterials. *Biomed. Mater.* **1**, R1–R9 (2006).
84. Diez-Escudero, A. *et al.* Heparinization of Beta Tricalcium Phosphate: Osteo-immunomodulatory Effects. *Adv. Healthc. Mater.* **7**, 1700867 (2018).
85. Diez-Escudero, A. *et al.* Focus Ion Beam/Scanning Electron Microscopy Characterization of Osteoclastic Resorption of Calcium Phosphate Substrates. *Tissue Eng. Part C Methods* **23**, 118–124 (2017).
86. Refai, A. K., Textor, M., Brunette, D. M. & Waterfield, J. D. Effect of titanium surface topography on macrophage activation and secretion of proinflammatory cytokines and chemokines. *J. Biomed. Mater. Res.* **70A**, 194–205 (2004).
87. Paul, N. E. *et al.* Topographical control of human macrophages by a regularly microstructured polyvinylidene fluoride surface. *Biomaterials* **29**, 4056–4064 (2008).
88. Mestres, G. *et al.* Inflammatory response to nano- And microstructured hydroxyapatite. *PLoS One* **10**, 1–20 (2015).
89. Chen, Z. *et al.* The effect of osteoimmunomodulation on the osteogenic effects of cobalt incorporated β-tricalcium phosphate. *Biomaterials* **61**, 126–138 (2015).
90. Kannan, R. Y., Salacinski, H. J., Sales, K., Butler, P. & Seifalian, A. M. The roles of tissue engineering and vascularisation in the development of micro-vascular networks: a review. *Biomaterials* **26**, 1857–1875 (2005).
91. Smith, M. K., Peters, M. C., Richardson, T. P., Garbern, J. C. & Mooney, D. J. Locally enhanced angiogenesis promotes transplanted cell survival. *Tissue Eng.* **10**, 63–71 (2004).

92. Rouwkema, J., Rivron, N. C. & van Blitterswijk, C. A. Vascularization in tissue engineering. *Trends Biotechnol.* **26**, 434–41 (2008).
93. Kohn, E. C., Alessandro, R., Spoonster, J., Wersto, R. P. & Liotta, L. A. Angiogenesis: role of calcium-mediated signal transduction. *Proc. Natl. Acad. Sci. U. S. A.* **92**, 1307–11 (1995).
94. Munaron, L. & Pla, A. Endothelial Calcium Machinery and Angiogenesis: Understanding Physiology to Interfere with Pathology. *Curr. Med. Chem.* **16**, 4691–4703 (2009).
95. Maier, J. A. M., Bernardini, D., Rayssiguier, Y. & Mazur, A. High concentrations of magnesium modulate vascular endothelial cell behaviour in vitro. *Biochim. Biophys. Acta - Mol. Basis Dis.* **1689**, 6–12 (2004).
96. Maier, J. A. M., Malpuech-Brugère, C., Zimowska, W., Rayssiguier, Y. & Mazur, A. Low magnesium promotes endothelial cell dysfunction: Implications for atherosclerosis, inflammation and thrombosis. *Biochim. Biophys. Acta - Mol. Basis Dis.* **1689**, 13–21 (2004).
97. Di Marco, G. S. *et al.* High phosphate directly affects endothelial function by downregulating annexin II. *Kidney Int.* **83**, 213–222 (2013).
98. Aguirre, A. *et al.* Control of microenvironmental cues with a smart biomaterial composite promotes endothelial progenitor cell angiogenesis. *Eur. Cells Mater.* **24**, 90–106 (2012).
99. Klenke, F. M. *et al.* Impact of pore size on the vascularization and osseointegration of ceramic bone substitutes in vivo. *J. Biomed. Mater. Res. - Part A* **85**, 777–786 (2008).
100. Chen, Y. *et al.* Enhanced effect of β-tricalcium phosphate phase on neovascularization of porous calcium phosphate ceramics: In vitro and in vivo evidence. *Acta Biomater.* **11**, 435–448 (2015).
101. Cairns, M. L., Meenan, B. J., Burke, G. A. & Boyd, A. R. Influence of surface topography on osteoblast response to fibronectin coated calcium phosphate thin films. *Colloids Surf. B. Biointerfaces* **78**, 283–90 (2010).
102. Zhang, J. *et al.* The size of surface microstructures as an osteogenic factor in calcium phosphate ceramics. *Acta Biomater.* **10**, 3254–63 (2014).
103. Eklou-Kalonji, E., Denis, I., Lieberherr, M. & Pointillart, A. Effects of extracellular calcium on the proliferation and differentiation of porcine osteoblasts in vitro. *Cell Tissue Res.* **292**, 163–171 (1998).
104. Maeno, S. *et al.* The effect of calcium ion concentration on osteoblast viability, proliferation and differentiation in monolayer and 3D culture. *Biomaterials* **26**, 4847–55 (2005).
105. Barradas, A. M. C. *et al.* A calcium-induced signaling cascade leading to osteogenic differentiation of human bone marrow-derived mesenchymal stromal cells. *Biomaterials* **33**, 3205–15 (2012).
106. Danoux, C. *et al.* Development of Highly Functional Biomaterials by Decoupling and Recombining Material Properties. *Adv. Mater.* **28**, 1803–1808 (2016).
107. ter Brugge, P. J., Wolke, J. G. C. & Jansen, J. A. Effect of calcium phosphate coating composition and crystallinity on the response of osteogenic cells in vitro. *Clin. Oral Implants Res.* **14**, 472–80 (2003).
108. Grellier, M., Bordenave, L. & Amédée, J. Cell-to-cell communication between osteogenic and endothelial lineages: implications for tissue engineering. *Trends Biotechnol.* **27**, 562–71 (2009).
109. Geneau, G. *et al.* Effect of endothelin-1 on osteoblastic differentiation is modified by the level of connexin43: Comparative study on calvarial osteoblastic cells isolated from Cx43+/-and Cx43+/+ mice. *Cell Tissue Res.* **340**, 103–115 (2010).
110. Bulnheim, U. *et al.* Endothelial cells stimulate osteogenic differentiation of mesenchymal stem cells on calcium phosphate scaffolds. *J. Tissue Eng. Regen. Med.* **8**, 831–40 (2014).
111. Thein-Han, W. & Xu, H. H. K. Prevascularization of a gas-foaming macroporous calcium phosphate cement scaffold via coculture of human umbilical vein endothelial cells and osteoblasts. *Tissue Eng. Part A* **19**, 1675–85 (2013).
112. Unger, R. E. *et al.* Tissue-like self-assembly in cocultures of endothelial cells and osteoblasts and the formation of microcapillary-like structures on three-dimensional porous biomaterials. *Biomaterials* **28**, 3965–76 (2007).

Chapter 2

Effect of nano and microstructural properties of biomimetic hydroxyapatite on osteoimmunomodulation

2.1 Introduction

Multiple processes occur during the bone healing following the surgical placement of a synthetic bone graft. Among them, immune reactions play an important role in determining the fate of the implant. The exogenous nature of biomaterials is recognized by the host as a foreign body, which usually triggers the release of cytokines and chemo-attractants by immune cells.[1] The osteoimmune environment generated at the vicinity of the bone graft by these regulatory molecules is of paramount importance, because it can lead to two opposite scenarios. In adverse conditions, it will lead to persistent excessive inflammation. On the contrary, in a favourable environment it will contribute to the regeneration of the bone tissue.

Among all immune cells, macrophages have attracted much interest due to their regulatory role in innate immune response and great plasticity in cellular polarization. In response to various stimuli, macrophages can polarize to pro-inflammatory M1 or anti-inflammatory M2 phenotypes.[2] Moreover, the polarization process is generally accompanied with changes in cell morphology, the release of inflammatory cytokines, and the production of reactive nitrogen and oxygen species.[1,3-6] For instance, the activation into M1 phenotype is characterised by the expression of pro-inflammatory cytokines such as tumour necrosis factor alpha (TNFα), interleukin 6 (IL-6) and interleukin 1 beta (IL-1β).[7,8] In contrast, polarized M2 macrophages produce anti-inflammatory cytokines, mainly interleukin 4 (IL-4), interleukin 10 (IL-10) and interleukin 13 (IL-13) accompanied with high expression of mannose receptors (CD163, CD206).[9]

This inflammatory microenvironment created by M1 and/or M2 immune cells was reported to greatly modulate bone healing events. The pro-inflammatory signals are recognised to stimulate osteoclastic response[10] and mesenchymal stem cell (MSCs) differentiation.[10-12] However, the prolonged exposure to these molecules will lead to chronic inflammation. In turn, the M2 profile participates in osteogenesis and angiogenesis through release of molecules such as bone morphogenetic protein-2 (BMP-2) or vascular endothelial growth factor (VEGF).[13,14] This intimate relation between immune cells and bone cells highlights the need for better monitoring of the initial stages after biomaterial implantation, redefining the requirements that a bone graft should meet. Hence, to trigger bone regeneration a bone graft should induce a favourable immune environment that results in the appropriate balance between osteogenesis and osteoclastogenesis.[1,15,16]

The response of immune cells is known to be influenced by various factors including topography[17-21], chemistry[16,22-26] or porosity.[27,28] The plasticity of macrophages to switch the phenotype in response to subtle changes opens the door to potential strategies in the development of bone substitutes with osteoimmunomodulatory properties. Hence,

modulating the physicochemical features of implants will likely induce various cytokine release profile from immune cells eliciting different effects on bone dynamics.

Calcium phosphate (CaPs) materials are interesting bone substitutes due to their close chemical resemblance to mineral phase of bone and osteoinductive/osteoconductive properties. Although countless studies have been devoted to the characterisation of their osteogenic and osteoindutive properties, little attention has been paid to their osteoimmunomodulatory properties. Only recently Chen *et al.* shed light on the osteoimmunomodulatory features of some CaPs, particularly sintered β-tricalcium phosphate (β-TCP) ceramics.[15,16,29]

On another hand, it has been recently shown, using model surfaces, that nanotopography also plays a vital role in regulating immune responses.[21,30] In this context, Xiao *et al.* proposed the concept of "nano-osteoimmunomodulation", as a strategy for the development of nanotopographies with osteoimmunomodulatory properties, able to regulate bone dynamics.[6]

This chapter intends to combine both concepts, taking advantage of the possibility to control the nanostructural features of calcium deficient hydroxyapatite (CDHA) materials using biomimetic processing routes. Hence, the work investigates the effect of nanostructures of biomimetic CDHA on the osteoimmunomodulation by unravelling the surface nanotopography and porosity of CDHA on the inflammatory cytokine production and osteoclastic differentiation, as well as the effect of the immune environment created by macrophages cultured on CDHA substrates on osteogenic differentiation of osteoblasts.

2.2 Materials and methods

2.2.1 Synthesis and characterisation of CDHA substrates

CDHA discs were prepared by the self-setting reaction of an hydraulic paste of α-tricalcium phosphate (α-TCP) powder at 37 °C, described in a previous work.[31] α-TCP was obtained by sintering a 1:2 molar mixture of calcium hydrogen phosphate ($CaHPO_4$, Sigma-Aldrich, St. Louis, USA) and calcium carbonate ($CaCO_3$, Sigma-Aldrich, St. Louis, USA) at 1400 °C for 15 h and subsequent quenching in air.

Previous studies showed that it was possible to tune the textural properties of the material by modifying the grain size of the starting α-TCP powder and the liquid-to-powder (L/P) ratio of the paste[32], this allowing the preparation of chemically identical CDHA substrates that varied in microstructure, specific surface area (SSA) and porosity.

Therefore, two milling protocols were applied with the purpose of obtaining the powder with coarse (C: 5.2 μm median size) and fine (F: 2.8 μm) particle size.[32] In order to

obtain a mouldable paste, the solid phase that consisted of α-TCP and 2 wt.% of precipitated hydroxyapatite (pHA; Merck 2143, Merck, Darmstardt, Germany) was mixed with an aqueous solution containing 2.5 wt.% of disodium hydrogen phosphate (Na_2HPO_4, Merck, Darmstadt, Germany). The samples were prepared with two different L/P ratios: 0.35 mL/g and 0.65 mL/g, transferred to Teflon moulds (6 mm of diameter, 2 mm of thickness) and left to set in water at 37 ºC for 7 days. The specimens were coded as C35, F35, C65 and F65, where C and F stand for coarse and fine powder respectively and 35 and 65 stand for the liquid to powder ratio of 0.35 and 0.65 mL/g respectively.

The microstructure of the substrates was characterised by Scanning Electron Microscopy (SEM, TESKAN MIRA3) with an acceleration voltage of 5 kV after depositing a thin layer of gold-palladium with EM SC005 Gold Coater (Leica). The surface roughness was characterized by optical interferometry (Veeco Wyko NT1100), using a 50x magnification and a scanned area of 47.5 x 63.4 μm^2. Images were acquired using Vision32 software.

2.2.2 Cell culture

Two cell lines, the murine-derived macrophage cell line RAW 264.7 (RAW) and human osteosarcoma cell line SaOS-2, were used in this study. Both cell lines were maintained in Dulbecco's Modified Eagle Medium (DMEM; Gibco®, Life Technologies Pty Ltd., Australia) supplemented with 10 % heat-inactivated fetal calf serum (FCS; In Vitro Technologies, Australia) and 1 % (50 U/mL and 50 µg/mL, respectively) penicillin/streptomycin (P/S; Gibco®, Life Technologies Pty Ltd., Australia) at 37 °C with a 5 % CO_2 humidified atmosphere.

2.2.3 Osteoimmunomodulatory effect of CDHA on macrophages under standard and inflammatory conditions

The behaviour of macrophages was evaluated after direct exposure to CDHA substrates. For that purpose, the discs were sterilised with 80 % ethanol, rinsed thrice with phosphate-buffered saline (PBS, Oxoid) and incubated overnight with complete medium. Subsequently, RAW cells were seeded at a density 7×10^5 cells/cm^2 for all experiments unless otherwise stated.

To induce the inflammatory environment 1 µg/mL of lipopolysaccharide (LPS, Escherichia coli 055:B5, R&D Systems) was added following previous protocols.[8,21] Briefly, after 12 hours of RAW cells seeding, standard medium was replaced with medium containing LPS and incubated for 2 hours. Subsequently, samples were

thoroughly washed with PBS, placed in new well plate and incubated following 6 hours in serum starvation medium.

2.2.4 Metabolic activity of RAW cells on CDHA substrates

The metabolic activity of RAW cells under standard conditions, was evaluated at day 1 and 3 trough MTT [3-(4,5-dimethylthiazol-2-yl)-2,5-diphenyl tetrazolium bromide] assay (R&D Systems). Briefly, the samples were washed with PBS and transferred to a new well plate, where 300 µL of 5 mg/mL of MTT solution was added to DMEM. After 4 h of incubation, MTT-DMEM solution was carefully removed and 150 µL of dimethyl sulfoxide (DMSO, Univar USA) was added in order to dissolve formazan crystals. Subsequently, the absorbance was read at 570 nm using microplate spectrophotometer (Benchmark Plus, Tacoma, Washington, USA).

2.2.5 Cell morphology

The morphology of RAW cells on CDHA substrates was observed at day 1 and 3 for standard conditions and 6 hours after incubation with LPS for inflammatory conditions. Images were acquired by SEM (TESKAN MIRA3) using an acceleration voltage of 5 kV, and by confocal microscopy (CLSM, Nikon A1).

For SEM visualisation, cells were thoroughly washed with PBS and subsequently fixed with 3 % glutaraldehyde. Samples were then rinsed with PBS and post-fixed with 1 % osmium tetraoxide incubation for 1 h. The process was followed by dehydration through consecutive washings with increasing concentrations of ethanol solution (50 %, 70 %, 90 %, 100 %) achieving a complete dehydration in hexamethyldisilazane (HMDS). Prior to visualisation, the discs were covered with a gold thin layer using EM SC005 Gold Coater (Leica).

For confocal microscopy, the cells were washed with PBS and fixed with 4 % paraformaldehyde solution (PFA). The membrane permeabilization was carried out through incubation with 0.1 % Triton X-100 in PBS during 15 min. For nitric oxide synthase (iNOS) staining, RAW cells were additionally incubated for 1 h with blocking solution consisting of 1 % bovine serum albumin (BSA) in PBS followed by 1 h incubation with primary and secondary antibodies, rabbit polyclonal iNOS in 1% BSA (1:100, Abcam) and Alexa Fluor488 Conjugate anti-rabbit IgG in 0.1 % Triton X-100 in PBS (1:1000, Cell Signaling Technology), respectively. For cytoskeleton and nuclei staining, cells were incubated with Rhodamine phalloidin for 1 h (1:300) and 4, 6-diamidino-2-phenylindole (DAPI) (1:1000) for 2 min, both in 0.1 % Triton X-100 in PBS solution. Between all steps, three rinses for 5 minutes with 0.15 % glycine in PBS were performed. Images were acquired using LASX software and processed using Fiji/Image-J package. Additionally, image analysis was performed in order to quantify the spreading area and elongation ratio (n=50) of macrophages.

2.2.6 Anti-inflammatory response of RAW cells to CDHA substrates

For standard conditions, RAW cells were seeded at a density of 7×10^5 cells/cm^2. After 6 hours of incubation the cell culture medium was replaced with serum free medium and the cells were incubated for additional 6 hours. Then, the substrate-conditioned medium (CM) was recovered for further experiments being stored at -80 ºC. For RNA extraction, samples were washed with PBS and total RNA from cells was extracted applying TRIzol reagent (Ambion™, Life Technologies Pty Ltd., Australia) following manufacturer instructions. Subsequently, the concentration of total RNA was quantified by NanoDrop ND-1000 spectrophotometer (NanoDrop technologies, Motchanin, DE, USA) and one thousand nanograms of total RNA were used for synthesis of complementary DNA using DyNAmo™ cDNA Synthesis Kit (Genesearch, QLD, Australia). Detection of inflammatory genes expression (IL-1β, IL-6, TNFα, iNOS, IL-10, CD206) was performed with a QuantstudioTM Real-Time PCR machine (Applied Biosystems, Foster City, California, USA) using SYBR Green qPCR Master Mix (Life Technologies). In all RT-qPCR runs, the specificity of primers was determined by melt curves analysis. The raw values were, then, expressed as relative fold applying the $2^{-\Delta\Delta Ct}$ method where:

$$\Delta\Delta Ct = (Ct_{sample}\,(\text{gene of interest}) - Ct_{sample}\,(\text{endogenous reference gene})) - (Ct_{TCPS}\,(\text{gene of interest}) - Ct_{TCPS}\,(\text{endogenous reference gene})) \quad \text{(Eq. 2.1.)}$$

and Ct represents the cycle threshold of sample.[33] The 18S ribosomal RNA gene expression was used as endogenous reference gene and the RAW cells cultured on TCPS condition were used for normalizing RT-qPCR data. The list of primers used for RT-qPCR experiments is specified in Table 2.1.

The same procedures were applied for extraction of the RNA and evaluation of the gene expression of RAW cells exposed to an inflammatory environment (after LPS stimulation, as explained in section 2.2.3.). Additionally, the cytokine release was analysed using enzyme-linked immunosorbent assay (ELISA). For that purpose, the supernatants were evaluated for the presence of IL-6 and TNFα using a mouse IL-6 Uncoated ELISA kit and a mouse TNFα Uncoated ELISA kit, respectively (Invitrogen).

Table 2.1. Primers' sequences used in this study.

Gene	Gene symbol	Primers' sequences (5'→3')
18S ribosomal RNA	18S	F:CGGAACTGAGGCCATGATTAAG R:GTATCTGATCGTCTTCGAACCTCC
Interleukin 1 beta	IL-1β	F:TGGAGAGTGTGGATCCCAAG R:GGTGCTGATGTACCAGTTGG
Interleukin 6	IL-6	F:ATAGTCCTTCCTACCCCAATTTCC R:GATGAATTGGATGGTCTTGGTCC
Tumor necrosis factor alpha	TNFα	F:CTGAACTTCGGGGTGATCGG R:GGCTTGTCACTCGAATTTTGAGA
Nitric oxide synthase	iNOS	F:CACCAAGCTGAACTTGAGCG R:CGTGGCTTTGGGCTCCTC
Oncostatin M	OSM	F:ACGGTCCACTACAACACCAG R:CCATCGTCCCATTCCCTGAAG
Transforming growth factor beta 1	TGFβ1	F:CAGTACAGCAAGGTCCTTGC R:ACGTAGTAGACGATGGGCAG
Vascular endotelial growth factor A	VEGF A	F:GTCCCATGAAGTGATCAAGTTC R:TCTGCATGGTGATGTTGCTCTCTG
Cathepsin K	CTSK	F:CCAGTTTTACAGCAGAGGTGTG R:CTTGCTTCCCTTCTGGGTG
Carbonic anhydrase 2	CAR2	F:AGCAGCGAGCAGATGTCTC R:TGAGCTGGACGCCAGTTG
Matrix metallopeptidase 9	MMP9	F:GGGCGTGTCTGGAGATTCG R:CACCTGGTTCACCTCATGGTC
Interleukin 10	IL-10	F:CAGGACTTTAAGGGTTACTTG R:ATTTTCACAGGGGAGAAATC
Mannose receptor C type	CD206	F:AGACGAAATCCCTGCTACTG R:CACCCATTCGAAGGCATTC
Runt-related transcription factor 2	Runx2	F:GACGAGGCAAGAGTTTCACC R:ATGAAATGCTTGGGAACTGC
Bone morphogenic protein 2	BMP-2	F:TGCCATTGTTCAGACGTTGG R:GTACTAGCGACACCCACAAC
Bone sialoprotein	BSP	F:TTTCTGCTACAACACTGGGCTATG R:TTGTTATATCCCCAGCCTTCTTG
Osteocalcin	OCN	F:GCAAAGGTGCAGCCTTTGTG R:GGCTCCCAGCCATTGATACAG
Collagen type I	COLL I	F:AGAACAGCGTGGCCT R:TCCGGTGTGACTCGT

2.2.7 Osteogenic and osteoclastogenic activity of macrophages

The osteogenic and osteoclastogenic activity of RAW cells was determined through detection of specific genes (osteogenesis: OSM, TGFβ1 and VEGF; osteoclastogenesis:

CTSK, CAR2, MMP9) following the specific time points and protocols detailed in section 2.2.5. The primers' sequences are those displayed in Table 2.1.

To assess cell morphology and substrate degradation, SEM images were acquired at day 3, following the fixation and visualisation protocols described in section 2.2.5

The ionic concentrations of Ca^{2+} and P_i of cell culture media with and without cells was quantified by inductively coupled plasma-optical emission spectrometry (ICP-OES, Perkin Elmer, MA, USA). The ionic concentration was determined at day 1 and 3 for standard conditions. Prior to quantification, the cell culture medium was diluted 5-fold with 2 % of ultrapure nitric acid.

2.2.8 The effect of the supernatant of RAW cells cultured on the CDHA substrate on the osteogenic differentiation of SaOS-2 cells

In order to investigate the effect of the osteoimmune environment created by the macrophages cultured onto the substrate, SaOS-2 cells were incubated with CM from section 2.2.6. For all experiments, except where otherwise stated, SaOS-2 cells were plated on TCPS at a density of 2.5×10^4 cells/cm^2. After 24 h the complete DMEM medium was replaced with RAW-substrate CM with 10 % of FCS and SaOS-2 cells were incubated for up to 3 days. Cells cultured with complete DMEM medium were used as a control.

2.2.8.1 Osteogenic-related gene expression and protein secretion by SaOS-2 cells

The bone-related gene expression was quantified through RT-qPCR at day 3 of cell culture. The RNA extraction and RT-pPCR protocols are detailed in section 2.2.6. The relative expressions of Runx2, BMP-2, BSP, OCN and COLL I (Table 2.1.) was determined using comparative Ct ($2^{-\Delta\Delta CT}$) method. 18S gene expression was used as endogenous reference gene and SaOS-2 cells cultured on tissue culture polystyrene (TCPS) at day 1 were used to normalize the data.

The evaluation of protein expression was carried out using Western Blot detection. Briefly, after incubation with CM, cell lysates were collected using RIPA lysis buffer. Subsequently, 20 μg of proteins from each sample were separated on SDS-PAGE gel followed by transfer onto nitrocellulose membranes (Pall Corporation, East Hills, New York, USA). The membranes were then blocked for 1 h in Odyssey blocking buffer (LI-COR Biosciences, Lincoln, Nebraska, USA). Afterwards, the membranes were incubated overnight at 4 ºC with primary antibodies against ALP, Runx2, COLL I and α-tubulin (all 1:1000, rabbit anti-human; Abcam, Cambridge, United Kingdom). The protein bands were visualised using the Odyssey infrared imaging system (LI-COR

Biosciences, Lincoln, Nebraska, USA). The relative intensities of protein bands were quantified using Fiji/Image-J package.

For the visualisation of cell morphology, SaOS-2 cells were seeded on glass coverslips placed inside 24-well plate following the seeding and incubation protocols described in section 2.2.6. Cytoskeleton and nuclei were stained using the immunocytochemistry methods detailed in section 2.2.5. Additionally cells were incubated with rabbit anti-human ALP (1:100, Abacam) followed by Alexa Fluor488 Conjugate anti-rabbit IgG secondary antibody (1:1000, Cell Signaling Technology, Danvers, MA) for ALP staining. The images were acquired using CLSM (Nikon A1) and processed with Fiji/Image-J package.

2.2.8.2 Mineralization of SaOS-2 cells

For the mineralization assay SaOS-2 cells were seeded at a semi-confluent density of 6×10^4 cells/cm^2. After 24h, the medium was replaced with CM combined with osteogenic medium at ratio 1:2. The supplements for osteogenic medium were 50 µg/mL ascorbic acid, 10 mM β-glycerophosphate and 100 nM dexamethasone. The medium was refreshed every third day. At 14 days of culture, SaOS-2 cells were washed with double distilled H_2O (ddH_2O) and fixed with 4 % of PFA for 15 min at RT. Afterwards, cells were stained using Alizarin red solution (ARS) at pH 4.2 for 20 min. The unbound stain was removed by various washings with ddH_2O. The images were acquired using a light microscope (Nikon ECLIPSE TS100) after previous air dying of the samples.

2.2.9 Statistical analysis

All statistical analyses were performed using SPSS software (IBM SPSS, Armonk, NewYork, USA). The data presented in graphs represents mean ± standard deviation (SD) (n=3 unless otherwise stated). Normality was checked through the Saphiro-Wilk test. Statistical differences between groups for non-parametric data were analysed through Mann-Whitney U test. Statistical differences between groups for parametric data were analysed using One-way ANOVA. The homogeneity of variance was assessed using Levene's test. In case of non-significant Levene's test, the Tukey's post hoc test was applied for data analysis. In case of significance, Tamhane's post hoc test was used. The level of significance for all tests was set at $p < 0.05$.

2.3 Results

2.3.1 Material characterisation

The detailed physicochemical characterisation regarding crystalline phases, porosity and pore size distribution and SSA of the biomimetic CDHA substrates analysed in this

study was previously described.[31,34] Table 2.2. displays the specific surface area and porosity of the CDHA substrates studied.

Table 2.2. Roughness, specific surface area (SSA) and porosity of the biomimetic calcium deficient hydroxyapatite substrates used in this study.

Substrate	Roughness Ra (µm)	SSA (m^2/g)[34]	Porosity (%)[34]
F35	1.12 ± 0.18	24.43 ± 0.03	34.3
F65	1.06 ± 0.42	27.32 ± 0.02	53.0
C35	1.94 ± 0.25	14.11 ± 0.01	33.4
C65	1.93 ± 0.48	14.42 ± 0.01	54.4

The microstructure of the fine (F35 and F65) and coarse (C35 and C65) substrates obtained by SEM is displayed in Figure 2.1. The use of fine particles resulted in a CDHA with agglomerates composed of needle-like crystals of nanometric size whilst coarse particles generated a CDHA with agglomerates presenting plate-like structure of micrometric size.

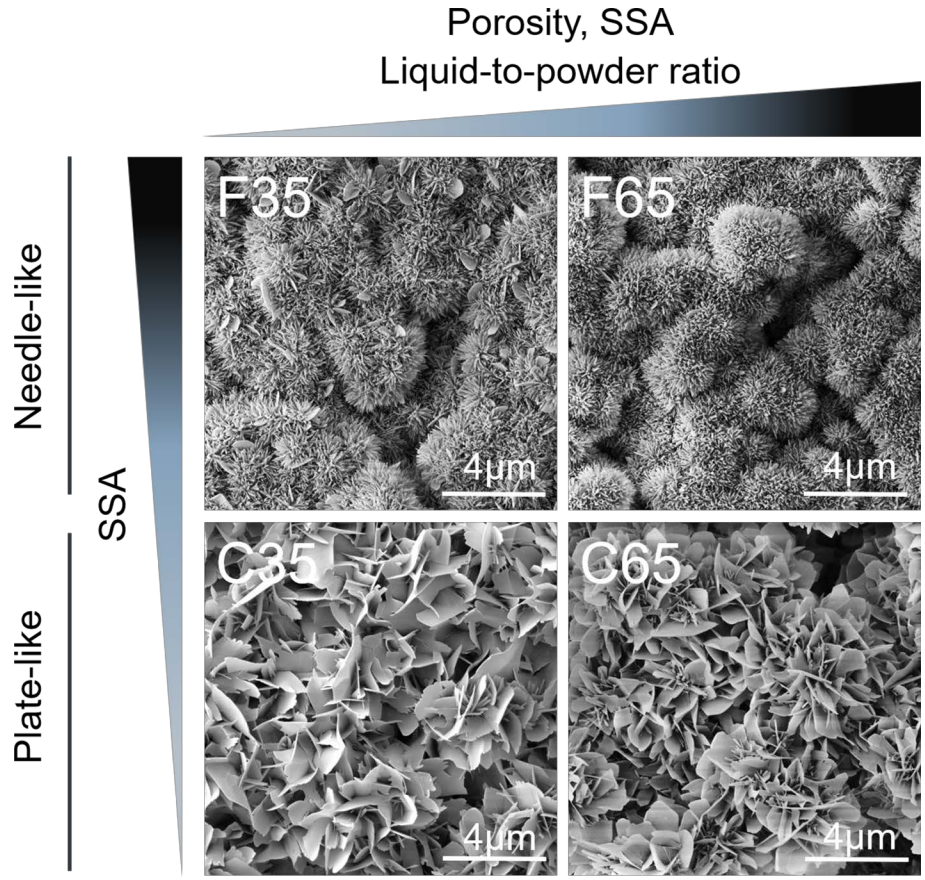

Figure 2.1. SEM images of surface microstructure of CDHA substrates.

2.3.2 Effect of CDHA substrates on the response of macrophage RAW cells under standard conditions

2.3.2.1 RAW cells proliferation and morphology

Similar metabolic activity was observed when RAW cells were cultured on the different CDHA discs for 1 and 3 days. The absorbance values at day 3 in the biomimetic substrates were significantly lower than that of the tissue culture polystyrene (TCPS) control group (Figure 2.2.).

The macrophages showed predominantly a round morphology in all substrates after 1 and 3 days of culture (Figure 2.3.A). Moreover, in all conditions cells organized into clusters. Higher spreading of RAW cells on all CDHA was observed at day 1 in comparison to the control group (Figure 2.3.B). At day 3, the cells cultured on F35 and C65 showed significantly different spreading area. Whilst on F35 the cells were less spread, on C65 they were more spread compared to control. No significant changes of cell elongation ratio were observed (Figure 2.3.C).

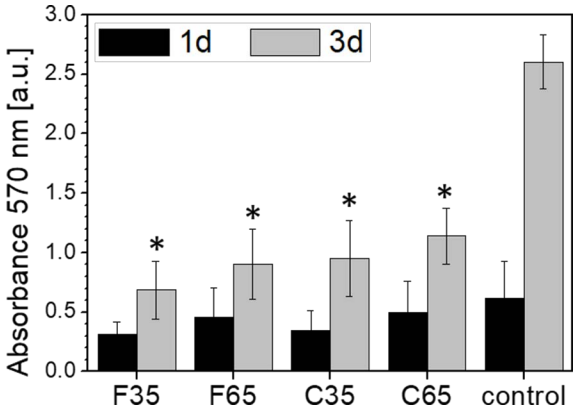

Figure 2.2. The metabolic activity of RAW cells on CDHA substrates at 1 and 3 day of culture, detected by MTT. No significant difference was found between various CDHA substrates. * indicates statistically significant difference ($p < 0.05$) compared to the control TCPS group at the corresponding time point.

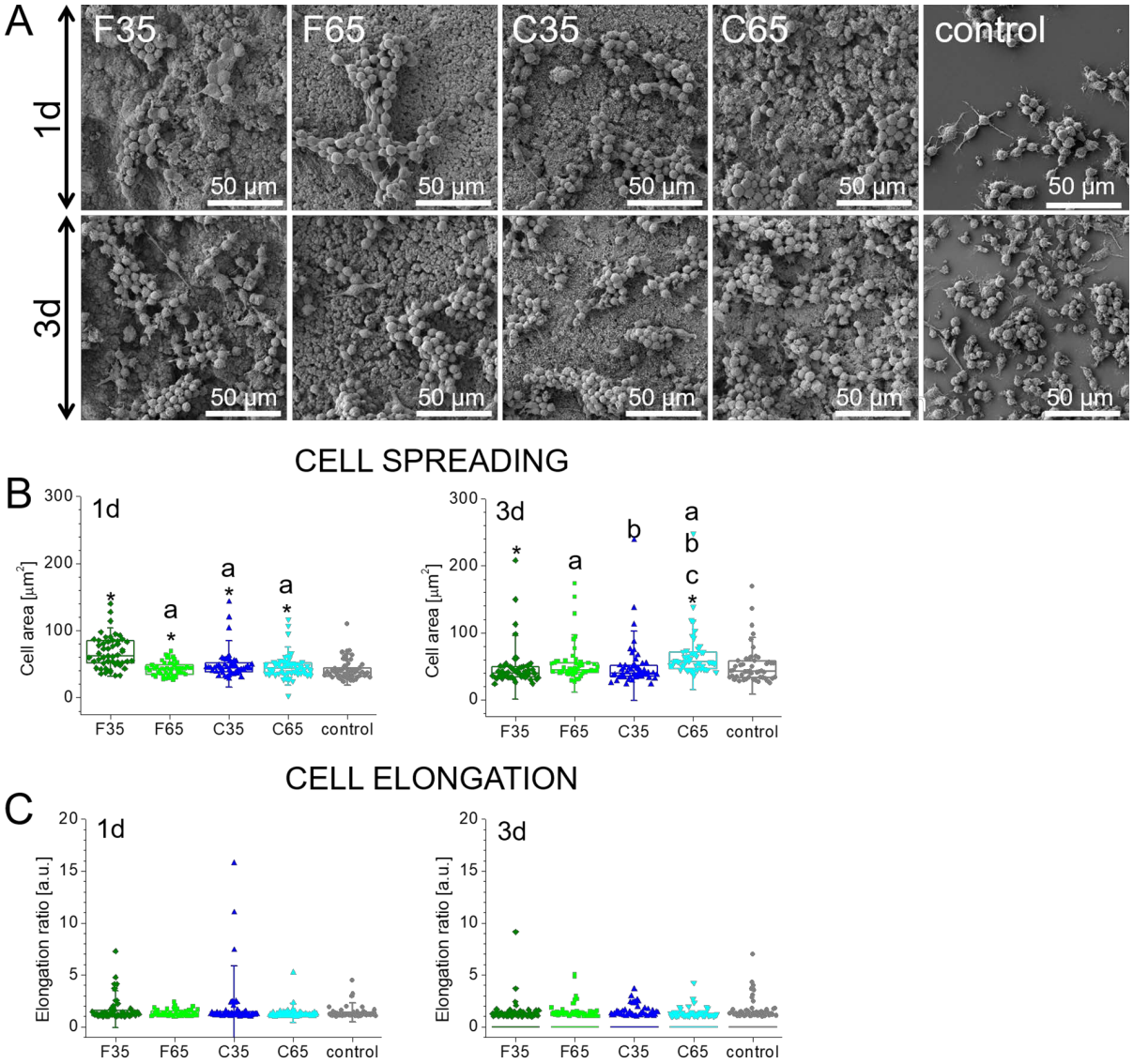

Figure 2.3. A) Morphology of RAW cells observed by SEM on CDHA substrates at 1 and 3 days. RAW cells cultured on glass coverslip were used as a control group. **B)** Cell spreading at 1 and 3 days of cell culture. **C)** Cell elongation ratio at 1 and 3 days of cell culture. In C and D graphs, symbols represent individual cells (n=50), the boxes represent 25th and 75th percentile, the middle line is the median and whiskers are standard deviation. * indicates statistically significant difference ($p < 0.05$) compared to the control group. Statistically significant differences between substrates were indicated with letters (a, b, c) where a, b and c indicates significant difference ($p < 0.05$) compared to F35, F65 and C35, respectively.

2.3.2.2 Inflammatory response of RAW cells

The expression of pro-inflammatory (IL-1β, IL-6, TNFα and iNOS) and anti-inflammatory (IL-10 and CD206) genes by RAW cells cultured on the CDHA was evaluated using RT-qPCR (Figure 2.4.). Overexpression of IL-1β and TNFα genes was observed for all CDHA substrates compared to TCPS being statistically significant for F35 in case of IL-1β expression and for F35, F65 and C35 in case of TNFα. The upregulation of IL-1β and IL-6 was more pronounced for F35 whilst both C35 and C65 coarse substrates upregulated the expression of TNFα. The gene expression of iNOS

and CD206 was lower when RAW cells were cultured on CDHA compared to TCP. However, this downregulation of was only statistically significant in case of expression of iNOS for C35. The expression of IL-10 genes was under the detection limit (data not shown).

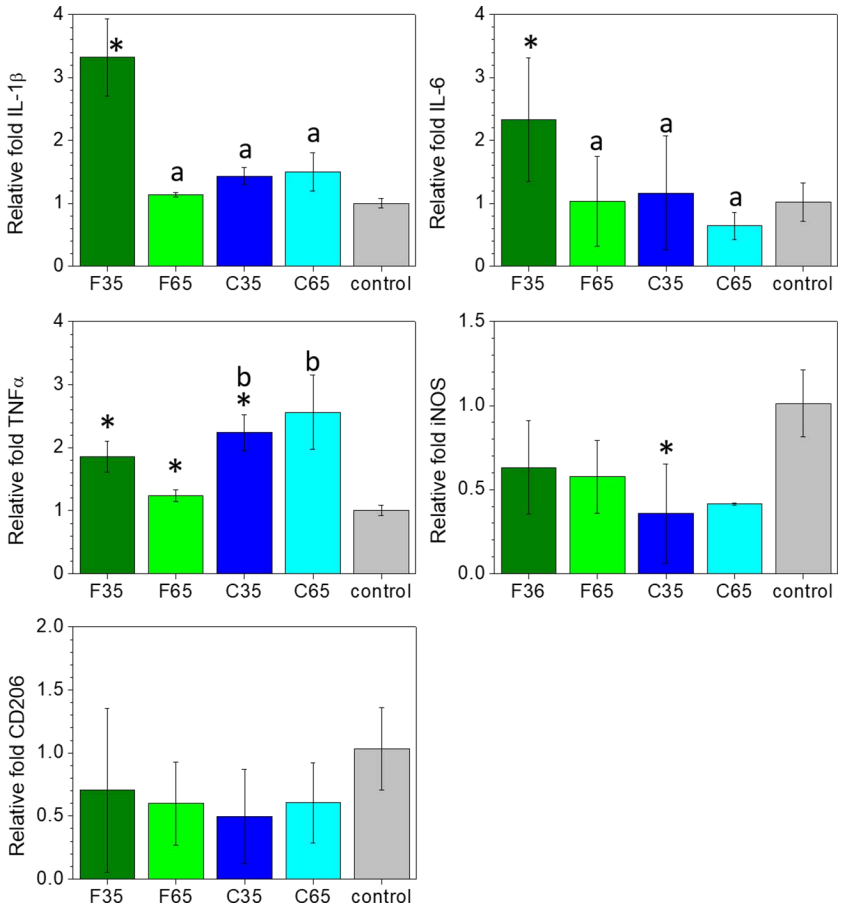

Figure 2.4. Relative expressions of inflammation related genes: IL-1β, IL-6, TNFα, iNOS (pro-inflammatory) and CD206 (anti-inflammatory) of RAW cells cultured on CDHA substrates for 12 h. The values were normalized with respect to housekeeping gene 18S using RAW cells cultured on TCPS as a control sample. * indicates statistically significant difference ($p < 0.05$) compared to the control group. Statistically significant differences between substrates were indicated with letters (a, b) where a and b indicate statistically significant differences ($p < 0.05$) compared to F35 and F65, respectively.

2.3.2.3 Osteogenic and osteoclastogenic activity of RAW cells

The gene expression of osteogenic (OSM, TGFβ and VEGF) and osteoclastogenic (CTSK, CAR2 and MMP9) markers are depicted in Figure 2.5.A and 2.5.B, respectively. In general, CDHA substrates showed similar osteogenic gene expression compared to the control except for F35 where lower levels of osteogenesis related markers were observed being statistically significant for TGFβ1 and VEGF. Noteworthy, cells cultured on C65 presented higher levels of osteogenic-related markers although only TGFβ1 gene expression was significantly higher compared to the other substrates. Moreover, C65 substrate also stimulated the gene expression of osteoclastogenic markers compared to TCPS, especially for CAR2 and MMP9 being

statistically significant for MMP9. Overall, the CDHA with high L/P ratio, F65 and C65, induced higher values of osteogenic and osteoclastogenic markers compared to their low L/P ratio equivalents, F35 and C35, and the same trend was observed when comparing the substrates with low SSA (C35 and C65) with their high SSA (F35 and F65) counterparts, the first inducing a higher expression than the last. However, the majority of this trends were not statistically significant.

The osteoclastic activity of RAW cells was also studied through visualisation of the morphology of the cells and the underlying substrate (Figure 2.5.C) and measurement of ionic concentrations in the cell culture medium (Figure 2.6.). Higher magnification SEM images (Figure 2.5.C, right panel) taken at day 3 revealed the presence of degraded crystals of CDHA in the regions near the macrophages compared to pristine needle and plate-like microstructure of the biomaterials.

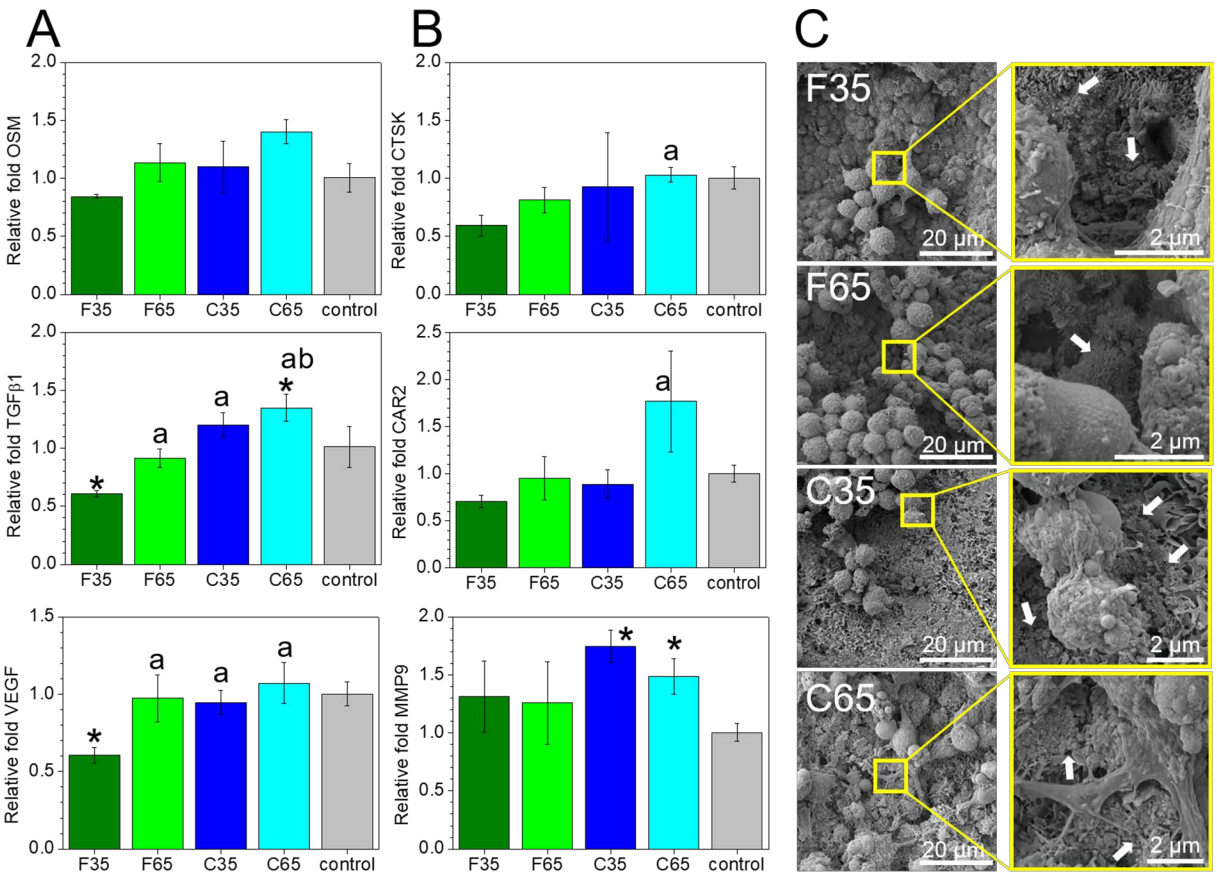

Figure 2.5. Osteogenic and osteoclastogenic activity of RAW cells cultured on CDHA substrates for 12 h. **A)** Relative expressions of osteogenesis related genes: OSM, TGFβ1 and VEGF. **B)** Relative expressions of osteoclastogenesis related genes: CTSK, CAR2, MMP9. In both A and B graphs, the values were normalized with respect to housekeeping gene 18S using RAW cells cultured on TCPS as a control sample. * indicates statistically significant difference ($p < 0.05$) compared to the control TCPS group. Statistically significant differences between substrates were indicated with letters (a, b, c) where a, b and c indicate statistically significant differences ($p < 0.05$) compared to F35, F65 and C35 respectively. **C)** SEM images of RAW cells on the CDHA substrates at day 3, showing degraded crystals (white arrows) presumably as a result of cell activity. Left panel: general view, right panel: detailed view.

The concentrations of calcium and phosphate ions in cell culture medium without cells were 1.89 ± 0.02 mM 1.24 ± 0.02 mM, respectively. No statistically significant changes of Ca^{2+} and P_i content were observed in presence of cells for TCPS group. In general, the levels of calcium decreased in presence of CDHA compared to TCPS, the decrease being more pronounced for F65. The presence of macrophages counteracted the decrease of Ca^{2+} increasing its concentration up to 15 % compared to the substrate alone (Figure 2.6.A and 2.6.B). This was observed at all time points for C35 and C65, whereas in F substrates the effect was more pronounced at day 3.

Little alterations of phosphate were noticed. Overall, P_i levels increased only in presence of F CDHA substrates, especially F65. There were no clear trends associated to the presence or absence of cells and phosphate concentration in the cell culture medium (Figure 2.6.C and 2.6.D).

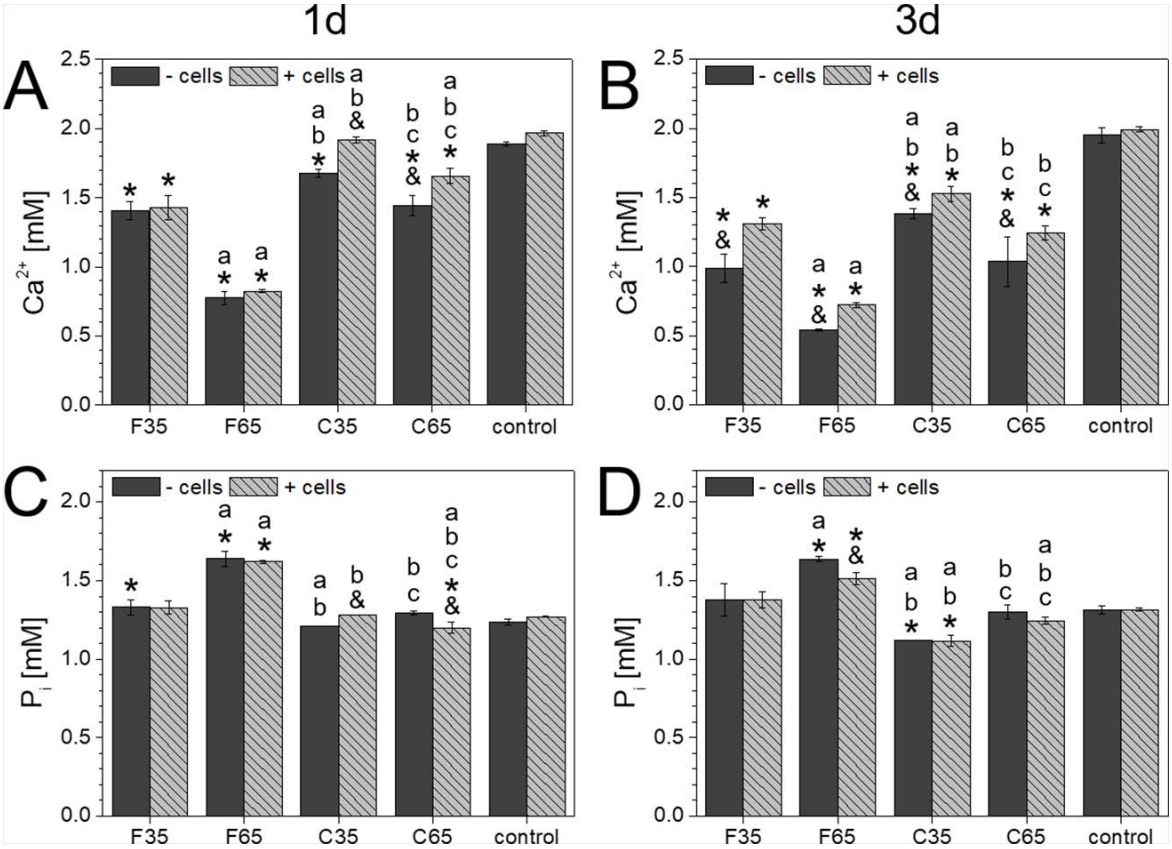

Figure 2.6. Calcium and phosphate concentrations in the cell culture medium in presence of CDHA, with (patterned columns) or without cells (plain columns), after 1 or 3 days. **A)** Calcium levels at day 1. **B)** Calcium levels at day 3. **C)** Phosphate levels at day 1. **D)** Phosphate levels at day 3. The ionic concentrations were evaluated for n=2 samples. For each substrate, & indicates statistically significant difference ($p < 0.05$) between ionic concentration of cell culture medium with or without cells. * indicates statistically significant difference ($p < 0.05$) compared to corresponding control group *i.e.* cell culture medium with or without cells. Statistically significant differences between substrates were indicated with letters (a, b, c) where a, b and c indicates significant difference ($p < 0.05$) compared to F35, F65 and C35, respectively.

2.3.2.4 The effect of CDHA and RAW cell conditioned medium on osteogenic differentiation of osteoblastic SaOS-2 cells

To study the effect of the microenvironment created by biomimetic substrates and macrophages on osteogenesis, osteoblast-like SaOS-2 cells were incubated with CDHA-RAW conditioned extracts. SaOS-2 cells were also cultured with conditioned extracts from RAW cells cultured on TCPS, "SaOS-2 control+", and with non-RAW-conditioned medium, "SaOS-2 control-".

The expression of the osteogenic markers alkaline phosphatase (ALP), Runt-related transcription factor 2 (Runx2), collagen type I (COLL I), bone morphogenic protein 2 (BMP-2), bone sialoprotein (BSP) and osteocalcin (OCN) was evaluated using RT-qPCR. The results showed an up-regulation of osteogenic-related genes in the cells cultured on the F CDHA substrates, this being especially pronounced for BMP-2, BSP and COLL I, and also for Runx2 and OCN in the case of F65. SaOS-2 cells incubated with extracts from plate-like substrates presented similar gene expression values compared to SaOS-2 control+, except for a decrease observed in the case of BSP (Figure 2.7.A).

Western blot analyses were performed to evaluate COLL I, Runx2 and ALP protein production. In general, no significant differences were observed between SaOS-2 cells stimulated with RAW extracts (SaOS-2 control+) and non-treated cells (SaOS-2 control-). Moreover, plate-like CDHA substrates induced lower protein levels compared to needle-like CDHA. Noteworthy, the protein levels of Runx2 and ALP was significantly higher in F35 substrate compared to all the other conditions (Figure 2.7.B).

The mineralization of SaOS-2 cells were assessed through Alizarin Red staining. Calcium deposition and nodule formation was observed to be fostered in the cells cultured in conditioned medium compared to SaOS-2 control- (Figure 2.7.C).

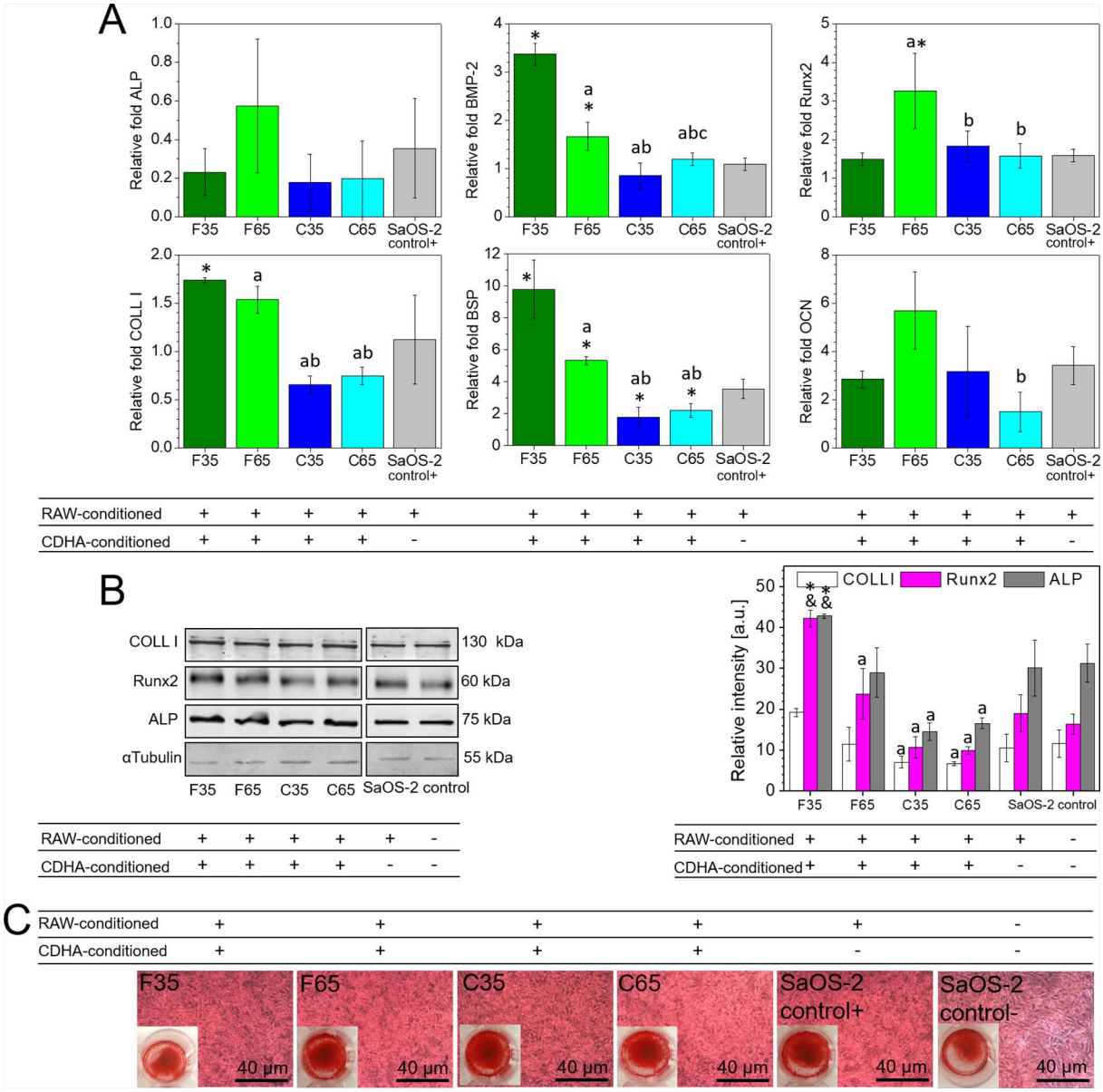

Figure 2.7. The effect of CDHA-RAW conditioned medium on osteogenic activity of SaOS-2. **A)** Relative expressions of osteogenesis related genes: ALP, Runx2, BMP-2, BSP, COLL I, OCN. **B)** Expression of osteogenesis related proteins (COLL I, Runx2, ALP) detected by Western blot and their relative intensity. **C)** Mineralization of SaOS-2 detected through Alizarin Red Staining. In all graphs, "SaOS-2 control+" refers to osteoblastic cells stimulated with RAW cells conditioned medium (without CDHA substrate) whilst "SaOS-2 control-" refers to osteoblastic cells in their standard cell culture medium. * and & indicates statistically significant difference ($p < 0.05$) compared to the SaOS-2 control+ and SaOS-2 control- group, respectively. Statistically significant differences between substrates were indicated with letters (a, b, c) where a, b and c indicate statistically significant differences ($p < 0.05$) compared to F35, F65 and C35 respectively.

The results of gene and protein expression were also confirmed by visualisation of ALP staining and semiquantitative analysis of images. Overall, osteoblastic cells incubated on RAW extracts from fine CDHA presented more intense ALP staining compared to controls or coarse substrates, being significantly higher for F35 (Figure 2.7.A and 2.7.B).

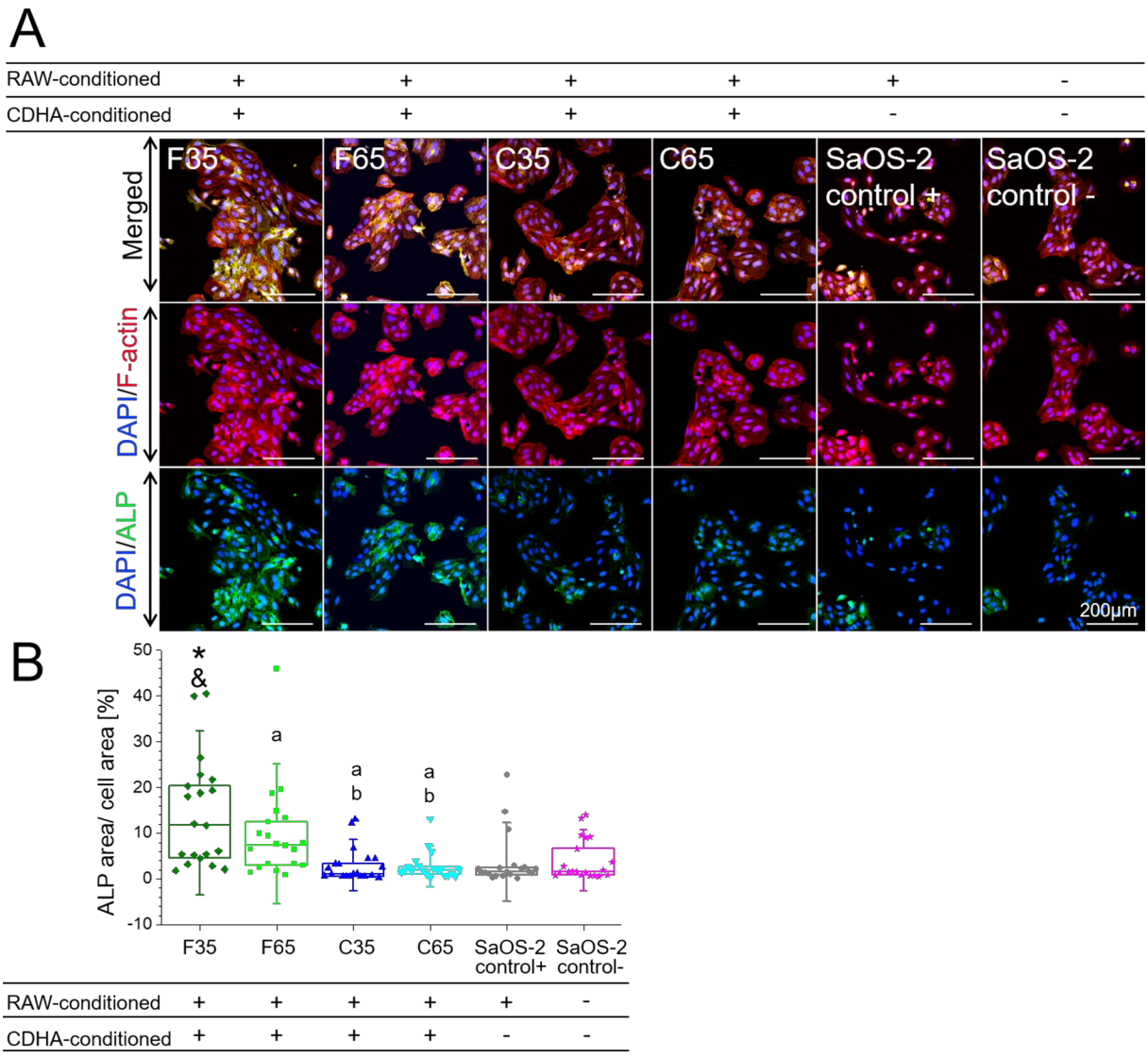

Figure 2.8. The effect of CDHA-RAW cells conditioned medium on ALP expression of SaOS-2. **A)** Representative confocal images of SaOS-2 morphology after 3 days of exposure to CDHA-RAW cells conditioned medium. Cells were stained for F-actin (red), nuclei (blue) and ALP (green). Scale bar in all images denotes 200 µm. The brightness and contrast of images was modified using Fiji/Image-J package. **B)** ALP area normalized to cell area after 3 days of culture. Symbols represent individual cells (n=20), the boxes represent 25th and 75th percentile, the middle line is the median and whiskers are standard deviation. * and & indicate statistically significant differences ($p < 0.05$) compared to the SaOS-2 control+ and SaOS-2 control- groups, respectively. Statistically significant differences between substrates were indicated with letters (a, b) where a and b indicate statistically significant differences ($p < 0.05$) compared to F35 and F65 respectively. In both figures, "SaOS-2 control+" refers to osteoblastic cells stimulated with RAW cells conditioned medium (without CDHA substrate) whilst "SaOS-2 control-" refers to osteoblastic cells in their standard cell culture medium.

2.3.3 The effect of CDHA substrates on the response of RAW cells under inflammatory conditions

In order to evaluate the behaviour of immune cells on CDHA samples under inflammatory environment, macrophages were stimulated with 1 µg/mL of LPS. Thereafter, morphological features of RAW cells as well as the expression of

inflammatory, osteogenic and osteoclastogenic markers were analysed. Over the following sections, “control+” group refers to RAW cells cultured on TCPS or glass coverslip and stimulated with LPS, whilst “control-“ refers to RAW cells cultured on TCPS or glass coverslip without any additional treatment.

2.3.3.1 RAW cells morphology

A combination of round-shaped cells with elongated cells was observed in all conditions (Figure 2.9.). Moreover, the rounded cells showed more flattened morphology on CDHA with high L/P ratio. Noteworthy, image analysis revealed that LPS activated cells presented more spread morphology compared to control- group (Figure 2.9.B). Even though, the spreading of macrophages on CDHA were less pronounced than cells cultured without any material and stimulated with LPS. The analysis of elongation ratio revealed higher elongation ratio for LPS stimulated cells.

2.3.3.1 Inflammatory, osteogenic and osteoclastogenic gene expression of RAW cells

The inflammatory response of the macrophages cultured on CDHA samples under inflammatory environment is depicted in Figure 2.10.A and 2.10.D. Overall, biomimetic substrates showed anti-inflammatory features downregulating the expression of pro-inflammatory cytokines (IL-1β, IL-6, TNFα) compared to control+ group. In general, the downregulation was more pronounced in the cells cultured on CDHA with low L/P ratio *i.e.* F35 and C35 compared to high L/P ratio equivalents. The evaluation of release of proinflammatory cytokines such as IL-6 and TNFα by ELISA (Figure 2.10.D) confirmed similar trends to those observed by analysis of gene expression (Figure 2.10.A). The expression of iNOS was slightly upregulated on C65 compared to control+.

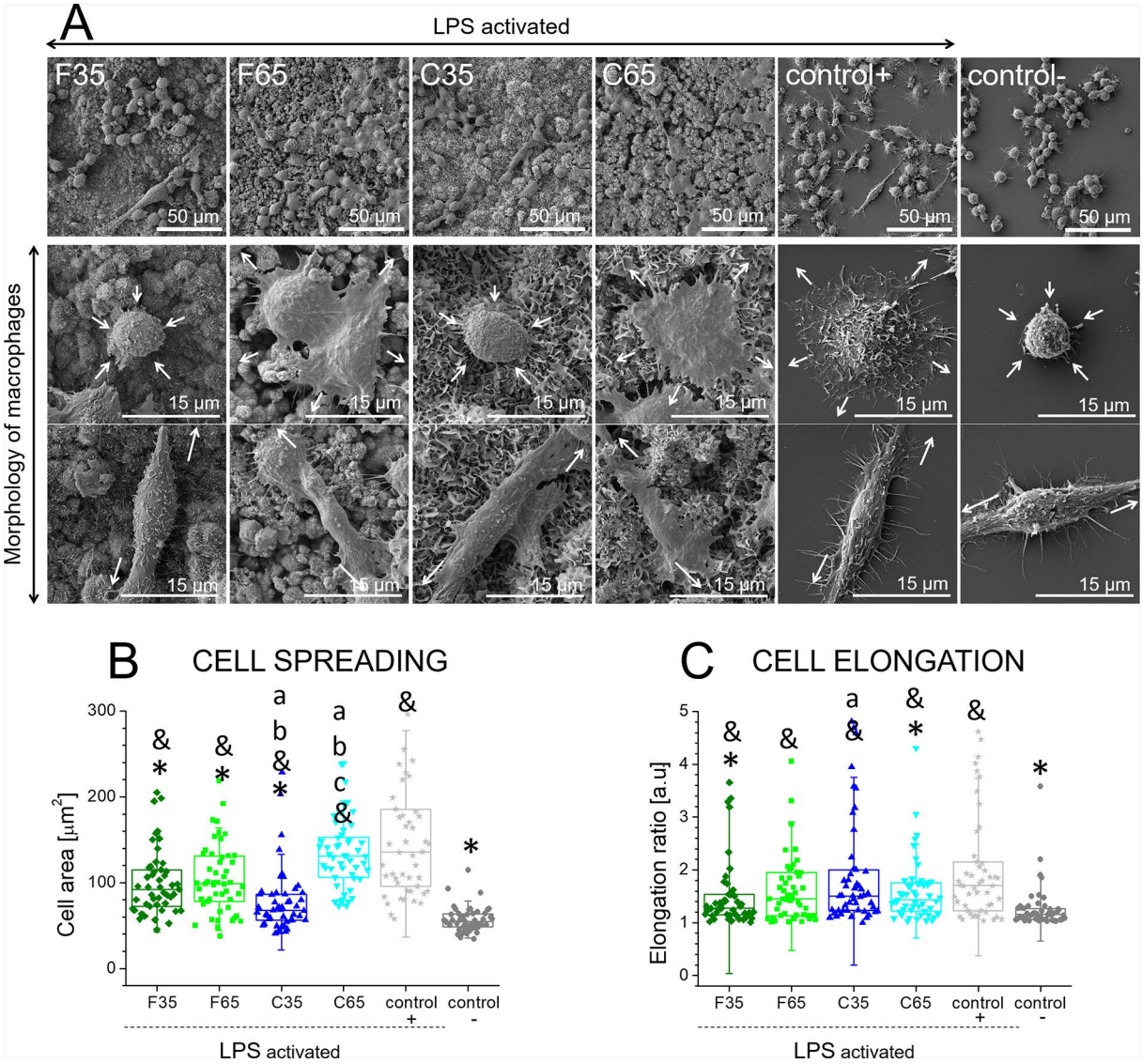

Figure 2.9. A) Morphology of RAW cells observed by SEM on CDHA at 6 hours of post- stimulation. RAW cells cultured on glass coverslip were used as control, where "control+" represents LPS stimulated RAW cells and "control-" non-stimulated cells. Upper panel: general view. Middle and lower panel: detailed view of macrophages morphology. Both rounded and elongated-shape cells were found on CDHA substrates. RAW cells cultured on high L/P CDHA *i.e.* F65 and C65 showed more flattened morphologies compared to F35 and C35. The white arrows indicate a putative direction of cell spreading **B)** Cell spreading after LPS stimulation **C)** Cell elongation after LPS stimulation. In B and C graphs, symbols represent individual cells (n=50), the boxes represent 25th and 75th percentile, the middle line is the median and whiskers are standard deviation. * and & indicate statistically significant differences ($p < 0.05$) compared to the control+ group and control- group, respectively. Statistically significant differences between substrates were indicated with letters (a, b, c) where a, b and c indicate statistically significant differences ($p < 0.05$) compared to F35, F65 and C35, respectively.

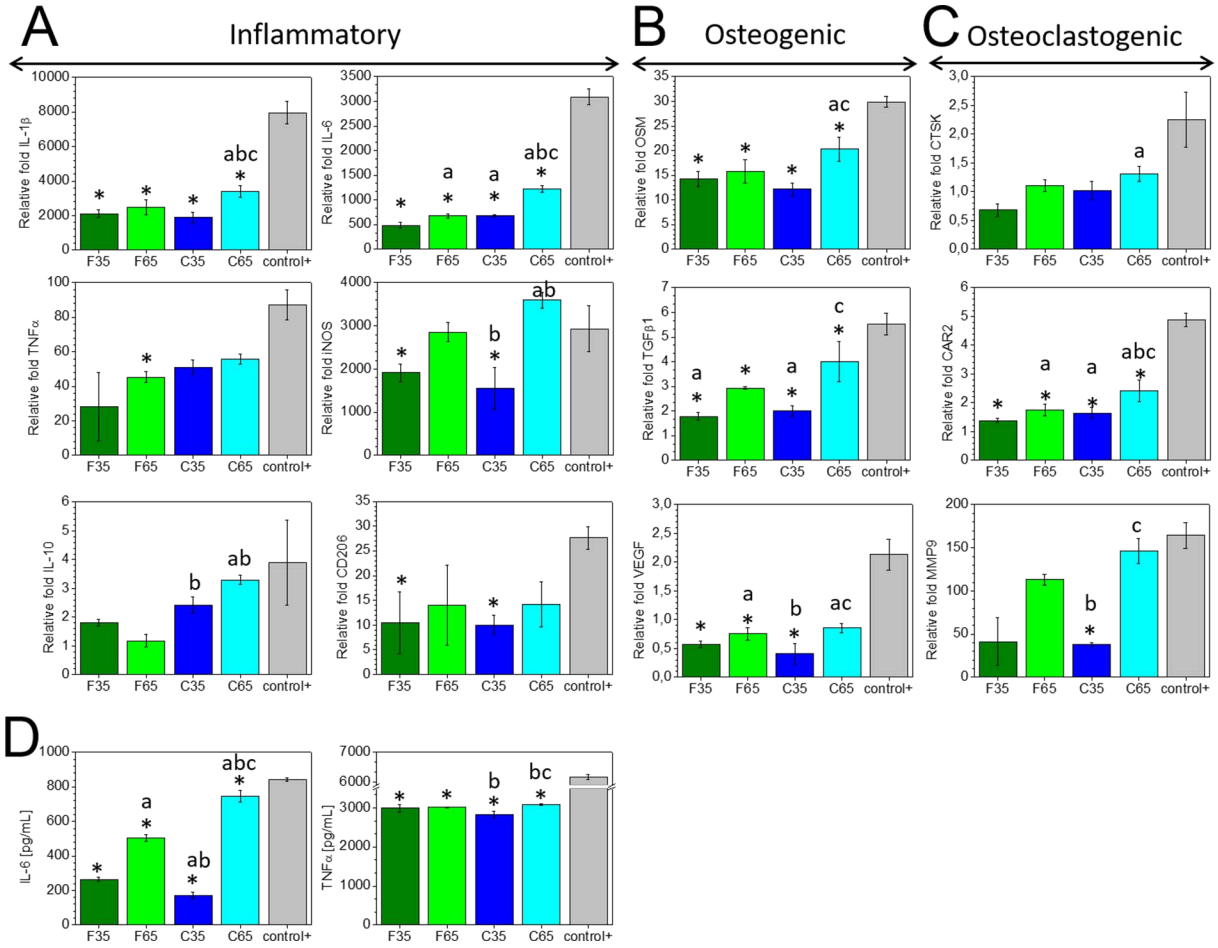

Figure 2.10. Inflammatory, osteogenic and osteoclastogenic activity of RAW cells on CDHA substrates under inflammatory environment. Cells were collected at 6 hours post-stimulation with 1 µg/mL of LPS. **A)** Relative expressions of inflammation related genes; M1 markers: IL-1β, IL-6, TNFα, iNOS; M2 markers: IL-10, CD206. **B)** Relative expressions of osteogenesis related genes: OSM, TGFβ1, VEGF. **C)** Relative expressions of osteoclastogenesis related genes: CTSK, CAR2, MMP9. Gene expression results normalized with respect to endogenous reference gene 18S using non-LPS stimulated RAW on TCPS as a calibrator sample. **D)** Release of inflammatory cytokines IL-6 and TNFα by RAW cells. Control+ represents LPS stimulated RAW cells cultured on TCPS. * indicates statistically significant differences ($p < 0.05$) compared to the control+ group. Statistically significant differences between substrates are indicated with letters (a, b, c) where a, b and c indicates statistically significant differences ($p < 0.05$) compared to F35, F65 and C35 respectively.

Regarding the expression of anti-inflammatory IL-10 and CD206, the levels of both were slightly lower on biomimetic hydroxyapatite compared to control+. Needle like CDHA downregulated the expression of IL-10 to greater extent than plate-like substrate (Figure 2.10.A).

Similar trends were observed for the osteogenic and osteoclastogenic activity of macrophages on the biomimetic CDHA substrates (Figure 2.10.B and 2.10C). Overall, downregulation of osteogenic (OSM, TGFβ and VEGF) and osteoclastogenic (CTSK, CAR2 and MMP) markers was observed on CDHA compared to control+, this trend being more pronounced for CDHA with low L/P ratio.

2.4 Discussion

In the field of synthetic bone grafts, biomimetic calcium deficient hydroxyapatite presents interesting properties due to its similar composition and structure to the mineral phase of bone, as well as its osteoinductive properties.[35] Moreover, unlike for sintered calcium phosphate ceramics, the microstructure and porosity of these materials can be easily tuned without modifying the chemical composition, covering a broad range of porosities and pore sizes and allowing to obtain nanostructured materials.[36] This makes this bone grafting material a very versatile platform to study the effect of textural properties on the interaction with cells.[34] Thus, the main motivation of this chapter was to study the relevance of some textural properties of CDHA *i.e.* surface topography, SSA and porosity, on immunomodulatory and osteoimmunomodulatory processes *in vitro*.

CDHA discs were obtained by cementitious reaction by the hydrolysis of α-TCP.[31] Changing the particle size of the α-TCP powder from fine (F) to coarse (C) shifted the size of the obtained crystals from the nano- to the micro-sized range, and the crystal morphology from needles to plates, respectively (Figure 2.1.). The modification of the textural properties of CDHA resulted in significant changes of the SSA and surface roughness (Table 2.2., Supplementary Figure 2.1.). F substrates presented approximately two-fold SSA values than C substrates. Moreover, using two different L/P ratios *i.e.* low 0.35 mL/g (F35 and C35) and high 0.65 mL/g (F65 and C65) allowed tailoring the material porosity (Table 2.2.).[32,34] Thus, chemically identical CDHA substrates were obtained, with distinct structural features. It is important to highlight that, unlike in the case of inert substrates, the variations in surface topography, SSA and porosity of CDHA are expected to affect the ionic exchange with the cell culture medium, which in turn may influence cell behaviour, as shown in previous studies.[37-39] Therefore, this creates a more complex scenario, since these indirect effects should be taken into consideration in addition to the direct effect of textural properties when evaluating immunomodulatory and osteoimmunomodulatory outcome of bioactive substrates.

In the present study the RAW 264.7 cells were used as a model to study immune cell response to biomimetic hydroxyapatite with tailored characteristics. The evaluation of proliferation and morphology of macrophages are interesting tools towards discovering the severity of inflammation and immune cells' activation stage.[40] The results revealed similar cell adhesion over all biomimetic substrates, comparable to the control (Figure 2.2.). However, RAW cell proliferation was reduced on the CDHA substrates. This is in accordance with previous reports where biomimetic hydroxyapatite reduced the proliferation of various cell types, which was attributed to a coupled effect of spiky microstructure and altered ionic release/uptake.[37-39] Similarly, Mestres *et al.* observed decreased cell number of RAW cells on CDHA at early days of cell culture being this

scenario more pronounced for needle-like samples.[41] However, we did not observe this behaviour, which can be probably due to the use of smaller sample size, which reduced the extent of ionic fluctuations (Figure 2.6.). The effect of ionic fluctuations on cellular behaviour will be discussed in Chapter 6.

Macrophage morphology is generally associated with their polarization state. The round shape is usually related to pro-inflammatory M1 phenotype whereas M2 phenotype exhibit more elongated shapes.[42,43] In addition, M1 type is also accompanied with enhanced cell spreading after induction with LPS.[44] Although there were no obvious changes in the elongation ratio of RAW cells (Figure 2.3.A and 2.3.C, Supplementary Figure 2.2.), immune cells presented different spreading areas, depending of CDHA substrate (Figure 2.2.A and 2.2.B, Supplementary Figure 2.2.). For instance, macrophages cultured on C65 presented enhanced spreading compared to the other biomimetic substrates and the control, suggesting a more inflammatory state. This agrees with findings by Mestres *et al.*, who reported a higher release of reactive oxygen species (ROS) for RAW cells cultured on plate-like substrates, suggesting a more inflammatory state compared to needle-like CDHA.[41]

Immediately after biomaterial implantation, immune cells are recruited and release pro-inflammatory molecules.[45] This process is particularly important due to the dual role of immune cells. Macrophages not only act as inflammatory mediators but also as wound and tissue healing regulators, determining further implant success or leading to chronic inflammation and graft rejection. Current strategies to control the foreign body response mostly focus on controlling inflammatory cytokines secretion. In this regard, modifications of the physicochemical features of biomaterials, including chemistry[24], roughness[46], stiffness[47] or geometry[48] have been reported to regulate macrophage activation. Interestingly, in present work higher values of pro-inflammatory cytokines IL-1β and IL-6 were observed on needle-like surfaces (F35), whereas TNFα was higher on plate-like surfaces. These results demonstrate that modifications at the nano- and micro-scale level influence differently macrophage activation, although in general the incubation with biomaterials fosters a pro-inflammatory status of immune cells as other authors previously described.[21,49,50] These findings suggest that in these substrates there is no clear link between surface topography of CDHA and polarization of macrophages. One possible explanation might be bioactive nature of CaP substrates. For bioinert biomaterials, the inflammatory molecule expression can be straightforwardly related to surface features in contrast to CDHA which ionic release/uptake might interfere with the effect of surface topography on cytokine expression.

It is generally accepted that adherent macrophages produce a degradative microenvironment that accelerates biomaterial resorption. In present study, both needle-like and plate-like microstructures induced the generation of multinucleated cells (Supplementary Figure 2.3.). Moreover, the degradation of hydroxyapatite crystals was

observed at the cell-substrate interface (Figure 2.5.C), suggesting cell-mediated degradation and osteoclastic-like behaviour of macrophages. Although the expression of osteoclastic genes on CDHA was generally lower or equal to control group, similar to reports[51], the incubation with C substrates lead to greater levels of CAR2 and MMP9 compared to their F counterparts of corresponding L/P ratio (C35 *vs*. F35 and C65 an F65), indicating that greater surface roughness may trigger some osteoclastic activity.[51,52] The presence of multinucleated macrophages (Supplementary Figure 2.3.) also suggests the morphology similar to that observed for osteoclastic cells. Another sign of osteoclastic behaviour of RAW cells was the higher ion concentration, especially calcium, in the cell culture media in presence of macrophages compared to the cell-free substrates (Figure 2.6.). In fact, the release of these ions into the medium can be associated to the dissolution of CDHA by the activity of immune cells, which counteracts the ionic exchange produced by the material itself, similarly to what was found in a previous study.[51] As previously reported, the immersion of biomimetic hydroxyapatite in cell culture medium resulted in a decrease of the calcium concentration and a slight increase of phosphate.[37] This ionic fluctuations are caused by the uptake of calcium by the substrate due to the calcium deficient nature of biomimetic apatite, and the replacement of phosphate in the CDHA structure by other ions present in cell culture medium, mainly carbonate.[53] Interestingly, the higher the porosity and the SSA of the substrate, the higher are the ionic fluctuations, being F65 the more reactive material. In presence of immune cells, an increase in Ca^{2+} concentration was observed for all substrates suggesting the cell-induced material degradation. However, is must be kept in mind that the differentiation of macrophages into fully functional osteoclasts[54] can be only achieved by additional stimulation with RANKL, OPG and M-CSF molecules.[55] Although the results suggest that RAW cultured on biomimetic substrates exhibit some osteoclastic features it cannot be clearly claimed that CDHA stimulate osteoclastic differentiation of macrophages.

The activation of immune cells and thus the simultaneous release of inflammatory molecules such as TNFα, TGFβ, INFγ and IL-17[12] or osteogenic factors like OSM, TGFβ1 and VEGF can also effectively stimulate osteoblastic differentiation. For instance, OSM, which is a pro-inflammatory cytokine of the IL-6 family secreted by M1 macrophages, was reported osteoblast differentiation and matrix mineralization[10] whereas VEGF is an anti-inflammatory cytokine produced by M2 macrophages that was recognised to be osteogenic and angiogenic inducer.[14] In contrast, TGFβ1 exhibits dual function; the inflammatory molecule can either stimulate osteogenesis[56] or lead to pathological fibrosis when its expression is prolonged.[57] Interestingly, in present study macrophages cultured on plate-like CDHA surfaces showed higher values of these gene markers compared to needle-like CDHA. On another hand, the results revealed additional effect of substrate porosity on stimulating the secretion of osteogenic molecules by macrophages. In this regard, samples with lower L/P ratio, *i.e.* low

porosity, decreased the expression of all three genes compared to their high L/P ratio *i.e.* high porosity, equivalents (Figure 2.5.A). In agreement with these results, Xiao *et al.* showed that that ceramic scaffolds with higher porosity led to increased expression of platelet-endothelial cell adhesion molecule (PECAM-1) and VEGF.[57]

To evaluate the influence of osteogenic factors and inflammatory molecules released by immune cells on osteoblastic differentiation, the SaOS-2 cells were exposed to extracts from RAW cells cultured on the different CDHA substrates. Although the expression of osteogenic molecules (OSM, TGFβ1 and VEGF) by RAW cells was generally lower for nanostructured needle-like substrates (Figure 2.5.A), the results showed that the immunoenvironment created by these CDHA materials stimulated to greater extent the expression of osteogenic-related genes as well as protein secretion in osteoblastic cells (Figure 2.7.A, 2.7.B and 2.8.). This inconsistency might suggest the involvement of other osteogenic factors and inflammatory molecules and it was previously observed in work of Chen *et al*.[21] Interestingly, macrophages cultured on needle-like surfaces overexpressed IL-1β and IL-6 cytokines, which might be the possible agents responsible for enhanced osteogenesis of SaOS-2 after exposure to RAW and needle-like CDHA immunoenvironment. In fact, both cytokines have been related to promote osteogenesis.[58-60] In contrary, plate-like structures did not stimulate osteoblast differentiation probably due to the inhibitory effects of TNFα secreted by macrophages.[61,62] However, the fact that the different substrates provoked different ionic fluctuations in the cell culture medium (Figure 2.6.) cannot be overlooked. Both calcium and phosphate, either separately or simultaneously, are known to affect the osteogenic commitment of bone forming cells.[63-65] Therefore, the specific response of SaOS-2 cells shouldn't be interpreted considering only the cytokines released in the supernatant by the macrophages. The changes in composition of the cell culture medium induced by the different substrates may also play a role, adding further complexity to the system and determining cell fate. However, in previous work the osteogenic differentiation of bone forming cells after exposure to CaPs modified cell culture medium[37] was not observed what suggests that osteogenic differentiation is accomplished due to the simultaneous effect of microenvironment created by substrate and the release of inflammatory molecules by macrophages as described by Chen *et al.*[16]

Finally, the effect of physiochemical properties of CDHA on modulating their anti-inflammatory capacity was also evaluated through activation of macrophages with LPS.[8] The activation of immune cells was confirmed through visualisation of iNOS (Supplementary Figure 2.4.), a common M1 phenotype reactive oxygen intermediate.[5] In general, the activation of immune cells led to different morphological (Figure 2.9., Supplementary Figure 2.5.) and gene expression (Figure 2.10.) responses to CDHA. This agrees with previous findings of Chen *et al.*, who reported different behaviour of RAW cells cultured under standard and inflammatory conditions with mesoporous silica

nanospheres.[8] The LPS stimulation led to immune cells with more spread morphologies and elongation ratios compared to non-stimulated cells. Interestingly, high L/P ratio CDHA led to enhanced spreading area compared to equivalent substrates with low L/P ratio, suggesting that higher porosity stimulates inflammation state to a greater extent. No clear effect of the needle- or plate-like microstructure was found. The results of inflammatory gene expression (Figure 2.10.A) and cytokine release (Figure 2.10.D) confirmed this trend. All the CDHA samples produced a reduction on the expression of inflammatory genes compared to the control after LPS induction, but the effect was more marked for the low L/P, this is, the less porous samples. The difference between F and C substrates, *i.e.* the effect of microstructure, was relevant only for the high L/P values, the F substrates showing lower expression of inflammation related genes. It has been observed previously that porous implants seem to modulate bone healing by inducing shifts in local macrophage phenotype into M1 phenotype which in turn contribute to better vascularization an finally better integration of implant.[27] On the other hand, topography also may play a role on anti-inflammatory effects of CDHA since needle-like structures reduced the expression of pro-inflammatory genes compared to plate-like structure, in accordance with a previous study.[41] Activated macrophages cultured on CDHA expressed higher amounts of osteogenic and osteoclastogenic genes compared to non-activated macrophages, although the levels were lower compared to the control. The results suggest a predominant role of substrate porosity under inflammatory environment; the incubation of macrophages with CDHA with high L/P led to higher pro-inflammatory signalling compared to low L/P equivalents.

Overall, the present chapter sheds light on the effect of structural differences of chemically identical calcium phosphate substrates on stimulating immunomodulatory, osteoimmunomodulatory and anti-inflammatory functions. The modification of surface topography and porosities of substrate will be an interesting tool for designing CaPs that trigger specific cellular responses of bone tissue.

2.5 Conclusions

The results obtained in this study demonstrated that the immune responses of macrophages can be modulated through distinct physicochemical properties of CDHA. Surface topography of CDHA plays an important role in stimulating the production of pro-inflammatory cytokines by macrophages, which in turn regulates osteogenic or osteoclastogenic processes. Moreover, the results showed that nanostructured neddle-like structures induce osteogenic activities of bone forming cells and porosity positively regulates the intensity of inflammation in CDHA substrates. Overall, the findings suggest that the favourable osteoimmune milieu for bone regeneration is not only related to the inflammatory cytokines released from activated immune cells, but also depends on the intrinsic microenvironment created by CDHA bioactivity.

2.6 Bibliography

1. Chen, Z. *et al.* Osteoimmunomodulation for the development of advanced bone biomaterials. *Mater. Today* **19**, 304–321 (2016).
2. Mokarram, N. & Bellamkonda, R. V. A Perspective on Immunomodulation and Tissue Repair. *Ann. Biomed. Eng.* **42**, 338–351 (2014).
3. Wu, X. Q. *et al.* Emerging role of microRNAs in regulating macrophage activation and polarization in immune response and inflammation. *Immunology* **148**, 237–248 (2016).
4. Vogel, D. Y. S. *et al.* Human macrophage polarization in vitro: Maturation and activation methods compared. *Immunobiology* **219**, 695–703 (2014).
5. Juhas, U., Ryba-Stanisławowska, M., Szargiej, P. & Myśliwska, J. Different pathways of macrophage activation and polarization. *Postepy Hig. Med. Dosw.* **69**, 496–502 (2015).
6. Chen, Z. *et al.* Nanotopography-based strategy for the precise manipulation of osteoimmunomodulation in bone regeneration. *Nanoscale* **9**, 18129–18152 (2017).
7. Michalski, M. N. & McCauley, L. K. Macrophages and skeletal health. *Pharmacol. Ther.* **174**, 43–54 (2017).
8. Han, S., Chen, Z., Han, P., Hu, Q. & Xiao, Y. Activation of Macrophages by Lipopolysaccharide for Assessing the Immunomodulatory Property of Biomaterials. *Tissue Eng. Part A* **23**, 1100–1109 (2017).
9. Mantovani, A., Biswas, S. K., Galdiero, M. R., Sica, A. & Locati, M. Macrophage plasticity and polarization in tissue repair and remodelling. *J. Pathol.* **229**, 176–185 (2013).
10. Guihard, P. *et al.* Induction of osteogenesis in mesenchymal stem cells by activated monocytes/macrophages depends on oncostatin M signaling. *Stem Cells* **30**, 762–772 (2012).
11. Ding, J. *et al.* TNFα and IL-1β inhibit RUNX2 and collagen expression but increase alkaline phosphatase activity and mineralization in human mesenchymal stem cells. *Life Sci.* **84**, 499–504 (2009).
12. Rifas, L. T-cell cytokine induction of BMP-2 regulates human mesenchymal stromal cell differentiation and mineralization. *J. Cell. Biochem.* **98**, 706–714 (2006).
13. Champagne, C. M., Takebe, J., Offenbacher, S. & Cooper, L. F. Macrophage cell lines produce osteoinductive signals that include bone morphogenetic protein-2. *Bone* **30**, 26–31 (2002).
14. Freytes, D. O., Kang, J. W., Marcos-Campos, I. & Vunjak-Novakovic, G. Macrophages modulate the viability and growth of human mesenchymal stem cells. *J. Cell. Biochem.* **114**, 220–229 (2013).
15. Chen, Z. *et al.* Osteoimmunomodulatory properties of magnesium scaffolds coated with β-tricalcium phosphate. *Biomaterials* **35**, 8553–8565 (2014).
16. Chen, Z. *et al.* Osteogenic differentiation of bone marrow MSCs by β-tricalcium phosphate stimulating macrophages via BMP2 signalling pathway. *Biomaterials* **35**, 1507–18 (2014).
17. Chen, S. *et al.* Characterization of topographical effects on macrophage behavior in a foreign body response model. *Biomaterials* **31**, 3479–3491 (2010).
18. Godek, M. L., Sampson, J. A., Duchsherer, N. L., McElwee, Q. & Grainger, D. W. Rho GTPase protein expression and activation in murine monocytes/macrophages are not modulated by model biomaterial surfaces in serum-containing in vitro cultures. J. Biomater. Sci. Polym. *Ed.* **17**, 1141–1158 (2006).
19. Bota, P. C. S. *et al.* Biomaterial topography alters healing in vivo and monocyte/macrophage activation in vitro. *J. Biomed. Mater. Res. - Part A* **95 A**, 649–657 (2010).
20. Wójciak-Stothard, B., Curtis, A., Monaghan, W., Macdonald, K. & Wilkinson, C. Guidance and activation of murine macrophages by nanometric scale topography. *Exp. Cell Res.* **223**, 426–435 (1996).
21. Chen, Z. *et al.* Tuning Chemistry and Topography of Nanoengineered Surfaces to Manipulate Immune Response for Bone Regeneration Applications. *ACS Nano* **11**, 4494–4506 (2017).
22. Arima, Y. & Iwata, H. Effect of wettability and surface functional groups on protein adsorption and cell adhesion using well-defined mixed self-assembled monolayers. *Biomaterials* **28**, 3074–3082 (2007).

23. Faucheux, N., Schweiss, R., Lützow, K., Werner, C. & Groth, T. Self-assembled monolayers with different terminating groups as model substrates for cell adhesion studies. *Biomaterials* **25**, 2721–2730 (2004).
24. Schutte, R. J., Parisi-Amon, A. & Reichert, W. M. Cytokine profiling using monocytes/macrophages cultured on common biomaterials with a range of surface chemistries. *J. Biomed. Mater. Res. - Part A* **88**, 128–139 (2009).
25. McBane, J. E., Matheson, L. A., Sharifpoor, S., Santerre, J. P. & Labow, R. S. Effect of polyurethane chemistry and protein coating on monocyte differentiation towards a wound healing phenotype macrophage. *Biomaterials* **30**, 5497–5504 (2009).
26. Ballotta, V., Driessen-Mol, A., Bouten, C. V. C. & Baaijens, F. P. T. Strain-dependent modulation of macrophage polarization within scaffolds. *Biomaterials* **35**, 4919–4928 (2014).
27. Sussman, E. M., Halpin, M. C., Muster, J., Moon, R. T. & Ratner, B. D. Porous implants modulate healing and induce shifts in local macrophage polarization in the foreign body reaction. *Ann. Biomed. Eng.* **42**, 1508–1516 (2014).
28. Bezuidenhout, D., Davies, N. & Zilla, P. Effect of well defined dodecahedral porosity on inflammation and angiogenesis. *ASAIO J.* **48**, 465–71 (2002).
29. Chen, Z. *et al.* The effect of osteoimmunomodulation on the osteogenic effects of cobalt incorporated β-tricalcium phosphate. *Biomaterials* **61**, 126–138 (2015).
30. Chen, Z. *et al.* Nanoporous microstructures mediate osteogenesis by modulating the osteo-immune response of macrophages. *Nanoscale* **9**, 706–718 (2017).
31. Ginebra, M. P. *et al.* Setting Reaction and Hardening of an Apatitic Calcium Phosphate *Cement. J. Dent. Res.* **76**, 905–912 (1997).
32. Espanol, M. *et al.* Intrinsic porosity of calcium phosphate cements and its significance for drug delivery and tissue engineering applications. *Acta Biomater.* **5**, 2752–62 (2009).
33. Livak, K. J. & Schmittgen, T. D. Analysis of relative gene expression data using real-time quantitative PCR and the 2-ΔΔCT method. *Methods* **25**, 402–408 (2001).
34. Diez-Escudero, A., Espanol, M., Beats, S. & Ginebra, M.-P. In vitro degradation of calcium phosphates: Effect of multiscale porosity, textural properties and composition. *Acta Biomater.* **60**, 81–92 (2017).
35. Barba, A. *et al.* Intrinsic osteoinduction of biomimetic nanostructured calcium phosphate scaffolds. *Front. Bioeng. Biotechnol.* **4**, 2–3 (2016).
36. Pastorino, D., Canal, C. & Ginebra, M. P. Multiple characterization study on porosity and pore structure of calcium phosphate cements. *Acta Biomater.* **28**, 205–214 (2015).
37. Sadowska, J.-M., Guillem-Marti, J., Montufar, E. B., Espanol, M. & Ginebra, M.-P. Biomimetic Versus Sintered Calcium Phosphates: The In Vitro Behavior of Osteoblasts and Mesenchymal Stem Cells. *Tissue Eng. Part A* **23**, 1297–1309 (2017).
38. Gustavsson, J., Ginebra, M. P., Planell, J. & Engel, E. Osteoblast-like cellular response to dynamic changes in the ionic extracellular environment produced by calcium-deficient hydroxyapatite. *J. Mater. Sci. Mater. Med.* **23**, 2509–20 (2012).
39. Engel, E. *et al.* Discerning the role of topography and ion exchange in cell response of bioactive tissue engineering scaffolds. *Tissue Eng. Part A* **14**, 1341–51 (2008).
40. Jenkins, S. J. *et al.* Local Macrophage Proliferation, Rather than Recruitment from the Blood, Is a Signature of TH2 Inflammation. *Science* (80-.). **332**, 1284–1288 (2011).
41. Mestres, G. *et al.* Inflammatory response to nano- And microstructured hydroxyapatite. *PLoS One* **10**, 1–20 (2015).
42. Sridharan, R. *et al.* Biomaterial based modulation of macrophage polarization: A review and suggested design principles. *Mater. Today* **18**, 313–325 (2015).
43. McWhorter, F. Y., Wang, T., Nguyen, P., Chung, T. & Liu, W. F. Modulation of macrophage phenotype by cell shape. *Proc. Natl. Acad. Sci.* **110**, 17253–17258 (2013).
44. Schmidt, A., Caron, E. & Hall, A. Lipopolysaccharide-Induced Activation of 2-Integrin Function in Macrophages Requires Irak Kinase Activity, p38 Mitogen- Activated Protein Kinase, and the Rap1 GTPase. *Mol. Cell. Biol.* **21**, 438–448 (2001).
45. Scatena, M., Eaton, K. V., Jackson, M. F., Lund, S. A. & Giachelli, C. M. Macrophages: The Bad, the Ugly, and the Good in the Inflammatory Response to Biomaterials in *The Immune*

Response to Implanted Materials and Devices (ed. Corradetti B.) 37–62 (Springer International Publishing, 2017).
46. Refai, A. K., Textor, M., Brunette, D. M. & Waterfield, J. D. Effect of titanium surface topography on macrophage activation and secretion of proinflammatory cytokines and chemokines. *J. Biomed. Mater. Res.* **70A**, 194–205 (2004).
47. Féréol, S. *et al.* Sensitivity of alveolar macrophages to substrate mechanical and adhesive properties. *Cell Motil. Cytoskeleton* **63**, 321–340 (2006).
48. Voskerician, G., Gingras, P. H. & Anderson, J. M. Macroporous condensed poly(tetrafluoroethylene). I. In vivo inflammatory response and healing characteristics. *J. Biomed. Mater. Res. - Part A* **76**, 234–242 (2006).
49. Paul, N. E. *et al.* Topographical control of human macrophages by a regularly microstructured polyvinylidene fluoride surface. *Biomaterials* **29**, 4056–4064 (2008).
50. Hotchkiss, K. M. *et al.* Titanium surface characteristics, including topography and wettability, alter macrophage activation. *Acta Biomater.* **31**, 425–434 (2016).
51. Ciapetti, G. *et al.* Osteoclast differentiation from human blood precursors on biomimetic calcium-phosphate substrates. *Acta Biomater.* **50**, 102–113 (2017).
52. Costa-Rodrigues, J., Fernandes, A., Lopes, M. A. & Fernandes, M. H. Hydroxyapatite surface roughness: Complex modulation of the osteoclastogenesis of human precursor cells. *Acta Biomater.* **8**, 1137–1145 (2012).
53. Cazalbou, S., Combes, C., Eichert, D., Rey, C. & Glimcher, M. J. Poorly crystalline apatites: evolution and maturation in vitro and in vivo. *J. Bone Miner. Metab.* **22**, 310–7 (2004).
54. ten Harkel, B. *et al.* The Foreign Body Giant Cell Cannot Resorb Bone, But Dissolves Hydroxyapatite Like Osteoclasts. *PLoS One* **10**, e0139564 (2015).
55. Teitelbaum, S. L. Bone resorption by osteoclasts. *Science* (80-.). **289**, 1504–1508 (2000).
56. Mizuno, M. & Kuboki, Y. TGF-β Accelerated the Osteogenic Differentiation of Bone Marrow Cells Induced by Collagen Matrix. *Biochem. Biophys. Res. Commun.* **211**, 1091–1098 (1995).
57. Chen, Z., Wu, C. & Xiao, Y. Convergence of Osteoimmunology and Immunomodulation for the Development and Assessment of Bone Biomaterials. in *The Immune Response to Implanted Materials and Devices* (ed. Corradetti B.) 107–124 (Springer International Publishing, 2017).
58. Lin, F.-H., Chang, J. B., McGuire, M. H., Yee, J. A. & Brigman, B. E. Biphasic effects of interleukin-1β on osteoblast differentiation in vitro. *J. Orthop. Res.* n/a-n/a (2010).
59. Huh, J. E. & Lee, S. Y. IL-6 is produced by adipose-derived stromal cells and promotes osteogenesis. Biochim. Biophys. *Acta - Mol. Cell Res.* **1833**, 2608–2616 (2013).
60. Cho, T. J. *et al.* Expression and role of interleukin-6 in distraction osteogenesis. *Calcif. Tissue Int.* **80**, 192–200 (2007).
61. Gilbert, L. *et al.* Inhibition of Osteoblast Differentiation by Tumor Necrosis Factor-α. Endocrinology **141**, 3956–3964 (2000).
62. Zhao, L. *et al.* Tumor necrosis factor inhibits mesenchymal stem cell differentiation into osteoblasts via the ubiquitin E3 ligase Wwp1. *Stem Cells* **29**, 1601–1610 (2011).
63. Barradas, A., Yuan, H., van Blitterswijk, C. & Habibovic, P. Osteoinductive biomaterials: current knowledge of properties, experimental models and biological mechanisms. *Eur. Cells Mater.* **21**, 407–429 (2011).
64. Barradas, A. M. C. *et al.* The influence of genetic factors on the osteoinductive potential of calcium phosphate ceramics in mice. *Biomaterials* **33**, 5696–705 (2012).
65. Yuan, H. *et al.* Osteoinductive ceramics as a synthetic alternative to autologous bone grafting. *Proc. Natl. Acad. Sci. U. S. A.* **107**, 13614–9 (2010).

2.7 Supplementary information

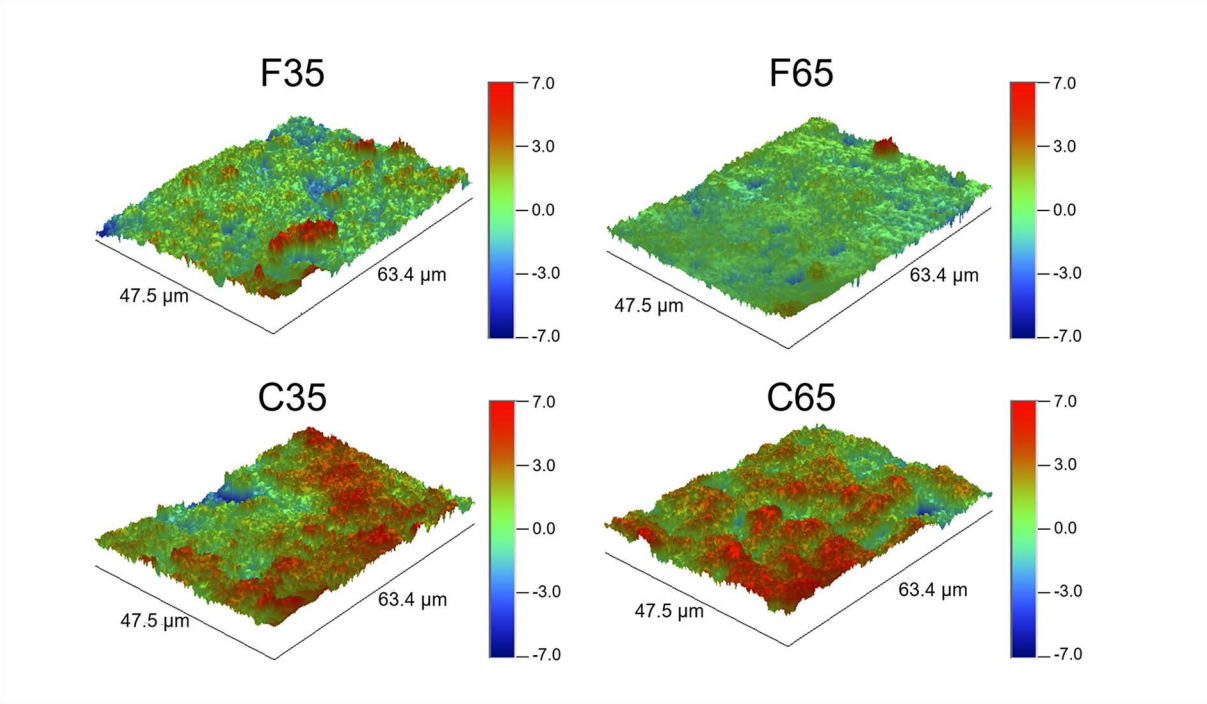

Supplementary Figure 2.1. Optical interferometry images of surface topography of CDHA substrates.

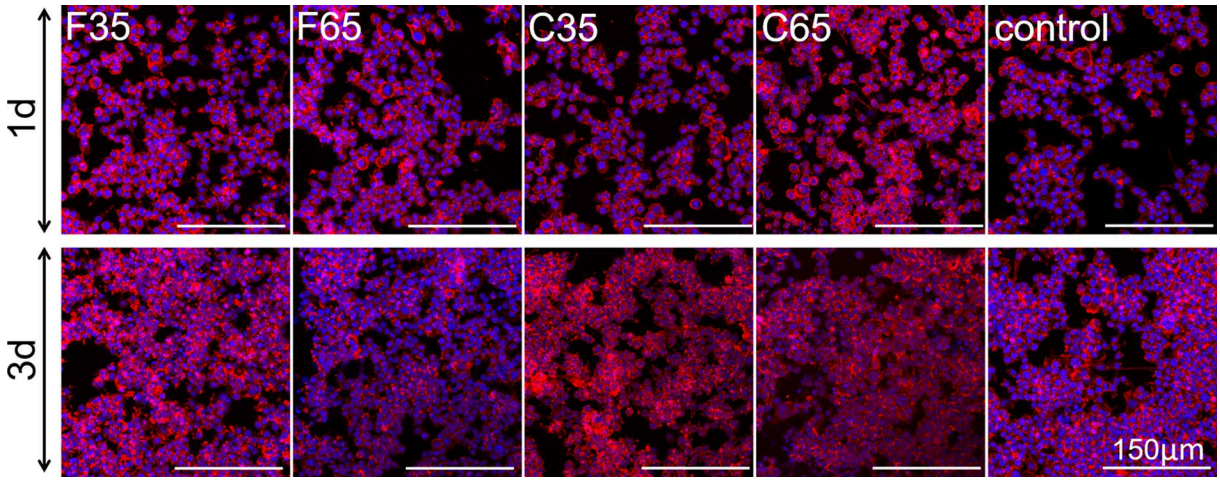

Supplementary Figure 2.2. Representative confocal images of morphology of RAW 264.7 cells on nano- and microstructured biomimetic hydroxyapatite at 1 and 3 day of cell culture. Cells were stained for F-actin (red) and nuclei (blue). RAW 264.7 seeded on glass coverslip were used as a control group. Scale bar in all images denotes 150 µm. The brightness and contrast of images was modified using Fiji/Image-J package.

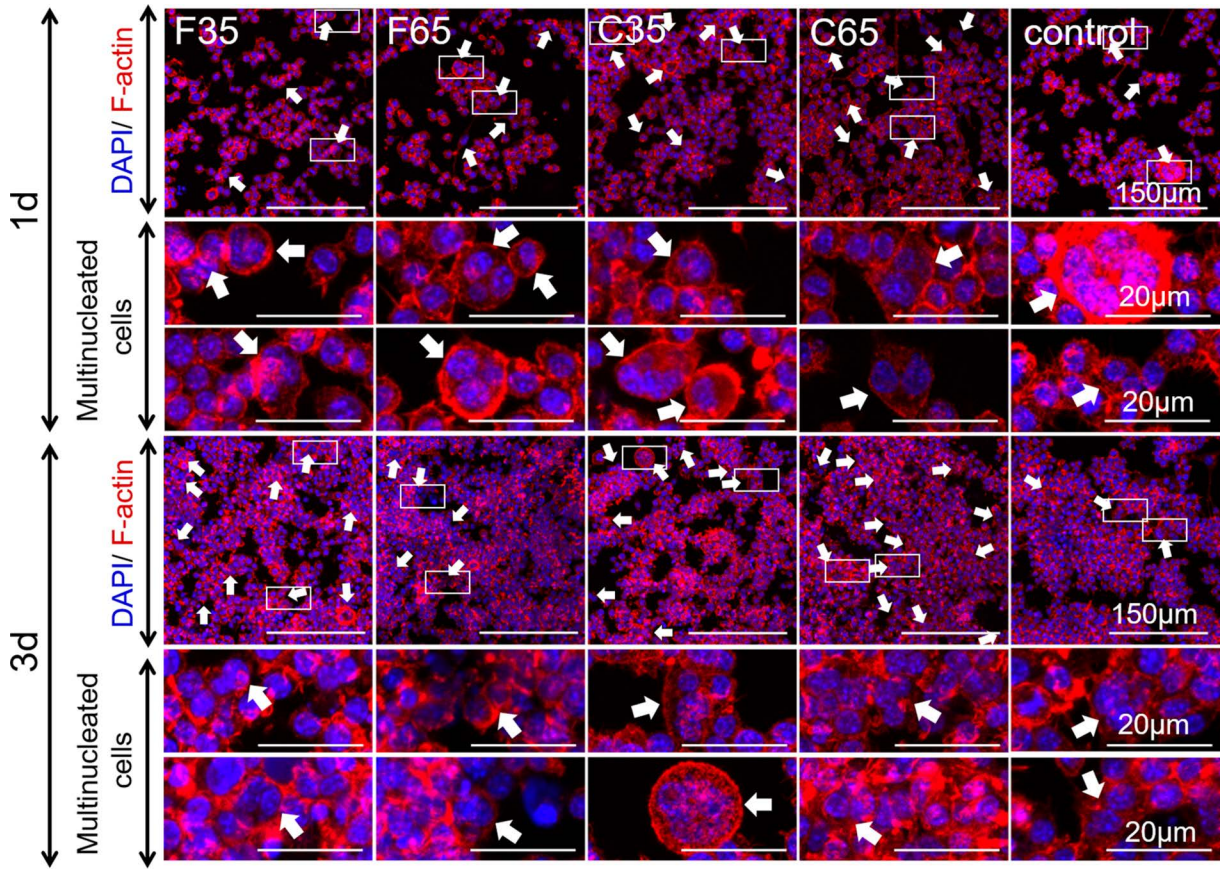

Supplementary Figure 2.3. The presence of multinucleated cells (white arrows) on nano- and microstructured hydroxyapatite at 1 and 3 day of cell culture. Cells were stained for F-actin (red) and nuclei (blue). RAW seeded on glass coverslip were used as a control group. The study revealed greater number of multinucleated cells on CDHA substrates compared to the control. Scale denotes 150 μm and for magnified images 20 μm. The brightness and contrast of images was modified using Fiji/Image-J package.

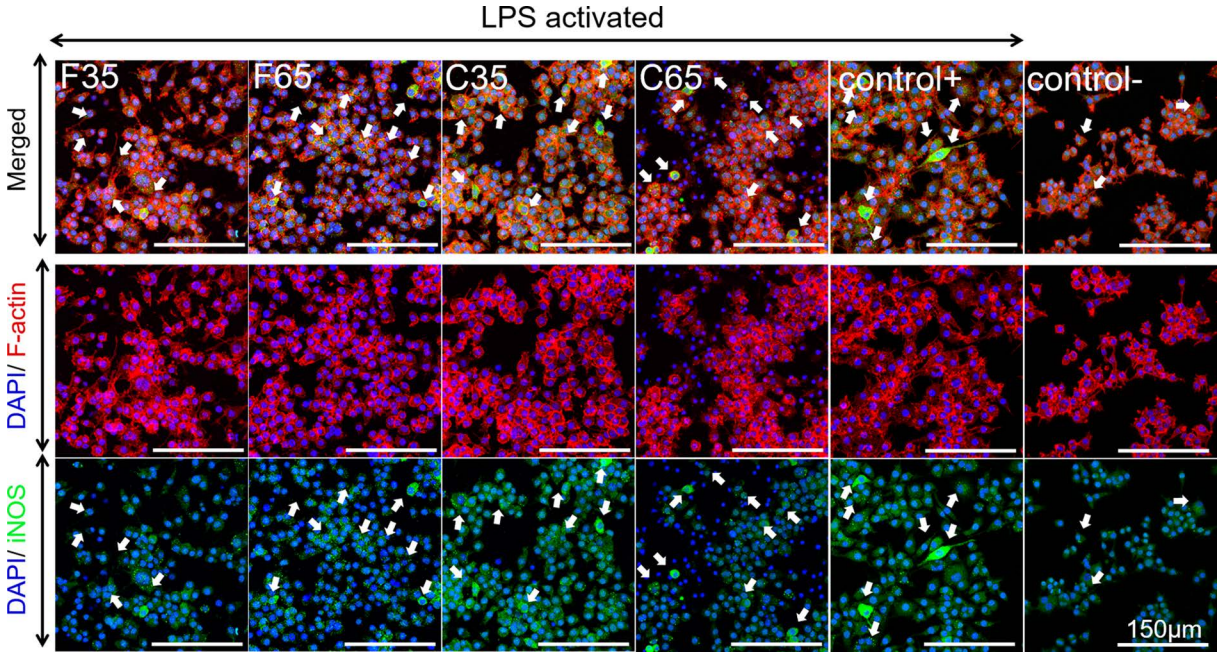

Supplementary Figure 2.4. The presence of iNOS-positively stained cells (white arrows) on CDHA substrates at 6 hours after post-stimulation. Cells were stained for F-actin (red), nuclei (blue) and iNOS (green). RAW cells seeded on glass coverslip were used as a control group. Control+ represents cells with LPS stimulation whilst control- cells without LPS stimulation. The iNOS staining of RAW cells confirmed successfully induced inflammatory environment on CDHA and control+. Scale denotes 150 µm. The brightness and contrast of images was modified using Fiji/Image-J package

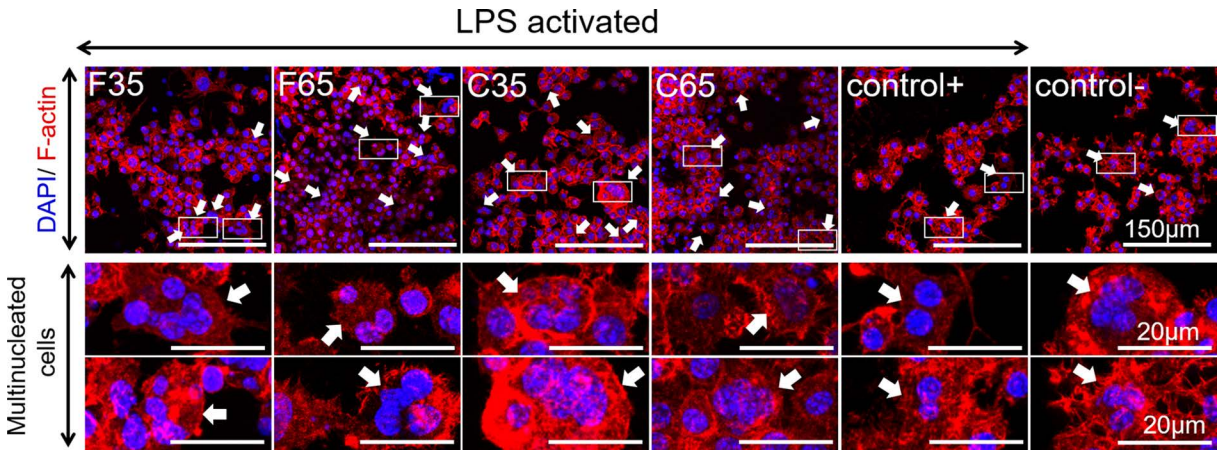

Supplementary Figure 2.5. The presence of multinucleated cells (white arrows) on nano- and microstructured hydroxyapatite at 6 hours of post LPS stimulation. Cells were stained for F-actin (red) and nuclei (blue). RAW cells seeded on glass coverslip were used as a control group. Control+ represents cells with LPS stimulation whilst control- cells without LPS stimulation. Scale denotes 150 µm and for magnified images 20 µm. The brightness and contrast of images was modified using Fiji/Image-J package.

Chapter 3

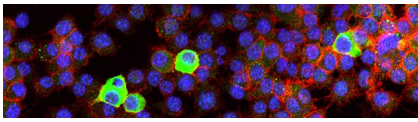

The influence of chemistry and surface topography of calcium phosphates on macrophage response under inflammatory environment

3.1 Introduction

The initial events after implantation of a biomaterial, this is, the inflammatory response provoked in the host, largely determines its long-term performance.[1-4] The inflammatory host response that involves the activation of numerous cell types, among them, macrophage polarization to either pro-inflammatory M1 or anti-inflammatory M2 phenotypes, with the consequent release of a wide range of mediator molecules[5,6], may result in different healing pathways.

In general, as a first step, the implantation of synthetic bone graft leads to the activation of M1 phenotype, which is coupled with the release of pro-inflammatory cytokines (mainly interleukin 6, IL-6; interleukin 1, IL-1 and tumour necrosis factor alpha, TNFα) and reactive species intermediates (reactive oxygen species, ROS and nitric oxide synthase NOS). This induces the necessary inflammatory phase, resulting in the recruitment of immune cells. Moreover, the chemoattractants and cytokines released in this phase stimulate the process of osteoclastogenesis.[7,8] The prolonged presence of the pro-inflammatory M1 phenotype produces chronic inflammation, including the expression of fibrous agents and granuloma formation and finally resulting in implant encapsulation and failure.[9] On contrary, the effective and timely switch from M1 to anti-inflammatory M2 phenotype will contribute to active bone tissue regeneration as the secretion of mannose receptors (CD206) and anti-inflammatory cytokines such as interleukin 10 (IL-10) from M2 macrophages[10] will attract bone cells and stimulate their osteogenic differentiation.[11,12] In general, the functionality of macrophages and thus their cytokine profile release is tightly linked to local environmental stimuli. The high plasticity of immune cells has fostered the development of different strategies to control macrophage polarization.[9] For instance, the exposure to microbial products such as lipopolysaccharide (LPS) activates M1 phenotype and is frequently applied to assess the anti-inflammatory capacity of biomaterials.[13]

Recently, the possibility to modulate macrophage polarisation by tuning biomaterial properties is attracting increasing attention. For instance, it has been shown that the functionality and polarization of immune cells can be influenced by chemical[14-19] or topographical[18-22] properties of biomaterials. Understanding how the macrophage-biomaterial interaction is translated into osteoclastic and osteogenic events would be of great interest in view of designing synthetic bone grafts with tailored features that foster bone formation.

In this context, CaPs are particularly relevant, since they are common bone substitutes due to their close resemblance to the mineral phase of bone and osteoinductive potential.[23-25] The effect of bulk CaPs on immune[26,27], osteoclastic[28-32] or bone forming cells[33] have been widely investigated. Nonetheless, there is a knowledge gap regarding the effect of the inflammatory environment created after CaPs implantation, on

osteoclastogenesis and osteogenesis processes. Although recent findings highlighted the role of some physicochemical properties of CaPs on modulating osteoimmune responses[34,35], the studies were limited to sintered ceramics such as β-tricalcium phosphate (β-TCP). Recently, biomimetic calcium phosphates, which are obtained at low temperature and have structural and compositional features much closer to the mineral phase of bone, were shown to have enhanced osteoinductive and osteogenic properties. Moreover, their structural features can be easily modified during synthesis process what allows obtaining biomimetic CaPs with various topographies from nano to micro range and trigger specific cell response. For instance, in previous chapter it was demonstrated that bringing the topography of biomimetic hydroxyapatite (CDHA) to nanoscale resulted in stimulation of osteogenic activities of bone forming cells whilst the increase of porosity of CDHA positively modulated its anti-inflammatory capacity.

The present chapter aims to study an interplay between the anti-inflammatory features of CaPs and the process of osteogenesis. The biomimetic CDHA is subjected to thermal treatment in order to obtained sintered β-TCP ceramic which is chemically different but presents similar Ca/P ratio and porosity. Afterwards, the anti-inflammatory and osteogenic capacity of biomimetic calcium deficient hydroxyapatite (CDHA) and a conventional β-TCP ceramic is investigated through evaluation of the release of inflammatory, osteoclastogenic and osteogenic factors from LPS-activated immune cells. Finally, the effect of the immune environment, created by immune cells and CaP substrate, on the osteogenic differentiation is assessed using bone marrow stromal cells and osteoblasts as a model of bone forming cells.

3.2 Materials and methods

3.2.1 Material preparation and characterisation

The synthesis of biomimetic CDHA and β-TCP samples was previously described.[36,37] Briefly, CDHA discs were prepared through a cementitious reaction using an α-tricalcium phosphate (α-TCP) paste. The solid phase, consisting of α-TCP powder with 2 wt.% of precipitated hydroxyapatite (pHA; Merck 2143, Merck, Darmstardt, Germany), was mixed with an aqueous solution of 2.5 wt.% disodium hydrogen phosphate (Na_2HPO_4; Panreac), at a 0.35 mL/g liquid-to-powder ratio (L/P) and transferred to Teflon moulds (6 mm of diameter, 2 mm of thickness). The samples were immersed in water at 37 ºC for 7 days to allow for complete reaction. The β-TCP discs were obtained by sintering the CDHA discs at 1100 ºC for 15 h.

The microstructure of CDHA and β-TCP was assessed by scanning electron microscopy (SEM; TESKAN MIRA3) with an acceleration voltage of 5 kV. Prior to visualisation, samples were sputtered with a thin layer of gold with EM SC005 Gold Coater (Leica). The surface roughness was determined by optical interferometry (Veeco Wyko

NT1100), using a 50x magnification and a scanned area of 47.5 x 63.4 μm^2. Images were acquired using Vision32 software.

3.2.2 Cell culture

The murine-derived macrophage cell line RAW 264.7 cells, human osteosarcoma cell line SaOS-2 and human BMSCs were used in current study. RAW 264.7 and SaOS-2 were expanded in Dulbecco's Modified Eagle Medium (DMEM; Gibco®, Life Technologies Pty Ltd., Australia Life Technologies) with heat-inactivated foetal calf serum (FCS; In Vitro Technologies, Australia FCS) and penicillin/streptomycin (50 U/ mL and 50 µg/ mL, respectively), (P/S; Gibco®, Life Technologies Pty Ltd., Australia Life Technologies). Cells were maintained at 37 °C with a 5 % CO_2 humidified incubator.

The BMSCs were isolated and cultured following the protocols established in previous reports.[18,38,39] Briefly, bone marrow was obtained from 50-60 year old patients undergoing knee or hip replacement. The informed consent was given from all donors and the procedure was approved by the Ethics Committee of Queensland University of Technology. The isolation of mononuclear cells from bone marrow was performed adding Lymphoprep (Axis-Shield PoC AS, Oslo, Norway) following the manufacturer's instructions. Subsequently, the cells were transferred to culture flasks with DMEM with 10 % of FCS and penicillin/streptomycin (50 U/mL and 50 µg/mL, respectively). Unattached hematopoietic cells were removed via medium changes. BMSCs in passage 4-5 were used in the current study.

3.2.3 Response of macrophages to CaPs substrates under inflammatory environment

CaPs samples were sterilised with 80 % of ethanol, rinsed three times with phosphate-buffered saline (PBS, Oxoid) and incubated overnight with complete DMEM. Afterwards, RAW cells were seeded on substrates at a density of 7×10^5 RAW cell/ cm^2. The anti-inflammatory capacity of CaPs substrates was studied through activation of M1 proinflammatory phenotype of macrophages with LPS treatment.[13,18] Briefly, the cell culture medium was replaced after 12 h with medium containing 1 µg/mL of LPS. After 2 h of incubation, LPS-containing medium was aspirated, samples were rinsed thrice with PBS and transferred to a new well plate. The RAW cells on CaPs substrates were then cultured additional 6 hours in serum-free cell culture medium. Subsequently, the CaPs-RAW conditioned medium were recovered for further experiments with BMSCs and SaOS-2 cells. Unless otherwise stated, the following experimental procedures were applied to LPS-stimulated RAW cells. The "control+" refers to RAW cells cultured on TCPS or glass coverslip and exposed to LPS stimulation whilst "control" refers to RAW cells cultured on TCPS or glass coverslip with standard cell culture DMEM media.

3.2.4 RAW cells morphology

The morphology of RAW cells cultured on CaP discs was evaluated using SEM (TESKAN MIRA3). Briefly, cells were washed with PBS and fixed with 3 % glutaldehyde at 4 ºC for 1 h. The process was followed by three risings with PBS and post-fixation with 1 % osmium tetraoxide for 1h. Subsequently, samples were incubated with increasing concentrations of ethanol (50 %, 70 %, 90 %, 100 %). Complete dehydration was achieved adding hexamethyldisilazane (HMDS). Samples were covered with a gold thin layer using EM SC005 Gold Coater (Leica) and visualised by SEM using 5 kV of an acceleration voltage.

The morphology of macrophages was additionally visualised using confocal microscopy (CLSM; Nikon A1) staining cells for F-actin, nuclei and nitric oxide synthase (iNOS). Cells were washed with PBS and fixed with 4 % paraformaldehyde (PFA) in PBS for 30 min. Then, cells were permeabilized with 0.1 % Triton X-100 in PBS for 15 min and blocked with 1 % bovine serum albumin (BSA) in PBS for 1 h. Cells were then incubated with rabbit polyclonal anti-iNOS in 1 % BSA (1:100, Abacam) for 1 h. Afterwards, cells were incubated with Alexa Fluor488 Conjugate anti-rabbit IgG (1:1000, Cell Signaling Technology, Danvers, MA) and Rhodamine phalloidin in 0.1 % Triton X-100 in PBS for 1 h (1:300) in the dark. The nuclei were counterstained through 2 min incubation with 4, 6-diamidino-2-phenylindole (DAPI) (1:1000) in 0.1 % Triton X-100 in PBS. Each step during all procedure was followed by three rinses for 5 min with 0.15 % glycine in PBS. Images were processed using Fiji/Image-J package and cell spreading, iNOS area and cell elongation ratio were determined semiquantitatively (n=20).

In parallel, RAW morphology on CaPs was also evaluated without LPS activation incubating RAW cells with CaPs substrates up to 3 days. Cell morphology was determined at day 1 and 3 through staining for F-actin and nuclei. Cell number was determined through nuclei counting using Fiji/Image-J package. Cell number was compared to control group (RAW seeded on glass coverslip) in order to discard cytotoxic effects of CaPs substrates.

3.2.5 Inflammatory, osteogenic and osteoclastogenic gene expression of macrophages

After the specified cell culture time, cells were lysed and total RNA was extracted using TRIzol reagent (Ambion™, Life Technologies Pty Ltd., Australia) following the manufacturer instructions. The concentration of total RNA was determined by NanoDrop ND-1000 spectrophotometer (NanoDrop technologies, Motchanin, DE, USA). Subsequently, 1000 ng of total RNA were reverse transcribed using DyNAmo™ cDNA Synthesis Kit (Genesearch, QLD, Australia). The cDNA template was amplified

with the Quantstudio TM Real-Time PCR machine (Applied Biosystems, Foster City, California, USA) using SYBR Green qPCR Master Mix (Life Technologies). The inflammatory RAW response to CaPs was determined analysing the gene expression of pro-inflammatory (IL-1β, IL-6, TNFα, iNOS) and anti-inflammatory (IL-10 and CD206) cytokines and surface markers. Osteogenic and osteoclastogenic activities of macrophages on CaPs were determined measuring the gene expression of specific markers (OSM, VEGF and TGFβ or CTSK, CAR2 and MMP9, respectively). The sequences of primers are listed in Table 3.1. The specificity of primers was determined by analysis of melt curves. The mean cycle threshold (Ct) value of each target gene was normalized against the Ct value of the endogenous control 18S. In order to compare the effect of two different chemistries of CaPs, the using comparative Ct ($2^{-\Delta\Delta CT}$) method[40] was applied where:

$$\Delta\Delta Ct = (Ct_{sample}\,(\text{gene of interest}) - Ct_{sample}\,(\text{endogenous reference gene})) - (Ct_{TCPS}\,(\text{gene of interest}) - Ct_{TCPS}\,(\text{endogenous reference gene})) \quad \text{(Eq. 3.1.)}$$

Control+ was used as a calibrator sample.

Table 3.1. Primers' sequences used in this study

Gene	Gene symbol	Primers' sequences (5'→ 3')
18S ribosomal RNA	18S	F:CGGAACTGAGGCCATGATTAAG R:GTATCTGATCGTCTTCGAACCTCC
Interleukin 1 beta	IL-1β	F:TGGAGAGTGTGGATCCCAAG R:GGTGCTGATGTACCAGTTGG
Interleukin 6	IL-6	F:ATAGTCCTTCCTACCCCAATTTCC R:GATGAATTGGATGGTCTTGGTCC
Tumor necrosis factor alpha	TNFα	F:CTGAACTTCGGGGTGATCGG R:GGCTTGTCACTCGAATTTTGAGA
Nitric oxide synthase	iNOS	F: CACCAAGCTGAACTTGAGCG R:CGTGGCTTTGGGCTCCTC
Interleukin 10	IL-10	F:CAGGACTTTAAGGGTTACTTG R:ATTTTCACAGGGGAGAAATC
Mannose receptor C type	CD206	F:AGACGAAATCCCTGCTACTG R:CACCCATTCGAAGGCATTC
Cathepsin K	CTSK	F:CCAGTTTTACAGCAGAGGTGTG R:CTTGCTTCCCTTCTGGGTG
Carbonic anhydrase 2	CAR2	F:AGCAGCGAGCAGATGTCTC R:TGAGCTGGACGCCAGTTG
Matrix metallopeptidase 9	MMP9	F:GGGCGTGTCTGGAGATTCG R:CACCTGGTTCACCTCATGGTC
Oncostatin M	OSM	F:ACGGTCCACTACAACACCAG R:CCATCGTCCCATTCCCTGAAG
Transforming growth factor beta 1	TGFβ1	F:CAGTACAGCAAGGTCCTTGC R:ACGTAGTAGACGATGGGCAG

Vascular endotelial growth factor A	VEGF A	F:GTCCCATGAAGTGATCAAGTTC R:TCTGCATGGTGATGTTGCTCTCTG
Runt-related transcription factor 2	Runx2	F:GACGAGGCAAGAGTTTCACC R:ATGAAATGCTTGGGAACTGC
Bone morphogenic protein 2	BMP-2	F:TGCCATTGTTCAGACGTTGG R:GTACTAGCGACACCCACAAC
Bone sialoprotein	BSP	F:TTTCTGCTACAACACTGGGCTATG R: TTGTTATATCCCCAGCCTTCTTG
Osteocalcin	OCN	F:GCAAAGGTGCAGCCTTTGTG R:GGCTCCCAGCCATTGATACAG
Collagen type I	COLL I	F:AGAACAGCGTGGCCT R:TCCGGTGTGACTCGT

3.2.6 Measurement of ion concentration of cell culture medium

The concentration of Ca^{2+} and P_i, with and without presence of RAW cells on CaPs, was evaluated in the medium by inductively coupled plasma-optical emission spectrometry (ICP-OES, Perkin Elmer, MA, USA). The sample supernatants were diluted 5-fold with 2 % of ultrapure nitric acid.

3.2.7 The effect of CaPs- RAW conditioned media on osteogenesis

The effect of the microenvironment created by the immune cells cultured on CaP substrates on osteogenesis was determined by incubating bone-forming cells with CaPs-RAW conditioned extracts. Briefly, BMSCs and SaOS-2 cells were separately seeded on tissue culture plastic (TCPS) at densities of 1×10^4 cells/cm^2 and 2.5×10^4 cells/cm^2, respectively. After 12 h of adhesion, cell culture medium was replaced with CaPs-RAW extract previously supplemented with 10 % of FCS and cells were incubated up to 3 days without medium change. Afterwards, the expression of osteogenesis-related genes (ALP, Runx2, COLL I, BSP, BMP-2 and OCN) was determined following the protocol described in section 2.5. The values of gene expression were normalised to 18S as a housekeeping gene and BMSCs+ and SaOS-2+ groups were used as a calibrator sample. Over following chapter "BMSCs+" and "SaOS-2+" refers to respectively mesenchymal and osteoblastic cells exposed to extracts from LPS-stimulated RAW cells.

Additionally, for SaOS-2 cells, the protein expression was determined through CLSM visualisation (for ALP) and western blot (for ALP, COLL I and Runx2). For CLSM analysis SaOS-2 cells were seeded on glass coverslip. Afterwards, standard fixation and staining protocol for CLSM visualisation were applied (section 3.2.4.). The rabbit anti-human ALP (1:100, Abacam) and Alexa Fluor488 Conjugate anti-rabbit IgG secondary antibody (1:1000, Cell Signalling Technology, Danvers, MA) were used as a primary and secondary antibody, respectively. Images were processed using Fiji/Image-J

package. The cell spreading, ALP area and cell elongation ratio was determined semiquantitatively (n=20) using the same software.

For western blot analysis, cells were lysed with RIPA buffer and total protein was quantified by Pierce™ BCA Protein Assay Kit (Thermo Fisher Scientific). Then, 20 µg of proteins were separated using SDS-PAGE, transferred onto a nitrocellulose membrane (Pall Corporation, East Hills, New York, USA) and blocked with Odyssey blocking buffer (LI-COR Biosciences, Lincoln, Nebraska, USA) for 1 h. The membrane was incubated overnight at 4 °C with antibodies against ALP, Runx2, COLL I or α-tubulin (all 1:1000, rabbit anti-human; Abcam, Cambridge, United Kingdom) followed by incubation with anti-mouse/rabbit IRDye 700/800 conjugated antibody (1:5000, Rockland, Gilbertsville, Pennsylvania, USA). In order to remove non-specific binding, washes with TBS-Tween buffer were performed between each incubation step. Bands were visualised by Odyssey infrared imaging system (LI-COR Biosciences, Lincoln, Nebraska, USA). The intensity of bands was determined through Fiji/Image-J package.

For the mineralization assay the BMSCs and SaOS-2 cells were seeded at a semi-confluent density of 3×10^4 cells/cm^2 and 6×10^4 cells/cm^2, respectively. After 24 h the medium was replaced with CaPs-RAW extracts combined with DMEM with osteogenic supplements: 50 µg/mL ascorbic acid, 10 mM β-glycerophosphate and 100 nM dexamethasone. The volume ratio between the CaPs-RAW extracts and DMEM with osteogenic supplements was 1:2. The medium was refreshed every third day. At 14 days of culture, cells were thoroughly washed with double distilled H_2O (ddH_2O) and the fixation was performed incubating cells with 4 % PFA for 15 min at RT. Afterwards, cells were incubated with Alizarin red solution (ARS) at pH 4.2 for 20 min. The unbound stain was removed through various rinsings with ddH_2O. The samples were air-dried and the images were acquired using a light microscope (Nikon ECLIPSE TS100).

3.2.8 Statistical analysis

The statistical analysis was performed using SPSS software (IBM SPSS, Armonk, NewYork, USA). The data was plotted as mean ± standard deviation (SD). The normality was checked through the Saphiro-Wilk test. In case of significance of Saphiro-Wilk test, the statistical differences between groups was determined by Mann-Whitney U test. In case of non-significant Saphiro-Wilk test, the statistical differences between groups was determined by T-Student test. For all tests, the level of significance was set for $p < 0.05$.

3.3 Results

3.3.1 Physicochemical characterisation of CaPs

SEM micrographs showed that the microstructure of biomimetic CDHA was formed of aggregates with plate-like crystals and average roughness (Ra) of 2.53 ± 0.72 µm. The sintering process applied to β-TCP led to coalescence of crystals within CDHA aggregates, resulting in polyhedral grain microstructure (Figure 3.1.) and lower Ra being 1.33 ± 0.23 µm. Further characterisation regarding substrates' SSA and porosity was described in a previous work[37] and displayed in Table 3.2.

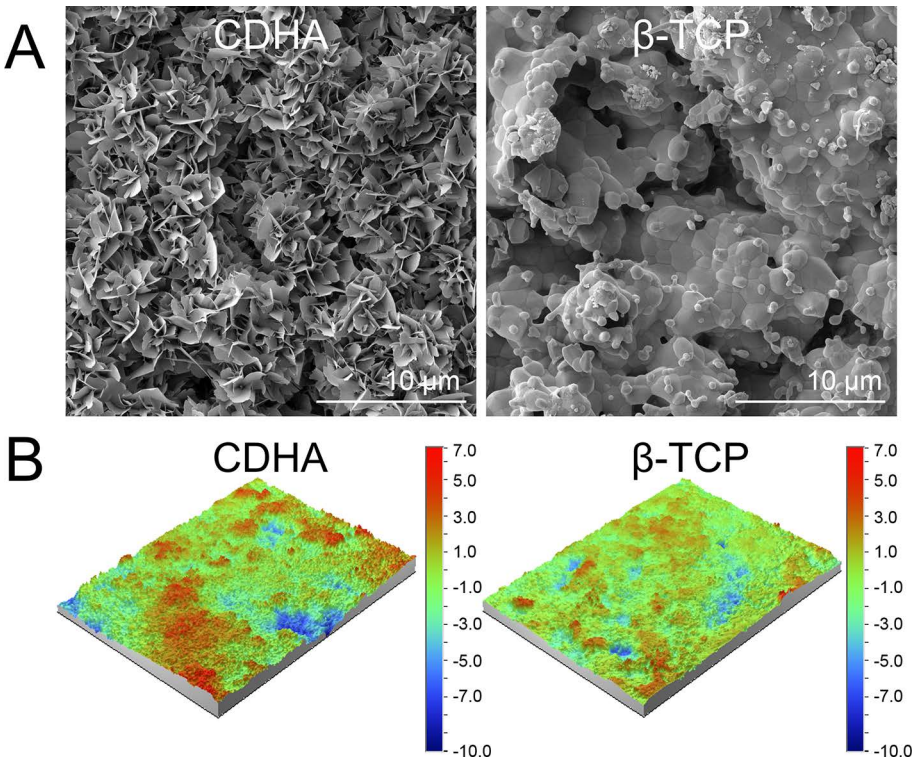

Figure 3.1. A) Representative SEM micrographs of CDHA and β-TCP surface morphology. **B)** Optical interferometry images of surface topography of CDHA and β-TCP substrates.

Table 3.2. Roughness, specific surface area (SSA) and porosity of CDHA and β-TCP.

Substrate	Roughness Ra (µm)	SSA (m^2/g)[37]	Porosity (%)[37]
CDHA	2.53 ± 0.72	14.11 ± 0.01	33.4
β-TCP	1.33 ± 0.23	0.38 ± 0.00	29.8

3.3.2 The response of RAW cells to CaP substrates under standard conditions

Macrophages adhered at similar numbers on CaP substrates and control. A progressive increase of cell number was observed from day 1 to day 3 of cell culture. β-TCP presented statistically significant higher number of RAW cells at day 3 compared to CDHA and control (Figure 3.2.).

In general, RAW cells cultured on CaPs and control presented a round-shaped morphology (Figure 3.3.). Moreover, macrophage organization into clusters was observed at day 3 for all conditions.

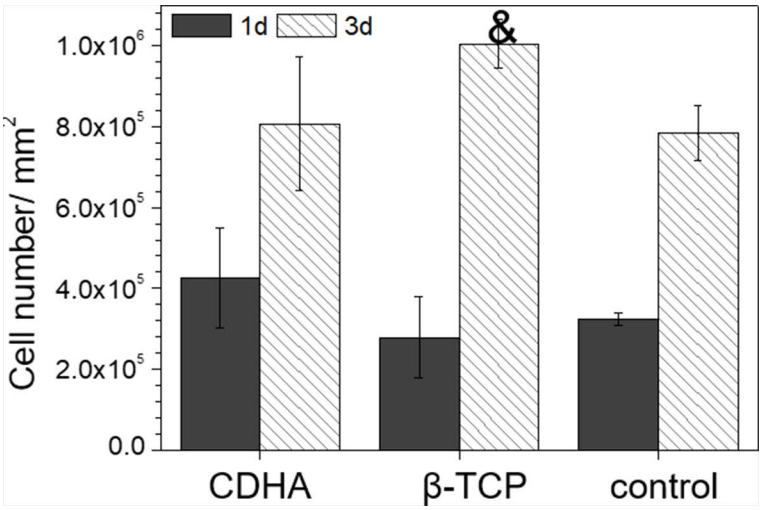

Figure 3.2. The number of attached RAW 264.7 cells to CaP substrates. The quantification was based on nuclei counting of CLSM images acquired at day 1 and day 3 of cell culture. "Control" refers to RAW 264.7 seeded on glass coverslip. & indicates statistically significant difference ($p < 0.05$) compared to control. No statistically significant difference ($p < 0.05$) was observed between CDHA and β-TCP substrate.

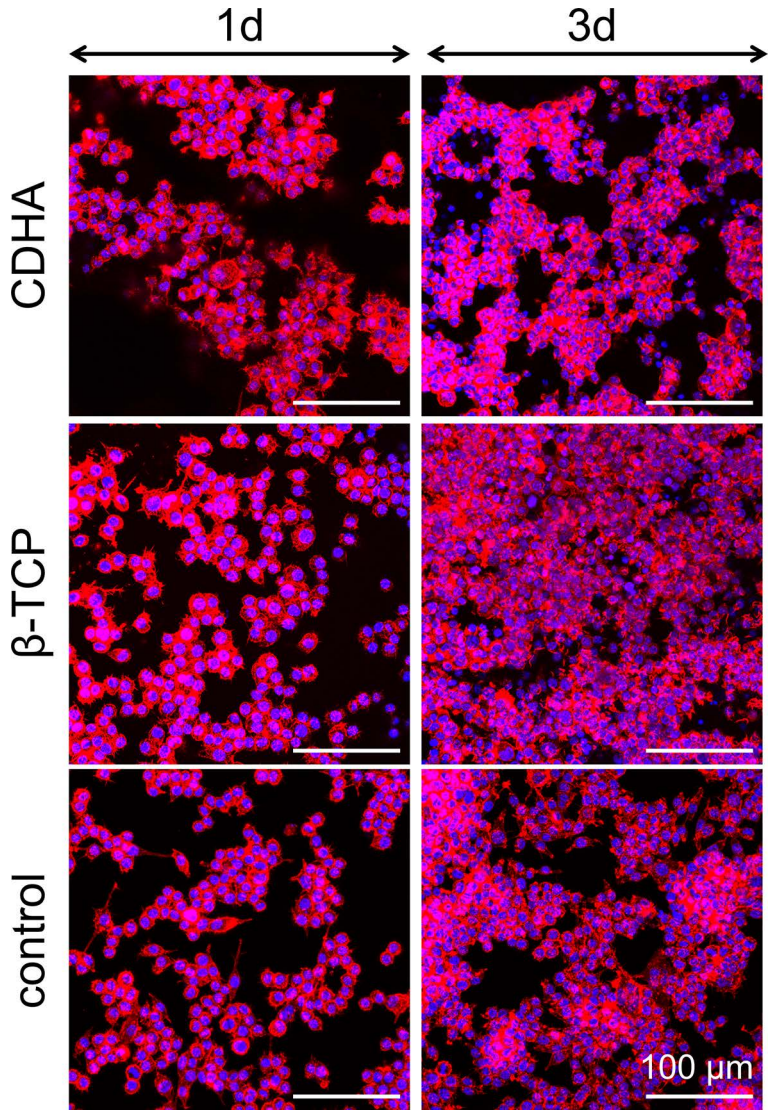

Figure 3.3. CLMS images of RAW 264.7 cells on CaP substrates at day 1 and 3 of cell culture. Cells were stained for F-actin (red) and nuclei (blue). "Control" refers to RAW 264.7 seeded on glass coverslip. The brightness and contrast of images were adjusted using Fiji/Image-J package.

3.3.3 The response of RAW cells to CaP substrates under inflammatory conditions

Inflammatory conditions were induced through incubation of RAW cells with LPS. Subsequently, the gene expression of macrophages cultured on CaPs was evaluated in terms of inflammatory, osteoclastic and osteogenic activities.

3.3.3.1 The inflammatory response of RAW cells cultured on CaPs

The gene expression of pro-inflammatory (IL-1β, IL-6, TNFα and iNOS) and anti-inflammatory (IL-10 and CD206) cytokines and surface markers are depicted in Figure 3.4.A. In general, RAW cells cultured on CaPs downregulated the expression of pro-inflammatory cytokines compared to cells cultured on TCPS (control+). These values

were approximately 4-fold (for IL-1 and IL-6) and 2-fold (for TNFα and iNOS) lower compared to control. Moreover, the downregulation of pro-inflammatory molecules was significantly more pronounced on β-TCP than on biomimetic CDHA. No statistically significant differences were observed for the expression of anti-inflammatory cytokine IL-10. However, CaP substrates downregulated the expression of anti-inflammatory surface marker CD206, more markedly in the case of β-TCP (Figure 3.4.A).

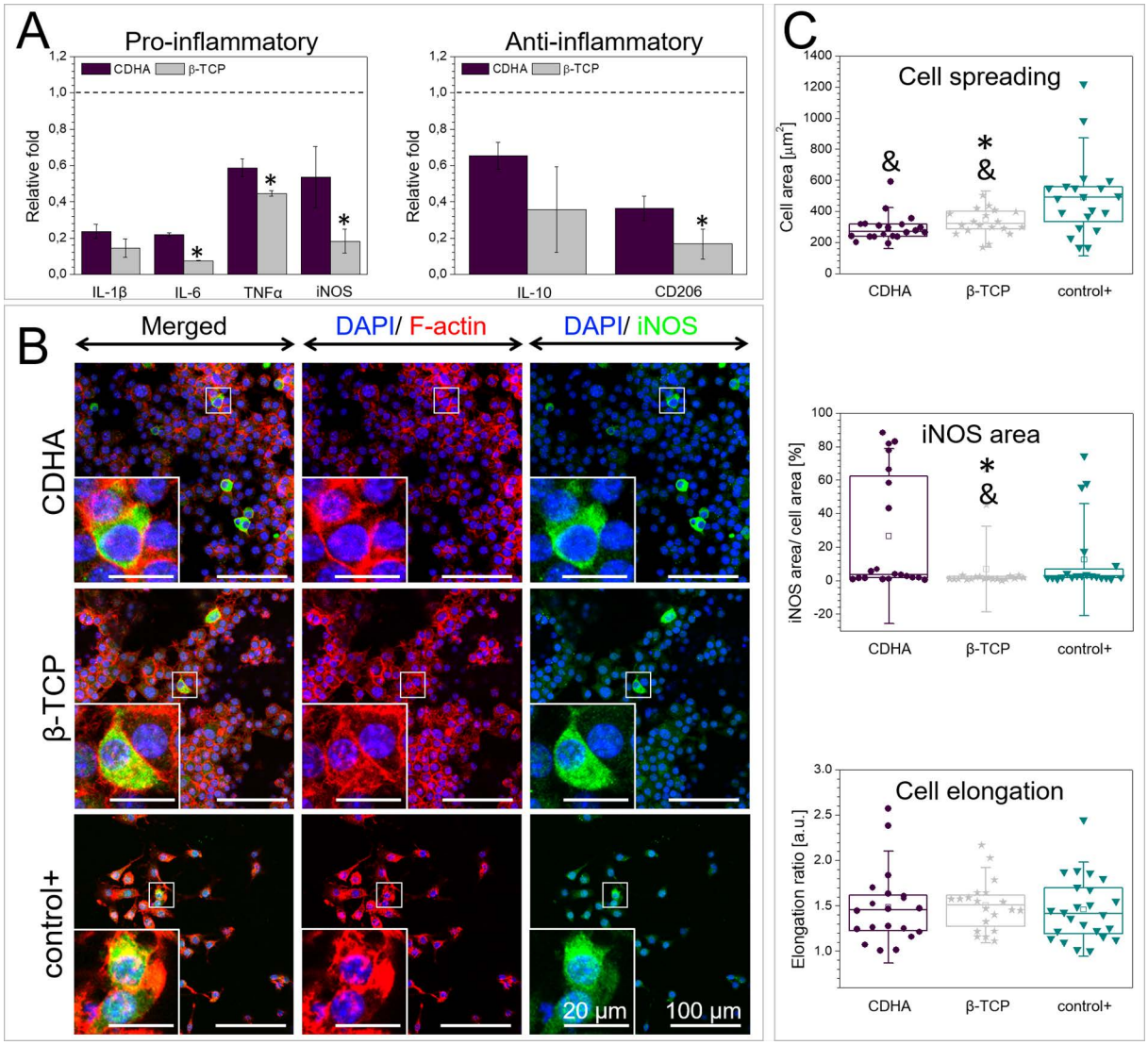

Figure 3.4. The response of RAW 264.7 cells to CaP substrates under inflammatory environment (6 hours after LPS stimulation). **A)** Relative expression of inflammation related genes: IL-1β, IL-6, TNFα, iNOS (pro-inflammatory) and IL-10 CD206 (anti-inflammatory) of RAW 264.7 cultured on CaP substrates. The values were normalised to 18S as an endogenous reference gene and using control+ as a calibrator sample. The dashed line indicates the relative fold equal to 1. * indicates statistically significant difference ($p < 0.05$) of β-TCP substrate compared to CDHA. **B)** Representative CLSM images of iNOS-positively stained RAW 264.7 cells on CaPs. Cells were stained for F-actin (red), nuclei (blue) and iNOS (green). The brightness and contrast of images were adjusted with Fiji/Image-J package. **C)** Semiquantitative analysis of RAW 264.7 spreading, iNOS occupied area and elongation ratio. Symbols represent individual cells (n=20), the boxes represent 25th and 75th percentile, the middle line is the median, the □ is the mean and whiskers are standard deviation. & indicates statistically significant difference ($p < 0.05$) compared to control+. * indicates statistically significant difference ($p < 0.05$) of β-TCP substrate compared to CDHA.

The anti-inflammatory capacity of CaPs was also assessed through visualisation of pro-inflammatory iNOS molecule (Figure 3.4.B). Thus, the reduction of iNOS-stained area of RAW were associated with higher anti-inflammatory capacity of the substrates. The presence of iNOS-positively stained RAW cells was observed in both CaP substrates. Nonetheless, β-TCP showed lower iNOS- stained area compared to CDHA and control+ group (Figure 3.4.C, middle graph).

The spreading area and elongation ratio of cells cultured on CaPs substrates provides an indication of the polarization of macrophages to either pro- or anti-inflammatory phenotype (Figure 3.4.C and Figure 3.5.).[41] RAW cells cultured on CaP substrates presented lower spreading area than the control+, this being more pronounced for macrophages cultured on CDHA (Figure 3.4.C, top). However, similar cell elongation ratios were observed for both substrates (Figure 3.4.C, bottom graph). The cell morphologies observed by SEM were compatible with both M1 and M2 macrophages on β-TCP and CDHA (Figure 3.5.).

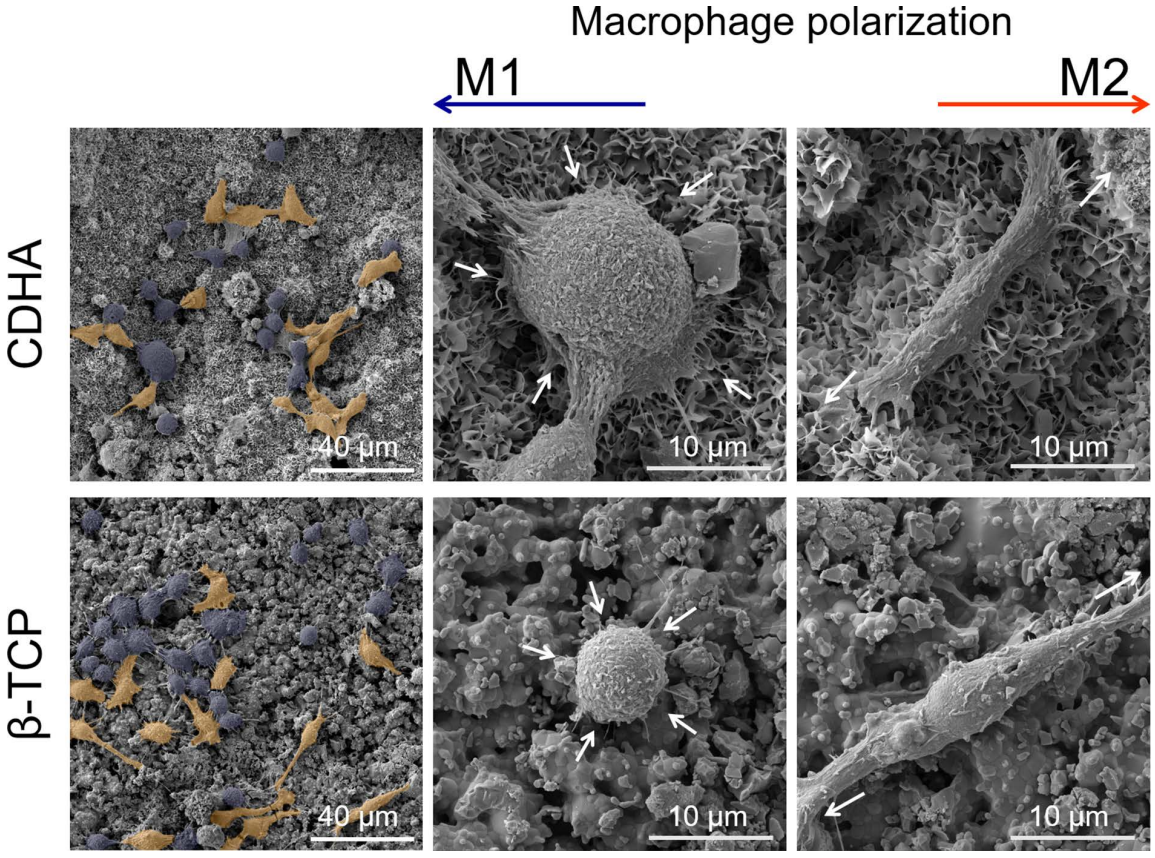

Figure 3.5. SEM micrographs of morphology of RAW264.7 on CaP substrates cultured under inflammatory environment (6 hours after LPS stimulation). Pseudo coloured blue and orange cells indicate macrophages with M1 and M2-like morphology, respectively. White arrows indicate putative direction of cell spreading.

3.3.3.2 Osteoclastic-like activity of RAW cells

The culture of RAW cells on CaP substrates resulted in the downregulation of osteoclastic marker genes (CTSK, CAR2 and MMP9) (Figure 3.6.). Similar decrease in the expression of CTSK and CAR2 genes was observed for CDHA and β-TCP, whilst the downregulation of MMP9 was more pronounced for β-TCP.

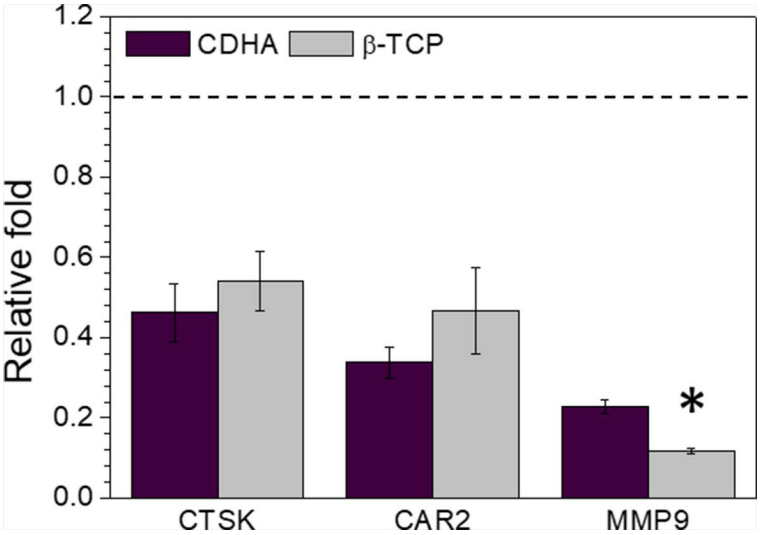

Figure 3.6. Relative expression of osteoclastogenesis related genes (CTSK, CAR2 and MMP9) of RAW 264.7 cells cultured on CaP substrates under inflammatory environment (6 hours after LPS stimulation). The values were normalised to 18S as an endogenous reference gene and using control+ as a calibrator sample. The dashed line indicates the relative fold equal to 1. *indicates statistically significant difference ($p < 0.05$) of β-TCP substrate compared to CDHA.

The levels of calcium and phosphate were monitored in presence or absence of cells (Figure 3.7.). The concentration of Ca^{2+} and P_i in the pristine cell culture medium were 1.66 ± 0.00 mM and 1.09 ± 0.02 mM, respectively. The immersion of CDHA in the cell culture medium resulted in a 17.19 ± 2.60 % decrease of Ca^{2+} concentration, which was counteracted by a slight increase in presence of the RAW cells (Figure 3.7.A). No alteration in Ca^{2+} concentration was observed for β-TCP. On the other hand, little alterations of phosphate were observed (Figure 3.7.B) in any of the culture conditions.

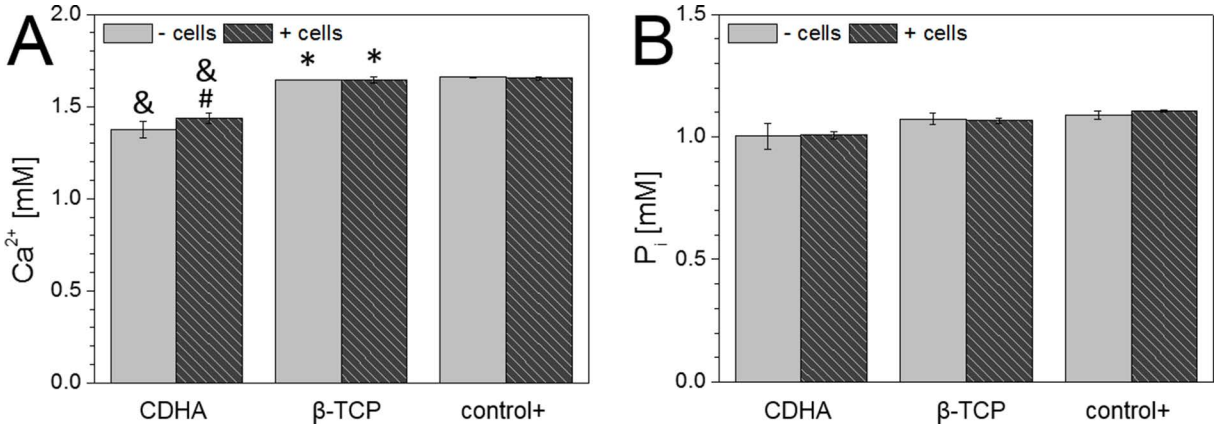

Figure 3.7. Ionic alterations of calcium and phosphate cause by CaP substrates in absence and presence of macrophages. Calcium and phosphate levels were determined after 6 hours of LPS-stimulation of RAW 264.7 cells. **A)** Ionic concentration of calcium **B)** Ionic concentration of phosphate. For each substrate, # indicates statistically significant difference ($p < 0.05$) between ionic concentration of cell culture medium with or without cells. & indicates statistically significant difference ($p < 0.05$) compared to corresponding control group *i.e.* cell culture medium with or without cells. * indicates statistically significant difference ($p < 0.5$) of β-TCP substrate compared to CDHA.

The resorptive activity of RAW on CaPs was also evaluated through SEM visualisation of the cell-material interphase (Figure 3.8.A). The morphology of the CaP substrate areas adjacent to the RAW cells was similar to the pristine substrate, with no signs of degraded crystals. Few multinucleated cells, which could be associated to a resorptive activity, were found on both CDHA and β-TCP (Figure 3.8.B).

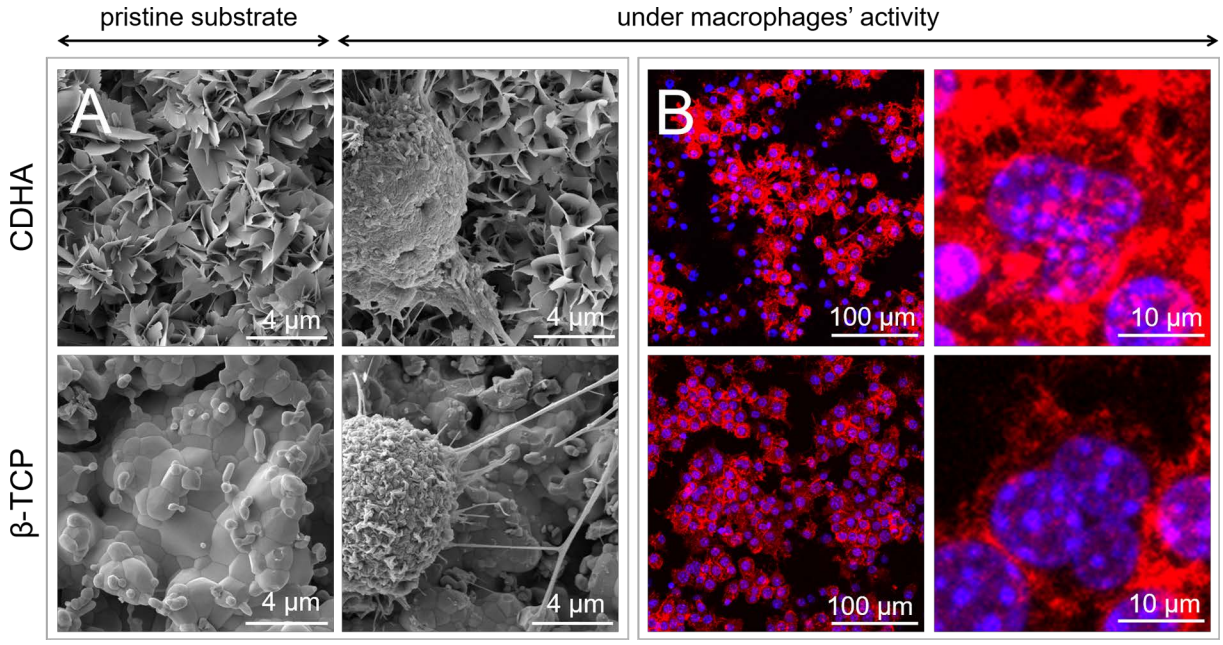

Figure 3.8. Osteoclastic activity of RAW 264.7 on CaP substrates under inflammatory environment (6 hours after LPS stimulation). **A)** Representative SEM micrographs: left panel: pristine CaP substrate, right panel: CaPs-RAW 264.7 interface. No signs of crystal degradation were observed. **B)** Representative CLMS images of multinucleated macrophages on CaPs: left panel: general view, right panel: detailed view. Cells were stained for F-actin (red) and nuclei (blue). The brightness and contrast of images were adjusted with Fiji/Image-J package.

3.3.4 The impact of RAW cells- CaP microenvironment on osteogenesis

The ability of macrophages cultured on CaP substrates to stimulate osteogenesis was analysed using two different strategies: i) evaluating the expression of osteogenic factors by RAW cells; ii) assessing the capacity of the macrophage-secreted molecules to induce the osteogenic differentiation of either BMSCs or SaOS-2, using RAW-CaPs extracts.

A downregulation of the expression of osteogenesis-related genes (OSM, TGFβ1 and VEGF) was observed when RAW cells were cultured on CaP substrates, more pronounced on CDHA than on sintered β-TCP, although the differences were no statistically significant for TGFβ1 and VEGF (Figure 3.9.A).

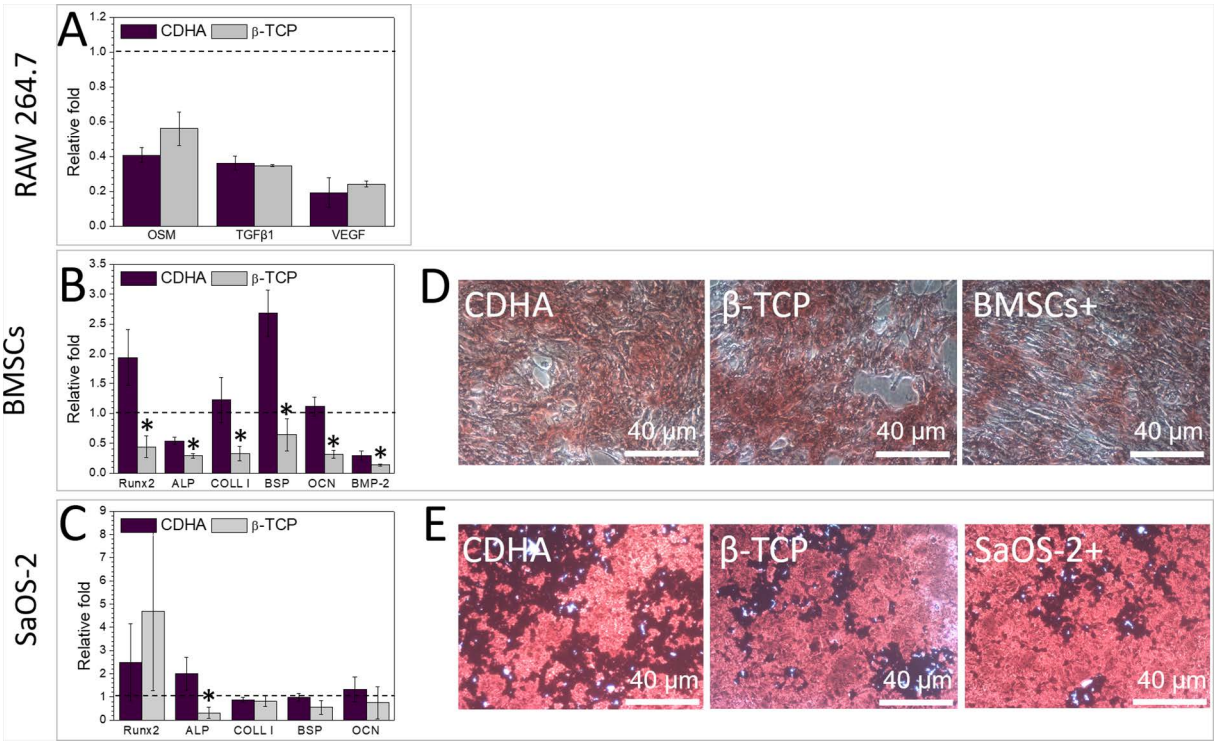

Figure 3.9. The impact of osteoimmune environment on osteogenesis. **A)** Relative expression of osteogenic factors (OSM, TGFβ and VEGF) from macrophages cultured on CaP substrates under inflammatory environment. **B)** and **C)** The effect of CaPs-RAW 264.7 conditioned medium on osteogenic gene expression of BMSCs (Runx2, ALP, COLL I, BSP, OCN, BMP-2) and SaOS-2 (Runx2, ALP, COLL I, BSP, OCN), respectively. For A, B and C, the values of gene expression were normalised to 18S as an endogenous reference gene. Respectively for A, B and C the control+, BMSCs+ and SaOS-2+ groups were used as a calibrator sample. The dashed line indicates the relative fold equal to 1. * indicates statistically significant difference ($p<0.05$) of β-TCP substrate compared to CDHA. The "BMSCs+" and "SaOS-2+" refers to cells incubated with extracts from LPS-stimulated RAW cells. **D)** and **E)** The effect of CaPs- RAW 264.7 conditioned medium on mineralization of BMSCs and SaOS-2, respectively.

Stimulation of BMSCs with RAW-β-TCP conditioned medium produced a significant downregulation on the gene expression of osteogenesis-related markers (Runx2, ALP, COLL I, BSP, OCN and BMP-2) compared to cells cultured with RAW-CDHA extracts (Figure 3.9.B). The incubation with RAW-CDHA extracts resulted in upregulation of Runx2 and BSP compared to BMSCs+. No significant impact on mineralization was observed showing similar ability of BMSCs to generate calcium deposits and nodule formation, irrespective of the RAW-CaP extract stimulation (Figure 3.9.D).

Overall, SaOS-2 cells showed to be less prone to extract stimulation compared to BMSCs. Incubation with RAW-β-TCP extract resulted in an increase of Runx2 gene expression and a decrease of BSP, OCN and ALP levels, being statistically significant only for ALP (Figure 3.9.C). Noteworthy, expression of BMP-2 was not detected for SaOS-2 cells. In general, little upregulation of osteogenic markers was observed for RAW-CaP extracts compared to SaOS-2+. Moreover, SaOS-2 cells presented a more intensive Alizarin Red staining suggesting higher calcium deposition and nodule formation compared to BMSCs (Figure 3.9.E). No differences in terms of mineralization were detected for SaOS-2 cells stimulated with either RAW-β-TCP or RAW-CDHA extract.

In general, the effect of RAW-CaP extracts on the osteogenic response of SaOS-2 cells was more pronounced in protein (Runx2, ALP and OPN) secretion evaluated through western blot (Figure 3.10.C and 3.10.D). Overall, the production of the three measured proteins was significantly higher in SaOS-2 cells stimulated with RAW-CaP conditioned medium compared to cells incubated with extracts from LPS-stimulated RAW cells (SaOS-2+) (Figure 3.10.D). Moreover, the secretion of COLL I by SaOS-2 cells was more pronounced after incubation with RAW-CDHA extracts. Additionally, the ALP protein expression was visualised using CLSM technique (Figure 3.10.A). The cell spreading area was higher in SaOS-2 cells cultured with RAW-CDHA extract compared to SaOS-2+ group (Figure 3.10.B, left graph). No impact of RAW-CaP conditioned medium on SaOS-2 morphology and elongation ratio was observed (Figure 3.10.B).

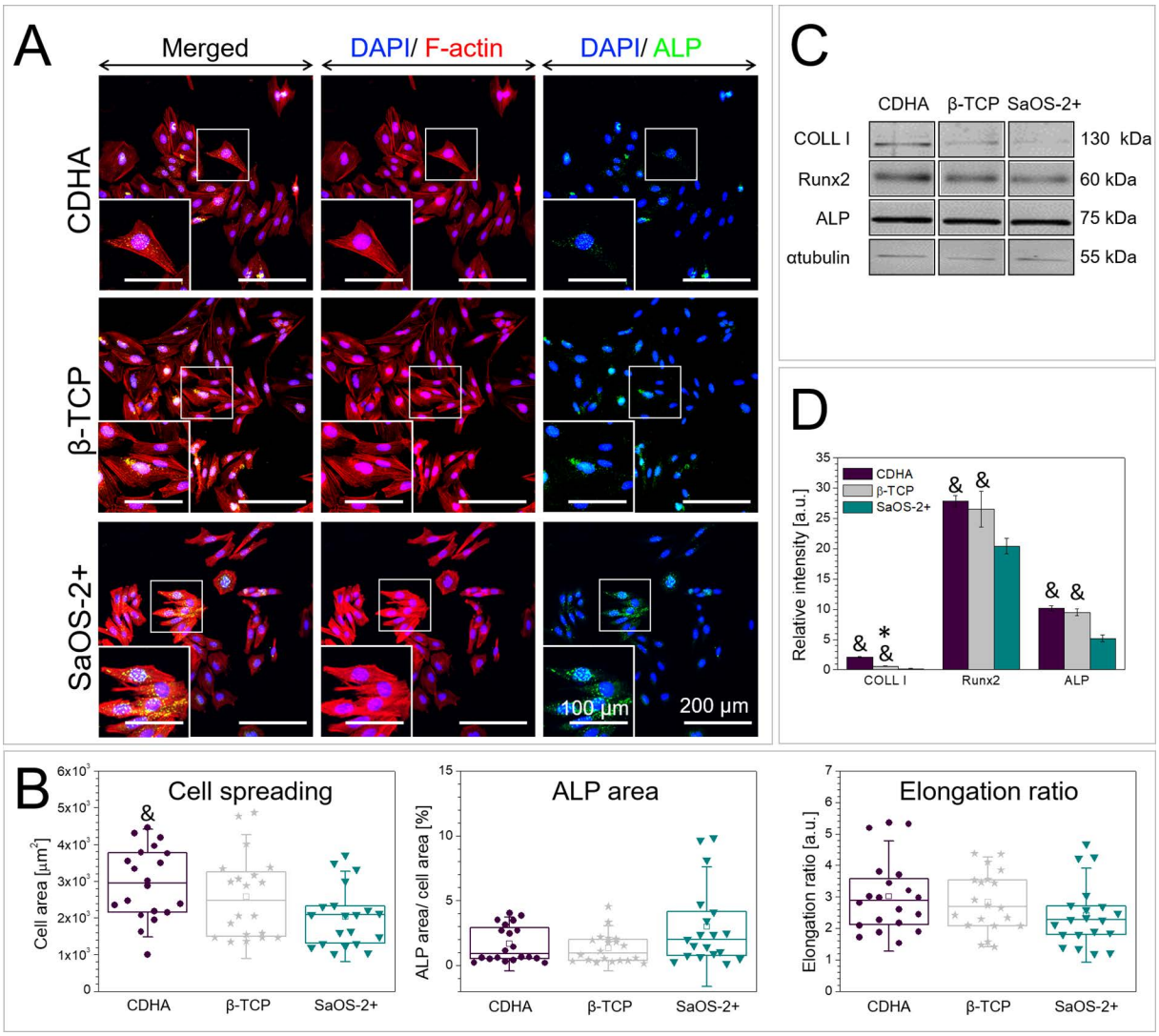

Figure 3.10. The effect of RAW cells-CaP conditioned medium on protein expression and morphology of SaOs-2 cells. **A)** Representative CLMS images of SaOS-2 after 3 day exposure to CaPs- RAW extracts. Cells were stained for F-actin (red), nuclei (blue) and ALP (green). The brightness and contrast of images was adjusted with Fiji/Image-J package. **B)** Semiquantitative analysis of SaOs-2 spreading, ALP occupied area and elongation ratio. Symbols represent individual cells (n=20), the boxes represent 25th and 75th percentile, the middle line is the median, the □ is the mean and whiskers are standard deviation. * indicates statistically significant difference ($p < 0.05$) compared to SaOS-2+. No significant differences were observed between substrates. **C)** Expression of osteogenesis related proteins (COLL I, Runx2, ALP) detected by Western blot **D)** Corresponding relative intensity of Western Blot bands. &Indicates statistically significant difference ($p < 0.05$) compared to control+. * indicates statistically significant difference ($p < 0.05$) compared to CDHA. In all figures, "SaOS-2 +" refers to cells incubated with with extracts from LPS-stimulated RAW cells.

3.4 Discussion

The capacity of biomaterials to modulate macrophage polarisation has been object of different studies.[2,16,18,20-22,42-44] In the field of synthetic bone grafts this is especially relevant, since tuning the inflammatory response may allow fostering the osteogenic properties of these materials. The present work addressed the interaction of two different bone substitutes, namely β-TCP and CDHA with immune cells. Although the elemental

composition of these two compounds is identical, both having a Ca/P ratio of 1.5, the different synthetic routes followed in each case, *i.e.* biomimetic precipitation for CDHA and high-temperature sintering for β-TCP, result in different crystal structure, surface topography, roughness and specific surface area (Figure 3.1., Table 3.2.).[37] The RAW 264.7 cell line was used as a model to study CaPs influence on immune cells response. The analysis of cell number revealed that both CaPs supported adhesion and proliferation of macrophages (Figures 3.2. and 3.3.), in agreement with previous studies.[45] This is particularly important as the accumulation of macrophages at early stage of inflammation is a contributing factor to wound repair.[46] Although CDHA caused a decrease of Ca^{2+} concentration in the cell culture medium, associated to the maturation of the apatitic phase, as reported previously for this type of material[47], the small sample size mitigated the extent of the ionic fluctuations, reducing the impact in cell proliferation.[37,48,49] Although immune cells have been reported to be sensitive to the textural features of the substrate, previous studies showed that the impact was rather in the phenotypic switch[3,50] and cytokine release[18,19,51] than in cell proliferation.

In order to assess the anti-inflammatory capacity of CaPs, macrophages were firstly stimulated with LPS. This molecule of bacterial origin activates pro-inflammatory M1 phenotype[52] and cytokine release[53] and is commonly used in inflammation related studies.[54] The induction of the pro-inflammatory state was confirmed by the presence of iNOS-positively stained cells for both CaP substrates (Figure 3.4.B). Interestingly, the cells cultured on β-TCP exhibited a significantly higher reduction of iNOS area (Figure 3.4.C, middle graph). Moreover, although both biomimetic CDHA and sintered β-TCP significantly downregulated the expression of pro-inflammatory cytokines compared to LPS-stimulated RAW cells (control+) (Figure 3.4.A), the reduction was more pronounced for β-TCP. The enhanced suppression of pro-inflammatory state by β-TCP is likely due to reduced levels of iNOS. For instance, Chamberlain *et al.* suggested a close relation between the reduction of local pro-inflammatory response and low levels of nitric oxides.[55]

The inflammatory activation of macrophages is normally associated to morphological changes.[52] Whereas the anti-inflammatory M2 phenotype is usually characterised by a more elongated aspect[9,41], pro-inflammatory macrophages exhibit rounded- like shapes accompanied with an enlargement of the spreading area.[9,56] The SEM images revealed a heterogeneous profile of the macrophages cultured on CDHA and β-TCP, with presence of both M1 and M2 morphological features (Figure 3.5.). Although no significant differences were found in terms of the elongation ratio (Figure 3.4., bottom graph), RAW cells presented smaller spreading areas on the CaP substrates compared to control+ (Figure 3.4.C, upper graph), which can be related to the downregulation of pro-inflammatory cytokines by CaPs (Figure 3.4.A).

Beyond the immune reaction, the macrophages are known to control osteogenesis and osteoclastogenesis through the release of a wide range of molecules. Moreover, macrophages, as osteoclast precursor cells, can exhibit some osteoclastic-like activity, such as the expression of osteoclastic enzymes, or the capacity to resorb CaP substrates.[34] Although previous studies reported a stimulatory effect of CaPs chemistry and topography osteoclastic differentiation[31,34], little osteoclastic activity of RAW cells cultured either on CDHA or on β-TCP was observed. For instance, no actin rings were present in the multinucleated RAW cells (Figure 3.8.), a morphological feature of osteoblastic-like cells through which they create sealed regions that can be subjected to acidic resorption.[57] Likewise, no signs of degradation were found in the CaP substrates (Figure 3.8.A), the microstructure of the substrate remaining intact in the cell-biomaterial interphases. There was no evidence either of ionic alterations, like an increase of calcium concentration in the cell culture medium, which might have been the result of the resorptive activity of cells (Figure 3.7.A and 3.7.B).[31,34] Moreover, little differences were observed in the expression of osteoclastogenic molecules (CTSK, CAR2 and MMP9) (Figure 3.7). Even though osteoclastic response of macrophages to bone grafts can be observed at short time of cell culture[29,34], the incubation of RAW cells with the CaP substrates without any additional stimulation probably prevented them from revealing their putative osteoclastic nature. Indeed, the RAW cells do not represent fully functional osteoclastic cells.[58] The full differentiation of monocytes/macrophages to osteoclasts, and hence specific osteoclastic behaviour can be only triggered through stimulation with RANKL, OPG and M-CSF.[59]

The crosstalk between immune cells and the bone forming cells is essential to complete the inflammation stage and to initiate the new bone formation. The release of inflammatory cytokines by macrophages is accompanied with the release of a wide range of factors like BMP-2, OSM[11,60], VEGF[10] or TGFβ1.[61] In this way, the immune cells create osteoimmune environment and actively participate in osteogenesis. Present chapter studied the simultaneous effect of secreted molecules from RAW cells cultured on CaPs and the ionic environment produced by the interaction of the CaP substrates with the cell culture medium, on the osteogenic differentiation of mesenchymal and osteoblastic cells (Figure 3.9. and 3.10.). For both CDHA and β-TCP, the expression of osteogenesis related molecules from RAW cells (TGFβ1 and VEGF) was observed (Figure 3.9.A). Noteworthy, the exposure of BMSCs to CDHA-RAW conditioned medium resulted in higher values of Runx2 and BSP (Figure 3.9.B). This result is particularly interesting since CDHA activated to greater extent the expression of pro-inflammatory cytokines by macrophages compared to β-TCP (Figure 3.4.A), which would be expected to result in attenuated osteogenic gene expression by bone forming cells.[62,63] However, some studies have underlined that the proper combination of pro-inflammatory molecules, e.g. IL-1β and TNFα, might also lead to enhanced osteogenic differentiation as well as formation of calcium deposits and nodules.[12,64,65] Another

interesting fact is that RAW cultured on CDHA simultaneously expressed higher levels of anti-inflammatory IL-10 and CD206 compared to β-TCP, which was previously associated with M2b macrophages - a subtype of anti-inflammatory immune cells.[66] Previous work demonstrated that incubation of MSCs with CaPs extracts, and thus exposing them to CaP-conditioned environment, was not sufficient stimulus to induce differentiation of MSCs into osteoblastic lineage.[37] Therefore, the enhanced osteogenic differentiation of BMSCs observed in current study should be likely associated with the release of osteogenic factors and inflammatory molecules from RAW cells cultured on CaP substrates rather than with the microenvironment created by CaPs after immersion in cell culture medium.

Finally, the effect of RAW-CaPs osteoimmune environment on osteoblastic SaOS-2 cells was assessed. In general, osteoblastic gene expression of SaOS-2 was not significantly affected when exposed to the RAW cells supernatants, except in the case of downregulation ALP for the β-TCP-RAW extract compared to CDHA-RAW extract (Figure 3.9.C). The semiquantitative analysis of CLMS images showed enhanced cell spreading[67] after exposure to RAW-CDHA supernatants, what might suggest greater capacity of microenvironment created by this substrate to induce osteogenic differentiation (Figure 3.10.A and 3.10.B).[67] Moreover, the effect of osteoimmune environment was reflected in protein expression (Runx2, COLL I and ALP) (Figures 3.10.C and 3.10.D). The results agree with those obtained for BMSCs, showing that more favourable environment for osteogenesis is obtained when immune cells are cultured on biomimetic CDHA. Nonetheless, better comprehending of this relation requires further *in vitro* investigation of signalling pathways responsible for enhanced osteogenic differentiation of bone forming cells.

3.5 Conclusions

In general, sintered β-TCP reduced to greater extent the release of inflammatory cytokines compared to biomimetic CDHA. Nonetheless, the microenvironment created after culturing macrophages on CDHA showed more potent osteogenic effects, fostering osteogenic differentiation of both BMSC and SaOS-2 cells, although more markedly in BMSCs.

Overall, the results from the present work demonstrated that chemically and texturally distinct calcium phosphates modulate differently the immune cell response. This opens the door to new strategies of design smart cell-instructive biomaterials that adapt their performance during all stages of bone healing process starting from early inflammatory phase until osteogenesis.

3.6 Bibliography

1. Franz, S., Rammelt, S., Scharnweber, D. & Simon, J. C. Immune responses to implants – A review of the implications for the design of immunomodulatory biomaterials. *Biomaterials* **32**, 6692–6709 (2011).
2. Chen, Z. *et al.* Osteoimmunomodulation for the development of advanced bone biomaterials. *Mater. Today* **19**, 304–321 (2016).
3. Chen, Z. *et al.* Nanotopography-based strategy for the precise manipulation of osteoimmunomodulation in bone regeneration. *Nanoscale* **9**, 18129–18152 (2017).
4. Chen, Z., Wu, C. & Xiao, Y. Convergence of Osteoimmunology and Immunomodulation for the Development and Assessment of Bone Biomaterials. in *The Immune Response to Implanted Materials and Devices* (ed. Corradetti B.) 107–124 (Springer International Publishing, 2017).
5. Jong, Y. K., Khang, D., Jong, E. L. & Webster, T. J. Decreased macrophage density on carbon nanotube patterns on polycarbonate urethane. *J. Biomed. Mater. Res. - Part A* **88**, 419–426 (2009).
6. Anderson, J. M., Rodriguez, A. & Chang, D. T. Foreign body reaction to biomaterials. *Semin. Immunol.* **20**, 86–100 (2008).
7. Devlin, R. D., Reddy, S. V., Savino, R., Ciliberto, G. & Roodman, G. D. IL-6 mediates the effects of IL-1 or TNF, but not PTHrP or 1,25(OH)2D3, on osteoclast-like cell formation in normal human bone marrow cultures. *J. Bone Miner. Res.* **13**, 393–399 (1998).
8. Abdel Meguid, M. H., Hamad, Y. H., Swilam, R. S. & Barakat, M. S. Relation of interleukin-6 in rheumatoid arthritis patients to systemic bone loss and structural bone damage. *Rheumatol. Int.* **33**, 697–703 (2013).
9. Sridharan, R. *et al.* Biomaterial based modulation of macrophage polarization: A review and suggested design principles. *Mater. Today* **18**, 313–325 (2015).
10. Wu, A. C., Raggatt, L. J., Alexander, K. A. & Pettit, A. R. Unraveling macrophage contributions to bone repair. *Bonekey Rep.* **2**, 1–7 (2013).
11. Guihard, P. *et al.* Induction of osteogenesis in mesenchymal stem cells by activated monocytes/macrophages depends on oncostatin M signaling. *Stem Cells* **30**, 762–772 (2012).
12. Rifas, L. T-cell cytokine induction of BMP-2 regulates human mesenchymal stromal cell differentiation and mineralization. *J. Cell. Biochem.* **98**, 706–714 (2006).
13. Han, S., Chen, Z., Han, P., Hu, Q. & Xiao, Y. Activation of Macrophages by Lipopolysaccharide for Assessing the Immunomodulatory Property of Biomaterials. *Tissue Eng. Part A* **23**, 1100–1109 (2017).
14. Arima, Y. & Iwata, H. Effect of wettability and surface functional groups on protein adsorption and cell adhesion using well-defined mixed self-assembled monolayers. *Biomaterials* **28**, 3074–3082 (2007).
15. Faucheux, N., Schweiss, R., Lützow, K., Werner, C. & Groth, T. Self-assembled monolayers with different terminating groups as model substrates for cell adhesion studies. *Biomaterials* **25**, 2721–2730 (2004).
16. Schutte, R. J., Parisi-Amon, A. & Reichert, W. M. Cytokine profiling using monocytes/macrophages cultured on common biomaterials with a range of surface chemistries. *J. Biomed. Mater. Res. - Part A* **88**, 128–139 (2009).
17. McBane, J. E., Matheson, L. A., Sharifpoor, S., Santerre, J. P. & Labow, R. S. Effect of polyurethane chemistry and protein coating on monocyte differentiation towards a wound healing phenotype macrophage. *Biomaterials* **30**, 5497–5504 (2009).
18. Chen, Z. *et al.* Tuning Chemistry and Topography of Nanoengineered Surfaces to Manipulate Immune Response for Bone Regeneration Applications. *ACS Nano* **11**, 4494–4506 (2017).

19. Christo, S. N. *et al.* The Role of Surface Nanotopography and Chemistry on Primary Neutrophil and Macrophage Cellular Responses. *Adv. Healthc. Mater.* **5**, 956–965 (2016).
20. Chen, S. *et al.* Characterization of topographical effects on macrophage behavior in a foreign body response model. *Biomaterials* **31**, 3479–3491 (2010).
21. Bota, P. C. S. *et al.* Biomaterial topography alters healing in vivo and monocyte/macrophage activation in vitro. *J. Biomed. Mater. Res. - Part A* **95 A**, 649–657 (2010).
22. Wójciak-Stothard, B., Curtis, A., Monaghan, W., Macdonald, K. & Wilkinson, C. Guidance and activation of murine macrophages by nanometric scale topography. *Exp. Cell Res.* **223**, 426–435 (1996).
23. Yuan, H. *et al.* A comparison of the osteoinductive potential of two calcium phosphate ceramics implanted intramuscularly in goats. *J. Mater. Sci. Mater. Med.* **13**, 1271–1275 (2002).
24. Barradas, A., Yuan, H., van Blitterswijk, C. & Habibovic, P. Osteoinductive biomaterials: current knowledge of properties, experimental models and biological mechanisms. *Eur. Cells Mater.* **21**, 407–429 (2011).
25. Barba, A. *et al.* Osteoinduction by Foamed and 3D-Printed Calcium Phosphate Scaffolds: Effect of Nanostructure and Pore Architecture. *ACS Appl. Mater. Interfaces* **9**, 41722–41736 (2017).
26. Xia, Z. *et al.* In vitro biodegradation of three brushite calcium phosphate cements by a macrophage cell-line. *Biomaterials* **27**, 4557–65 (2006).
27. Mestres, G. *et al.* Inflammatory response to nano- And microstructured hydroxyapatite. *PLoS One* **10**, 1–20 (2015).
28. Shiwaku, Y. *et al.* The crosstalk between osteoclasts and osteoblasts is dependent upon the composition and structure of biphasic calcium phosphates. *PLoS One* **10**, 1–17 (2015).
29. Bernhardt, A., Schumacher, M. & Gelinsky, M. Formation of Osteoclasts on Calcium Phosphate Bone Cements and Polystyrene Depends on Monocyte Isolation Conditions. *Tissue Eng. Part C Methods* **21**, 160–170 (2015).
30. Davison, N. L. *et al.* Osteoclast resorption of beta-tricalcium phosphate controlled by surface architecture. *Biomaterials* **35**, 7441–7451 (2014).
31. Ciapetti, G. *et al.* Osteoclast differentiation from human blood precursors on biomimetic calcium-phosphate substrates. *Acta Biomater.* **50**, 102–113 (2017).
32. Diez-Escudero, A. *et al.* Focus Ion Beam/Scanning Electron Microscopy Characterization of Osteoclastic Resorption of Calcium Phosphate Substrates. *Tissue Eng. Part C Methods* **23**, 118–124 (2017).
33. Samavedi, S., Whittington, A. R. & Goldstein, A. S. Calcium phosphate ceramics in bone tissue engineering: a review of properties and their influence on cell behavior. *Acta Biomater.* **9**, 8037–45 (2013).
34. Chen, Z. *et al.* Osteoimmunomodulatory properties of magnesium scaffolds coated with β-tricalcium phosphate. *Biomaterials* **35**, 8553–8565 (2014).
35. Diez-Escudero, A. *et al.* Heparinization of Beta Tricalcium Phosphate: Osteo-immunomodulatory Effects. *Adv. Healthc. Mater.* **7**, 1700867 (2018).
36. Ginebra, M. P. *et al.* Setting Reaction and Hardening of an Apatitic Calcium Phosphate *Cement. J. Dent. Res.* **76**, 905–912 (1997).
37. Sadowska, J.-M., Guillem-Marti, J., Montufar, E. B., Espanol, M. & Ginebra, M.-P. Biomimetic Versus Sintered Calcium Phosphates: The In Vitro Behavior of Osteoblasts and Mesenchymal Stem Cells. *Tissue Eng. Part A* **23**, 1297–1309 (2017).
38. Singh, S., Jones, B. J., Crawford, R. & Xiao, Y. Characterization of a Mesenchymal-Like Stem Cell Population from Osteophyte Tissue. *Stem Cells Dev.* **17**, 245–254 (2008).
39. Mareddy, S., Crawford, R., Brooke, G. & Xiao, Y. Clonal Isolation and Characterization of Bone Marrow Stromal Cells from Patients with Osteoarthritis. *Tissue Eng.* **13**, 819–829 (2007).

40. Livak, K. J. & Schmittgen, T. D. Analysis of relative gene expression data using real-time quantitative PCR and the 2-ΔΔCT method. *Methods* **25**, 402–408 (2001).
41. McWhorter, F. Y., Wang, T., Nguyen, P., Chung, T. & Liu, W. F. Modulation of macrophage phenotype by cell shape. *Proc. Natl. Acad. Sci.* **110**, 17253–17258 (2013).
42. Brodbeck, W. G. *et al.* Biomaterial surface chemistry dictates adherent monocyte/macrophage cytokine expression in vitro. *Cytokine* **18**, 311–319 (2002).
43. Godek, M. L., Sampson, J. A., Duchsherer, N. L., McElwee, Q. & Grainger, D. W. Rho GTPase protein expression and activation in murine monocytes/macrophages are not modulated by model biomaterial surfaces in serum-containing in vitro cultures. *J. Biomater. Sci. Polym. Ed.* **17**, 1141–1158 (2006).
44. Sussman, E. M., Halpin, M. C., Muster, J., Moon, R. T. & Ratner, B. D. Porous implants modulate healing and induce shifts in local macrophage polarization in the foreign body reaction. *Ann. Biomed. Eng.* **42**, 1508–1516 (2014).
45. Fernandes, K. R., Zhang, Y., Magri, A. M. P., Renno, A. C. M. & van den Beucken, J. J. J. P. Biomaterial Property Effects on Platelets and Macrophages: An in Vitro Study. *ACS Biomater. Sci. Eng.* **3**, 3318–3327 (2017).
46. Jenkins, S. J. *et al.* Local Macrophage Proliferation, Rather than Recruitment from the Blood, Is a Signature of TH2 Inflammation. *Science* (80-.). **332**, 1284–1288 (2011).
47. Pascaud, P. *et al.* Interaction between a bisphosphonate, tiludronate and nanocrystalline apatite: In vitro viability and proliferation of HOP and HBMSC cells. *Biomed. Mater.* **7**, (2012).
48. Gustavsson, J., Ginebra, M. P., Planell, J. & Engel, E. Osteoblast-like cellular response to dynamic changes in the ionic extracellular environment produced by calcium-deficient hydroxyapatite. *J. Mater. Sci. Mater. Med.* **23**, 2509–20 (2012).
49. Engel, E. *et al.* Discerning the role of topography and ion exchange in cell response of bioactive tissue engineering scaffolds. *Tissue Eng. Part A* **14**, 1341–51 (2008).
50. Bartneck, M. *et al.* Induction of specific macrophage subtypes by defined micro-patterned structures. *Acta Biomater.* **6**, 3864–3872 (2010).
51. Paul, N. E. *et al.* Topographical control of human macrophages by a regularly microstructured polyvinylidene fluoride surface. *Biomaterials* **29**, 4056–4064 (2008).
52. Mantovani, A., Biswas, S. K., Galdiero, M. R., Sica, A. & Locati, M. Macrophage plasticity and polarization in tissue repair and remodelling. *J. Pathol.* **229**, 176–185 (2013).
53. Meng, F. & Lowell, C. A. Lipopolysaccharide (LPS)-induced Macrophage Activation and Signal Transduction in the Absence of Src-Family Kinases Hck, Fgr, and Lyn. *J. Exp. Med.* **185**, 1661–1670 (1997).
54. Zhang, W., Shen, X., Xie, L., Chu, M. & Ma, Y. MicroRNA-181b regulates endotoxin tolerance by targeting IL-6 in macrophage RAW264.7 cells. *J. Inflamm.* (United Kingdom) **12**, 1–9 (2015).
55. Chamberlain, L. M., Brammer, K. S., Johnston, G. W., Chien, S. & Jin, S. Macrophage Inflammatory Response to TiO Nanotube Surfaces. *J. Biomater. Nanobiotechnol.* **2**, 293–300 (2011).
56. Schmidt, A., Caron, E. & Hall, A. Lipopolysaccharide-Induced Activation of 2-Integrin Function in Macrophages Requires Irak Kinase Activity, p38 Mitogen- Activated Protein Kinase, and the Rap1 GTPase. *Mol. Cell. Biol.* **21**, 438–448 (2001).
57. Sørensen, M. G. *et al.* Characterization of osteoclasts derived from CD14+ monocytes isolated from peripheral blood. *J. Bone Miner. Metab.* **25**, 36–45 (2007).
58. ten Harkel, B. *et al.* The Foreign Body Giant Cell Cannot Resorb Bone, But Dissolves Hydroxyapatite Like Osteoclasts. *PLoS One* **10**, e0139564 (2015).
59. Teitelbaum, S. L. Bone resorption by osteoclasts. *Science* (80-.). **289**, 1504–1508 (2000).

60. Chen, Z. *et al.* Osteogenic differentiation of bone marrow MSCs by β-tricalcium phosphate stimulating macrophages via BMP2 signalling pathway. *Biomaterials* **35**, 1507–18 (2014).
61. WAHL, S. M., McCARTNEY-FRANCIS, N., ALLEN, J. B., DOUGHERTY, E. B. & DOUGHERTY, S. F. Macrophage Production of TGF-beta and Regulation by TGF-beta. *Ann. N. Y. Acad. Sci.* **593**, 188–196 (1990).
62. Chen, Z. *et al.* Immunomodulatory effects of mesoporous silica nanoparticles on osteogenesis: From nanoimmunotoxicity to nanoimmunotherapy. *Appl. Mater. Today* **10**, 184–193 (2018).
63. Chen, Z. *et al.* The effect of osteoimmunomodulation on the osteogenic effects of cobalt incorporated β-tricalcium phosphate. *Biomaterials* **61**, 126–138 (2015).
64. Lin, F.-H., Chang, J. B., McGuire, M. H., Yee, J. A. & Brigman, B. E. Biphasic effects of interleukin-1β on osteoblast differentiation in vitro. *J. Orthop. Res.* n/a-n/a (2010). doi:10.1002/jor.21099
65. Ding, J. *et al.* TNFα and IL-1β inhibit RUNX2 and collagen expression but increase alkaline phosphatase activity and mineralization in human mesenchymal stem cells. *Life Sci.* **84**, 499–504 (2009).
66. Mosser, D. M. The many faces of macrophage activation. *J. Leukoc. Biol.* **73**, 209–212 (2003).
67. McBeath, R., Pirone, D. M., Nelson, C. M., Bhadriraju, K. & Chen, C. S. Cell Shape, Cytoskeletal Tension, and RhoA Regulate Stem Cell Lineage Commitment. *Dev. Cell* **6**, 483–495 (2004).

Chapter 4

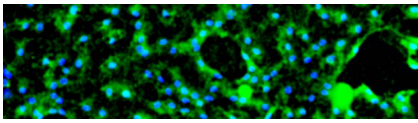

The influence of physicochemical properties of biomimetic hydroxyapatite on the *in vitro* behavior of endothelial progenitor cells and their interaction with mesenchymal stem cells

4.1 Introduction

Bone healing is a complex process that involves multiple interdependent and overlapping-in-time steps.[1] For instance, the timely angiogenesis serves not only as a source of oxygen and nutrients, but also controls the recruitment and differentiation of stem cells, the osteoblastic activity and consequently further new bone formation.[2,3] Therefore, the interplay between vessel-forming endothelial cells (ECs) and bone-forming cells is critical during the bone healing process. The ability of these cells to communicate, both through autocrine/paracrine routes and through direct gap junctional cell-to-cell contacts, results in a tight coupling between angiogenesis and osteogenesis.[2] For instance, mesenchymal stem cells (MSCs) and osteoblasts secrete angiogenic factors such as vascular endothelial growth factor (VEGF)[4], fibroblasts growth factor (FGF)[5] and protein deglycase 1 (DJ 1)[6] whose goal is to enhance ECs proliferation and subsequent vessel growth. On the other hand, ECs express bone morphogenetic protein 2 (BMP-2) and endothelin 1 (EDH 1), which fulfil dual function by regulating angiogenesis as well as stimulating bone formation.[7–10]

Despite the remarkable self-regenerative capacity of bone tissue, large defects cannot be bridged unless some support structures, namely bone grafts, are implanted to support the healing process. Calcium phosphates (CaPs) have been shown to be excellent synthetic bone grafts, due to their close compositional resemblance to the mineral phase of bone. Furthermore, some of them such as sintered β-TCP or low temperature CDHA[11,12] were reported to possess osteoconductive/osteoinductive properties that might foster the osteogenesis-related processes.

Great efforts have been made in CaPs research towards investigating to which extent and how their particular physicochemical features such as macroporosity, chemistry, ionic release/uptake, and surface topography affect the osteoinductive/osteoconductive potential.[13,14] Nonetheless, since bone healing process is complex, involving not only bone- forming cells but also immune or endothelial cells, the implant should actively participate in the former stages of bone regeneration exhibiting anti-inflammatory and angiogenic properties as well as stimulating the proper crosstalk between the different cell types implicated in restoring of bone function.

Recently, some advances have been made in modulating the angiogenic performance of CaP-based materials. The macroporosity[15,16], functionalisation/loading of scaffold with biomolecules like RGD[16] or VEGF[17,18] or incorporation of ions like cooper[19] or cobalt[20] have been investigated as strategies for potentiating the angiogenic features of CaPs. Moreover, the *in vitro* prevascularisation of bone grafts was also studied as an interesting approach for the preparation of constructs with enhanced angiogenic performance. For instance, Chen *et al.* and Thein-Han *et al.* showed that coculturing of endothelial and bone forming cells on microporous calcium phosphate scaffolds had

positive impact on stimulating the formation of microcapillary network as well as the expression of genes involved in both angiogenesis and osteogenesis.[16,21] Although the pathways involved in activation of positive crosstalk of endothelial and bone cells have been widely investigated[22,23], little attention has been paid to the effect of particular features of CaPs on the angiogenic and osteogenic events in coculture conditions.

Therefore, the current study tackles two main goals. The first was to investigate to which extent the particular cues of CDHA affect the behaviour of endothelial progenitor and mesenchymal stem cells separately. Two chemically identical biomimetic calcium deficient hydroxyapatite, consisting of either needle-like or plate-like crystals were compared to sintered β-TCP in terms of its effect on rEPCs and rMSCs proliferation, PECAM-1 production and osteogenic/angiogenic gene expression. As a second goal, the outcome of physicochemical features of CaPs on the interaction of rEPCs and rMSCs were investigated through coculture system evaluating angiogenic and osteogenic gene expression and the secretion of connexin43 (Cx43), a junctional protein responsible for cell-to-cell communication. Additionally, the expression of protein deglycase 1 (DJ 1) and endothelin 1 (EDH 1) was analysed, as possible mediators of rEPCs and rMScs crosstalk.

4.2 Materials and methods

4.2.1 Material preparation

CDHA was obtained by hydrolysis of α-tricalcium phosphate (α-TCP) via a cementitious reaction, as previously described.[24] Briefly, α-TCP powder was prepared by heating at 1400 °C for 15 h a 2:1 molar mixture of calcium hydrogen phosphate ($CaHPO_4$, Sigma-Aldrich, St. Louis, USA) and calcium carbonate ($CaCO_3$, Sigma-Aldrich, St. Louis, USA), followed by quenching in air. α-TCP powders with two different sizes were obtained by milling according to two different protocols. The α-TCP powder with larger size (coarse, C: 5.2 μm median size) was obtained my milling in agate ball mill (Pulverisette 6, Fritsch GmbB) with 10 balls (d=30 mm) for 15 min at 450 rpm. The α-TCP powder with smaller size (fine, F: 2.8 μm) was first milled with 10 balls (d= 30 mm) for 60 min at 450 rpm followed by second milling with 10 balls (d=30 mm) for 40 min at 500 rpm and the third one with 100 balls (d=10 mm) for 60 min at 500 rpm.[25]

CDHA discs were obtained by mixing a solid phase consisting of α-TCP powder and 2 wt.% of precipitated hydroxyapatite (pHA; Merck 2143, Merck, Darmstardt, Germany) with a liquid phase of 2.5 wt.% disodium hydrogen phosphate (Na_2HPO_4, Merck, Darmstadt, Germany), with a liquid to powder ratio of 0.35 mL/g. The paste was transferred to Teflon moulds (15 mm diameter and 2 mm thickness) and immersed in

water at 37 ºC for 7 days for complete reaction. The products obtained were coded as C-CDHA or F-CDHA depending on the size of the starting powder.

β-tricalcium phosphate discs were obtained by sintering C-CDHA at 1100 ºC for 15 hours, followed by slow cooling inside the furnace.

4.2.2 Material characterisation

Phase composition of the different CaPs was assessed by X-ray diffraction (XRD, D8 Advance, Brucker, Karlsruhe, Germany). The diffractometer equipped with a Cu Kα X-ray anode was operated at 40 kV and 40 mA. The data was collected in 0.02 ° steps over the 2θ range of 10 °-80 ° with a counting time of 4 s per step. The phases were identified by comparison to the diffraction patterns of HA (JCPDS 82-1943), α-TCP (JCPDS 09-0348) and β-TCP (JCPDS 70-2065). The microstructure of materials was analysed by Scanning Electron Microscopy (SEM, Zeiss Neon 40, Oberkochen, Germany) at an acceleration voltage of 5 kV. To impart conductivity, surfaces were coated with gold-palladium layer prior to imaging. The surface roughness was characterized by optical interferometry (Veeco Wyko NT1100), using a 50x magnification and a scanned area of 47.5 x 63.4 μm^2. Images were acquired using Vision32 software. The SSA and porosity of materials used in current study was described in previous reports.[26]

4.2.3 Cell culture study

The protocol of isolation of rat mesenchymal stem cells (rMSCs) and rat endothelial progenitor cells (rEPCs) was described elsewhere.[27] Briefly, cells were obtained from the tibias and femurs of Lewis rats at the Institute for Bioengineering of Catalonia (IBEC). Flow cytometry was performed in order to assess cell phenotype.[28]

rMSCs were grown in Advanced Dulbecco's Modified Eagle Medium (AdvDMEM) supplemented with 10 % of foetal bovine serum (FBS), 2 mM L-glutamine, penicillin/streptomycin (50 U/mL and 50 μg/mL, respectively) and 20 mM 4-(2-hydroxyethyl)-1-piperazineethanesulfonic acid (HEPES) buffer, provided from Invitrogen.

rEPCs were expanded in microvascular endothelial cell medium 2 (EGM2-MV, Lonza) containing endothelial cell basal medium (EBM-2, Lonza) supplemented with EGM-2 bullet kit and 5 % FBS.

All experiments, except where stated, were performed with a seeding density of 12×10^3 cells/well using rMSCs and rEPCs at passages 3-5.

4.2.3.1 Determination of coculture ratio of rEPCs and rMSCs

For the coculture studies, both cell types were expanded separately in their corresponding cell culture media till 70-80 % of confluence. Afterwards, rEPCs and rMSCs were detached and seeded at rEPCs:rMSCs ratios of 1:0, 4:1, 2:1, 1:1, 1:2, 1:4 and 0:1 onto 24-well plates. Cells were cultured up to 21 days in EGM-2 MV medium at 37 ºC in a humidified 5 % CO_2 incubator replacing the medium every other day. The optimum ratio for coculture conditions was chosen evaluating cell proliferation, cell differentiation, and cell mineralization.

4.2.3.1.1 Cell proliferation by lactate dehydrogenase (LDH) activity

Cell number was quantified at 1, 7, 14 and 21 days of cell coculture by evaluating lactate dehydrogenase (LDH) activity. At specific time points, cells were rinsed with PBS and subsequently lysed with M-PER® (Mammalian Protein Extraction Reagent, Thermo Scientific, Waltham, MA, USA). Prior to evaluation, cell lysates were stored at -80 ºC. LDH activity was measured with Citotoxicity Detection Kit LDH (Roche Applied Science, Penzberg, Germany). Absorbances were evaluated spectrophotometrically at 492 nm with Synergy HTX multi-mode microplate reader (Bio-Tek Instruments, Inc.). In order to express the absorbances' values as a cell number, a calibration curve with a decreasing number of cells was prepared.

4.2.3.1.2 Alkaline phosphatase (ALP) activity

Cell differentiation and mineralization were determined at 21 days through measurements of alkaline phosphatase (ALP) activity and Alizarin Red Staining (ARS), respectively.

ALP activity was quantified using SensoLyte® pNPP Alkaline Phosphate Assay Kit (AnaSpec Inc., CA, USA). The same lysates as for the cell proliferation assay were used. The ALP activity was measured at 405 nm using Synergy HTX multi-mode microplate reader (Bio-Tek Instruments, Inc.). The given values were normalized to the cell number from proliferation assay and divided by the time of incubation.

4.2.3.1.3 Alizarin Red Staining (ARS)

The calcification of cellular matrix in the different rEPCs:rMSCs ratios was analysed at day 21 using Alizarin Red S (ARS) staining method (Sigma-Aldrich). Cells were washed with PBS and then fixed with 4 % (v/v) paraformaldehyde (PFA) for 20 min at RT. The fixation was followed by three rinsings with Mili- Q water and subsequently 500 µL/well of 40 mM ARS (pH 4.2) was added. The incubation with stain was performed at RT for 20 min and with continuous shaking. The excess of dye was removed by rinsing with Milli-Q. Stained cells was examined under a fluorescence stereoscopy (Leica Microsystems, Germany). Subsequently, the stain was eluted with a cetylpyridinium chloride (CPC) buffer (10 % (w/v) in 10 mM NaH_2PO_4, pH 7)

incubating 30 min at RT. The absorbance of collected supernatants was measured at 570 nm with Synergy HTX multi-mode microplate reader (Bio-Tek Instruments, Inc.).

4.2.3.2 Monoculture and coculture of rECPS and rMSCs on CaPs

C-CDHA, F-CDHA and β-TCP discs (12-15 mm of diameter, 2 mm of height) were sterilised with 70 % ethanol, rinsed with PBS and pre-incubated overnight with complete EGM-2 MV medium at 37 ºC. Subsequently the corresponding cells were seeded on the substrates. The ratio 1:2 was used for coculture condition on discs considering the results obtained in the previous study. For both coculture[29] and monoculture of rEPCs and rMSCs[30], EGM-2 MV medium was used. In all assays, the medium was refreshed after 6 hours of cell adhesion and then every other day throughout the whole culture period. Tissue culture polystyrene (TCPS) was used as corresponding control for each monoculture/coculture condition. Cell number was evaluated at 6 hours, 3, 7, 14 and 21 days by measuring LDH activity following the previously detailed protocol. For cells cultured on CaPs discs, results were normalised versus the area of the discs and then expressed as relative fold to TCPS at 6 h.

4.2.3.2.1 Ionic concentrations of cell culture media

At specific time points, the supernatants from mono- and cocultures on CaPs were collected and stored at -20 ºC for further analysis. Subsequently, the concentration of calcium and phosphorus were determined. The Ca^{2+} was quantified applying o-cresolphthalein complexone method.[31,32] The concentration of P_i was evaluated by Phosphate Colorimetric Assay Kit (Sigma-Aldrich) measuring the absorbance at 650 nm with Synergy HTX multi-mode microplate reader (Bio-Tek Instruments, Inc.).

4.2.3.2.2 Immunostaining

Monocultured rEPCs, rMSCs and coculture were stained for nuclei, F-actin and Cx43. Monocultured rEPCs and coculture were additionally incubated with endothelial specific platelet endothelial cell adhesion molecule (PECAM-1, CD31). The staining was performed at 14 days and 21 days of cell culture. The samples were rinsed with PBS (x3) and cells were fixed with 4 % (v/v) PFA solution in PBS. Afterwards, the permeablization process was carried out with 0.1 % Triton X-100 (Sigma-Aldrich) in PBS during 15 min. Subsequently, cells were incubated 30 min at RT with blocking solution consisting of 1 % bovine serum albumin (BSA) (Sigma-Aldrich) in PBS. The discs were incubated with the primary antibody rabbit anti-PECAM-1 (Santa Cruz Biotechnologies) at 1:100 in 1 % BSA in PBS for one hour. The step was followed by incubation with secondary antibody Alexa Fluor 488 chicken anti-rabbit (1:1000) and Alexa Fluor 546 Phalloidin (1:300) in 0.1 % Triton X-100 in PBS (all from Invitrogen). For nuclei staining, 4',6-diamidino-2-phenylindole (DAPI) (1:1000 in 0.15 % glycine in PBS) was added and samples were incubated for 2 minutes. Between all steps, three rinses for 5 minutes with 0.15 % glycine (Sigma-Aldrich) in PBS were performed. For

Cx43 staining the manufacturer instructions was followed in terms of cell fixation, dilution and incubation times. The primary antibody was mouse-anti Connexin43 C terminus (Millipore) and the secondary antibody was Alexa Fluor 488 goat anti-mouse (Invitrogen). The cells seeded on glass coverslip were used as a control group. Samples were mounted with Mowiol 4-88 (Sigma-Aldrich) and visualised using inverted LSM 800 ZEISS confocal microscope (CLSM). Images were acquired using LASX software and processed using Fiji/Image-J package.

4.2.3.2.3 Angiogenic and osteogenic gene expression of cocultured rEPCs and rMSCs on CaPs

Angiogenic and osteogenic gene expression was evaluated at 1, 7 and 14 days of mono- and cocultures by quantitative real-time polymerase chain reaction (RT-qPCR).Total RNA was extracted from mono and cocultures at the given time points using RNeasy® Mini Kit (Qiagen, Hilden, Germany) as recommended by the manufacturer. Total RNA quantity was determined by NanoDrop ND-1000 spectrophotometer (NanoDrop Technologies, Montchanin, DE, USA) and subsequently 130 ng of the total RNA were used as template for single strand complementary DNA (cDNA) synthesis using QuantiTect Reverse Transcription Kit (Qiagen). Quantitative real-time PCR (RT-qPCR) assays were performed and monitored in triplicate using a StepOnePlus Real-Time PCR System (Applied Biosystems, Foster City, CA, USA). The cDNA template was amplified with the QuantiTect SYBR Green RT-PCR Kit (Qiagen) and specific primers for angiogenic and osteogenic markers (Listed in Table 1). No-RNA control, the melt curve analysis and no-RT control were run to ensure the specificity of primers and the absence of genomic DNA, respectively. The expression of all studied genes were normalised by expression of β-actin (ACTB) and relative fold changes (FC) were related to 1 day gene expression value of either rEPCs monocultured on TCPS with EGM-2 MV (for angiogenesis markers: VEGF A, VEGF R2, endothelin-1) or rMSCs monocultured on TCPS with advDMEM (for osteogenic markers: ALP, BMP-2, OC, DJ 1). The fold change was calculated with the formula:

$$FC = E_{target}^{\Delta Cq\ target\ (TCPS\ 6h - sample)} / E_{reference}^{\Delta Cq\ reference\ (TCPS\ 6h - sample)} \quad \text{(Eq 4.1.)}$$

Cq respresents the median value of the quantification cycle of the triplicate of each sample. E corresponds to the efficiency of amplification and is determined through following formula $E = 10^{[-1/slope]}$ where slope value proceeds from slope of the log-linear portion of the calibration curve.

Table 4.1. Primers' sequences used in this study

Gene	Gene symbol	Primers' sequences (5'→3')
β-actin	ACTB	F:CCCGCGAGTACAACCTTCT R: CGTCATCCATGGCGA ACT
Bone morphogenetic protein-2	BMP-2	F: CCCCTATATGCTCGACCTGT R: AAAGTTCCTCGATGGCTTCTT
Alkaline phosphatase	ALP	F GCACAACATCAAGGACATCG R:TCAGTTCTGTTCTTGGGGTACT
Osteocalcin	OCN	F:ATAGACTCCGGCGCTACCTC R: CCAGGGGATCTGGGTAGG
Vascular endothelial growth factor A	VEGF A	F:CGGAGCGCAACGTCACTATG R: TGGTCTGCATTCACATCTGC
Vascular endothelial growth factor receptor 2	VEGF R2	F: AAAGAGAGGGACTTTGGCCG R: GTCGCCACTTGGACAAAACCC
Parkinsonism associated deglycase	DJ-1	F: ATGCGACGGTACTGACCTG R: TCAGTGTTTGGCTATCCCTGT
Endothelin-1	EDH 1	F:TGTCTACTTCTGCCACCTGGA R: CCTAGTCCATACGGGACGAC

4.2.4 Statistical analysis

All data were plotted as means ± standard error (SE). Statistical significance was determined by ANOVA with Tukey HSD post-hoc analysis defining statistical significance by $p < 0.05$. Non- parametric data was additionally subjected to Kruskal Wallis test followed by multiple pairwise comparison. Significance level was set for $p < 0.05$. Statistical analysis were performed using SPSS 23.0 software (SPSS, ICN., Chicago, IL)

4.3 Results

4.3.1 Optimisation for coculture conditions

The Figure 4.1. summarises the proliferation (Figure 4.1.A), osteogenic differentiation (Figure 4.1.B) and mineralisation (Figure 4.1.C and 4.1.D) of rEPCs and rMSCs in coculture conditions on TCPS. The efficiency of cell adhesion was similar between all coculture ratios and similar proliferative potential was observed in all conditions.

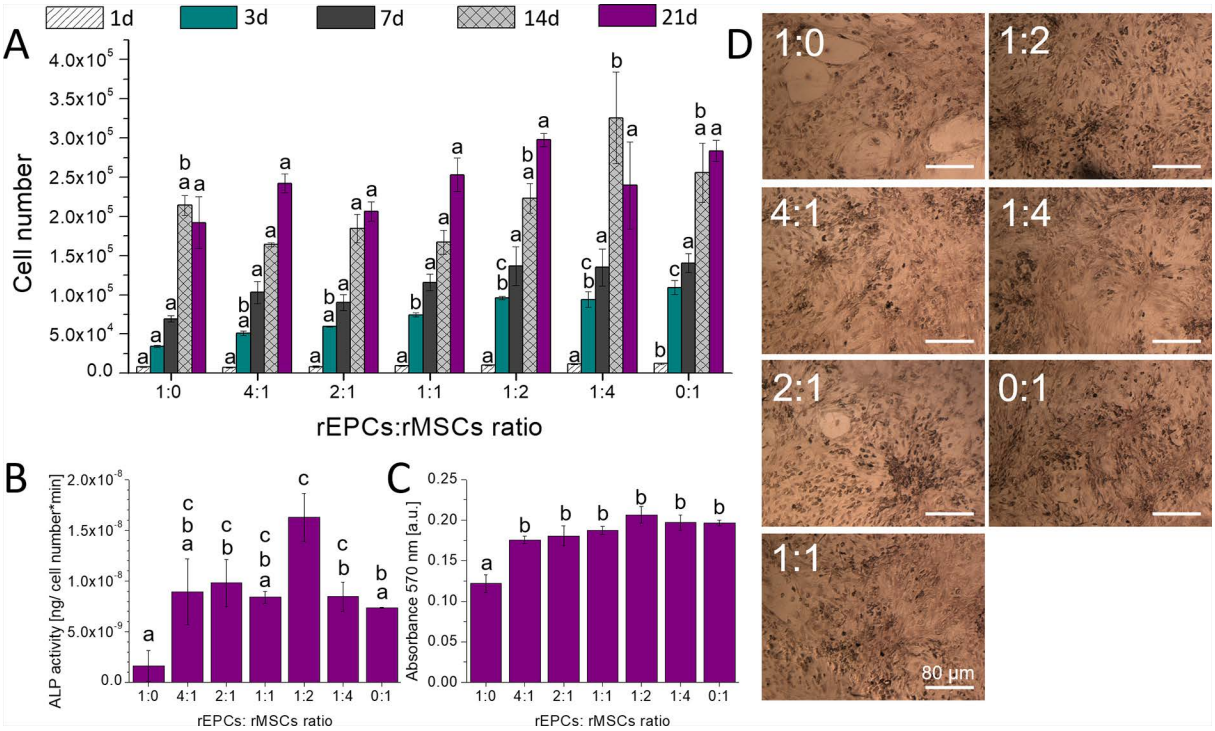

Figure 4.1. A) Proliferation of cocultured rEPCs and rMSCs after 6 hours, 3 days, 7 days, 14 days and 21 days. **B)** ALP activity of cocultured rEPCs and rMSCs at 21 days. The results were normalized versus corresponding cell number evaluated through LDH. **C** and **D)** Alizarin red staining of cocultured rECPs and rMSCs at day 21. Scale bar denotes 80 µm. Numbers on photographs indicate the ratio rEPCs: rMSCs. In all graphs, the same letter (a,b or c) indicates conditions with no statistically significant differences ($p > 0.05$) at specific time point.

Cell differentiation and calcification at day 21 were evaluated by measuring the ALP activity (Figure 4.1.B) and by Alizarin Red staining (Figure 4.1.C and 4.1.D), respectively. As expected, monocultured rEPCs exhibited poor ALP activity. Cells cultured at ratio 1:2 revealed the highest ALP activity that was over two fold higher than monocultured rMSCs. Moreover, cocultured cells revealed similar amount of alizarin red compared to rMSCs (Figure 4.1.C). No rearrangements in cell morphology and little calcium deposits were observed in all conditions (Figure 4.1.D). The ratio 1:2 was chosen for further experiments since it showed high cell proliferation together with high ALP activity and ARS.

4.3.2 Physicochemical characterisation of CaPs

The XRD diffraction confirmed that CaPs are phase-pure (Figure 4.2.C) except for C-CDHA, where traces of unreacted α-TCP were observed (< 3%). The sintered β-TCP showed sharp diffraction peaks whilst broad peaks were observed for C-CDHA and especially for F-CDHA substrates. Whereas all materials presented similar porosities (Figure 4.2.D), clear differences were observed in terms of microstructure. C-CDHA consisted of plate-like crystals, whereas F-CDHA presented nanometric sized needle-like crystals, organised in agglomerates. The sintering process of β-TCP led to the formation of polyhedral crystals (Figure 4.2.A). The microstructural differences resulted

in higher SSA for the biomimetic CDHA compared to sintered β-TCP. C-CDHA presented higher average roughness values than F-CDHA and sintered β-TCP (1.33 ± 0.23) (Figure 4.2.B).

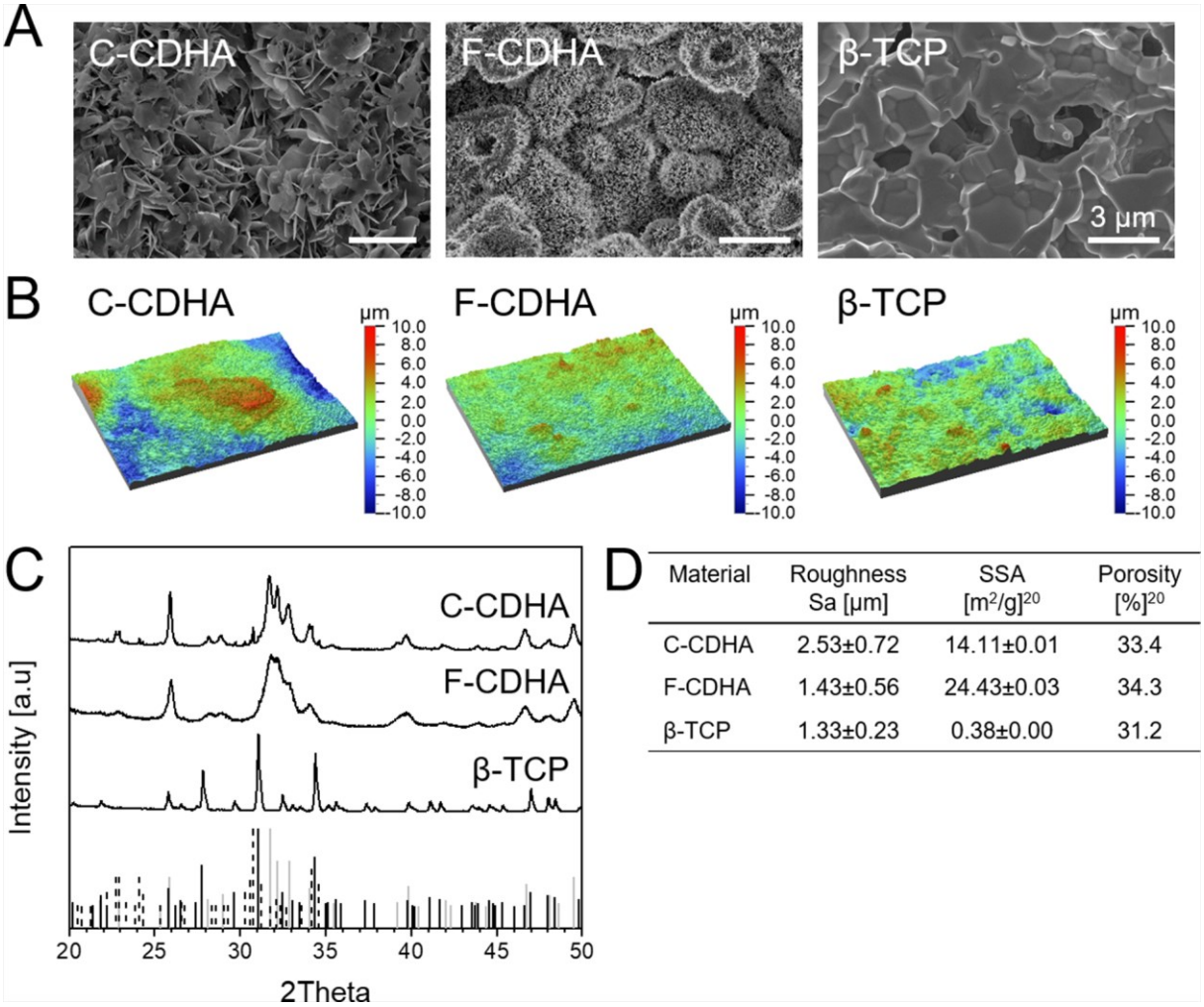

Figure 4.2. Physicochemical characterisation of CaPs **A)** SEM micrographs of surface morphology. Scale bare denotes 3µm. **B)** Optical interferometry images of C-CDHA, F-CDHA and β-TCP. **C)** XRD patterns of the different calcium phosphate substrates. The vertical lines represent the patterns of HA (JCPDS 82-1943), α-TCP (JCPDS 09-0348) and β-TCP (JCPDS 70-2065) from the Joint Committee on powder Diffraction Standards. **D)** Values of roughness, specific surface area (SSA) and total porosity.[20]

4.3.3 Initial cell adhesion and proliferation in monocultures and cocultures

Similar adhesion of monocultured rEPCs was observed in all substrates (Figure 4.3.A). Monocultured rEPCs progressively increased their number in all CaPs with slightly slower proliferation rate on biomimetic CDHA substrates. Moreover, lower number of monocultured rEPCs on β-TCP at day 3 was observed compared to TCPS.

In monocultured rMSCs, the cellular adhesion was lower on CDHA substrates whilst β-TCP presented similar number of adhered cells compared to the control. Overall, the

proliferative potential of monocultured rMSCs was lower when cultured on CaP substrates. This scenario was especially pronounced for biomimetic substrates where the cellular proliferation was significantly slowed down or impaired on C-CDHA and F-CDHA, respectively. Moreover, the β-TCP showed significantly lower number of monocultured rMSCs at day 21 compared to the control.

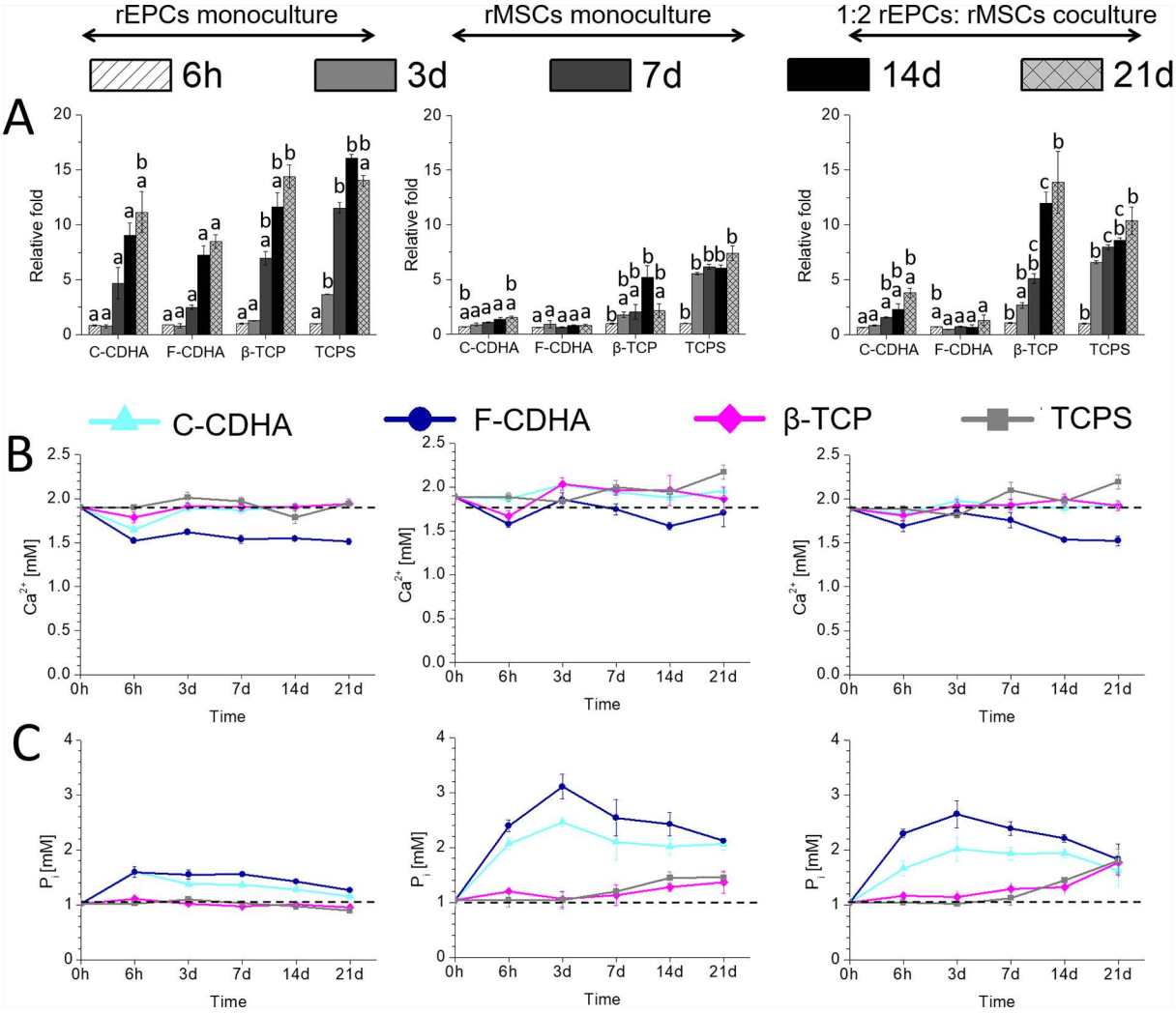

Figure 4.3. A) Proliferation of monocultured rEPCs, monocultured rMCSs and cocultured cells with ratio 1:2 of rEPCs and rMSCs on various CaPs. Cell numbers were quantified at 6 hours, 3 days, 7 days, 14 days and 21 days. The values were expressed as relative fold change compared to cell number obtained on corresponding TCPS at 6 hours. In all graphs, the same letter (a,b or c) indicate groups with no statistically significant differences ($p > 0.05$) at specific time point. **B)** Calcium concentration in EGM-2 MV medium in presence of cells. **C)** Phosphorus concentration in EGM-2 MV medium in presence of cells.

In coculture system, the cellular adhesion was also lower on CDHA compared to β-TCP and TCPS. The cells presented low proliferation rate on biomimetic CDHA being this scenario especially pronounced on F-CDHA, where similar cell numbers were observed over the cell culture times. Nonetheless, the proliferative potential of cells on C-CDHA was higher on coculture condition compared to monocultured rMSCs. The enhanced proliferation rate on coculture was also observed for β-TCP compared to monocultured rMSCs.

4.3.4 Ionic concentration

The evolution of calcium and phosphate concentration in the EGM-2 MV culture medium in presence of cells is displayed in Figure 4.3.B and 4.3.C, respectively. The initial value of Ca^{2+} concentration was 1.89 ± 0.05 mM. In general, irrespective of the cell type, little alteration of calcium levels was observed for C-CDHA and β-TCP. In monocultured rEPCs, F-CDHA up took Ca^{2+} ions from the medium, this resulting in a 20% decrease in calcium concentration compared to the control throughout the whole culture period. In rMSCs monoculture, the decrease of Ca^{2+} by F-CDHA was observed at 6 h and 14 d of cell culture whilst this trend for coculture was noted at 6 h, 14 and 21 d.

The initial experimental value of P_i was 1.02 ± 0.01 mM. In general, higher Pi levels were detected in presence of the biomimetic substrates, whereas the values registered for the β-TCP substrates were similar to TCPS. Despite using the same cell culture medium, different trends were observed for the biomimetic substrates depending on cell type. For rEPCs monoculture, the CDHA increased approximately 50 % the P_i concentration compared to TCPS at 6 hours. In contrast, for rMSCs monoculture and coculture on biomimetic CDHA highest levels of P_i were observed at day 3, reaching approximately 170 % and 130 % P_i concentration compared to TCPS, respectively. Comparing the two biomimetic substrates, F-CDHA led to more pronounced changes of P_i content. In all cell culture conditions on CDHA, slow and progressive decrease of P_i concentration was observed after reaching the aforementioned highest levels.

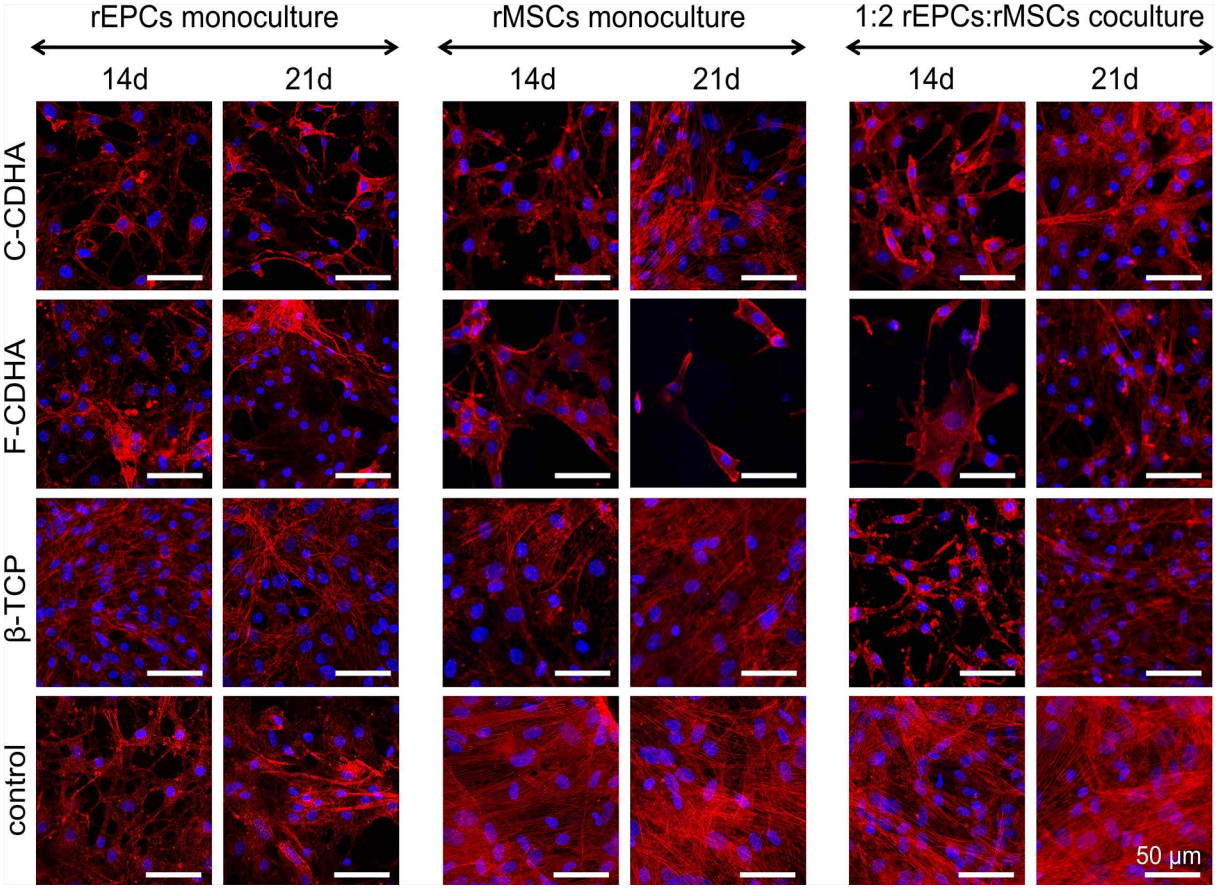

Figure 4.4. Merged fluorescence images of monocultured rEPCs, monocultured rMSCs and cocultured cells with ratio 1:2 of rEPCs and rMSCs on various CaPs. Cells were stained for F-actin (red) and nuclei (blue). The images were acquired at 14 days and 21 days of cell culture. The cells seeded on glass coverslip were used as a control. Scale bar denotes 50 μm.

4.3.5 Cell morphology

Cellular morphology in mono- and coculture on CaPs substrates at 14 and 21 days were studied through visualisation with a CLSM. For that purpose, cells were stained for F-actin and nuclei (Figure 4.4.). In all conditions, the cells presented a spread morphology with well-defined cytoskeleton except for monocultured rMSCs on F-CDHA at day 21.

Cx43, a gap-junction protein, was visualised in all CaPs substrates over all cell culture conditions at days 14 and 21 (Figure 4.5.). The analysis revealed that Cx43 protein was mainly colocalised with F-actin in cells cultured on CaPs being this scenario similar to that observed in control group. In all conditions the presence of Cx43 was mainly localized in the outer part of the cellular membrane.

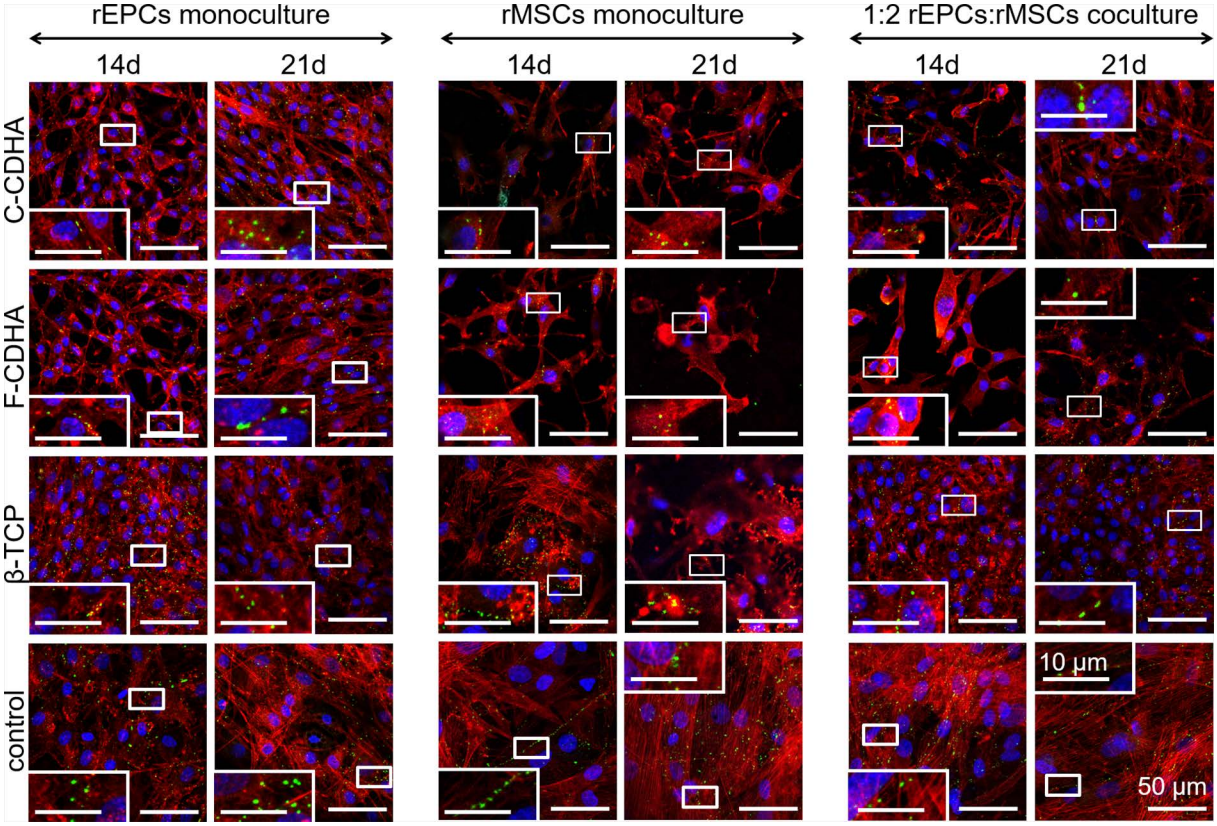

Figure 4.5. Merged fluorescence images of monocultured rEPCs, monocultured rMSCs and cocultured cells with ratio 1:2 of rEPCs and rMSCs on C-CDHA, F-CDHA and β-TCP at 14 and 21 days of cell culture. Cells were stained for Connexin43 (green), F-actin (red) and nuclei (blue). Scale bars denote 50 μm in the main images and 10 μm in the insets.

In order to distinguish rEPCs at coculture conditions, cells were additionally incubated with endothelial specific PECAM-1 and compared to monocultured rEPCs (Figure 4.6.A). Whilst PECAM-1 was well visible in rEPCs monoculture, a small number of PECAM-1 positively stained cells were observed in coculture. Semiquantitative analysis of CLSM images revealed that at day 14 the PECAM-1 stained area in rEPCs monoculture was slightly lower on C-CDHA and β-TCP sample whilst the F-CDHA showed similar values to that observed on control group (Figure 4.6.B). In case of coculture, increased values of PECAM-1 stained area were observed for C-CDHA at day 14 (Figure 4.6.C) compared to other CaPs and control. These differences between substrates were not statistically significant and they disappeared at day 21.

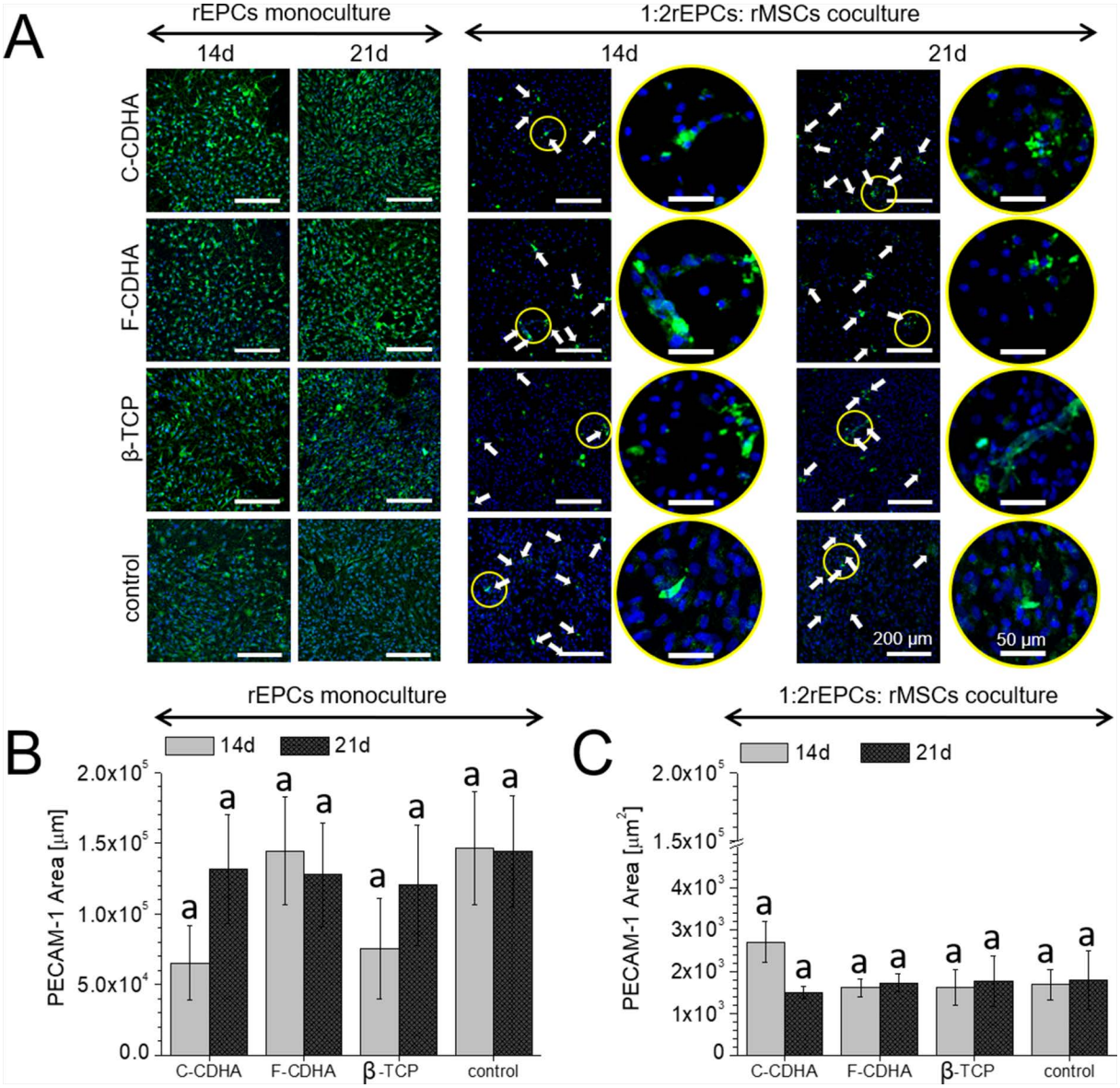

Figure 4.6. A) Merged fluorescence images of monocultured rEPCs and cocultured cells at ratio 1:2 of rEPCs and rMSCs on C-CDHA, F-CDHA and β-TCP at 14 and 21 days of cell culture. Cells were stained for PECAM-1 (green) and nuclei (blue). For coculture images, cells stained with both PECAM-1 and nuclei correspond to rEPCs whilst cells without PECAM-1 staining represent rMSCs. Scale bar denotes 200 µm for the main images and 50 µm for magnified images. **B)** Semiquantitative evaluation of area of PECAM-1 staining in monoculutred rEPCs on CaPs at 14 and 21 days. **C)** Semiquantitative evaluation of the area of PECAM-1 staining in cocultured 1:2 rEPCs and rMSCs on CaPs at 14 and 21 days. In graphs B and C, the same letter indicates groups with no statistically significant differences ($p > 0.05$) at specific time point.

4.3.6 Gene expression

4.3.6.1 Osteogenic gene expression

The expression of genes related to osteogenesis is depicted in Figure 4.7. In general, an upregulation of the osteogenic genes was detected on the CaP substrates, both in mono- and coculture conditions. A considerable upregulation of the ALP expression was

observed on the F-CDHA substrate, irrespective of cell type. In monocultured rMSCs the maximum value was attained at day 1, decreasing at 7 and 14 days. In contrast, in monocultured rEPCs and in the cocultures the ALP expression increased at 1 and 7 days, strongly decreasing at day 14. The expression of BMP-2 was higher for monocultured rEPCs compared to the other culture conditions in all substrates at day 1, decreasing afterwards. Conversely, monocultured rMSCs and coculture continuously increased their BMP-2 expression until day 7, especially for F-CDHA, and they maintained similar levels at day 14 irrespective of the substrate. Regarding OC expression, it was upregulated at early time points in the rEPCs, whilst in rMSCs and coculture the increase was shifted to 7 or 14 days. Moreover, the upregulation was higher on F-CDHA substrate in comparison to the other CaPs, irrespective of the cell type. The expression levels of DJ 1were higher in the two CDHA substrates compared to β-TCP. These levels were especially high in monocultured rEPCs and coculture at day 1 in both C-CDHA and F-CDHA. Subsequently, they decreased in all substrates except for rEPCs cultured on F-CDHA. Monocultured rMSCs on C-CDHA showed also a high upregulation at day 7.

4.3.6.2 Angiogenic gene expression

The expression of angiogenic markers is depicted in Figure 4.8. VEGF A was overexpressed by cells cultured on F-CDHA at all time points, especially by rEPCs but also in the 1:2 rEPCs: rMSCs cocultures an in the rMSC monocultures. In contrast, the cells cultured on C-CDHA and sintered β-TCP produced similar VEGF A expression pattern: an initial peak at day 1, followed by a brusque decrease at days 7 and 14. The expression profile of VEGF R2 was strongly dependent of cell type and substrate, although an overexpression was observed on all CaP substrates. In general, biomimetic substrates showed to cause more fluctuations in VEGF R2 expression rather than sintered β-TCP, which maintained similar VEGF R2 values over cell culture. For biomimetic CaPs, the overexpression of VEGF R2 was mainly observed in rEPCs monoculture presenting the highest values at days 7 and 14 for C-CDHA and F-CDHA, respectively. The expression of EDH 1 was strongly enhanced by F-CDHA at day 1 and 7 for rEPCs monoculture and at day 14 for coculture. In contrast, overexpression of EDH1 was observed in the rEPCs monoculture on β-TCP at day 14.

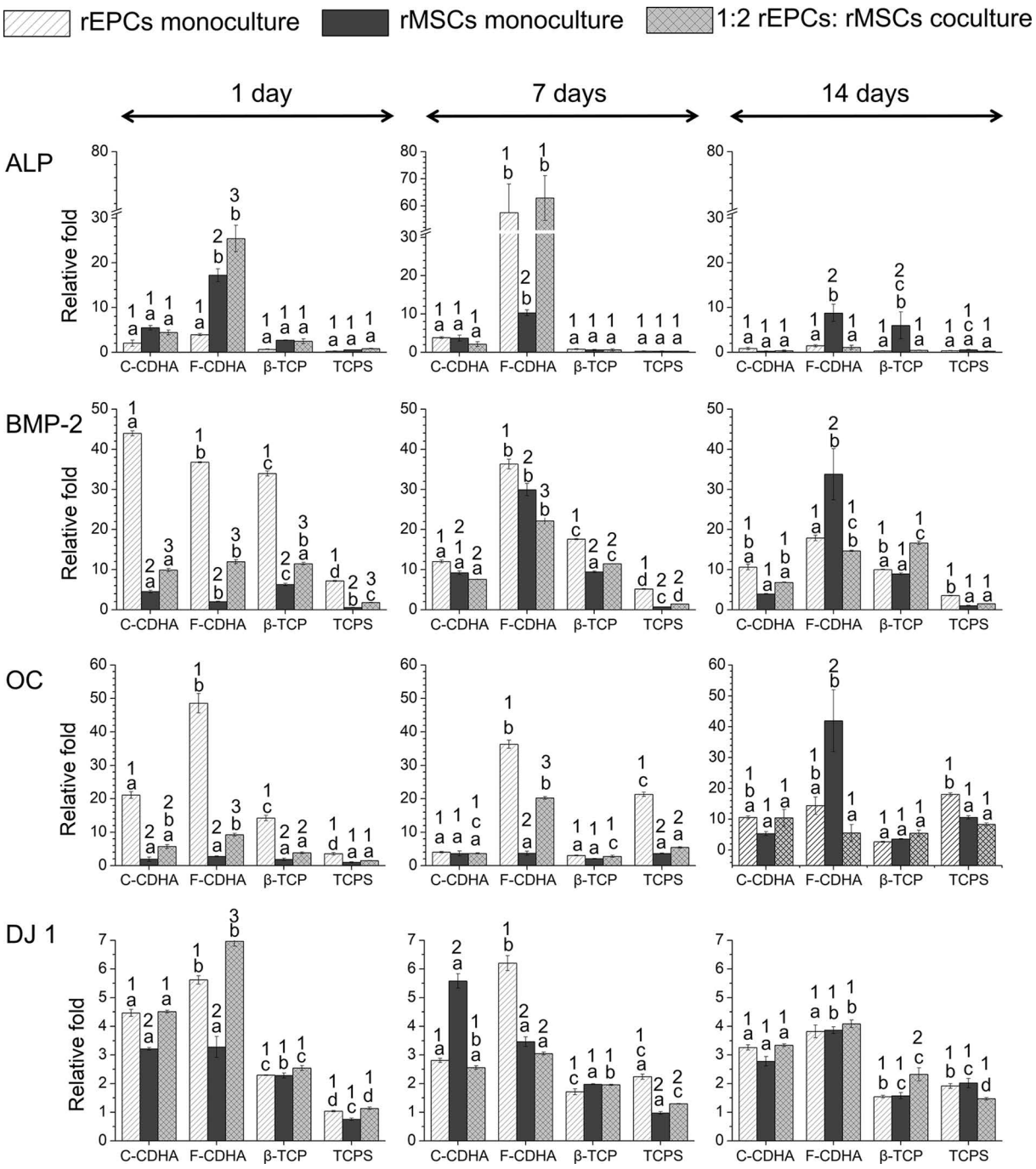

Figure 4.7. Gene expression of osteogenic markers in monocultured rEPCs, monocultured rMSCs and coculture on three calcium phosphate substrates. Expressions levels were determined by quantitative real time RT-PCR, normalised versus monocultured rMSCs on TCPS at 6 hours and displayed relative to their housekeeping gene. In all graphs, the same letter (a, b, c or d) indicates no statistically significant differences ($p > 0.05$) between substrates for each specific cell culture condition (rEPCs monoculture, rMSCs monoculture, rEPCs: rMSCs coculture). The same number (1, 2 or 3) indicates no statistically significant differences ($p > 0.05$) between cell culture conditions for each substrate (C-CDHA, F-CDHA, β-TCP, TCPS).

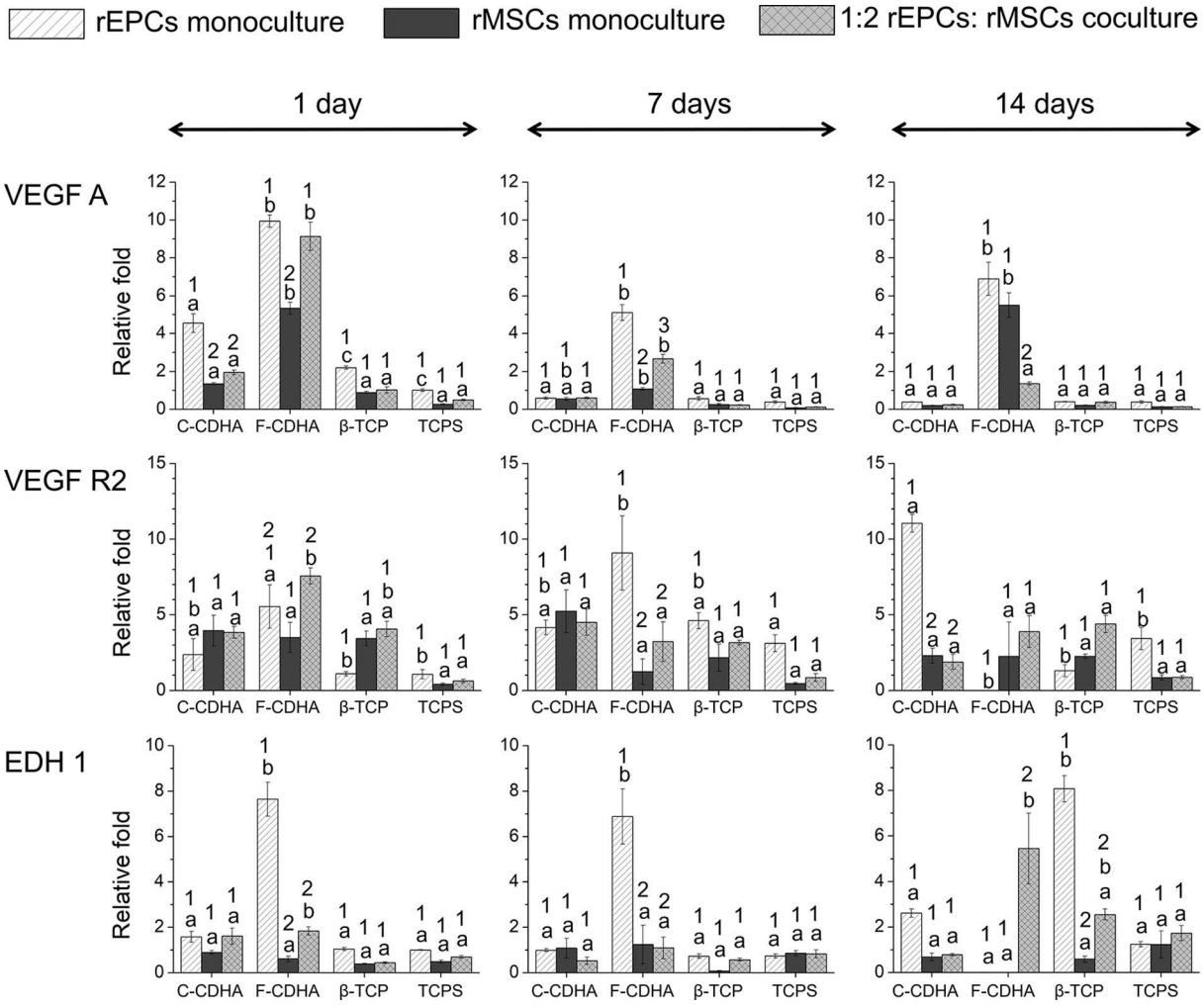

Figure 4.8. Gene expression of angiogenic markers in monocultured rEPCs, monocultured rMSCs and coculture on three calcium phosphate substrates. Expressions levels were determined by quantitative real time RT-PCR, normalised versus monocultured rEPCs on TCPS at 6 h. and displayed relative to their housekeeping gene. In all graphs, the same letter (a, b, c or d) indicates no statistically significant differences ($p > 0.05$) between substrates for each specific cell culture condition (rEPCs monoculture, rMSCs monoculture, rEPCs: rMSCs coculture). The same number (1, 2 or 3) indicates no statistically significant differences ($p > 0.05$) between cell culture conditions for each substrate (C-CDHA, F-CDHA, β-TCP, TCPS).

4.3.6.3 The effect of rEPCs and rMSCs coculture on osteogenic and angiogenic gene expression

The effect of coculture on the expression of osteogenic and angiogenic markers is presented in Figure 4.9. Upregulation of osteogenic markers in coculture condition was substrate and gene dependent. In general, the F-CDHA substrate led to higher values of upregulation of osteo-specific genes compared to other biomimetic C-CDHA and to sintered β-TCP. For F-CDHA, the main upregulation peak of osteogenic genes was detected at day 1 or day 7 of coculture. Both biomimetic C-CDHA and sintered β-TCP showed similar patterns for BMP-2, OC and DJ 1 showing dual upregulation peak at day 1 and 14.

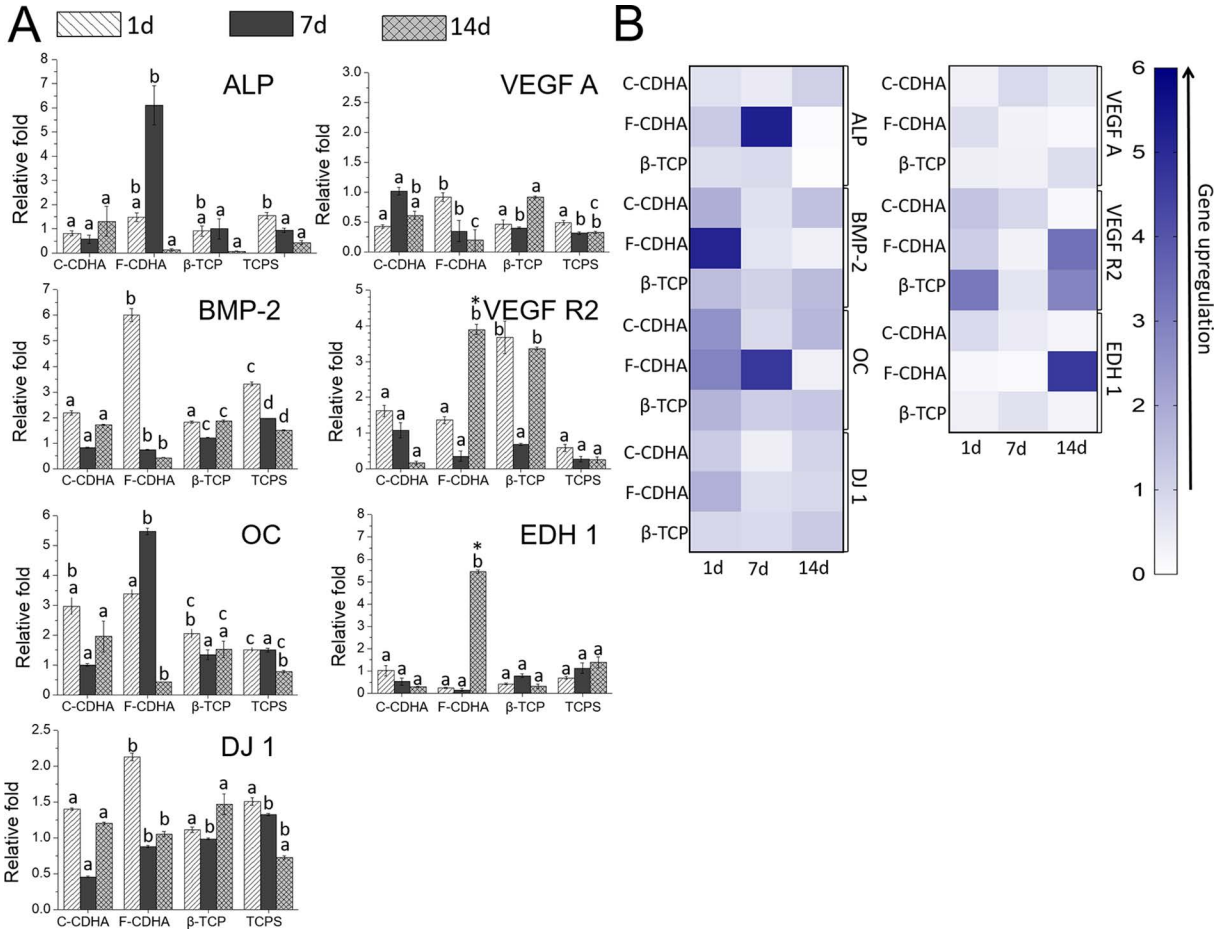

Figure 4.9. A) Effect of culturing both rEPCS and rMSCs on the gene expression of osteogenesis and angiogenesis related genes compared to monocultured cells. In order to see either specific gene is upregulated in coculture system the gene expression was normalised versus gene expression in monocultured rMSCs or monocultured rEPCs for osteogenic (ALP, BMP-2, OC, DJ 1) or angiogenic (VEGF A, VEGF R2, EDH 1) genes, respectively. For samples where gene expression in monoculture was not detected the mean value obtained in coculture was plotted (*). B) Heat map of gene upregulation in coculture system.

With regards to angiogenic gene expression, the cocultue of rEPCs and rMSCs resulted in strong upregulation of VEGF R2 and EDH 1 when the cells were cultured on F-CDHA and β-TCP, mainly at day 14 of coculture. The expression of EDH 1 was enhanced by F-CDHA whilst VEGF R2 expression was upregulated by both F-CDHA and β-TCP substrates (Figure 4.9.).

4.4 Discussion

4.4.1 Proliferation of rEPCs and rMSCs on the different substrates

The proliferation of rEPCs and rMSCs was clearly affected by the substrate to different extents, being slower in general on the biomimetic CDHA (Figure 4.3.A). The reduction of the proliferation rate was more pronounced for the rMSCs and the cocultures,

particularly on F-CDHA. This can be attributed to various factors. For instance, medium composition, surface topography as well as the ratio between cell types in coculture system were reported to influence cell proliferation.[33–35] Following previous reports, we decided to use EGM-2 MV, a medium for the culture of endothelial cells, both for coculture and monocultures instead of a mixture of cell culture media to guarantee endothelial cell survival.[21,36–38] Even if the use of endothelial cell culture medium for rMSCs monoculture is not a common choice, several studies have demonstrated little effects on phenotypic features of MSCs when cultured in EGM-2.[30,39,40] Moreover, the use of the same culture medium for all cultures is a clear advantage when comparing bioactive materials, which are known to interact with the cell culture medium. Using a single cell culture medium allows discarding any interactions due to the interaction of the material with the cell culture media of different compositions.

The analysis of cell behaviour on CaPs substrates requires to take into consideration not only their physicochemical features but also their intrinsic reactivity with aqueous environment. The reactive behaviour of CaPs *in vitro* and its further effect on bone cell behaviour, more pronounced for substrates with high SSA, has been widely reported.[13,41–43] For instance, we previously showed that CDHA altered ionic concentration to a higher extent than sintered ceramics[44], which can be related not only to the high SSA, but also to the presence of non-apatitic domains on their crystal surface.[45,46] Moreover, the distinct structural features of chemically identical substrates used in the present study, *i.e.* F-CDHA and C-CDHA, might produce different ionic fluctuations and thereby affect the cellular behaviour to different extents. Another interesting issue is that expected ionic fluctuations might vary depending of medium composition[42,44] as well as presence or not of cells. In the latter case, the layer of cells might reduce the exposure of the substrate to different extents depending on the degree of surface coverage, which in turn would decrease the ionic exchange.[47] In the current study we observed that CDHA substrates exhibited greater P_i release compared to sintered β-TCP and TCPS. In accordance with a previous report[48], this scenario was more pronounced for F-CDHA due to its higher SSA compared to C-CDHA. Although the monocultures and coculture on CaPs were performed using the same cell culture medium, the release of P_i was different over the same substrate. For instance, the P_i release from F-CDHA was 2-fold more pronounced in monocultured rMSCs compared to monocultured rEPCs (Figure 4.3.C) at 6 h of culture. However, since little differences of cellular adhesion on the biomimetic CDHA were observed at 6 hours of cell culture, different P_i release cannot be explained with the hypothesis that the layer of cells might cover the surface of substrate reducing the ionic exchange.[47] Therefore, we hypothesize that the different ionic behaviour observed in monocultures and coculture could be attributed to the cellular activity that occurs in contact with the substrate, which may buffer/increase the P_i content in cell culture medium.

In our study, monocultured rEPCs showed similar proliferative potential on all CaPs with slightly lower proliferation rate for biomimetic substrates (Figure 4.3. and 4.4.). Previous studies with bioinert substrates showed that topographical cues of biomaterials have little impact on proliferation of endothelial cells.[49] For instance, Xu *et al.* observed similar adhesion and proliferation of ECs cultured on randomly electrospun PLLA substrates with either nano- or micro-roughness.[49] It is important to highlight that, unlike in the case of inert materials, calcium phosphates control cellular behaviour also through fluid- mediated effects *i.e.* the ionic exchange with cell culture medium. This makes the scenario far more complex as the cell response is affected simultaneously by both textural properties of CaPs as well as indirect effects. This aspect must be taken into consideration when interpreting the *in vitro* performance of highly reactive biomaterials.

In contrast, reduced proliferation was observed for biomimetic substrates in comparison to β-TCP in rMSCs monoculture. This might be attributed to two simultaneously affecting factors: the microstructure of CDHA and its intrinsic ionic reactivity. We previously demonstrated that ionic fluctuations caused by CDHA particularly affect rMSCs causing a reduction on the number of focal adhesions and cell shrinkage and leading to cell death via apoptosis.[44] Interestingly, although the F-CDHA possesses the same chemical composition as C-CDHA, it leads to a more pronounced reduction of MSCs number. A similar behaviour was previously observed for osteoblastic cells.[48] The more pronounced release of P_i caused by F-CDHA due to its smaller crystal size and thus the higher SSA could be the responsible for this reduced proliferation. For instance, Liu *et al.* demonstrated that even small changes of P_i concentrations in cell culture medium reduce the proliferation of MSCs.[50] The effect of topography on cellular proliferation cannot be overlooked. For instance, it was previously demonstrated that the contact of cells with topography of CaP substrate slowed down the proliferation rate compared to cells exposed exclusively to CaP extracts without the additional effect of microstructure.[44]

Slowed cell proliferation on coculture system was also observed for CDHA, also especially for F-CDHA. Since the greater part of cells was constituted of rMSCs, we hypothesize that this behaviour can be also attributed to microstructure and ionic fluctuations of CDHA as above described for the rMSCs monoculture. Interestingly, the PECAM-1 staining revealed few number of rEPCs in coculture system, irrespective of the substrate (Figure 4.6.). The possible explanation of this scenario might be the growth rate of cells that might change when exposed to coculture conditions.[33] Bidarra *et al.* showed that MSCs and ECs cultured alone exhibited different proliferation rate as when they were cocultured. The authors observed that ECs stimulated the expansion of MSCs what might contribute to curtail ECs capability to grow in coculture. This led to lower proliferation rate for EC in coculture compared to EC in monolayer what was also observed in our study.[33] Similarly, Fuchs *et al.* demonstrated low proliferative potential

of ongrowth endothelial cells (OECs) when exposed to coculture conditions. Coculturing bone cells with OECs at ratio 3:2 lead to two opposite behaviours: whilst bone cells increased their number over time, a decrease was observed for OECs.[51] In our study, the low number of rECPs was interestingly observed in both CaPs and control group (Figure 4.6.). The high proliferation rate of coculture for control group and β-TCP combined with low number of PECAM-1 positively stained cells suggest an increased growth of MSCs what might contribute to curtail effect over rEPCs (Figure 4.3.A). Instead, the low cellular number of coculture observed on CDHA substrates suggests other parameters involved in reducing the rEPCs proliferation since this cannot be associated with increased rate of rMSCs proliferation. One possible explanation for this scenario might be the increased levels of phosphate from CDHA, since levels above 2.5 mM were reported to induce apoptosis in ECs.[52,53]

4.4.2 Angiogenic differentiation of rEPCs and rMSCs on the different substrates

In order to evaluate the angiogenic potential of CaPs, the expression of VEGF A and VEGF R2 was measured in mono- and coculture conditions (Figure 4.8.). Additionally, cell cultures were subjected to the endothelial specific PECAM-1 staining to reveal whether rEPCs form microcapillary-like structures on CaPs substrates (Figure 4.6.).

VEGF A plays a pivotal role in the angiogenesis process, regulating the recruitment of endothelial progenitor cells as well as promoting its proliferation and differentiation.[23] VEGF A has been also suggested to mediate the secretion of osteogenic factors such as BMP-2, thus stimulating bone cell behaviour.[54] Interestingly, VEGF A is known to be expressed not only by endothelial cells, but also by pre-osteoblasts during differentiation[55], thereby paracrinely stimulating angiogenesis. In our study, early VEGF A overexpression at 1 day was found when rEPCs were cultured on biomimetic substrates, notably more pronounced on F-CDHA (Figure 4.8.). Whilst rEPCs cultured on C-CDHA showed a decrease of VEGF A after 1 day expression peak, rEPCs on F-CDHA sustained high values of VEGF A. Furthermore, VEGF A expression was also upregulated for monocultured rMSCs and coculture on F-CDHA. This behaviour was not observed for other CaPs substrates. Several authors studied the effect of bioactive character of substrates such as bioglasses on high expression of VEGF A in endothelial cells. However, they rather point the stimulatory effect of the release of calcium, which was not altered in our study.[56,57] On the other hand, the surface roughness also plays an important role in regulating angiogenic gene expression. For instance, the upregulation of VEGF A was observed in bioinert materials with surface roughness (Ra) of approximately 2 μm.[58] Although the bioactive character of CDHA hinder to interrelate the enhanced VEGF A expression with the topography of the substrate, we hypothesize that the roughness of CDHA might contribute to present scenario. The expression of

VEGF R2 as the main receptor and major mediator of the angiogenic effects of VEGF on endothelial cells[59,60] was also studied. We found that the enhanced expression of VEGF A from endothelial cells cultured on F-CDHA substrate correlated with higher levels of their VEGF R2 at early time of cell culture. Interestingly, strongly enhanced values of VEGF A at 1 day for monocultured rEPCs on F-CDHA (Figure 4.8.) also corresponded in time with upregulation of EDH 1 and DJ 1 (Figure 4.7.) as well as sustained expression of BMP-2 (Figure 4.7.)- potent angiogenic inducers.[8,61] Hence, we hypothesize that greater expression of VEGF A might be coupled with combined effect of the enhanced expression of these genes as well as upregulation of VEGF R2. For instance, Jung-Min *et al.* demonstrated a positive effect of DJ 1 on VEGF A expression in endothelial cells through involvement of autocrine and paracrine mechanisms.[62]

Positively PECAM-1 stained cells were observed in both monocultured rEPCs and cocultured conditions (Figure 4.6.A). Nevertheless, we did not observe capillary-like networks in any of the studied CaP substrate. In both mono- and coculture conditions rEPCs were present in the form of patches rather than showing aligned morphology.

4.4.3 Osteogenic differentiation of rEPCs and rMSCs on the different substrates

The commitment of mono and cocultured rEPCs and rMSCs towards osteoblastic lineage was also evaluated through RT-qPCR. Alkaline phosphatase (ALP) expression and osteocalcin (OCN) are commonly used markers of early and late osteogenic gene expression, respectively. Whilst ALP is implicated in the regulation of local concentrations of inorganic phosphates fostering the mineralization[63], OC regulates the quality and size of newly-formed mineral crystals.[64] The gene expression of BMP-2 and DJ 1 were also evaluated since both participate in osteogenesis process as well as they are potent enhancers of angiogenesis.[6,65,66]

Different trends of expression of ALP, OC, BMP-2 and DJ 1 were observed for mono and coculture conditions (Figure 4.7.). Moreover, the expression of each individual osteogenic marker was also time- and substrate-dependent. In general, cells cultured on CaPs materials showed higher gene expression at early time point compared to TCPS. This effect was observed for both mono- and coculture condition being more pronounced for biomimetic substrates. The result is coinci dent with other studies where stimulatory effect of CaPs on osteogenic expression was demonstrated.[29,48] For instance, we previously reported that biomimetic materials induce the differentiation of MSCs to greater extent than sintered ceramic.[44] This stimulatory effect is likely due to the coupled effect of subtle ionic fluctuations and surface topography- pivotal parameters in controlling osteogenic cell commitment.[67,68] The little changes of calcium content in EGM-2 MV medium after immersion of CDHA allowed the cell survival and further differentiation. This accords with our previous finding where differentiation of MSCs

into osteoblastic lineage cultured on CDHA was observed only when great ionic changes were mitigated. Interestingly, although both biomimetic CDHA own the same chemistry, the osteogenic differentiation was more pronounced for needle-like F-CDHA substrate suggesting the important role of surface topography.[48] This scenario, indeed, might contribute to curtail proliferation rate of MSCs (Figure 4.3.A) inasmuch as osteogenic differentiation is usually accompanied by slower cellular proliferation.

4.4.4 Angiogenic and osteogenic differentiation of rEPCs and rMSCs in coculture

The impact of coculturing rEPCs with rMSCs on angio- and osteogenesis was depicted in Figure 9. Overall, the F-CDHA stimulated to a greater extent the gene expression in coculture conditions compared to rMSCs monocultured on the same substrate. Interestingly, this upregulation was more pronounced for osteogenic-related genes, which were upregulated either at 1 day (BMP-2, OC and DJ1) or 7 days (ALP and OC) (Figure 4.9.). Regarding the angiogenic gene expression, there were no impact of coculturing rEPCs and rMSCs on upregulation of VEGF A, the main regulator of angiogenic events, on any of studied CaPs substrates.

The previous reports showed that there are several parameters that might orchestrate this behaviour in coculture. For instance, Salani *et al.* underlined that a direct cell contact, through gap junctional proteins like Cx43, is a fundamental condition for stimulation of gene expression in endothelial and bone cells in in vitro coculture systems.[69] However, since monocultured and cocultured cells presented similar secretion of Cx43 (Figure 4.5.), the enhanced expression of osteogenic genes for coculture on F-CDHA should be attributed to other events that orchestrate this behaviour. The great influence of potent osteogenic enhancers like BMP-2, EDH 1 and DJ 1 was also mentioned in literature. Kaigler *et al.* demonstrated that direct cell-cell contact mediate BMP-2 signalling from endothelial cells enhancing the ALP activity and OCN production of bone cells.[70] The effect of EDH 1, although frequently associated only with angiogenic events, was also reported to stimulate differentiation of osteoprogenitor cells.[23] Moreover, previous reports demonstrated that DJ 1 not only mediates the endothelial-bone cells' crosstalk but also induces osteogenesis through FGFR-1 signalling.[6] Since no enhanced expression of BMP-2 and EDH 1 in coculture was observed for F-CDHA substrate we hypothesize that the higher levels of DJ 1 might contribute to the osteogenic potential of F-CDHA.

4.5 Conclusions

The results demonstrate that distinct chemical features of CaPs substrate trigger various cell responses in terms of proliferation as well as angiogenic and osteogenic gene expression. In general, ionically more reactive CDHA affect proliferation rate to greater

extent than sintered β-TCP. The F-CDHA led to more pronounced ionic changes than C-CDHA significantly reducing proliferation rate of rMSCs and the coculture of rECPs: rMSCs. For β-TCP, where cells were exposed to little ionic exchange, the coculture resulted in enhanced growth of rMSCs compared to monocultured rMSCs.

With regards to coculture condition, the cellular crosstalk was not reflected in enhanced secretion of gap junctional protein Cx43 but through upregulation of osteogenic-related genes. This behaviour was mainly observed for F-CDHA substrate and might be related to enhanced expression of osteogenic inducer DJ 1.

4.6 Bibliography

1. Hu, K. & Olsen, B. R. Osteoblast-derived VEGF regulates osteoblast differentiation and bone formation during bone repair. **126,** 509–526 (2016).
2. Kusumbe, A. P., Ramasamy, S. K. & Adams, R. H. Coupling of angiogenesis and osteogenesis by a specific vessel subtype in bone. *Nature* **507,** 323–328 (2014).
3. Stegen, S., van Gastel, N. & Carmeliet, G. Bringing new life to damaged bone: The importance of angiogenesis in bone repair and regeneration. *Bone* **70,** 19–27 (2015).
4. Mayer, H. *et al.* Vascular endothelial growth factor (VEGF A) expression in human mesenchymal stem cells: Autocrine and paracrine role on osteoblastic and endothelial differentiation. *J. Cell. Biochem.* **95,** 827–839 (2005).
5. Javerzat, S., Auguste, P. & Bikfalvi, A. The role of fibroblast growth factors in vascular development. *Trends Mol. Med.* **8,** 483–489 (2002).
6. Kim, J.-M. *et al.* DJ-1 promotes angiogenesis and osteogenesis by activating FGF receptor-1 signaling. *Nat. Commun.* **3,** 1296 (2012).
7. Raida, M., Heymann, a C., Günther, C. & Niederwieser, D. Role of bone morphogenetic protein 2 in the crosstalk between endothelial progenitor cells and mesenchymal stem cells. *Int. J. Mol. Med.* **18,** 735–9 (2006).
8. Smadja, D. M. *et al.* Bone morphogenetic proteins 2 and 4 are selectively expressed by late outgrowth endothelial progenitor cells and promote neoangiogenesis. *Arterioscler. Thromb. Vasc. Biol.* **28,** 2137–2143 (2008).
9. Dyer, L. A., Pi, X. & Patterson, C. The role of BMPs in endothelial cell function and dysfunction. *Trends Endocrinol. Metab.* **25,** 472–80 (2014).
10. Parfitt, A. M. The mechanism of coupling: a role for the vasculature. *Bone* **26,** 319–323 (2000).
11. Barba, A. *et al.* Intrinsic osteoinduction of biomimetic nanostructured calcium phosphate scaffolds. *Front. Bioeng. Biotechnol.* **4,** 2–3 (2016).
12. Barba, A. *et al.* Osteoinduction by Foamed and 3D-Printed Calcium Phosphate Scaffolds: Effect of Nanostructure and Pore Architecture. *ACS Appl. Mater. Interfaces* **9,** 41722–41736 (2017).
13. Danoux, C. *et al.* The Effects of Crystal Phase and Particle Morphology of Calcium Phosphates on Proliferation and Differentiation of Human Mesenchymal Stromal Cells. *Adv. Healthc. Mater.* **5,** 1775–1785 (2016).
14. Danoux, C. *et al.* Development of Highly Functional Biomaterials by Decoupling and Recombining Material Properties. *Adv. Mater.* **28,** 1803–1808 (2016).
15. Xiao, X. *et al.* The promotion of angiogenesis induced by three-dimensional porous beta-tricalcium phosphate scaffold with different interconnection sizes via activation of PI3K/Akt pathways. *Sci. Rep.* **5,** 9409 (2015).
16. Chen, W., Thein-Han, W., Weir, M. D., Chen, Q. & Xu, H. H. K. Prevascularization of biofunctional calcium phosphate cement for dental and craniofacial repairs. *Dent. Mater.* **30,** 535–44 (2014).
17. Patel, Z. S. *et al.* Dual delivery of an angiogenic and an osteogenic growth factor for bone regeneration in a critical size defect model. *Bone* **43,** 931–940 (2008).
18. Zhang, H. X. *et al.* In vitro and in vivo evaluation of calcium phosphate composite scaffolds containing BMP-VEGF loaded PLGA microspheres for the treatment of avascular necrosis of the femoral head. *Mater. Sci. Eng. C* **60,** 298–307 (2016).
19. Barralet, J. *et al.* Angiogenesis in Calcium Phosphate Scaffolds by Inorganic Copper Ion Release. *Tissue Eng. Part A* **15,** 1601–1609 (2009).
20. Bose, S., Fielding, G., Tarafder, S. & Bandyopadhyay, A. Understanding of dopant-induced osteogenesis and angiogenesis in calcium phosphate ceramics. *Trends Biotechnol.* **31,** 594–605 (2013).
21. Thein-Han, W. & Xu, H. H. K. Prevascularization of a gas-foaming macroporous calcium phosphate cement scaffold via coculture of human umbilical vein endothelial cells and osteoblasts. *Tissue Eng. Part A* **19,** 1675–85 (2013).
22. Deckers, M. M. L. *et al.* Bone Morphogenetic Proteins Stimulate Angiogenesis through Osteoblast-Derived Vascular Endothelial Growth Factor A. *Endocrinology* **143,** 1545–1553 (2002).

23. von Schroeder, H. ., Veillette, C. ., Payandeh, J., Qureshi, A. & Heersche, J. N. . Endothelin-1 promotes osteoprogenitor proliferation and differentiation in fetal rat calvarial cell cultures. *Bone* **33,** 673–684 (2003).
24. Ginebra, M. P. *et al.* Setting Reaction and Hardening of an Apatitic Calcium Phosphate Cement. *J. Dent. Res.* **76,** 905–912 (1997).
25. Espanol, M. *et al.* Intrinsic porosity of calcium phosphate cements and its significance for drug delivery and tissue engineering applications. *Acta Biomater.* **5,** 2752–62 (2009).
26. Diez-Escudero, A., Espanol, M., Beats, S. & Ginebra, M.-P. In vitro degradation of calcium phosphates: Effect of multiscale porosity, textural properties and composition. *Acta Biomater.* **60,** 81–92 (2017).
27. Aguirre, A., González, A., Planell, J. A. & Engel, E. Extracellular calcium modulates in vitro bone marrow-derived Flk-1+ CD34+ progenitor cell chemotaxis and differentiation through a calcium-sensing receptor. *Biochem. Biophys. Res. Commun.* **393,** 156–161 (2010).
28. Aguirre, A., Planell, J. A. & Engel, E. Dynamics of bone marrow-derived endothelial progenitor cell/mesenchymal stem cell interaction in co-culture and its implications in angiogenesis. *Biochem. Biophys. Res. Commun.* **400,** 284–91 (2010).
29. Bulnheim, U. *et al.* Endothelial cells stimulate osteogenic differentiation of mesenchymal stem cells on calcium phosphate scaffolds. *J. Tissue Eng. Regen. Med.* **8,** 831–40 (2014).
30. Janeczek Portalska, K. *et al.* Endothelial Differentiation of Mesenchymal Stromal Cells. *PLoS One* **7,** (2012).
31. Stern, J. & Lewis, W. H. P. The colorimetric estimation of calcium in serum with o-cresolphthalein complexone. *Clin. Chim. Acta* **2,** 576–580 (1957).
32. Gitelman, J. An Improved Automated Procedure of Calcium in Biological for the Determination Specimens. *Anal. Biochem.* **18,** 521–531 (1967).
33. Bidarra, S. J. *et al.* Phenotypic and proliferative modulation of human mesenchymal stem cells via crosstalk with endothelial cells. *Stem Cell Res.* **7,** 186–97 (2011).
34. Ma, J. *et al.* Coculture of osteoblasts and endothelial cells: optimization of culture medium and cell ratio. *Tissue Eng. Part C. Methods* **17,** 349–357 (2011).
35. Kang, Y., Kim, S., Fahrenholtz, M., Khademhosseini, A. & Yang, Y. Osteogenic and angiogenic potentials of monocultured and co-cultured human-bone-marrow-derived mesenchymal stem cells and human-umbilical-vein endothelial cells on three-dimensional porous beta-tricalcium phosphate scaffold. *Acta Biomater.* **9,** 4906–15 (2013).
36. Sun, W. *et al.* Co-culture of outgrowth endothelial cells with human mesenchymal stem cells in silk fibroin hydrogels promotes angiogenesis. *Biomed. Mater.* **11,** 35009 (2016).
37. Pedersen, T. O. *et al.* Mesenchymal stem cells induce endothelial cell quiescence and promote capillary formation. *Stem Cell Res. Ther.* **5,** 23 (2014).
38. Liu, X. *et al.* Co-Seeding Human Endothelial Cells with Human-Induced Pluripotent Stem Cell-Derived Mesenchymal Stem Cells on Calcium Phosphate Scaffold Enhances Osteogenesis and Vascularization in Rats. *Tissue Eng. Part A* **23,** 546–555 (2017).
39. Bouacida, A. *et al.* Pericyte-Like Progenitors Show High Immaturity and Engraftment Potential as Compared with Mesenchymal Stem Cells. *PLoS One* **7,** (2012).
40. König, J. *et al.* Amnion-derived mesenchymal stromal cells show angiogenic properties but resist differentiation into mature endothelial cells. *Stem Cells Dev.* **21,** 1309–20 (2012).
41. Knabe, C. *et al.* Evaluation of calcium phosphates and experimental calcium phosphate bone cements using osteogenic cultures. *J. Biomed. Mater. Res.* **52,** 498–508 (2000).
42. Gustavsson, J., Ginebra, M. P. P., Engel, E. & Planell, J. Ion reactivity of calcium-deficient hydroxyapatite in standard cell culture media. *Acta Biomater.* **7,** 4242–52 (2011).
43. Gustavsson, J., Ginebra, M. P., Planell, J. & Engel, E. Osteoblast-like cellular response to dynamic changes in the ionic extracellular environment produced by calcium-deficient hydroxyapatite. *J. Mater. Sci. Mater. Med.* **23,** 2509–20 (2012).
44. Sadowska, J.-M., Guillem-Marti, J., Montufar, E. B., Espanol, M. & Ginebra, M.-P. Biomimetic Versus Sintered Calcium Phosphates: The In Vitro Behavior of Osteoblasts and Mesenchymal Stem Cells. *Tissue Eng. Part A* **23,** 1297–1309 (2017).
45. Vandecandelaere, N., Rey, C. & Drouet, C. Biomimetic apatite-based biomaterials: On the critical impact of synthesis and post-synthesis parameters. *J. Mater. Sci. Mater. Med.* **23,** 2593–

2606 (2012).
46. Cazalbou, S. *et al.* Ion exchanges in apatites for biomedical applications. **6,** 405–409
47. Ciapetti, G. *et al.* Osteoclast differentiation from human blood precursors on biomimetic calcium-phosphate substrates. *Acta Biomater.* **50,** 102–113 (2017).
48. Engel, E. *et al.* Discerning the role of topography and ion exchange in cell response of bioactive tissue engineering scaffolds. *Tissue Eng. Part A* **14,** 1341–51 (2008).
49. Xu, C., Yang, F., Wang, S. & Ramakrishna, S. In vitro study of human vascular endothelial cell function on materials with various surface roughness. *J. Biomed. Mater. Res. - Part A* **71,** 154–161 (2004).
50. Liu, Y. K. Y. K. *et al.* The effect of extracellular calcium and inorganic phosphate on the growth and osteogenic differentiation of mesenchymal stem cells in vitro: implication for bone tissue engineering. *Biomed. Mater.* **4,** 25004 (2009).
51. Fuchs, S. *et al.* Dynamic processes involved in the pre-vascularization of silk fibroin constructs for bone regeneration using outgrowth endothelial cells. *Biomaterials* **30,** 1329–1338 (2009).
52. Di Marco, G. S. *et al.* High phosphate directly affects endothelial function by downregulating annexin II. *Kidney Int.* **83,** 213–222 (2013).
53. Di Marco, G. S. *et al.* Increased inorganic phosphate induces human endothelial cell apoptosis in vitro. *Am. J. Physiol. Renal Physiol.* **294,** F1381-7 (2008).
54. Peng, H. *et al.* VEGF Improves, Whereas sFlt1 Inhibits, BMP2-Induced Bone Formation and Bone Healing Through Modulation of Angiogenesis. *J. Bone Miner. Res.* **20,** 2017–2027 (2005).
55. Akeno, N., Robins, J., Zhang, M., Czyzyk-Krzeska, M. F. & Clemens, T. L. Induction of Vascular Endothelial Growth Factor by IGF-I in Osteoblast-Like Cells Is Mediated by the PI3K Signaling Pathway through the Hypoxia-Inducible Factor-2α. *Endocrinology* **143,** 420–425 (2002).
56. Eldesoqi, K. *et al.* High calcium bioglass enhances differentiation and survival of endothelial progenitor cells, inducing early vascularization in critical size bone defects. *PLoS One* **8,** (2013).
57. Aguirre, A. *et al.* Control of microenvironmental cues with a smart biomaterial composite promotes endothelial progenitor cell angiogenesis. *Eur. Cells Mater.* **24,** 90–106 (2012).
58. Olivares-Navarrete, R. *et al.* Rough titanium alloys regulate osteoblast production of angiogenic factors. *Spine J.* **13,** 1563–1570 (2013).
59. Ferrara, N., Gerber, H.-P. & LeCouter, J. The biology of VEGF and its receptors. *Nat. Med.* **9,** 669–676 (2003).
60. Koch, S. & Claesson-Welsh, L. Signal transduction by vascular endothelial growth factor receptors. *Cold Spring Harb. Perspect. Med.* **2,** 1–21 (2012).
61. Salani, D. *et al.* Endothelin-1 Induces an Angiogenic Phenotype in Cultured Endothelial Cells and Stimulates Neovascularization In Vivo. *Am. J. Pathol.* **157,** 1703–1711 (2000).
62. Seghezzi, G. *et al.* Fibroblast growth factor-2 (FGF-2) induces vascular endothelial growth factor (VEGF) expression in the endothelial cells of forming capillaries: an autocrine mechanism contributing to angiogenesis. *J. Cell Biol.* **141,** 1659–73 (1998).
63. Golub, E. E., Harrison, G., Taylor, a G., Camper, S. & Shapiro, I. M. The role of alkaline phosphatase in cartilage mineralization. *Bone Miner.* **17,** 273–278 (1992).
64. Roach, H. I. Why does bone matrix contain non-collagenous proteins? The possible roles of osteocalcin, osteonectin, osteopontin and bone sialoprotein in bone mineralisation and resorption. *Cell biology international* **18,** 617–628 (1994).
65. Vasseur, S. *et al.* DJ-1/PARK7 is an important mediator of hypoxia-induced cellular responses. *Proc. Natl. Acad. Sci.* **106**, 1111–1116 (2009).
66. Hoogendam, J., Bent, C. V. a N. D. E. R., Papapoulos, S. E. & Lo, C. W. G. M. through Osteoblast-Derived Vascular Endothelial Growth Factor A. *Endocrinology* **143,** 1545–1553 (2014).
67. McBeath, R., Pirone, D. M., Nelson, C. M., Bhadriraju, K. & Chen, C. S. Cell Shape, Cytoskeletal Tension, and RhoA Regulate Stem Cell Lineage Commitment. *Dev. Cell* **6,** 483–495 (2004).
68. Kilian, K. A., Bugarija, B., Lahn, B. T. & Mrksich, M. Geometric cues for directing the differentiation of mesenchymal stem cells. *Proc. Natl. Acad. Sci. U. S. A.* **107,** 4872–7 (2010).
69. Villars, F. *et al.* Effect of HUVEC on human osteoprogenitor cell differentiation needs

heterotypic gap junction communication. *Am. J. Physiol. Cell Physiol.* **282,** C775-85 (2002).
70. Kaigler, D. *et al.* Endothelial cell modulation of bone marrow stromal cell osteogenic potential. *FASEB J.* **19,** 665–7 (2005).

Chapter 5

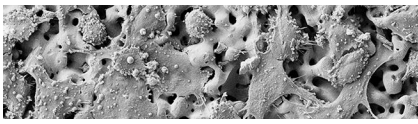

Biomimetic versus sintered calcium phosphates: The *in vitro* behavior of osteoblasts and mesenchymal stem cells

5.1 Introduction

Synthetic bone grafts represent an advantageous alternative to autographs and allographs from various points of view.[1-3] On the one hand, because they are of synthetic origin, availability is not a concern. Moreover, they do not cause immunogenic reactions or disease transmission. However, despite all these advantages, the success of these synthetic bone grafts depends on their capacity to actively stimulate bone regeneration, while maintaining a tight synchronization between bone formation and reabsorption.

Calcium phosphates have been extensively used as bone substitutes.[4-6] Traditionally, they are obtained by high temperature sintering routes. However, in recent years the potential of using more mild reaction conditions, that is, biomimetic routes based on dissolution/precipitation reactions that occur at room or body temperature has been disclosed.[7,8] The reason for this shift is to attempt to mimic the processes by which the human body fabricates the mineral phase in bone, which is also a calcium phosphate. Thus, using biomimetic routes, it is now possible to obtain nanostructured calcium-deficient hydroxyapatite (CDHA) materials that are more similar to the mineral phase in bone in terms of morphology, texture, composition, specific surface area (SSA), and crystallinity. It is hypothesized that, due to the higher reactivity resulting from the mentioned properties, this biomimetic hydroxyapatite would be more closely recognized by autologous bone and would consequently undergo similar remodelling processes as bone.

The high reactivity of biomimetic CDHA has, however, direct implications when assessing the *in vitro* cell response to this material. Previous studies showed that biomimetic CDHA significantly altered the ionic composition of the cell culture medium[9], affecting cellular behaviour. This was demonstrated by growing cells on porous membranes (inserts) placed on top of the materials to allow ionic and protein exchanges through the membrane, but preventing direct contact of cells with the material.[10] Although the results proved the effect of the materials' reactivity, the effect of topography was not addressed in this study even if *in vivo* both, reactivity and topography, contribute simultaneously.

Moreover, the extent to which these changes could affect cellular behaviour compared to traditional sintered calcium phosphates and the relative importance of the composition and surface texture must still be deciphered. Thus, the aim of this work is to investigate how biomimetic and sintered calcium phosphates alter the composition of the cell culture medium and the extent to which this change and the different textural properties affect cell behaviour.

For this purpose, two cell types that are relevant to the osteogenic process, namely, osteoblastic cells and mesenchymal stem cells, were cultured in direct contact with the

surface of the materials and indirectly, that is, in contact with the media modified by the material, but without contacting the surface of the materials.

For the indirect studies, a novel strategy was explored, in which the cells were seeded on glass coverslips that were placed on top of the materials so that cells could continuously sense the average ionic environment caused by the diffusion of ions in and out of the material. The use of glass coverslips was preferred over the use of commercial Transwell systems not only for economic reasons but also because it allowed easy monitoring of the cells by optical microscopy. This is not possible when cells are grown on the porous membranes (inserts) of the Transwell systems.

Biomimetic CDHA ($Ca_9(HPO_4)(PO_4)_5(OH)$) obtained by hydrolysis of α-tricalcium phosphate (α-TCP) at 37 ºC and sintered α-TCP (α-$Ca_3(PO_4)_2$) and β-tricalcium phosphate (β-TCP) (β-$Ca_3(PO_4)_2$), both of which were obtained by heat treatment of CDHA, were used as materials. The two sintered materials were chosen based on two considerations: (1) the sintering step results in materials with identical elemental compositions to CDHA (e.g., Ca/P = 1.5), and (2) α-TCP and β-TCP have been widely used as synthetic bone grafts. Moreover, an additional material was prepared as a control, that is, stoichiometric hydroxyapatite ($Ca_{10}(PO_4)_6(OH)_2$), which was obtained by sintering the same reagents used for the fabrication of CDHA.

5.2 Materials and methods

5.2.1 Material preparation

Biomimetic CDHA discs were obtained by a cementitious reaction based on the hydrolysis of α-TCP, as previously described.[7] Briefly, α-TCP powder containing 2 wt.% of precipitated hydroxyapatite (Merck 2143; Merck, Darmstardt, Germany) was mixed with a 2.5 wt.% aqueous solution of disodium hydrogen phosphate (Na_2HPO_4; Panreac, Darmstadt, Germany) at a liquid to powder ratio of 0.65 mL/g. The paste was placed in Teflon moulds to produce discs (15 mm diameter and 2 mm thickness), which were immersed in 37 ºC water for 7 days to ensure complete hydrolysis of the α-TCP powder to CDHA. Afterward, a thermal treatment was applied to the CDHA discs to obtain either β-TCP discs (1100 ºC/9 h, followed by slow cooling inside the furnace) or α-TCP discs (1400 ºC/4 h, followed by quenching in air).

The α-TCP powder used for the cementitious reaction was obtained by heat-treating a 2:1 molar mixture of $CaHPO_4$ (Sigma-Aldrich, St. Louis, MO) and $CaCO_3$ (Sigma-Aldrich) at temperatures up to 1400 ºC for 15 h, which was subsequently quenched in air. Afterward, the α-TCP was milled in a planetary ball mill (Pulverisette 6, Fritsch GmbB) for 15 min at 450 rpm using 10 agate balls (d=30 mm).

Moreover, stoichiometric hydroxyapatite (HA) discs were prepared by mixing $CaHPO_4$ and $CaCO_3$ powders at a calcium/ phosphorous molar ratio of 1.67. Then, 0.6 g of the mixture was uniaxially compacted at 80 MPa to obtain 15 mm discs. Afterward, the discs were sintered at 1100 ºC for 20 h.

5.2.2 Material characterisation

The dimensions and weights of the discs were recorded after the synthesis/sintering process. The phase composition of the discs was determined by X-ray diffraction (XRD; D8 Advance; Bruker, Karlsruhe, Germany). The diffractometer equipped with a Cu Ka X-ray tube was operated at 40 kV and 40 mA. Data were collected in 0.02 º steps over the 2θ range of 10-80 º, with a counting time of 2 s per step. For phase identification, the diffraction patterns were compared with the Joint Committee on Powder Diffraction Standards for HA (JCPDS 82-1943), α-TCP (JCPDS 09-0348), and β-TCP (JCPDS 70-2065). Semiquantitative XRD analysis of the products was carried out using the reference intensity ratio method.[11]

Infrared analyses were performed on a Perkin Elmer Frontier Fourier transform infrared spectroscopy spectrometer in the attenuated total reflection mode to check the typical functional groups present in the samples. All spectra were obtained in the range of 225-4000 cm^{-1} with a spectral resolution of 4 cm^{-1} by averaging 32 scans. The microstructure of the samples was examined using scanning electron microscopy (SEM; Zeiss Neon 40, Oberkochen, Germany) at an acceleration voltage of 5 kV after the surface was coated with a thin gold-palladium layer.

The surface roughness was characterised by confocal microscopy (Sensofar, PIm 2300), using a 50x magnification and a scanned area of 240 x 180 mm^2. The SSA was determined by nitrogen adsorption (ASAP 2020; Micromeritics, Norcross, GA) using the Brunauer-Emmett-Teller method. The skeletal density was measured by helium pycnometry (AccuPyc 133; Micromeritics). Finally, the porosity and pore size distribution were measured by mercury intrusion porosimetry (MIP; AutoPore IV 9500).

5.2.3 Cell culture study

Primary rat mesenchymal stem cells (rMSCs) were used to evaluate the osteoinductive potential of the different materials, that is, their capacity to induce the differentiation of undifferentiated stromal cells to the osteoblastic phenotype. The effect of the materials on osteoblastic cells was assessed using human osteoblast-like SaOS-2 cells (ATCC, Manassas, VA). Although SaOS-2 cells are an osteosarcoma cell line, their suitability as osteoblast cell model has been widely demonstrated.[12-14]

SaOS-2 cells were maintained in McCoy's medium (Sigma-Aldrich) supplemented with 10 % foetal bovine serum (FBS), 2 mM L-glutamine, penicillin/streptomycin (50 U/mL

and 50 mg/mL, respectively), and 20 mM 4-(2-hydroxyethyl) piperazine-1-ethanesulfonic acid buffer (HEPES), all from Invitrogen.

rMSCs were isolated from the tibias and femurs of Lewis at the Institute for Bioengineering of Catalonia (IBEC) as previously described.[15] The mesenchymal stem cell phenotype was previously characterized by flow cytometry.[16] Cells were expanded in Advanced Dulbecco's modified Eagle medium (DMEM) supplemented with 10 % FBS, 2 mM L-glutamine, penicillin/streptomycin (50 U/mL and 50 mg/mL, respectively), and 20 mM HEPES buffer, all from Invitrogen. Cells at passages 4 to 5 were used in all experiments

5.2.4 Direct contact cell cultures

The discs were sterilized by immersion in 70 % ethanol and rinsed thrice with phosphate- buffered saline (PBS). Then, the discs (n=3 per each independent experiment) were placed in 24-well plates and incubated with the corresponding complete media overnight. Afterward, 80×10^3 cells/well were seeded and incubated for 4 or 6 h (SaOS-2 cells or rMSCs, respectively), and then cultured up to 7 days; the media were refreshed every day. Tissue culture polystyrene (TCPS) was used as control.

5.2.5 Indirect contact cell cultures

The cells were cultured in indirect contact with the calcium phosphate discs using glass coverslips (d=8 mm) to determine the effect of ionic exchanges. For this purpose, the coverslips were first sterilized by immersion in 70 % ethanol, rinsed thrice with PBS, and then placed in a 48-well plate and incubated with FBS for 4 h. Subsequently, 20×10^3 cells (SaOS-2 cells) or 5×10^3 cells (rMSCs) were seeded on the coverslips and incubated overnight.

The initial number of each type of cells was determined in a previous assay to prevent confluence and subsequent detachment from the glass coverslips at the end of the assay. The coverslips were then transferred to 24-well plates and placed on top of the sterilized and preconditioned calcium phosphate discs as shown in Supplementary Figure 5.1 (preconditioning was carried out as described in the direct contact assays). The discs remained stable on top of the samples throughout the assay. The cells were incubated for the same time periods as the direct cell cultures, and the media were refreshed every day. Glass coverslips on TCPS were used as the control.

5.2.6 Cell proliferation

The cells were lysed with 300 mL of M-PER® (Mammalian Protein Extraction Reagent; Thermo Scientific, Waltham, MA) after transferring the calcium phosphate discs (direct culture) or the coverslips (indirect cell culture) onto a new 24-well plate at each specified

time. Cell proliferation was evaluated at 4 or 6 h (SaOS-2 cells or rMSCs, respectively), 3 and 7 days of cell culture. At each time point, cells were lysed with 300 mL of M-PER. The cell number was evaluated using the Cytotoxicity Detection Kit lactate dehydrogenase (LDH; Roche Applied Science, Penzberg, Germany), according to the manufacturer's instructions. The LDH activity was measured spectrophotometrically at 492 nm with PowerWave HT Microplate Reader (BioTek Instruments, Inc., Winooski, VT)[17]. A calibration curve with a decreasing number of cells was prepared to express the results as cell numbers. Finally, the results were expressed as a relative fold change compared to the cell number obtained on TCPS at 4 or 6 h (SaOS-2 cells or rMSCs, respectively). The experiments were performed in triplicate.

5.2.7 Cell differentiation

The alkaline phosphatase (ALP) activity was quantified as a marker of osteogenic differentiation. The ALP activity was determined in the same extracts used for the cell proliferation assay, which did not contain osteogenic factors, using a SensoLyte® *p*NPP Alkaline Phosphate Assay Kit (AnaSpec, Inc., Fremont, CA), according to the manufacturer's instructions. The ALP levels were measured spectrophotometrically at 405 nm using a PowerWave HT Microplate Reader (BioTek Instruments, Inc.). The results were normalized to the number of cells obtained in the proliferation assay at each corresponding time point and divided by the assay incubation time. The experiments were performed in triplicate.

5.2.8 Cell morphology

Cell morphology in the direct contact test was observed by SEM (Zeiss Neon 40) at each specified time point. The cell-seeded discs were washed in PBS (x3) and fixed in a 2.5 % glutaraldehyde solution in PBS for 1 h at 4 ºC. Subsequently, the fixed samples were washed in PBS (x3) and dehydrated in a 50 %, 70 %, 90 %, 96 %, and 100 % ethanol series. Complete dehydration was achieved in hexamethyldisilazane, and the discs were stored inside a desiccator. The dried discs were covered with a thin gold-palladium layer using vapour deposition (EMITECH K950X).

5.2.9 Apoptosis/necrosis assay

Flow cytometry analyses were performed to determine the cell death pathways for both the direct and indirect cell cultures on the CDHA samples. Briefly, either SaOS-2 cells or rMCSs were seeded on CDHA as described above (Direct Contact Cell Culture and Indirect Contact Cell Culture). After adhesion, the cells were detached with TrypLE (Invitrogen) and centrifuged at 300 rcf for 5min, followed by rinsing with cold PBS. Subsequently, the cells were stained with the Dead Cell Apoptosis Kit with annexin V-Alexa Fluor 488 and propidium iodide (PI) (Invitrogen), according to the manufacturer's

protocol. All incubations were performed in the dark. TCPS and glass coverslips were used as the controls for the direct and indirect contact cell cultures, respectively.

Ten thousand events were analysed on the Gallios Flow Cytometer (Beckman Coulter, Brea, CA) by measuring the fluorescence emission at 530 nm (FL1) and >575 nm (FL4) for annexin V and PI detection, respectively. The samples were analysed using Summit 4.3 Software.

5.2.10 Measurements of the pH and ion concentrations in the cell culture media

The supernatants of the direct cell cultures were collected at each specified time point. First, the pH was measured using a selective electrode (CRISON INSTRUMENTS, MultiMeter MM 41). Afterward, the calcium and phosphorous concentrations in samples that had been diluted 10-fold with 2 % ultrapure nitric acid were quantified by inductively coupled plasma-optical emission spectrometry (Perkin Elmer Optima 3200 RL).

5.2.11 Statistical analysis

The results are displayed as means ± standard errors (SE). The Kruskal-Wallis nonparametric test, followed by the Mann-Whitney test, with Bonferroni's correction were used to determine the statistically significant ($p < 0.05$) differences between the means of the different groups.

5.3 Results

5.3.1 Material characterisation

The XRD results revealed that samples were phase-pure, except for β-TCP, where some additional peaks were visible that represented the presence of traces of hydroxyapatite (~5 wt.%) (Supplementary Figure 5.2.). Similarly, FTIR results confirmed the presence of the typical vibrational bands in the different CaPs (Supplementary Figure 5.3.). The skeletal densities measured by helium pycnometry were in agreement with the theoretical values (Table 5.1.). All sintered materials (α-TCP, β-TCP, and HA) exhibited low SSA values (< 1 m^2/g), whereas CDHA presented higher SSA values (~20 m^2/g).

Table 5.1. Physicochemical properties of the calcium phosphates used in the study.

Material	CDHA	α-TCP	β-TCP	HA
Nominal Ca/P ratio	1.5	1.5	1.5	1.67
Solubility at 37 ºC (-log K_{ps})	85.1[a]	28.5	29.6	117.2
Theoretical density (g/mL)	d.n.f.	2.87	3.07	3.15
Diameter of the discs (mm)	15.00 ± 0.04	13.02 ± 0.04	12.97± 0.09	14.00± 0.02
Roughness,Sa (µm)	3.12 ± 0.44	4.15 ± 0.88	3.78± 1.27	3.35± 0.65
SSA (m^2/ g)	19.13 ± 0.04	0.22 ± 0.00	00.71± 0.00	0.54± 0.03
Skeletal density (g/ mL)	2.84 ± 0.03	2.7 8± 0.02	3.05± 0.07	3.20± 0.02
Porosity (%)	50.04	32.84	42.73	47.09

Average values ± standard deviation are displayed for the experimental values.[18-20]
[a] Solubility at 25 ºC.

These results correlated very well with the microstructures observed by SEM. The morphology of CDHA (Figure 5.1.A and 5.1.B) consisted of aggregates of entangled nanometric plate-like crystals (high magnification) that were formed around the initial α-TCP particles. The presence of aggregates and nanometric plate-like crystals led to a bimodal pore size distribution, as determined by MIP, containing intraaggregate pores in the 6-200 nm range and interaggregate pores centred ~1 mm (Figure 5.1.C).

The sintering process applied to CDHA to obtain α-TCP (Figure 5.1.D ad 5.1.E) and β-TCP (Figure 5.1.G and 5.1.H) led to a phase transformation accompanied by the growth and coalescence of the crystals within the original CDHA aggregates, resulting in smoother textures and the disappearance of the nanoscale porosity (Figure 5.1.F and 5.1.I). The α-TCP and β-TCP discs showed polygonal crystals, with some protuberances in the case of β-TCP due to the lower sintering temperature, with the pores between the crystals resulting from the original interaggregate pores observed in CDHA.

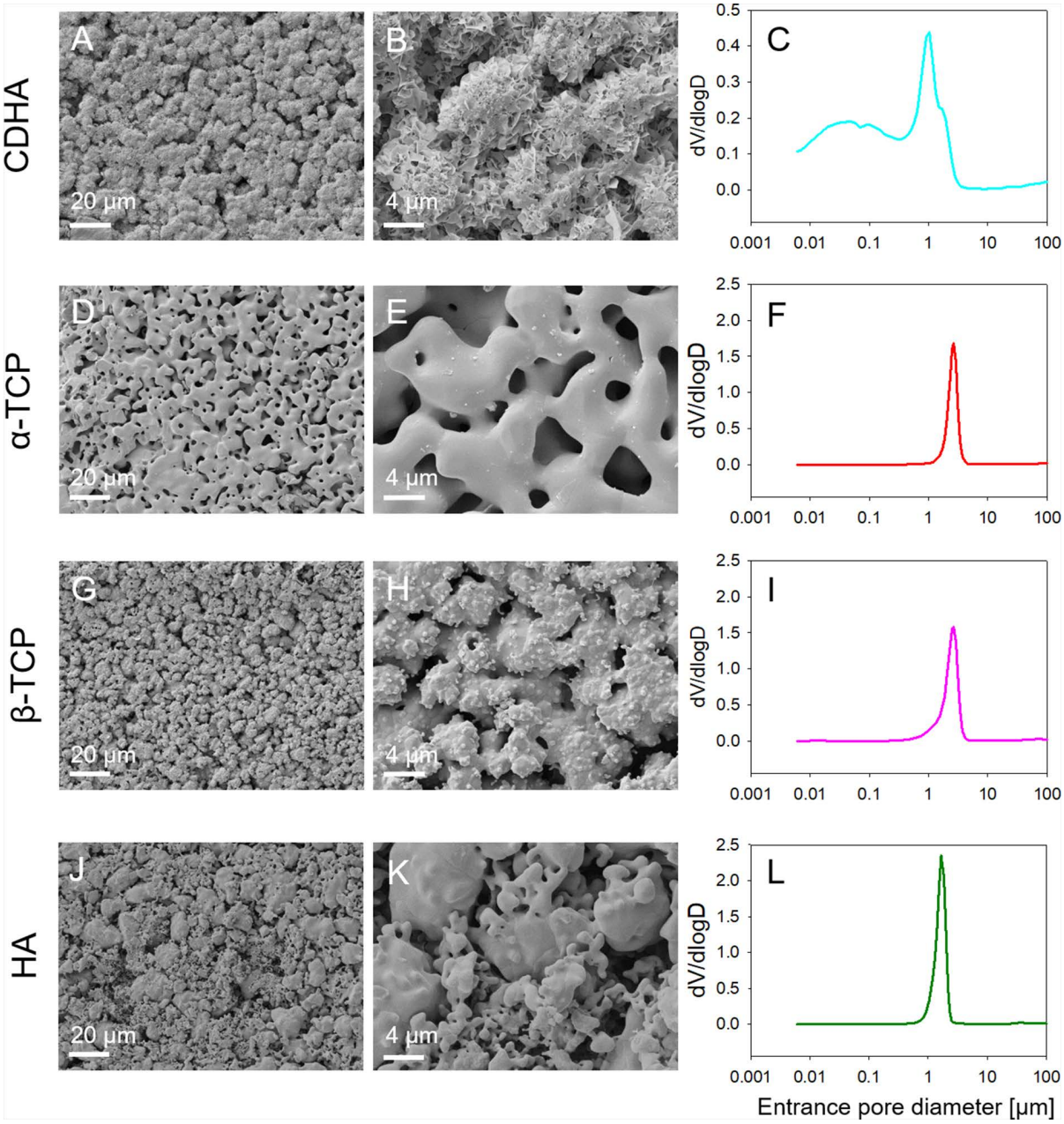

Figure 5.1. SEM images of the surfaces of CDHA **(A, B)**, α-TCP **(D, E)**, β-TCP **(G, H)**, and HA **(J, K)**. Pore entrance size distribution curves obtained by MIP for CDHA **(C)**, α-TCP **(F)**, β-TCP **(I)**, and HA **(L)**.

As a result, the microscale porosity increased, leading to a sharp monomodal pore size distribution cantered at 2.6 mm, which was slightly narrower for α-TCP due to the higher sintering temperature. Sintered HA (Figure 5.1.J and 5.1.K) also consisted of smooth polygonal crystals, with a sharp monomodal pore size distribution (Figure 5.1.L) cantered approximately at 1.7 mm. However, the microstructure was more heterogeneous than the other sintered materials because HA was produced by sintering a compacted mixture of $CaCO_3$ and $CaHPO_4$, with different granulometries.

Similar values of the average roughness (Sa) were found for the different substrates as displayed in Table 5.1., which was consistent with the fact that the same starting powder

and L/P ratios were used for their fabrication. In terms of total porosity, CDHA and HA presented the highest porosity values of approximately 50 %, whereas β-TCP and α-TCP had porosities ranging between ~30 % and 40 % (Table 5.1.). As expected, the porosities of α-TCP and β-TCP were inversely proportional to the sintering temperature.

5.3.2 Cell proliferation

The efficiency of SaOS-2 cell adhesion in direct cultures after 4 h was similar in all CaPs, except for β-TCP, where cell adhesion was slightly higher (Figure 5.2.A). On days 3 and 7, there was a decrease in the number of cells on CDHA, whereas the number of cells increased slightly on α-TCP, β-TCP, and HA, but at a much slower rate than on TCPS. Regarding the rMSCs, CDHA and HA showed reduced cell adhesion compared to the other CaPs (Figure 5.2.B). Moreover, the number of rMSCs on β-TCP, and more markedly on CDHA, decreased with time. In contrast, the number of cells on α-TCP increased with time, as it did also on HA, although at a lower rate.

The morphological studies performed by SEM showed that both osteoblasts and mesenchymal stem cells were able to adhere on the different surfaces (Figure 5.3 and 5.4). At 4 h of culture, there were no visible differences in SaOS-2 cell spreading and morphology on the various CaPs. There was a continuous increase in the number of SaOS-2 cells grown on all CaPs with time, except for CDHA, where only few cells were observed after 3 and 7 days (Figure 5.3.B and 5.3.C). On day 7, the highest SaOS-2 cell density was observed on α-TCP (Figure 5.3.F), where the cells formed a multilayer. The rMSCs (Figure 5.4.) showed similar behaviours as the SaOS-2 cells. However, at 6 h of culture, the rMSCs were flatter and spread more than the SaOS-2 cells.

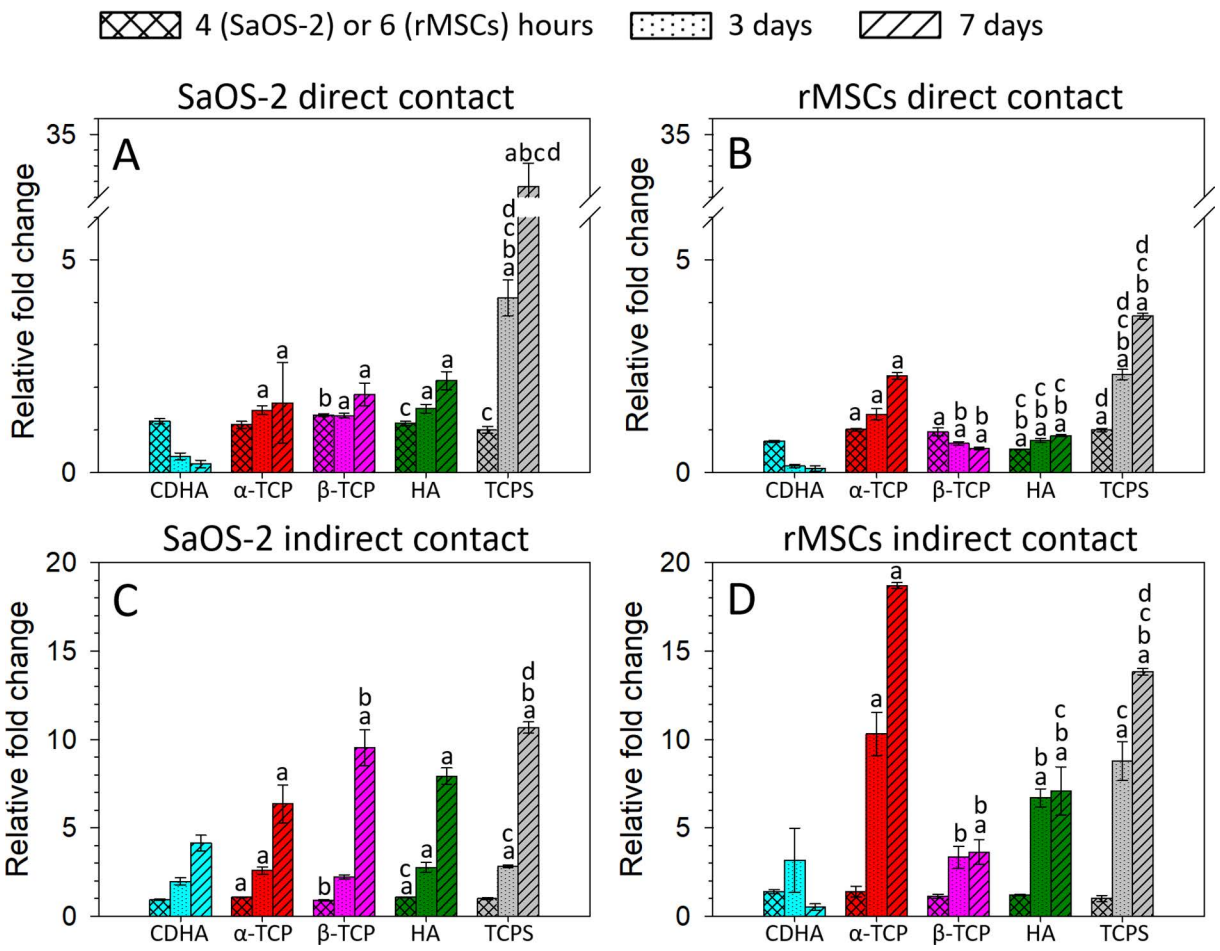

Figure 5.2. Proliferation of SaOS-2 cells grown in direct **(A)** and indirect contact **(C)** with the CaPs after 4 h, 3 and 7 days. Proliferation of rMSCs in direct **(B)** and indirect contact **(D)** with CaPs after 4 h, 3 and 7 days. The results were expressed as relative fold changes compared to the cell number obtained on TCPS at 4 or 6 h (SaOS-2 cells or rMSCs, respectively). At each time point, the letters (a, b, c and d) indicate a significant difference ($p < 0.05$) compared with CDHA, α-TCP, β-TCP and HA, respectively.

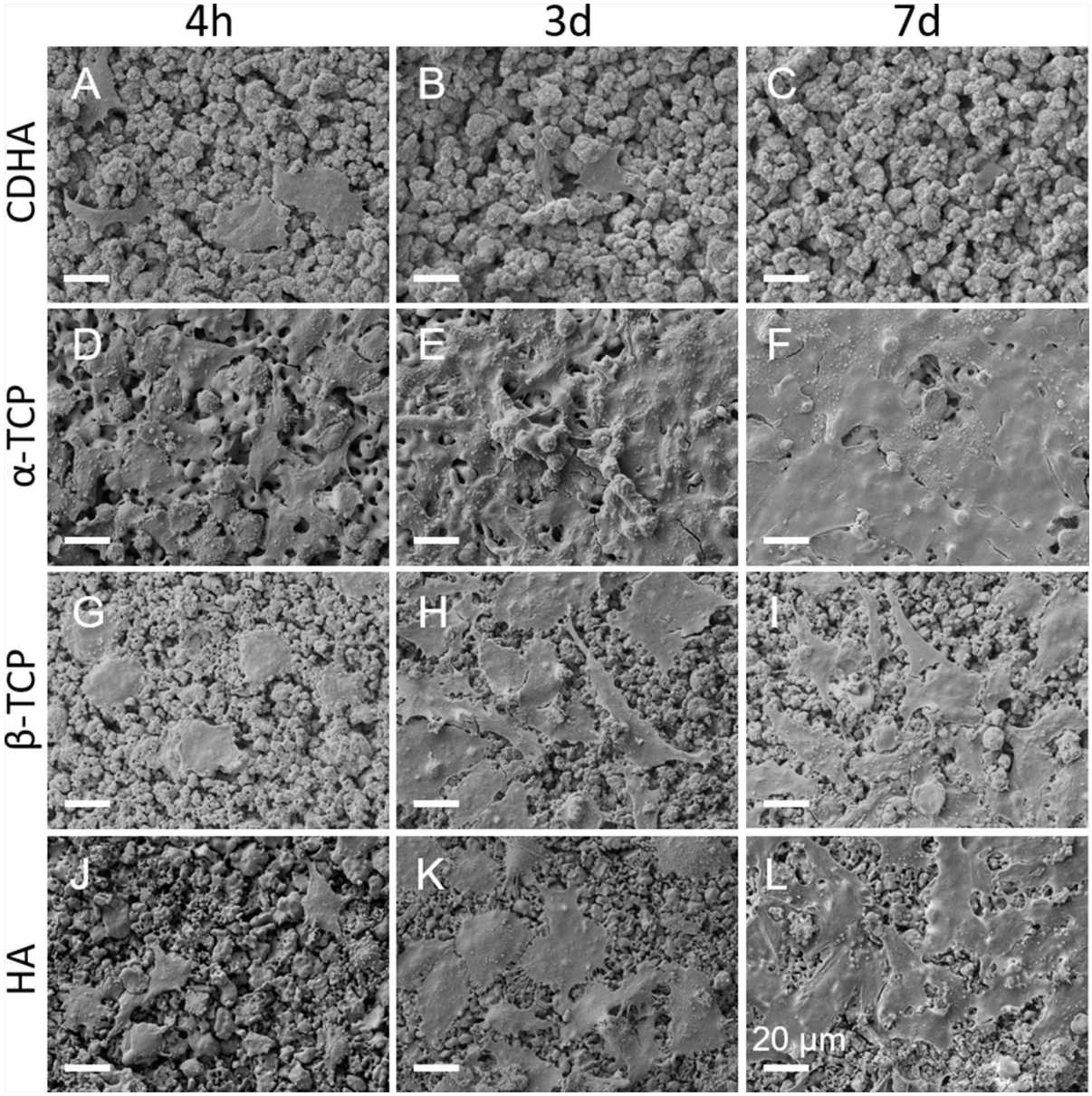

Figure 5.3. Morphology of SaOS-2 observed by SEM at 4 h, 3 and 7 days of cell culture on CDHA **(A-C)**, α-TCP **(D-F)**, β-TCP **(G-I)** and HA **(J-L)**. Scale bar denotes 20 µm.

In the indirect cell cultures, the initial number of SaOS-2 cells for all CaPs was similar to TCPS and increased with culture time (Figure 5.2.C). However, the cell growth rate for CDHA was slower than the other groups. Regarding the rMSCs, the initial cell number was similar for all CaPs (Figure 5.2.D). For CDHA, the number of rMSCs increased on day 3, followed by a decrease on day 7. For β-TCP and HA, the cell number increased on day 3 and remained constant on day 7. α-TCP produced constant cell growth with time, reaching even higher values than TCPS.

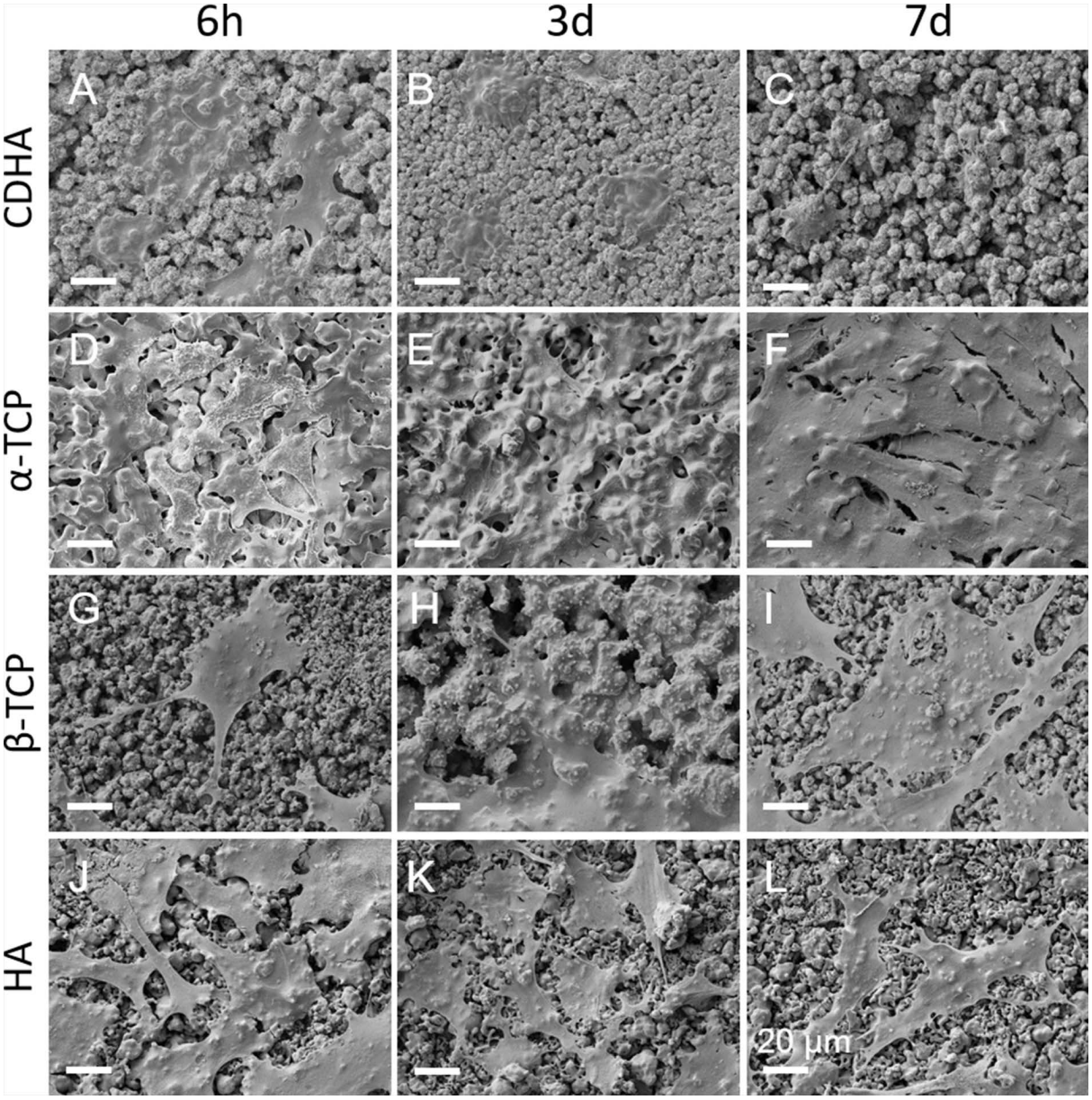

Figure 5.4. Morphology of rMSCs observed by SEM at 4 h, 3 and 7 days of cell culture on CDHA **(A-C)**, α-TCP **(D-F)**, β-TCP **(G-I)** and HA **(J-L)**. Scale bar denotes 20 µm.

5.3.3 Cell differentiation

When the SaOS-2 cells were cultured directly on the substrates in the absence of osteogenic medium, different trends were observed for the different materials (Figure 5.5.A). Although α-TCP and β-TCP exhibited a maximum activity on day 3, followed by a decrease on day 7, showing similar or smaller values than the control (TCPS), the ALP activity values for cells grown on CDHA continued to increase on day 7, reaching significantly higher values than the other substrates.

As expected, the rMSCs had smaller ALP activity values than the SaOS-2 cells. At 6 h, the ALP activity in the cells cultured on HA were two-fold higher than the other CaPs and the control (Figure 5.5.D), but they decreased on days 3 and 7; the same trend was

observed for α-TCP. Although the ALP activity began increasing on β-TCP, it was markedly decreased on 7 days. In contrast, rMSCs cultured on CDHA showed a continuous increase in the ALP activity during the cell culture.

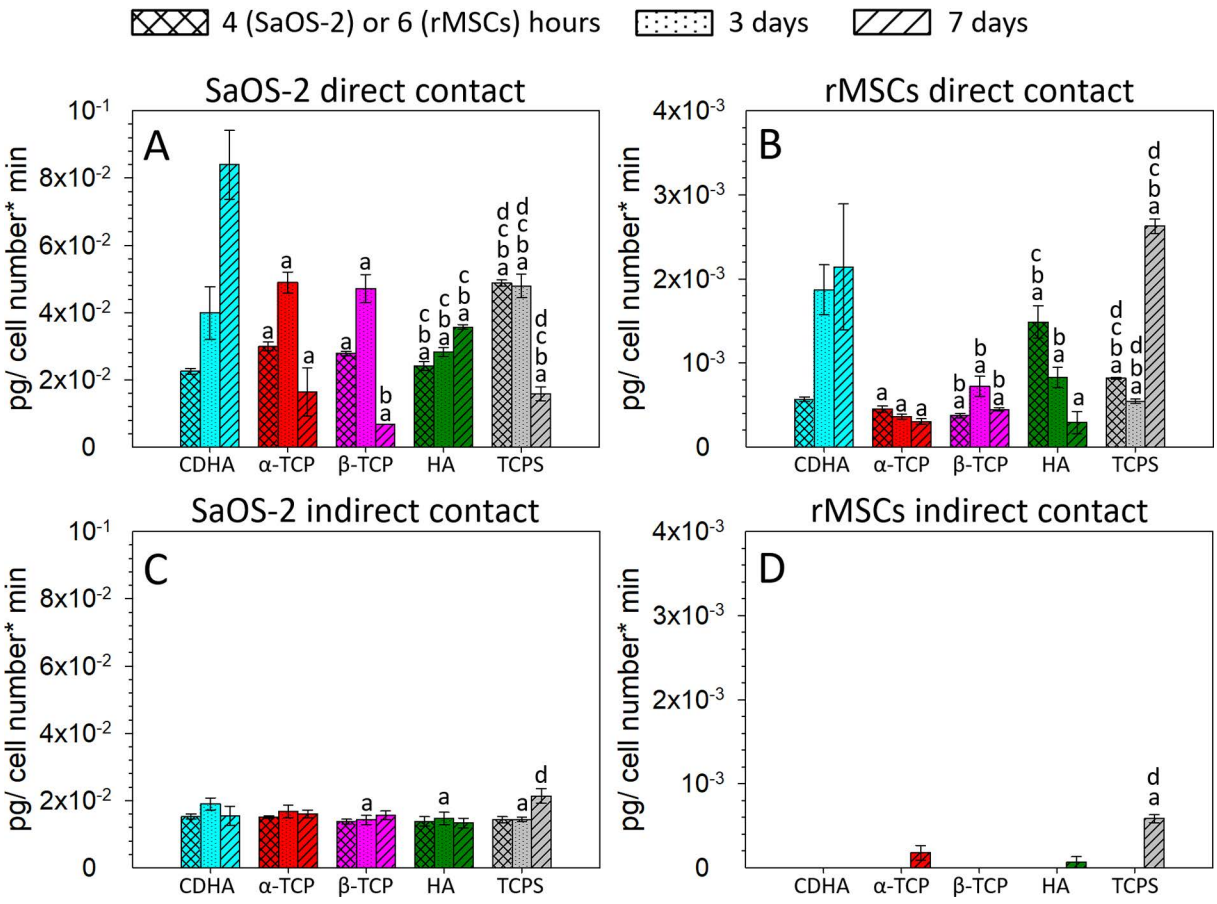

Figure 5.5. ALP activity in SaOS-2 cells grown in direct **(A)** and indirect contact **(C)** with CaPs after 4 h, 3 and 7 days. ALP activity in rMSCs grown in direct **(B)** and indirect contact **(D)** with CaPs after 4 h, 3 and 7 days. The results were normalized to their corresponding number of cells. At each time point, letters (a, b, c and d) indicate a significant difference ($p < 0.05$) compared with CDHA, α-TCP, β-TCP and HA, respectively.

The ALP activity values for SaOS-2 cells in indirect contact were similar for the different CaPs at all time points (Figure 5.5.C). Notably, these ALP activity values were slightly lower than the values obtained when cells were in direct contact with the substrates. In contrast, rMSCs in indirect contact did not show any ALP activity at 6 h and on day 3 (Figure 5.5.D). Only low ALP activity levels were observed for HA, α-TCP, and TCPS on day 7.

5.3.4 Ionic exchange in the cell culture medium during the cell culture studies

The variations in pH with time for the various CaPs in McCoy's and advDMEM cell culture media are presented in Figure 5.6.A and 5.6.B, respectively. The initial pH values for McCoy's and advDMEM media were 7.4 and 7.6, respectively, and they

increased after 6 h of incubation with the cells to 8.53 and 8.10, respectively. Regarding McCoy's medium, α-TCP and β-TCP exhibited similar trends as TCPS. CDHA and HA reduced the pH slightly at 6 h. For the advDMEM medium, all CaPs exhibited similar behaviours as TCPS, except for CDHA, which reduced the pH at 6 h.

The results of the variations in the Ca^{2+} and inorganic phosphate (P_i) ion concentrations after the various materials were exposed to McCoy's media and advDMEM are summarized in Figure 5.6.C-F. It is important to highlight that the chemical compositions of both media are slightly different, particularly in terms of the Ca^{2+} and P_i contents. The initial Ca^{2+} and P_i concentrations of McCoy's medium were 1.17 and 4.34 mM, respectively, whereas for advDMEM, the concentrations were 1.87 and 1.16 mM, respectively. The Ca^{2+} concentrations were not altered in the media that was in contact with α-TCP and HA (Figure 5.6.C and 5.6.D).

In contrast, there was a strong decrease in the Ca^{2+} concentrations in both media that were in contact with CDHA and β-TCP, particularly for advDMEM. Regarding the P_i concentrations, both HA and β-TCP decreased the levels in both media, whereas α-TCP maintained it constant (Figure 5.6.E and 5.6.F). In contrast, P_i release was observed for CDHA, which was notably higher in advDMEM (Figure 5.6.E) than in McCoy's medium (Figure 5.6.F).

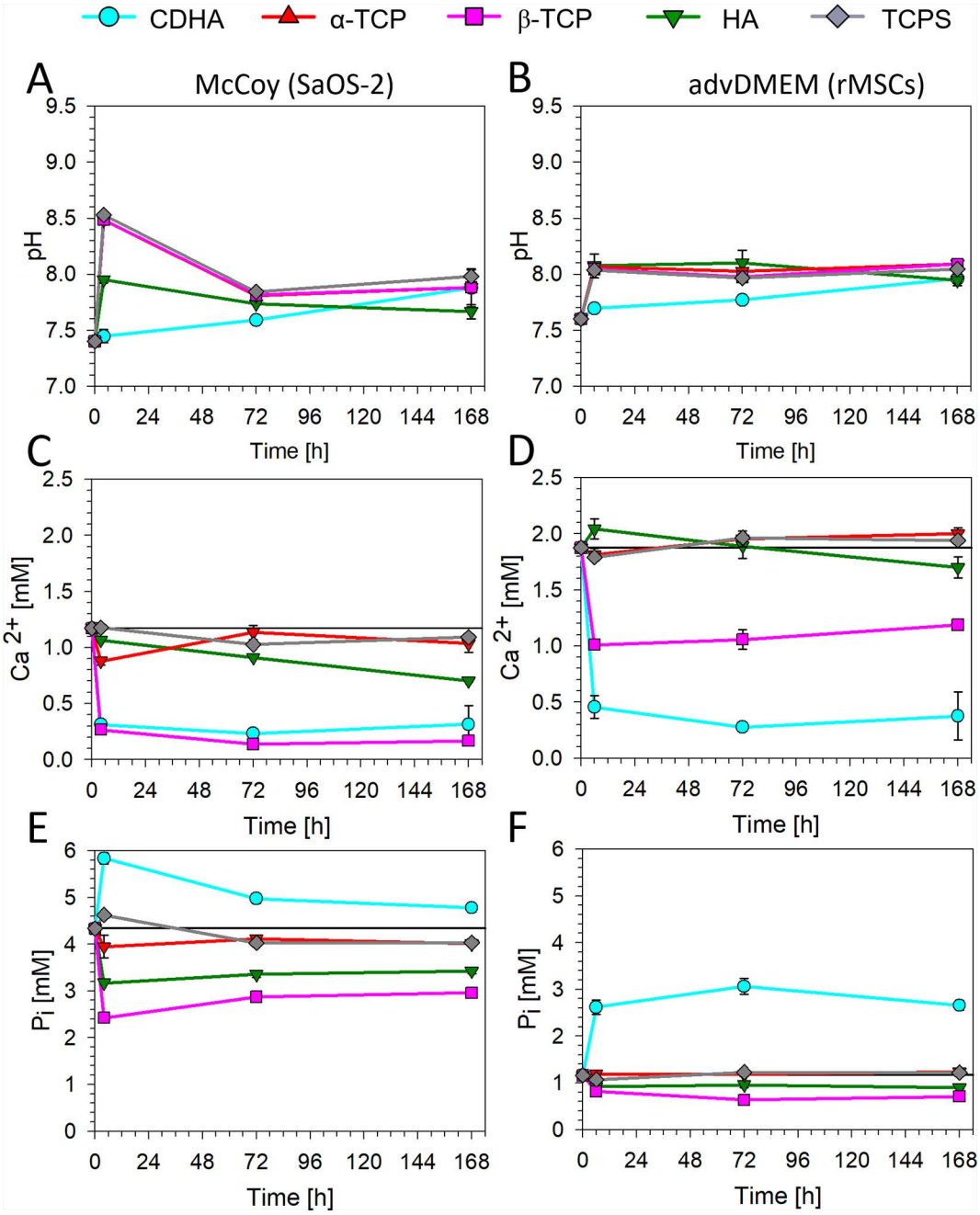

Figure 5.6. Evolution of pH values and calcium and phosphorous concentrations in the cell culture media when the cells were cultured on the different materials: McCoy's cell culture medium in presence of SaOS-2 cells (A, C, E), and advDMEM in the presence of rMSCs (B, D, F). The black horizontal line indicates the starting experimental values for the pH, Ca^{2+}, and P_i in McCoy's medium (A, C, E) and advDMEM (B, D, F). The pH values for α-TCP are not visible in Figure 7a because they overlap with the values for β-TCP.

5.3.5 Apoptosis/necrosis assay

The cell death pathway involved in the CDHA samples was evaluated by flow cytometry. Figure 5.7. presents the contour diagrams of the annexin V-Alexa Fluor 488/PI of SaOS-2 cells (Figure 5.7.A, 5.7.B, 5.7.E and 5.7.F) and rMSCs (Figure 5.7C, 5.7.D, 5.7.G and 5.7.H) in direct and indirect cell cultures on CDHA with their

corresponding responding controls (TCPS and glass coverslip, respectively). The bottom left quadrant of the cytograms represents viable cells, which are negatively stained for PI and Alexa Fluor 488-annexin V. Necrotic cells, which are PI positive and Alexa Fluor 488-annexin V negative, are located in the top left quadrant. The bottom right quadrant corresponds to apoptotic cells that are positively stained for Alexa Fluor 488-annexin V, but negatively stained for PI. Finally, the upper right quadrant represents late apoptotic cells, which show positive staining for both Alexa Fluor 488-annexin V and PI.

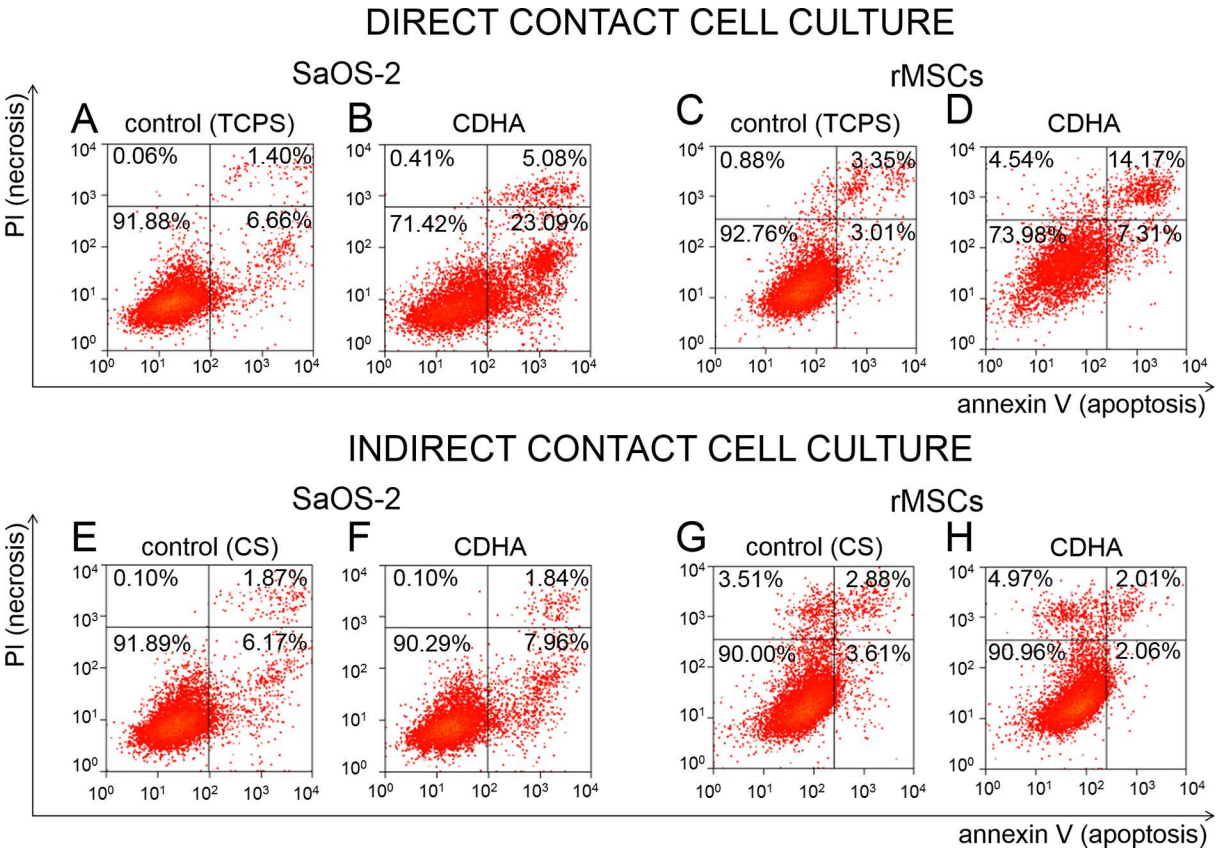

Figure 5.7. Apoptosis/necrosis assay by flow cytometry. The graphs represent the cell death pathways for SaOS-2 cells **(A, B, E, F)** or rMSCs **(C, D, G, H)** grown in direct or indirect cell culture with CDHA. Cells that were positively stained for annexin V-FITC and negatively stained for PI were considered apoptotic. Cells that were positively stained for both annexin V-FITC and PI were considered late apoptotic. Cells that were negatively stained for annexin V-FITC and positively stained for PI were considered necrotic. The percentage of each type of cells is presented in the corresponding square of each graph.

For the direct cell cultures, the percentage of viable cells on CDHA decreased compared to TCPS, where the percentage of viable cells was > 90 %. This decrease in cell viability was similar for both SaOS-2 cells and rMSCs. The percentages of apoptotic and late apoptotic SaOS-2 cells in contact with CDHA were 23.09 % and 5.08 %, respectively. Lower percentages of necrotic SaOS-2 cells in direct contact with CDHA were detected. In contrast, for rMSCs, the percentage of apoptotic cells in direct contact with CDHA

was lower than the SaOS-2 cells, but there was an increase in the percentages of late apoptotic and necrotic cells.

For the indirect cell culture studies, the percentage of viable cells in CDHA was similar to TCPS for both cell types, with ~90 % viability and similar percentages of apoptotic, late apoptotic, and necrotic cells.

5.4 Discussion

The objective of this study was to analyse the *in vitro* cell response of bone-related cells to biomimetic and high-temperature sintered calcium phosphates. The calcium phosphates compared differed not only in chemical phase but also in the textural properties, which strongly affected their reactivity. The cell culture studies showed very different trends for the biomimetic CDHA and the sintered calcium phosphates, both when the cells were cultured directly on the surface of the materials or on glass coverslips placed on the substrates.

Cell proliferation was strongly reduced when cells were cultured in direct contact with all substrates in comparison to TCPS, more significantly for SaOS-2 cells (Figure 5.2.). The most striking results were those obtained for biomimetic CDHA, where the cell number, both for SaOS-2 and rMSCs, strongly decreased with time, even if the cells initially adhered (6 h) to a similar extent as on the other substrates. In rMSCs, a decrease in cell number was observed also for β-TCP. In contrast, both cell types did proliferate on α-TCP and HA, although at a slower rate than on TCPS.

SEM observations (Figures 5.3. and 5.4.) revealed that both rMSCs and SaOS-2 cells were less spread on CDHA. Similar findings on MSC attachment and proliferation on octacalcium phosphate substrates with similar morphologies to CDHA were reported in previous studies.[21-23] One possible explanation could be the sharp morphology of the mineral crystals, which might have hindered cell adhesion. However, microstructure and ionic exchange are intrinsically linked parameters, and to better understand the effect that the material-induced ionic fluctuations of the cell culture medium could have on cell response, ionic concentrations in the cell culture medium were monitored at the different time points.

The ionic composition of the cell culture media was altered to various extents by the different materials, depending not only on the composition and therefore the solubility of the materials but also on their textural properties, since an increase in the SSA and the presence of interconnect pores in the samples increase the surface available for reaction with the surrounding medium. Moreover, the modification in the ionic concentrations depended on the nature of cell culture medium, which had different initial concentrations of Ca^{2+} and P_i.[10] This aspect is crucial, as fluctuations in the ionic

environment have been reported to directly control cell function and specifically osteoblast and MSC proliferation, in a dose-dependent manner.[24-27]

The supplementation with HEPES buffer greatly helped to preserve relatively stable pH values of most of the materials. A pronounced and maintained calcium depletion from the culture medium was registered both for McCoy's and advDMEM media in the presence of CDHA and, to a minor extent, β-TCP (Figure 5.6C and D). The Ca^{2+} levels remained unchanged for stoichiometric HA and α-TCP. The uptake of Ca^{2+} was previously described for biomimetic calcium phosphates, such as octacalcium phosphate[22,23] and CDHA.[9,10,28,29] This behaviour was attributed to the maturation process to stoichiometric HA that is more thermodynamically stable[30,31] and was fostered by the high SSA of the materials and the presence of non-apatitic domains on their crystal surface, giving them a higher reactivity compared with high-temperature sintered materials.[30]

The ionic reactivity of the different materials with cell culture media in terms of P_i also varied depending on the material. P_i release was registered for CDHA, which could be explained by the replacement of P_i ions on the CDHA crystal surface or lattice structure with ions available in the culture medium, typically carbonate, which is known to replace superficial phosphate.[32] The highest P_i release observed in advDMEM could be associated to the highest carbonate content in this culture medium compared to McCoy's medium.[10] Interestingly, β-TCP, which is more soluble than CDHA and had a much smaller SSA, sequestered both P_i and Ca^{2+} from the medium. This behaviour could be explained by the dissolution and subsequent re-precipitation of CaP on the recessed regions of the material where supersaturation could most easily be maintained.

In the indirect contact studies, the SaOS-2 cells were able to proliferate on the glass coverslips placed on top of the substrates, despite the modifications of the ionic concentrations in McCoy's culture medium caused by the different materials to varying extents. These results agree with previous studies that suggest that SaOS-2 cells are quite robust in terms of ionic fluctuations.[33]

Thus, the effect on cell proliferation when compared to TCPS was small on HA and α-TCP, where the materials caused slight modifications in calcium and phosphorous concentrations in the cell culture medium, and no difference was observed on β-TCP, despite the stronger ionic fluctuations registered (decrease of both calcium and phosphate concentrations) (Figure 5.6.). A significant reduction in the proliferation rate was found only on CDHA, where a strong depletion of calcium and release of phosphate were observed. In contrast, a higher sensitivity to the ionic fluctuations was noticed in the rMSCs.

Lower rates of cell proliferation were observed in the indirect culture for all materials except α-TCP, the effects being more marked in the materials where the ionic fluctuations were more pronounced, that is, β-TCP and especially CDHA. Particularly, for CDHA, although the number of cells increased at day 3, it strongly decreased at day 7. As in the case of SaOS-2, this behaviour might be associated to the concomitant decrease in Ca^{2+} and increase in P_i concentrations, which is in good agreement with previous studies, which were reported to reduce cell proliferation, both osteoblast-like cells[25] and MSCs.[34]

The particular decrease in the number of cells grown in contact with CDHA after the initial cell adhesion was further analysed by flow cytometry using markers for apoptosis and necrosis to reveal the cell death pathway. The results showed that the direct contact of cells with CDHA induced apoptosis already after a 6 h interaction (Figure 5.7.). rMSCs exhibited a more advanced apoptosis stage, with a permeabilised plasma membrane (late apoptosis), than the SaOS-2 cells (Figure 5.7.D).

Low levels of apoptosis were observed when the cells were cultured on coverslips in indirect contact with CDHA (Figure 5.7.F and 5.7.H). This agrees with the results of cell proliferation under this condition (Figure 5.2.C and 5.2.D), where cell number increased for SaOS-2 and for rMSCs decreased only at 7 days of culture (Figure 5.2.D). This suggests that the fluctuations in Ca^{2+} and P_i impacted cell proliferation at later stages after cell adhesion, as previously described[25,34] and the induction of apoptosis after 6h of cell culture was associated with the direct interaction with the substrate.

The results of the cell differentiation experiments obtained measuring the ALP activity[35] showed very different trends depending on the test type (direct vs. indirect cell culture) (Figure 5.5.). As expected, rMSCs presented less ALP activity than SaOS-2 cells.[36] SaOS-2 cells in the indirect assays showed low and constant ALP levels, whereas the rMSCs had an almost non-existent ALP activity. No differences were observed between the different materials, despite the marked differences in Ca^{2+} and P_i concentrations in the respective cell culture media.

The indirect study revealed that direct cell contact with the biomaterial surface and chemistry was a requisite for promoting osteoblast differentiation. This is very relevant for the *in vivo* application since it evidences that cell differentiation cannot be stimulated by the ionic fluctuations caused by materials in their vicinity. Thus, this prevents undesirable new bone formation in remote areas in a similar way as ectopic mineralization occurs due to the migration of osteoinductive molecules.

Notably higher ALP levels were measured in the direct contact assays, and significant differences were found for CDHA compared to the other materials. The ALP activity of SaOS-2 in direct contact with α-TCP, β-TCP, and HA was similar or lower than on

TCPS (Figure 5.5.A), whereas a 4-fold ALP activity was recorded on CDHA, with respect to TCPS on day 7, in agreement with previous studies that reported a high ALP activity of osteoblastic cells on CDHA.[28] A continuous increase in the ALP activity was also recorded for the rMSCs cultured on CDHA, similar to what was observed in other biomimetic substrates like octacalcium phosphate.[23]

Noteworthy, this increase in the ALP activity on CDHA samples in both types of cells coincided with a decrease in cell number. However, although the number of cells was low in these conditions, the ALP activity values were significant when compared to indirect studies where also a decrease in cell numbers was observed. A direct effect of topography cannot be excluded, as it has been identified as a parameter controlling differentiation in both mesenchymal and osteoblastic cells when cultured on inert materials like poly(methyl methacrylate), titanium, or titanium oxide.[37-42] This effect is associated with the increased cytoskeletal tension, which is known to drive osteogenesis.[42,43] However, the situation is far more complex in highly reactive calcium phosphates.

The present chapter showed that the ionic exchange is magnified in materials with high SSA (Figure 5.6.), and this may result in complex ionic gradients that are difficult to measure. Thus, it could seem contradictory that cells cultured on CDHA, which induced a strong decrease of Ca^{2+} in the cell culture medium, presented higher ALP activity, since it is known that Ca^{2+} has a stimulatory effect on the differentiation of MSCs.[15,26] However, one should expect that the uptake of calcium by the material, which results in a decrease in the average Ca^{2+} concentration in the cell culture medium, lead simultaneously to an increased Ca^{2+} concentration on the surface of the material, where the cells are located. This could contribute, together with the topographical cues, to the enhanced differentiation suggested by the higher ALP activity levels when the cells are cultured directly on the material surface.

5.5 Conclusions

The results obtained show that the distinct physicochemical features of biomimetic and ceramic calcium phosphates modified differently the composition of the culture media, this in turn affecting cellular behaviour in terms of proliferation and differentiation, although to different extents for SaOS-2 cells and rMSCs. The use of glass coverslips was useful to separately determine the effects of the ionic fluctuations and direct contact with the surface, although this approach has some limitations, since the coverslip cells were not able to sense the ionic gradients that take place in the close vicinity of the surface.

Overall, this work highlights the inherent limitations of static cell culture assays, particularly for the assessment of reactive materials such as biomimetic CDHA. The drastic changes in the ionic composition in contact with the cell culture media caused

by the high SSA and the non-stoichiometry of these materials can potentially affect cell behaviour to the extent that the materials could appear to be cytotoxic, even if they function well *in vivo*. Dynamic cell culture assays that more closely simulate the *in vivo* scenario might contribute to advance in this direction.

5.6 Bibliography

1. LeGeros, R. Z. & LeGeros, J. P. in *Key Engineering Materials* **240–242**, 3–10 (2003).
2. Bohner, M. Calcium orthophosphates in medicine: From ceramics to calcium phosphate cements. *Injury* **31**, 37–47 (2000).
3. Vallet Regi, M. Calcium phosphates as substitution of bone tissues. *Prog. Solid State Chem.* **32**, 1–31 (2004).
4. Hench, L. L. Bioceramics. *J. Am. Ceram. Soc.* **81**, 1705–1728 (2005).
5. LeGeros, R. Z. Calcium phosphate-based osteoinductive materials. *Chem. Rev.* **108**, 4742–53 (2008).
6. Dorozhkin, S. V & Epple, M. Biological and medical significance of calcilum phosphates. *Angew. Chemie Int. Ed.* **41**, 3130–3146 (2002).
7. Ginebra, M. P. *et al.* Setting Reaction and Hardening of an Apatitic Calcium Phosphate *Cement. J. Dent. Res.* **76**, 905–912 (1997).
8. Habraken, W., Habibovic, P., Epple, M. & Bohner, M. Calcium phosphates in biomedical applications: materials for the future? *Mater. Today* **19**, 69–87 (2015).
9. Gustavsson, J., Ginebra, M. P. P., Engel, E. & Planell, J. Ion reactivity of calcium-deficient hydroxyapatite in standard cell culture media. *Acta Biomater.* **7**, 4242–52 (2011).
10. Gustavsson, J., Ginebra, M. P., Planell, J. & Engel, E. Osteoblast-like cellular response to dynamic changes in the ionic extracellular environment produced by calcium-deficient hydroxyapatite. *J. Mater. Sci. Mater. Med.* **23**, 2509–20 (2012).
11. Chung, F. H. Quantitative Interpretation of X-Ray Diffraction Method, Patterns of Mixtures. I. Matrix-Flushing for Quantitative Multicomponent Analysis. *J. Appl. Crystallogr.* **7**, 519–525 (1974).
12. Pautke, C. *et al.* Characterization of osteosarcoma cell lines MG-63, Saos-2 and U-2 OS in comparison to human osteoblasts. *Anticancer Res.* **24**, 3743–3748 (2004).
13. Saldaña, L., Bensiamar, F., Boré, A. & Vilaboa, N. In search of representative models of human bone-forming cells for cytocompatibility studies. *Acta Biomater.* **7**, 4210–4221 (2011).
14. Czekanska, E. M., Stoddart, M. J., Richards, R. G. & Hayes, J. S. In search of an osteoblast cell model for in vitro research. *Eur. Cells Mater.* **24**, 1–17 (2012).
15. González-Vázquez, A. *et al.* Extracellular calcium and CaSR drive osteoinduction in mesenchymal stromal cells. *Acta Biomater.* **10**, 2824–2833 (2014).
16. Aguirre, A., Planell, J. A. & Engel, E. Dynamics of bone marrow-derived endothelial progenitor cell/mesenchymal stem cell interaction in co-culture and its implications in angiogenesis. *Biochem. Biophys. Res. Commun.* **400**, 284–91 (2010).
17. Allen, M., Millett, P., Dawes, E. & Rushton, N. Lactate dehydrogenase activity as a rapid and sensitive test for the quantification of cell numbers in vitro. *Clin. Mater.* **16**, 189–194 (1994).
18. Dorozhkin, S. V. Calcium Orthophosphates in Nature, Biology and Medicine. *Materials (Basel).* **2**, 399–498 (2009).
19. Carrodeguas, R. G. & De Aza, S. α-Tricalcium phosphate: synthesis, properties and biomedical applications. *Acta Biomater.* **7**, 3536–46 (2011).
20. Elliott, J. C. General chemistry of calcium orthophosphates. in *Structure and Chemistry of the Apatites and Other Calcium Orthophosphates* (Elsevier, 1994).
21. Guo, H., Su, J., Wei, J., Kong, H. & Liu, C. Biocompatibility and osteogenicity of degradable Ca-deficient hydroxyapatite scaffolds from calcium phosphate cement for bone tissue engineering. *Acta Biomater.* **5**, 268–78 (2009).
22. Anada, T. *et al.* Dose-Dependent Osteogenic Effect of Octacalcium Phosphate on Mouse Bone Marrow Stromal Cells. *Tissue Eng. Part A* **14**, 965–978 (2008).

23. Danoux, C. *et al.* The Effects of Crystal Phase and Particle Morphology of Calcium Phosphates on Proliferation and Differentiation of Human Mesenchymal Stromal Cells. *Adv. Healthc. Mater.* **5**, 1775–1785 (2016).
24. Dvorak, M. M. *et al.* Physiological changes in extracellular calcium concentration directly control osteoblast function in the absence of calciotropic hormones. *Proc. Natl. Acad. Sci. U. S. A.* **101**, 5140–5 (2004).
25. Meleti, Z., Shapiro, I. M. & Adams, C. S. Inorganic phosphate induces apoptosis of osteoblast-like cells in culture. *Bone* **27**, 359–366 (2000).
26. Barradas, A. M. C. *et al.* A calcium-induced signaling cascade leading to osteogenic differentiation of human bone marrow-derived mesenchymal stromal cells. *Biomaterials* **33**, 3205–15 (2012).
27. Danoux, C. B. S. S. *et al.* Elucidating the individual effects of calcium and phosphate ions on hMSCs by using composite materials. *Acta Biomater.* **17**, 1–15 (2015).
28. Engel, E. *et al.* Discerning the role of topography and ion exchange in cell response of bioactive tissue engineering scaffolds. *Tissue Eng. Part A* **14**, 1341–51 (2008).
29. Knabe, C. *et al.* Evaluation of calcium phosphates and experimental calcium phosphate bone cements using osteogenic cultures. *J. Biomed. Mater. Res.* **52**, 498–508 (2000).
30. Vandecandelaere, N., Rey, C. & Drouet, C. Biomimetic apatite-based biomaterials: On the critical impact of synthesis and post-synthesis parameters. *J. Mater. Sci. Mater. Med.* **23**, 2593–2606 (2012).
31. Rollin-Martinet, S., Navrotsky, A., Champion, E., Grossin, D. & Drouet, C. Thermodynamic basis for evolution of apatite in calcified tissues. *Am. Mineral.* **98**, 2037–2045 (2013).
32. Cazalbou, S., Combes, C., Eichert, D., Rey, C. & Glimcher, M. J. Poorly crystalline apatites: evolution and maturation in vitro and in vivo. *J. Bone Miner. Metab.* **22**, 310–7 (2004).
33. Chou, Y.-F., Huang, W., Dunn, J. C. Y., Miller, T. A. & Wu, B. M. The effect of biomimetic apatite structure on osteoblast viability, proliferation, and gene expression. *Biomaterials* **26**, 285–95 (2005).
34. Liu, Y. K. Y. K. *et al.* The effect of extracellular calcium and inorganic phosphate on the growth and osteogenic differentiation of mesenchymal stem cells in vitro: implication for bone tissue engineering. *Biomed. Mater.* **4**, 25004 (2009).
35. Stein, G. S. & Lian, J. B. Molecular mechanisms mediating proliferation/differentiation interrelationships during progressive development of the osteoblast phenotype. *Endocrine Reviews* **14**, 424–442 (1993).
36. Rodan, S. B. *et al.* Characterization of a Human Osteosarcoma Cell Line (Saos-2) with Osteoblastic Properties Characterization of a Human Osteosarcoma Cell Line (Saos-2) with Osteoblastic Properties. 4961–4966 (1987).
37. Dalby, M. J., McCloy, D., Robertson, M., Wilkinson, C. D. W. & Oreffo, R. O. C. Osteoprogenitor response to defined topographies with nanoscale depths. *Biomaterials* **27**, 1306–15 (2006).
38. Schneider, G. B., Zaharias, R., Seabold, D., Keller, J. & Stanford, C. Differentiation of preosteoblasts is affected by implant surface microtopographies. *J. Biomed. Mater. Res. A* **69**, 462–8 (2004).
39. Masaki, C., Schneider, G. B., Zaharias, R., Seabold, D. & Stanford, C. Effects of implant surface microtopography on osteoblast gene expression. *Clin. Oral Implants Res.* **16**, 650–6 (2005).
40. Schwartz, Z. *et al.* Implant Surface Characteristics Modulate Differentiation Behavior of Cells in the Osteoblastic Lineage. *Adv. Dent. Res.* 13, 38–48 (1999).
41. Oh, S. *et al.* Stem cell fate dictated solely by altered nanotube dimension. *Proc. Natl. Acad. Sci. U. S. A.* **106**, 2130–2135 (2009).

42. McBeath, R., Pirone, D. M., Nelson, C. M., Bhadriraju, K. & Chen, C. S. Cell Shape, Cytoskeletal Tension, and RhoA Regulate Stem Cell Lineage Commitment. *Dev. Cell* **6**, 483–495 (2004).
43. Kilian, K. A., Bugarija, B., Lahn, B. T. & Mrksich, M. Geometric cues for directing the differentiation of mesenchymal stem cells. *Proc. Natl. Acad. Sci. U. S. A.* **107**, 4872–7 (2010).
44. Drouet, C. Apatite Formation: Why It May Not Work as Planned, and How to Conclusively Identify Apatite Compounds. *Biomed Res. Int.* **2013**, 1–12 (2013).
45. Carrodeguas, R. G. & De Aza, S. α-Tricalcium phosphate: synthesis, properties and biomedical applications. *Acta Biomater.* **7**, 3536–46 (2011).

5.7 Supplementary Information

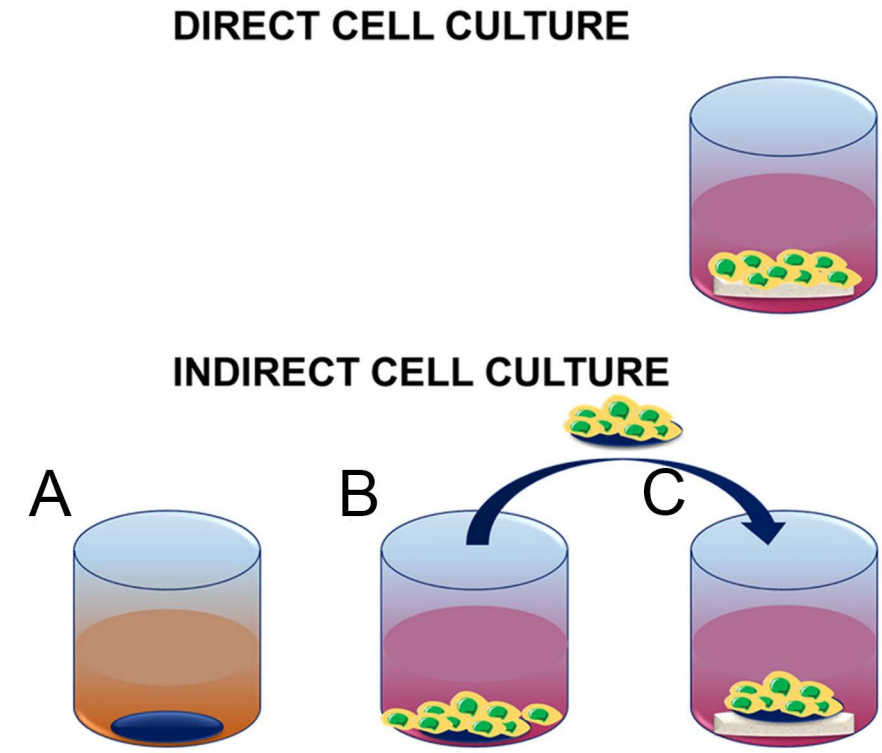

Supplementary Figure 5.1. Illustration of the methodology for the direct and indirect cell cultures. For indirect cell culture the cells were cultured on glass coverslips that were placed on top of the material surface. Glass coverslips were preconditioned 4 hours in FBS **(A)** and subsequently 20×10^3 cells/ well (SaOS-2) or 5×10^3 cells/ well (rMSCs) were seeded **(B)**. After ensuring cell adhesion, glass coverslips were transferred to new 24-well plate and placed on top of the material **(C)**.

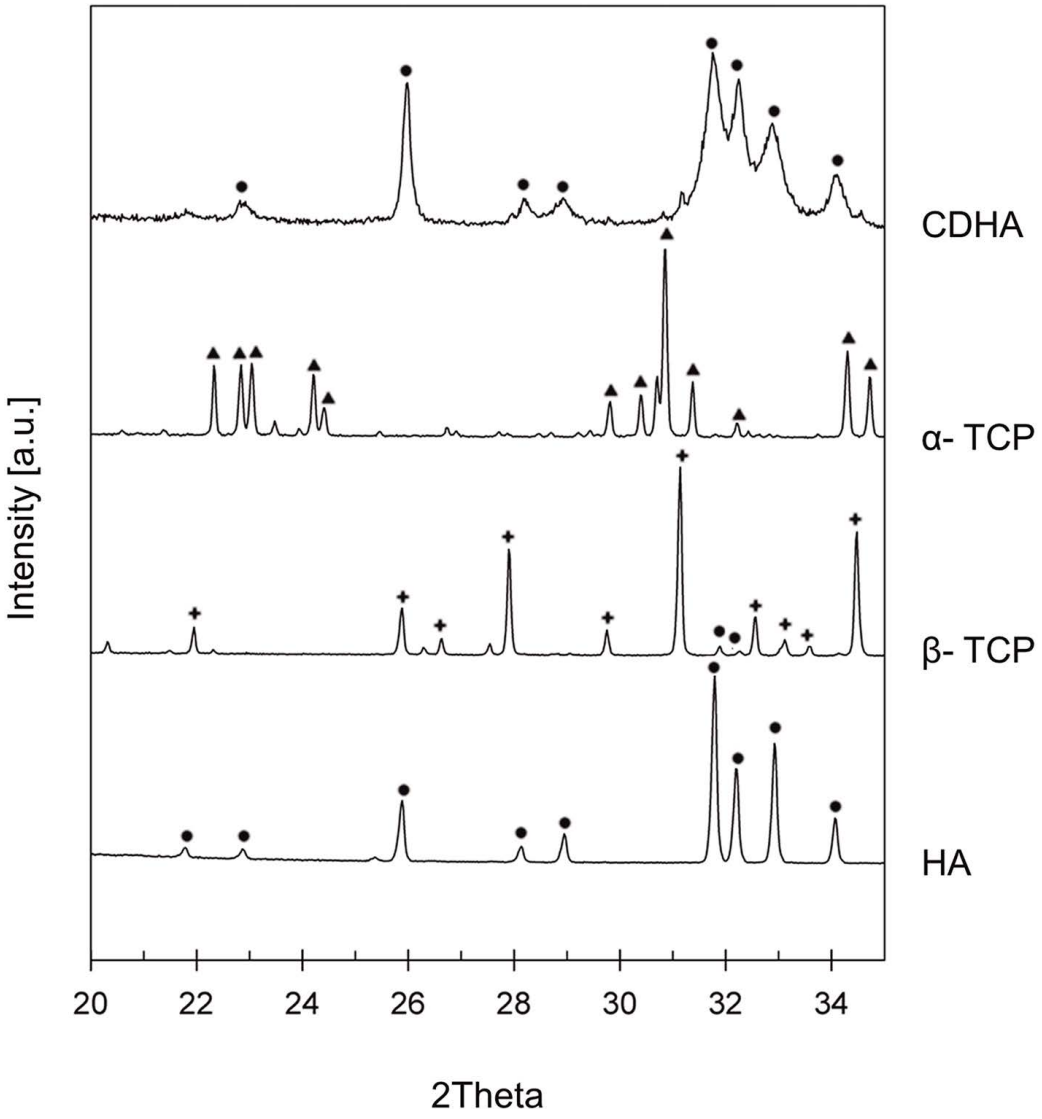

Supplementary Figure 5.2. XRD patterns of obtained CaPs. XRD were compared with the Joint Committee on Powder Diffraction Standards for (●) HA (JCPDS 82-1943), (▲) α-TCP (JCPDS 09-0348) and (+) β-TCP (JCPDS 70-2065).

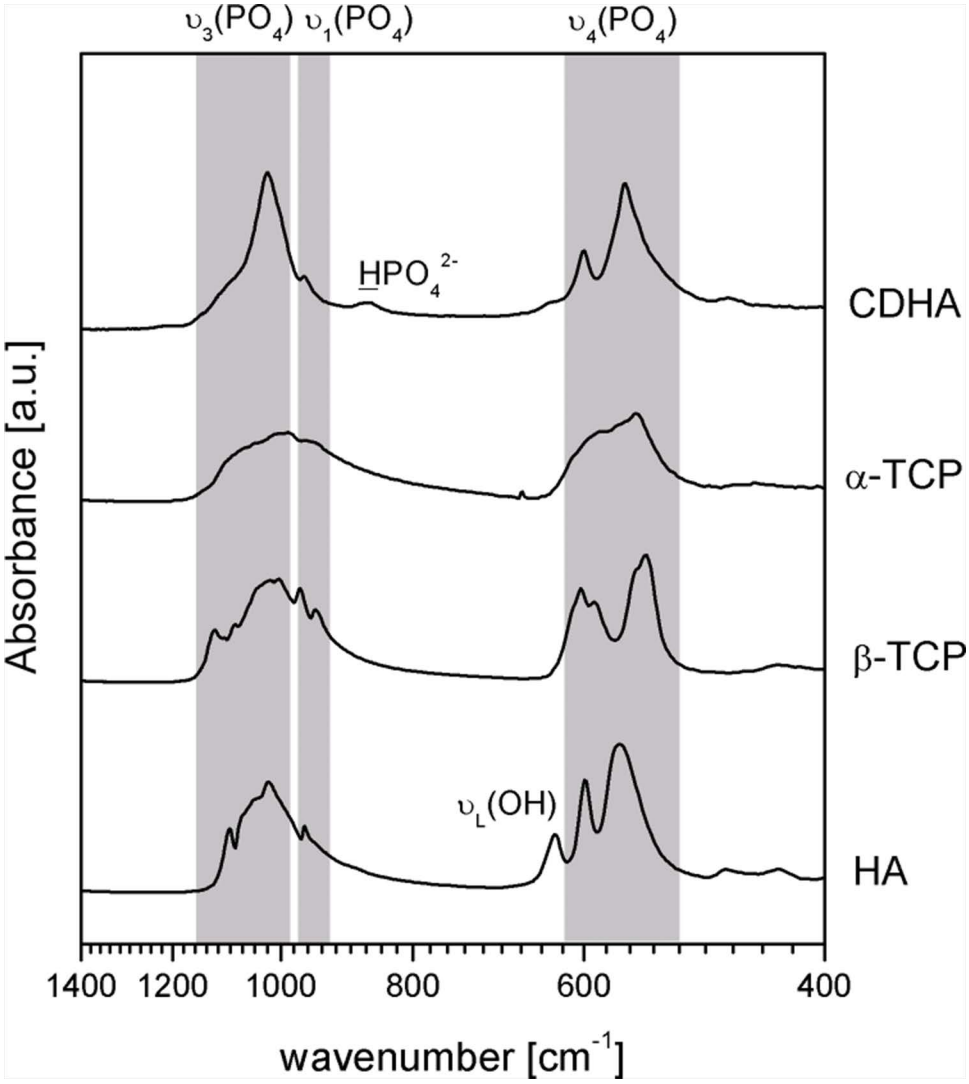

Supplementary Figure 4.3. Characteristic FTIR spectra for different CaPs in the vibration range: 400-1400 cm $^{-1}$. Band assignation was done following the works by Drouet *et al*. and Carrodeguas *et al*.[44,45]

Chapter 6

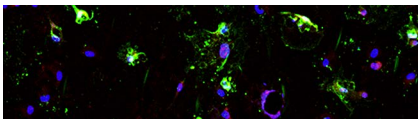

In vitro response of mesenchymal stem cells to biomimetic hydroxyapatite substrates: a new strategy to assess the effect of ion exchange

6.1 Introduction

Calcium phosphates are increasingly used as bone graft substitutes due to their similarity to the mineral phase of bone and their osteogenic potential. However, although some advances have been made in the last years, the design of synthetic bone grafts that outperform autografts remains an open challenge. For this to be possible, it would be necessary to have a more systematic knowledge of the effect of the different material properties on the biological response.[1]

Topography and textural properties, like the micro/nanostructure or porosity have been shown to influence the biological performance of calcium phosphates both *in vitro* and *in vivo*, affecting for instance the bioactivity, osteogenic and osteoinductive properties.[2-6] This has been often attributed to the sensitivity of adherent cells to the topography of the substrate. Whereas this can be a straightforward conclusion for bioinert substrates, the situation in the case of bioactive materials like CaPs is far more complex. In addition to the direct contact effects, materials can influence cell behaviour indirectly, through fluid-mediated effects, that is, through the interaction with the body fluids where the cells are immersed. For instance, it is well accepted that, amongst the parameters that contribute to the excellent performance of calcium phosphates as bone substitute materials, the ionic exchange promotes the creation of a favourable microenvironment leading to bone formation.[1,7-11]

The complexity arises because topography and ionic exchange are strictly coupled variables. The ionic exchange between material and the surrounding fluid is dependent on both the chemical composition and the microstructure or topography of the material. For a given chemical composition, the ionic exchange with the surrounding medium will be modified if the materials' topography, and consequently the specific surface area is modified. Hence, the difficulty to analyse these two parameters independently, and the risk to wrongly attribute to topography and effect that in reality can be chemical, *i.e.* associated to the modification of the soluble ions present in solution, which come into contact with the cells.

The identification of the individual effects of topography and ionic exchange is particularly relevant in the *in vitro* studies where, due to the specific conditions, some materials, especially those having high specific surface areas, as biomimetic apatites can induce considerable ionic exchange in the cell culture medium.[12,13] In these cases, the interpretation of the results and the extrapolation to the *in vivo* scenario, where continuous fluid renewal occurs, becomes especially challenging.[14]

In previous works it was demostrated that sintered ceramics and biomimetic calcium deficient hydroxyapatite (CDHA, $Ca_9(HPO_4)(PO_4)_5(OH)$) altered the ionic composition of the cell culture media to different extents, affecting the behaviour of osteoblastic and

mesenchymal stem cells.[15] This was especially striking in the case of biomimetic CDHA, a material that while having an excellent *in vivo* response, with superior osteogenic and osteoinductive properties[16], drastically impaired the viability of rat mesenchymal stem cells (rMSCs). This effect was confirmed by seeding the cells either in direct contact with the surface of CDHA discs or on glass coverslips on top of the CDHA substrates. The results demonstrated that rMSCs were highly sensitive to the ionic fluctuations caused by the biomaterial in the cell culture medium, reaching cytotoxic levels that prevented to study further the cell-material interactions.[15] Paradoxically, the same particular topographical and chemical features of these materials responsible for the excellent *in vivo* response, namely, its nanostructure, large specific surface area (SSA), deficiency in calcium and low crystallinity caused this poor *in vitro* response.[15] Whereas a further understanding of the specific mechanisms governing the cell-material interaction would be of great interest in view of designing enhanced synthetic bone grafts, the mutual interdependence between nanostructure and ionic exchange hampered the identification of the individual roles of these parameters.

In the present work, a new strategy is proposed to overcome the poor *in vitro* results usually obtained with highly reactive biomimetic CDHA, and to discern the role of ionic exchange and topographical features in the response of rMSCs. The strategy consisted in establishing culture conditions that, within the limitations of the static cultures, mimicked better the *in vivo* situation. This was done by adjusting the volume ratio between cell culture medium and biomaterial (V_{CM}/V_B). Thus, cells were cultured either at low (V_{CM}/V_B ~5) or at high (V_{CM}/V_B ~300) volume ratios, which exposed them to the same surface chemistry and topography but to different ionic concentrations. We further analysed the effect of the ionic environment on the intracellular free cytoplasmic calcium content and the subsequent processes related to it, such as the adhesion mechanisms, apoptosis and the osteogenic differentiation of rMSCs. β-tricalcium phosphate (β-TCP) was used as a control, as this sintered ceramic is directly obtained by thermal treatment of CDHA, this assuring the same elemental composition and minimising possible interferences from different reagents.

6.2 Materials and methods

6.2.1 Material preparation

The synthesis of biomimetic CDHA and β-TCP was described elsewhere.[15,17] Briefly, CDHA was obtained through a cementitious reaction involving the hydrolysis of α-TCP. The solid phase, consisting of α-TCP powder with a 2 wt.% of precipitated hydroxyapatite (Merck 2143; Merck, Darmstardt, Germany) was mixed with the help of a spatula with a liquid phase consisting of 2.5 wt.% disodium hydrogen phosphate (Na_2HPO_4; Panreac) at a 0.40 mL/g liquid to powder ratio. The paste was then transferred to Teflon moulds. Subsequently, the discs were immersed in water at 37 °C

for 7 days to allow for the complete hydrolysis reaction of α-TCP to CDHA to take place. Two dimensions of discs were prepared: i) Large discs: 15 mm diameter x 2 mm thickness (CDHA-L); and ii) Small discs: 5.5 mm diameter x 0.30 mm thickness (CDHA-S) (Figure 5.1.B). The β-TCP-L and β-TCP-S discs were obtained by sintering the CDHA-L and CDHA-S discs respectively at 1100 °C during 15 h.

6.2.2 Material characterisation

The surface microstructure was characterised by scanning electron microscopy (SEM, Zeiss Neon 40) with an acceleration voltage of 5 kV after coating the surface with gold-palladium sputtering with EMITECH K950X. The surface roughness was characterised by optical interferometry (Wyko NT1100; Veeco Instruments, USA), using a 50x magnification and a scanned area of 47.5 x 63.4 μm^2. Images were acquired using Vision32 software (Veeco Instruments).

6.2.3 Cell culture study

Rat mesenchymal stem cells (rMSCs) were isolated from the tibias and femurs of young Lewis rats (2-4 weeks old) and expanded in Advanced Dulbecco's Modified Eagle's Medium (advDMEM) supplemented with 10 % foetal bovine serum (FBS), 2 mM L-glutamine, penicillin/streptomycin (50 U/mL and 50 µg/mL, respectively) and 20 mM HEPES, all from Invitrogen (complete advDMEM). HEPES was used as pH buffer to prevent the acidification of the medium by CDHA.[12] For all the experiments, rMSCs at passage 3 and 4 were seeded at a density of 300 cells/mm^2 except where otherwise stated. For cell culture assays, 2 mL of complete advDMEM medium were used, giving rise to two cell culture conditions: i) low volume ratio between culture medium and biomaterial (V_{CM}/V_B ~5), when large discs were used (CDHA-L or β-TCP-L); and ii) high volume ratio between culture medium and biomaterial (V_{CM}/V_B ~300) for the small discs (CDHA-S or β-TCP-S) (Figure 5.1.B).

6.2.3.1 Initial cell attachment and proliferation

The discs were sterilized by immersion in 70 % ethanol and subsequently rinsed thrice with PBS. Afterwards, the discs were placed in 24-well plate and incubated overnight with complete advDMEM. Cells were seeded and after the initial cell attachment (6 hours) samples were transferred to new 24-well plate to discard attached cells at the bottom of well-plate in the small discs. Subsequently, rMSCs were incubated with samples for 6 hours, 3 days, 7 days and 14 days, renewing the medium every day. Tissue culture polystyrene (TCPS) was used as control. At each specified time point, discs were transferred to new 24-well plate, washed thrice with PBS and lysed with 300 µl M-PER® (Mammalian Protein Extraction Reagent, Thermo Scientific, Waltham, MA, USA). Cell number was quantified by Cytotoxicity Detection Kit (Roche Applied Science, Penzberg, Germany) following the manufacturer's protocol. A calibration

curve with increasing numbers of cells was prepared. LDH activity was evaluated at 492 nm with Synergy HTX multi-mode microplate reader (Bio-Tek). Results of cell number detected by LDH activity were normalized versus the area of the corresponding substrate. Two independent runs of experiment were performed.

6.2.3.2 Scanning electron microscopy

Cell morphology was evaluated by scanning electron microscopy (SEM, Zeiss Neon 40) with an acceleration voltage of 5 kV. After placing the discs in new 24-well plate, three rinses with PBS were performed and cells were fixed in 2.5 % glutaraldehyde solution in PBS. Afterwards, discs were incubated for 1 h at 4 °C and subsequently washed in PBS (x3) and dehydrated in 50, 70, 90, 96 and 100 % ethanol series. Dehydration process was completed by adding hexamethyldisilazane (HMDS). A thin layer of gold-palladium was deposited on discs by vapour deposition (EMITECH K950X). Image analysis with Fiji/Image-J package was performed in order to quantify spreading area and aspect ratio of rMSCs over cell culture (n=15).

6.2.3.3 Measurement of pH, Ca^{2+} and Pi concentration in the cell culture medium

For the evaluation of calcium and phosphate concentrations, at each specified time point, the supernatants *i.e.* the cell culture medium in contact with the CaP substrates were collected. Then, Ca^{2+} content was quantified through calcium o-cresolphthalein complexone method[18,19] whereas P_i through Phosphate Colorimetric Assay Kit (Sigma-Aldrich) following the manufacturer's instructions. The results were measured spectrophotometrically by Synergy HTX multi-mode microplate reader (Bio-Tek) at 570 nm and 650 nm for Ca^{2+} and P_i, respectively. The pH measurements were performed using a selective electrode (CRISON INSTRUMENTS, MultiMeter MM 41). The experiments were performed in two independent runs.

6.2.3.4 Evolution of the CDHA exposed to the cell culture medium

To analyse the effect of prolonged exposure of CDHA to cell culture medium, CDHA-L and CDHA-S discs were sterilised with 70 % ethanol, rinsed thrice with double distilled water (dd H_2O) and incubated overnight with 2 mL of advDMEM without FBS supplementation (FBS was not included to avoid the contribution of the ions bound to proteins as they could interfere upon protein adsorption on the material). The medium renewal was performed every day up to 21 days of incubation. Before incubation, as well as after 14 and 21 days, the discs were broken into two halves and one of them was milled in an agate mortar. The remaining half discs and the powders were then washed three times with dd H_2O and allowed to dry at 37 °C. To determine the superficial changes in composition, the surface of CDHA-L discs was scraped with a scalpel and the powder was analysed by Fourier transform infrared spectroscopy in the attenuated

total reflection mode (ATR-FTIR, Nicolet 6700). Data was acquired in 64 scans with a resolution of 4 cm^{-1} from 4000 to 675 cm^{-1} with a Germanium crystal.

The Ca/P ratio was measured from the milled CDHA halves by inductive coupled plasma-mass spectroscopy (ICP-MS; Agilent 7700x, Agilent Technologies, Japan). The powders were dissolved in 69 % HNO_3 (w/w) (HNO_3, TraceSELECT®, Sigma Aldrich, Switzerland) and diluted 1:1000 in a solution of demineralized H_2O containing 3% HNO_3, 2% HCl (HCl, Rotipuran® Supra, Carl Roth, Switzerland) and 0.01 % HF (HF, TraceSELECT® Ultra, Sigma Aldrich, Switzerland). The solutions were analyzed using ICP-MS. ^{44}Ca and ^{31}P signals were calibrated against a custom-made certified standard solution containing Ca and P ions in a molar ratio of 1.55, and ^{23}Na, ^{25}Mg and ^{88}Sr signals were calibrated against a multi-element standard solution (both: Inorganic Ventures, USA). Calibration drifts were corrected according to the Ca-P standard measured after every 8^{th} sample and according to a 20 ppb internal Sc standard solution (Inorganic Ventures, USA) measured along with each sample. Finally, the mean values of four measurements per sample were determined.

6.2.3.5 Measurment of intracellular Ca^{2+}

To analyse potential effects of the extracellular calcium fluctuations on the intracellular calcium, this parameter was measured for the cells cultured on CDHA, the substrate that induced higher changes of calcium concentration following the two culture conditions. Cells were seeded on CDHA-L and CDHA-S as described above (section 6.2.3.1.). After 6 hours of adhesion, samples were transferred to new 24-well plate and adherent cells were detached with trypsin. Both trypsinised cells and supernatants were centrifuged at 300 x g for 5 min. Afterwards, cells were incubated with 5 µM Fluo-4-acetoxymethyl ester, a dye which binds to free cytoplasmic calcium of living cells, (Fluo-4 AM; Molecular Probes) in FBS- free advDMEM for 20 min at 37 °C. Subsequently, cells were centrifuged and resuspended in PBS. The fluorescence emission at 530 nm was measured by a Gallios Flow Cytometer (Beckman Coulter, Brea, CA, USA). A total of 5000 events were evaluated. Afterwards, the flow cytometry data was plotted as forward scatter versus side scatter and gate was determined manually using the unstained rMSCs and rMSCs stained with Fluo-4 AM as a controls. The dead and fragmented cells were excluded from analysis. Summit 4.3 and FlowJo Softwares were used for sample analysis.

6.2.3.6 Apoptosis/necrosis assay

After 6 hours of adhesion of rMSCs to CDHA-L and CDHA-S, cells were detached as above described (section 6.2.3.5.), centrifuged and the cell pellet was resuspended using cold PBS. Subsequently, rMSCs were stained with Alexa Fluor 488 Annexin V and Propidium Iodide (PI) using the Dead Cell Apoptosis Kit (Invitrogen) and following manufacturer protocol. TCPS was used as control. The samples were stored on ice till

analysis. A total of 5000 events for each condition were analysed by a Gallios Flow Cytometer (Beckman Coulter, Brea, CA, USA) measuring the fluorescence emission at 530 nm (FL1) and > 575 nm (FL4) for annexin V and PI staining, respectively. Summit 4.3 Software was used for sample analysis.

Additionally, apoptosis/necrosis pathway on CDHA-L and CDHA-S samples was analysed by visualization in confocal microscopy. For that purpose, CDHA-L and CDHA-S were washed with cold PBS and stained with Dead Cell Apoptosis Kit. Afterward, cells were fixed with 4% paraformaldehyde (PFA) solution in PBS. For nuclei visualisation, discs were incubated with 4',6-diamidino-2-phenylindole (DAPI, 1:1000 in 0.15 % glycine in PBS) for 2 minutes. Cells seeded on glass coverslip were used as a control. Samples were visualized in a TCS SPE confocal microscope (Leica Microsystems). Images were acquired using the LASX software and processed using Fiji/Image-J package.

6.2.3.7 Immunofluorescence staining

Cell morphology and adhesion on CDHA-L and CDHA-S was investigated by staining of cytoskeleton, focal adhesions and fibronectin (FN) secretion. rMSCs seeded on glass coverslip were used as a control. The study was performed at 6 hours, and 1, 2 and 3 days of cell culture. Attached cells were rinsed with PBS (x3) and fixed in 4% PFA solution in PBS. Afterwards, cells were permeabilized with 300 µL of 0.1 % Triton X-100 (Sigma-Aldrich) in PBS for 15 minutes and blocked with 1 % bovine serum albumin (BSA) (Sigma-Aldrich) in PBS for 30 min. Then, the discs were incubated for 1 hour with the following primary antibodies: mouse anti-vinculin (Sigma-Aldrich), rabbit anti-fibronectin (Sigma-Aldrich) or rabbit anti- phospho-FAK (pFAK; pTyr397 specific, Santa Cruz Biotechnologies), all at 1:100 in 1 % BSA in PBS. Afterwards, appropriate secondary antibodies were added: Alexa Fluor 488 goat anti- mouse (1:1000) or Alexa Fluor 488 goat anti-rabbit (1:1000) were incubated with Alexa Fluor 546 Phalloidin (1:300) for 1 hour in 0.1 % Triton X-100 in PBS (all from Invitrogen). For nuclei staining, the discs were incubated with DAPI (1:1000 in 0.15 % glycine in PBS) for 2 minutes. Between all steps, three rinses for 5 minutes with 0.15 % glycine (Sigma-Aldrich) in PBS were performed. Discs were mounted with Mowiol 4-88 (Sigma-Aldrich) and visualized using a TCS SPE confocal microscope (Leica Microsystems, Germany). Cells seeded on glass coverslip were used as a control. Images were acquired using LASX software and processed using Fiji/Image-J package. Additionally, image analysis was performed in order to quantify the evolution of spreading area and aspect ratio (n=15) on CDHA discs at short time points. The pFAK area (n=10) was measured at day 3 of cell culture.

6.2.3.8 Gene expression

The differentiation of rMSCs to osteoblastic phenotype was assessed on CDHA-S and β-TCP-S by measuring gene expression of osteoblastic markers by real time quantitative polymerase chain reaction (qRT-PCR). Total RNA was extracted at 6 hours, 1 day and 3 days using RNeasy® Mini Kit (Qiagen, Hilden, Germany) and following manufacturer instructions. Samples were previously transferred to new 24-well plates and rinsed thrice in PBS. Subsequently, total RNA was quantified by NanoDrop ND-1000 spectrophotometer (NanoDrop Technologies, Montchanin, DE, USA) and 150 ng of RNA were used for synthesis of complementary DNA (cDNA) using the QuantiTect Reverse Transcription Kit (Qiagen). cDNA templates were amplified using the QuantiTect SYBR Green RT-PCR Kit (Qiagen) in a StepOnePlus Real-Time PCR System (Applied Biosystems, Foster City, CA, USA) using specific primers for osteoblastic markers (Table 6.1.). In all RT-qPCR runs, specificity of primers was determined by melt curves analysis. Moreover, negative controls *i.e.* no- RNA control and no- RT control were run in parallel in order to ensure that contamination and genomic DNA were not present. The values were normalised by expression of reference gene *i.e.* β-actin (ACTB) and relative fold changes (FC) were related to TCPS at 6h of culture using the following Equation 6.1.[20]

$$FC = E_{target}^{\Delta Cq\ target\ (TCPS\ 6h - sample)} / E_{reference}^{\Delta Cq\ reference\ (TCPS\ 6h - sample)} \qquad \text{(Eq 6.1.)}$$

Cq respresents the median value of the quantification cycle of the triplicate of each sample. E corresponds to the efficiency of amplification and is determined through following formula $E = 10^{[-1/slope]}$ where slope value proceeds from slope of the log-linear portion of the calibration-curve. The experiment was performed in three independent runs. No osteogenic medium was used for CDHA-S and β-TCP-S except for the evaluation of OCN gene expression, where osteogenic medium (OM) containing 50 µm/mL ascorbic acid, 10 mM β-glycerophosphate and 100 nM dexamethasone in complete medium was used. The osteogenic medium was added 6 hours after cell seeding.

Table 6.1. Primers' sequences used in this study

Gene	Gene symbol	Primers' sequences (5'→3')
β-actin	ACTB	F:CGTCATCCATGGCGA ACT R: CCCGCGAGTACAACCTTCT
Alkaline phosphatase	ALP	F:TCAGTTCTGTTCTTGGGGTACAT R: GCACAACATCAAGGACATCG
Bone morphogenic protein-2	BMP-2	F:CCCCTATATGCTCGACCT CT R: AAAGTTCCTCGATGGCTTCTT
Collagen I	COLLI	F:CATGTTCAGCTTTGTGGACCT R: GCAGCTGACTTCAGGGATGT
Osteocalcin	OCN	F:CCAGGGGATCTGGGTAGG R: ATAGACTCCGGCGCTACCTC
Osteonectin	ONN	F:GGTTCTGGCAGGGGTTTT R: GTTTGAAGAAGGTGCAGAGGA
Osteopontin	OPN	F:GGCTACAGCATCTGAGTGTTTG R: CGGTGAAAGTGGCTGAGTTT

6.2.4 Statistical analysis

The experiments were performed in triplicate, with three independent runs in each test, except where otherwise stated. The results are presented as mean ± standard error (SE). Statistical analysis for parametric data (the results of flow cytometry) was performed using T-Student test. For non-parametric data, Kruskal-Wallis test was applied, followed by multiple pairwise comparison. Significance level was set as p-value < 0.05.

6.3 Results

6.3.1 Material characterisation

SEM micrographs revealed that the topography of CDHA consisted of aggregates of plate-like crystals, whilst the sintering process led to a polyhedral grain structure for β-TCP. The average roughness was higher for CDHA (Sa=2.53 ± 0.72 μm) compared to β-TCP (Sa=1.33 ± 0.23 μm) (Figure 1A). Further physicochemical characterisation of both CaP materials can be found in a previous work.[15]

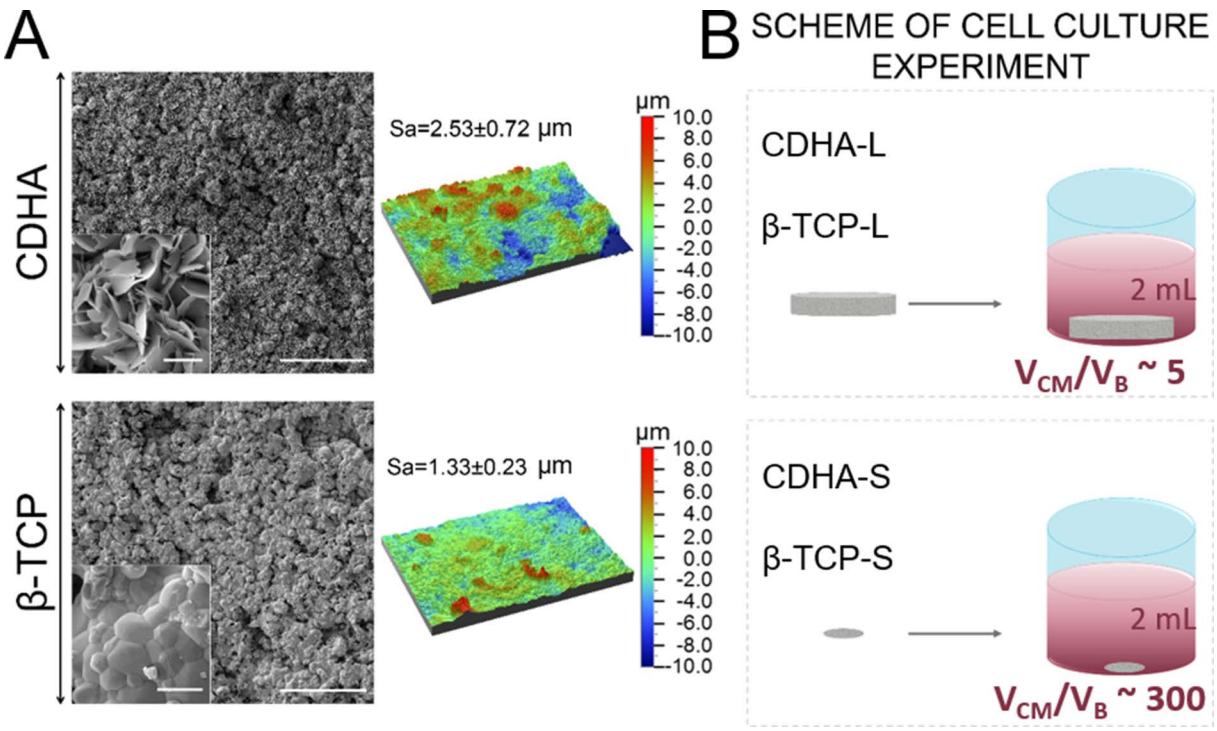

Figure 6.1. A) Scanning electron microscopy (left panel) and optical interferometry (right panel) images of CDHA and β-TCP substrates. Scale bar denotes 40 µm in the main images and 2 µm in the insets with magnified micrographs; **B)** Scheme of cell culture experiment.

6.3.2 Initial cell adhesion and proliferation

Cell proliferation was slower in the four CaP substrates than in TCPS, and in general cell number was larger in β-TCP than in CDHA. Interestingly, different trends were found in relation to the effect of V_{CM}/V_B on cell proliferation when comparing CDHA and β-TCP. Whereas cell number increased with time on β-TCP irrespective of the V_{CM}/V_B used, on the CDHA cell proliferation was significantly affected by the V_{CM}/V_B (Figure 6.2.A). When cells were cultured on the large CDHA discs (CDHA-L) cell number decreased over time. In contrast, this tendency was reversed and a slow increase in cell number was observed when cells were cultured on the small discs (CDHA-S), although the values reached were significantly lower than those observed for β-TCP and TCPS.

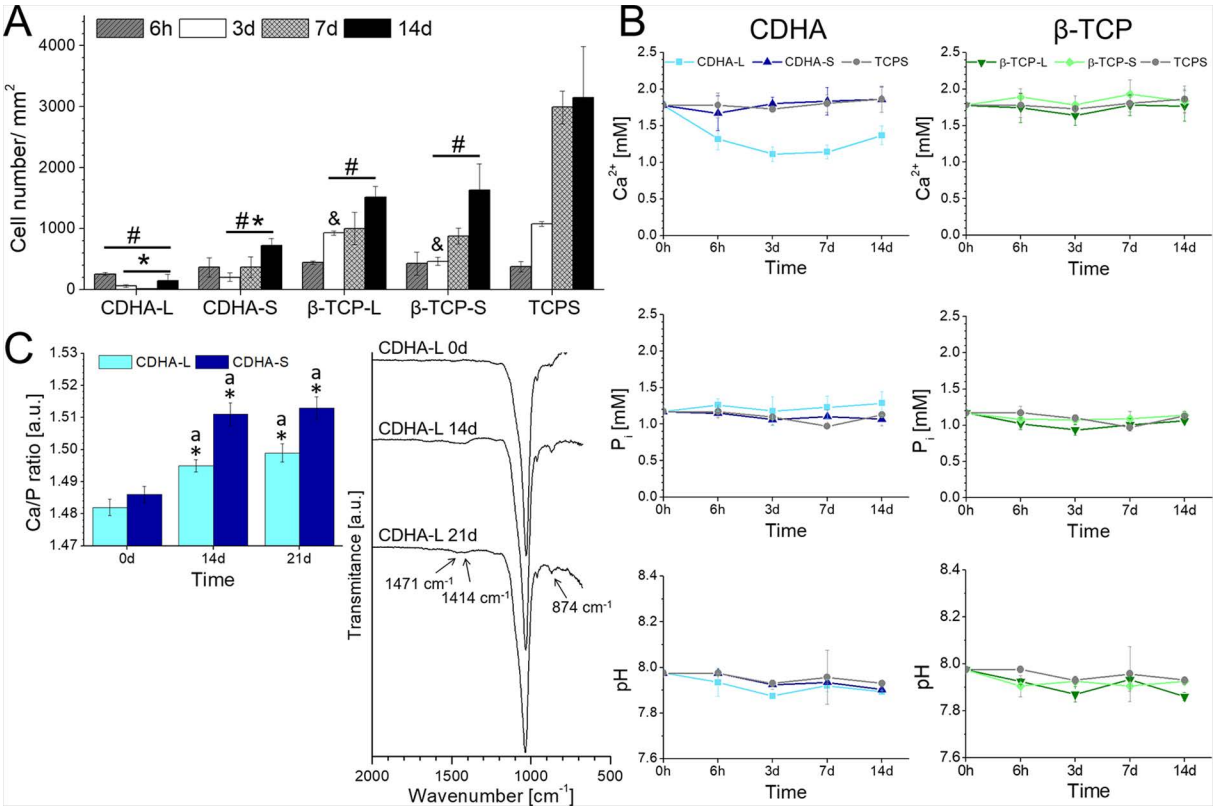

Figure 6.2. A) Proliferation of rMSCs at 6 hours, 3, 7 and 14 days. Bars represent means ± standard deviation (SD) of three experiments. * indicates significant differences ($p < 0.05$) between CDHA- L and CDHA- S at each time point. & indicates significant differences ($p < 0.05$) between β-TCP- L and β-TCP- S at each time point. # Indicates significant differences ($p < 0.05$) compared with TCPS at each time point; **B)** upper panel: Concentration of Ca^{2+} in the supernatants at 6 hours, 3, 7 and 14 day of cell culture; middle panel: Concentration of P_i in the supernatants at 6 hours, 3, 7 and 14 day of cell culture; bottom panel: pH of the supernatants at 6 hours, 3, 7 and 14 day of cell culture. The evaluation of ionic composition and pH of supernatants was performed in presence of cells. **C)** The effect of cell culture medium on CDHA chemistry; left: The Ca/P ratio of CDHA-L and CDHA-S discs after 0, 14 and 21 days of incubation with culture media; right: The ATR- FTIR spectra of CDHA-L surface. The evaluation of CDHA-L and CDHA-S substrates was performed without presence of cells in culture medium. * indicates significant differences ($p < 0.05$) between CDHA-L and CDHA-S at each time point. Letters (a,b) identify differences ($p < 0.05$) between the time points within the same sample.

6.3.3 Interactions between the CDHA substrates and the cell culture medium

The evolution of extracellular Ca^{2+} and P_i over time in presence of cells is displayed in Figure 6.2.B. The experimental value of Ca^{2+} in complete advDMEM cell culture medium was 1.78 ± 0.17 mM. Different trends were found in relation to the effect of V_{CM}/V_B when comparing CDHA and β-TCP. Whereas the Ca^{2+} concentration in the culture medium was unaltered in contact with β-TCP discs, irrespective of its size, a significant decrease of calcium concentration was produced in contact with the CDHA-L discs, which did not happen for the small CDHA discs. After 6 hours, the Ca^{2+} concentration decreased approximately 25 % of the initial experimental value and continued decreasing up to 40 % at days 3 and 7. At day 14 the calcium concentration

increased slightly, reaching similar values to those at 6 hours, which reflected that the uptake of Ca^{2+} was slowly becoming saturated.

Small changes of P_i concentration in the cell culture medium were observed for all the substrates, the concentration remaining closer to the initial value (1.17 ± 0.10 mM) (Figure 6.2.B, middle panel). Little variation was observed in the pH of the cell culture medium throughout the cell culture study in all CaP discs (Figure 6.2.B, bottom panel).

Regarding the CDHA substrates, no changes were observed by SEM in the microstructure of the surface of the discs after exposure to FBS-free advDMEM for 21 days. Both CDHA-L and CDHA-S exhibited the typical plate- like crystal morphology already revealed on the pristine substrates (Supplementary Figure 6.1.). Interestingly, FTIR analysis of the surface of the discs revealed the presence of carbonate bands on CDHA-L samples exposed to the cell culture medium (Figure 6.2.C, right panel). The bands at 1471 and 1419 cm^{-1} can be ascribed to a B-type substituted apatite whilst the one observed at 874 cm^{-1} can be assigned to either HPO_4^{2-} or to a B-type carbonate substituted apatite.[21-23] The remaining bands at 964 and 1030 cm^{-1} correspond to typical vibrational modes of phosphate in apatite.[24] The modification of the discs surface chemistry was further confirmed through X-ray photoelectron spectroscopy (XPS) (Supplementary Figure 6.2.A and 6.2.B). In addition, ICP-MS analyses performed after dissolution of powdered discs led to an increase in the Ca/P ratio of 0.90 ± 0.13 % and 1.67 ± 0.24 % for CDHA-L and CDHA-S at 14 day, respectively (Figure 6.2.C, left panel). It is worth stressing that these values are an average of the whole volume of the samples, and do not to correspond to the surface. There were no significant changes in Ca/P ratio between 14 and 21 day of incubation. Similar trends were observed for the Mg/P and Na/P ratios (Supplementary Figure 6.3.).

6.3.4 Cell morphology

The micrographs of the morphological studies performed by SEM are shown in Figure 6.3. Cells were well adhered after 6 hours, presenting similar flattened morphology in all CaPs. Nonetheless, after 3 days of culture rMSCs exhibited differences in shape depending on the substrate. In both β-TCP-L and β-TCP-S, rMSCs maintained their initial flattened and spread morphology showing similar cell spreading area as well as aspect ratio (Figures 6.3.B and 6.3.C). In contrast, on CDHA-S the rMSCs became more spindle-shaped, with a higher aspect ratio compared to the initial time point (Figure 6.3.C).

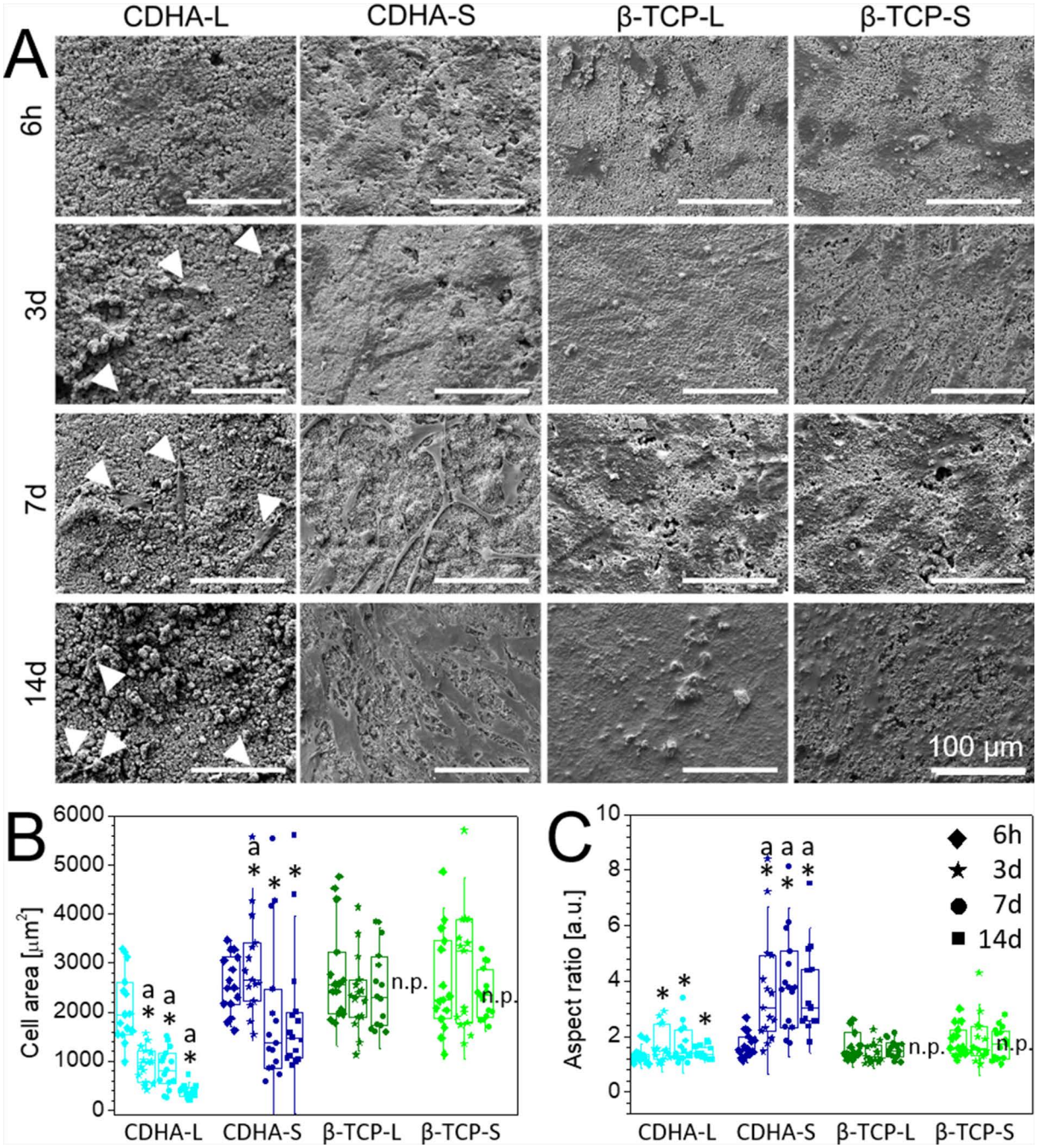

Figure 6.3. A) Morphology of rMSCs observed by SEM on CDHA-L, CDHA-S, β-TCP-L and β-TCP-S at 6 hours, 3, 7 and 14 days. To better distinguish rMSCs on CDHA-L, some cells are labelled with white arrows. Scale bar denotes 100 µm; **B)** Cell spreading and **C)** aspect ratio on CaPs substrates over cell culture. Symbols represent individual cells (n=15), the boxes represent 25th and 75th percentile, the middle line is the median and whiskers are standard deviation. n.p.- not provided: due to the high density of cells on β-TCP-L and β-TCP-S at day 14, the quantification of morphological features of rMSCs was precluded. * indicates significant differences ($p < 0.05$) between L (CDHA-L and β-TCP-L) and S (CDHA-L and β-TCP-L) substrates at each time point; a indicates significant differences ($p < 0.05$) compared with 6h for each sample. No other statistically significant differences were detected.

The most remarkable changes occurred for the low V_{CM}/V_B ratio, that is, for CDHA-L discs. In this case, although rMSCs showed flattened morphology at 6 hours a progressive decrease in cell spreading was observed over time, together with a reduction

in cell number (Figures 6.3.A and 6.3.B). Moreover, the cells cultured on CDHA-L presented a significantly lower aspect ratio compared to CDHA-S, remaining round-shaped throughout the cell culture (Figure 6.3.C).

6.3.5 Free-intracellular calcium

The free-intracellular calcium for the cells cultured on CDHA is displayed in Figure 6.4. The dead and fragmented cells were excluded from the analysis and the fluorescence was normalized by cell size.[25,26] Thus, the values of median fluorescence of Fluo-4 represent the levels of intracellular calcium of viable, gated cells (Figure 6.4.A, coloured dots). A shift of fluorescence emission of Fluo-4 was observed when rMSCs were cultured on CDHA-L and CDHA-S compared to TCPS (Figure 6.4.B). The results showed a no statistically significant decrease of 4.86 ± 21.01 % of median fluorescence of Fluo-4 for CDHA- L (Median=0.067 ± 0.01) compared to TCPS (Median= 0.0705 ± 0.00). In contrast, the Fluo-4 fluorescence levels for CDHA-S (Median=0.11 ± 0.02) were 61.87 ± 33.72 % higher than the TCPS values (Figure 6.4.D). The experiment was performed in four independent runs.

6.3.6 Cell death pathways

The pathway of rMSCs death was evaluated for CDHA-L and CDHA-S discs (Figure 6.5.) and represented as a contour diagram of Annexin V Alexa Fluor 488/ PI intensity staining. The viable cells appear negatively stained for PI and Alexa Fluor 488-Annexin V and are represented at left lower quadrant. The positively stained cells for Alexa Fluor 488-Annexin V and negatively stained for PI are considered apoptotic cells and are represented in the right lower quadrant. The left upper quadrant represents necrotic cells that positive stain for PI but are negative for Alexa Fluor 488- Annexin V. Late apoptotic cells display binding for both PI and Alexa Fluor 488- Annexin V and are represented in the right upper quadrant. The percentage of viable was significantly reduced for CDHA-L (65.20 %) compared to the control, and non-viable cells were mainly late apoptotic cells (21.64 %), although there was also a percentage of apoptotic and necrotic cells (6.6 and 6.56 % respectively). The percentage of viable cells increased when the ratio V_{CM}/V_B increased. Thus, when the small discs were used (CDHA-S), the percentage of viable cells was 82.58 %, with 8.53 % of late apoptotic cells, 7.88 % of apoptotic cells and very few necrotic cells. The results were confirmed through the visualisation by confocal microscope (Figures 6.5.D-I)

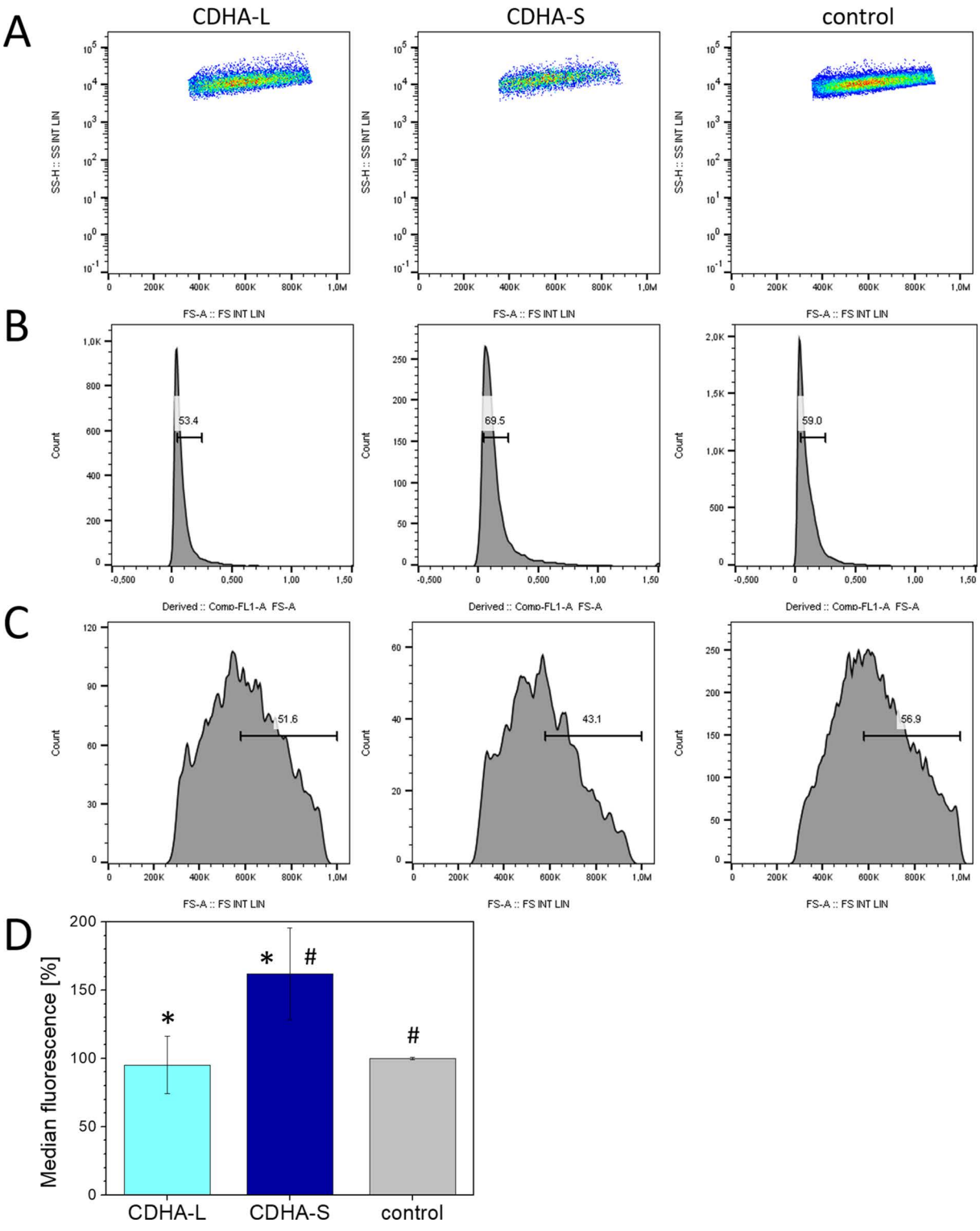

Figure 6.4. Flow cytometric analysis of intracellular calcium of CDHA-L, CDHA-S and control at 6 hours. **A)** The dot plots show the gate (coloured dots) of viable cells that was set for analysis of Fluo-4 fluorescence; **B)** Histograms of fluorescence of Fluo-4 normalised versus forward scatter (cell size); **C)** Histograms of cell size (forward scatter); **D)** Mean ± standard error of median fluorescence of Fluo-4 from three independent runs. The median fluorescence for CDHA-L and CDHA-S was represented as a percentage of median fluorescence of the control (TCPS) establishing that it is equal to 100 %. * and # indicates groups with significant differences ($p < 0.05$).

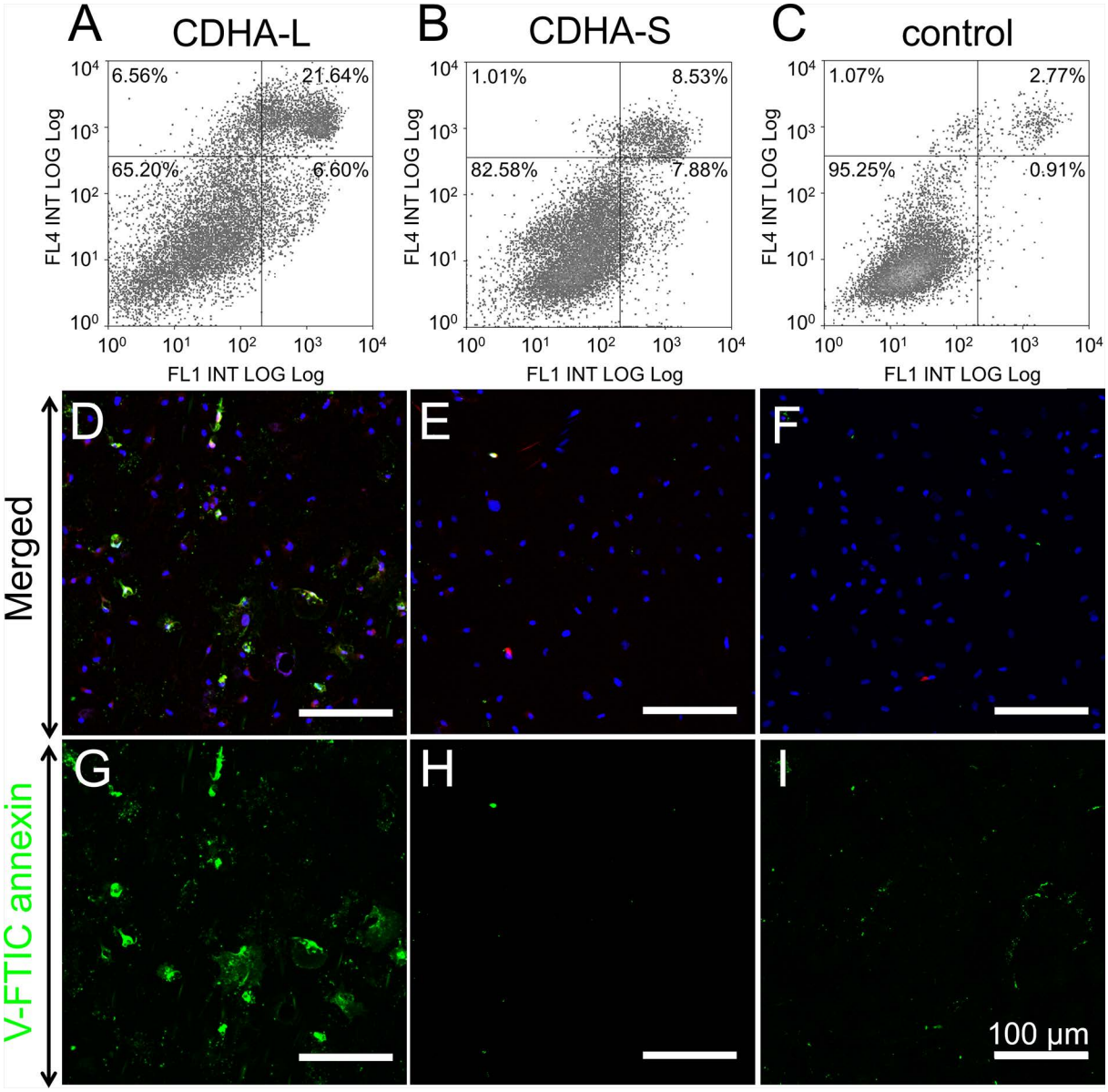

Figure 6.5. A), **B)** and **C)** apoptosis/necrosis assay by flow cytometry. Cells positively stained for Alexa Fluor 488 annexin V and negatively for PI were considered as apoptotic. Cells positively stained for both Alexa Fluor 488 annexin V and PI were considered as late apoptotic. Cells negatively stained for Alexa Fluor 488 annexin V and positively for PI are considered necrotic. The percentage of each population of cells is presented in corresponding square of each graph; **D)**, **E)** and **F)**: Representative merged confocal images of rMSCs stained for apoptosis (green)/necrosis (red) with annexin V/PI and nuclei (blue) ; **G)**, **H)** and **I)**: Representative confocal images of rMSCs stained for apoptosis (green). Scale bar denotes 100 µm. The brightness and contrast of images was adjusted using Fiji/Image-J package.

6.3.7 Immunofluorescence staining

The morphology of rMSCs on CDHA-L and CDHA-S was studied by immunofluorescence, staining the nuclei, the actin cytoskeleton and either FN (Figure 6.6.) or pFAK (Figure 6.7.).

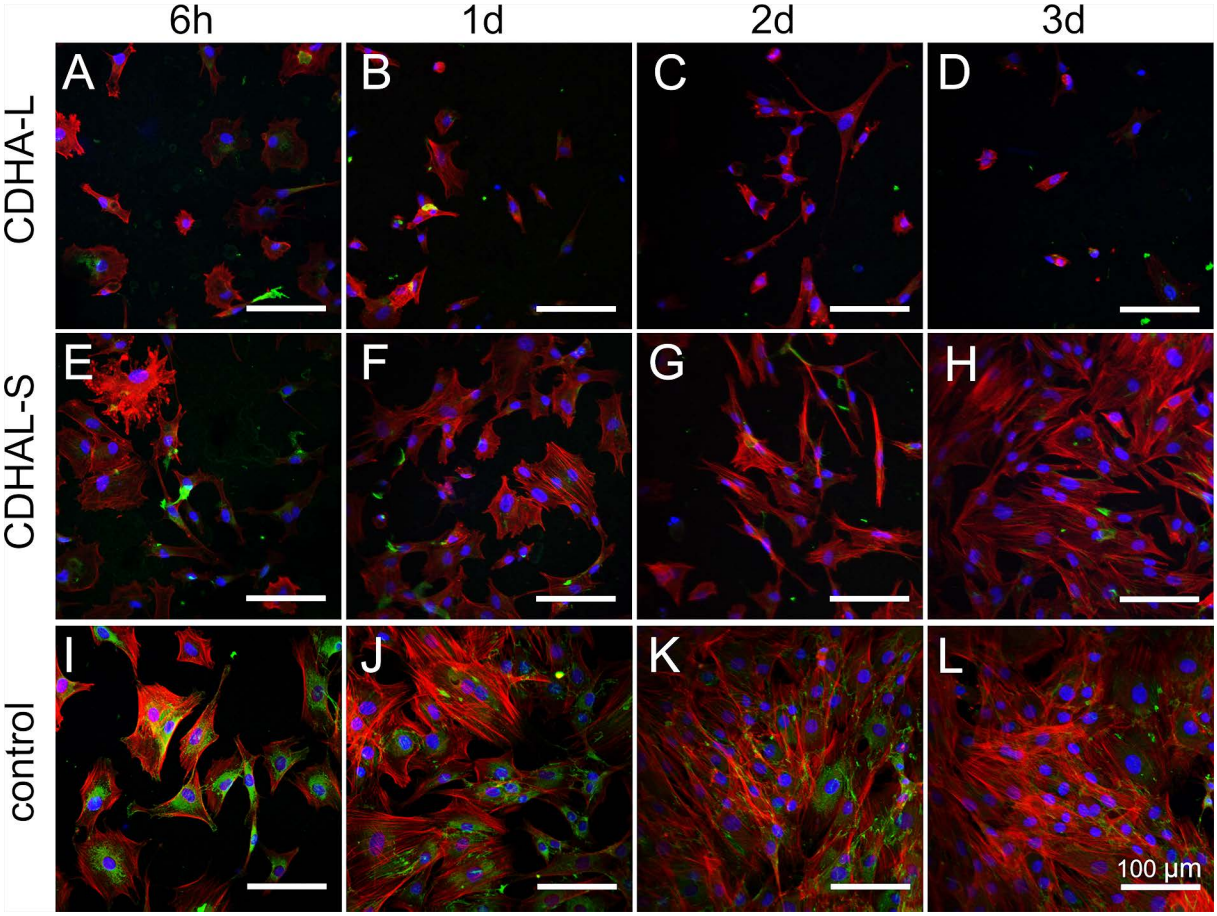

Figure 6.6. Merged images of rMSCs stained for F-actin (red), nuclei (blue) and fibronectin (green) on CDHA-L (A, B, C, D), CDHA-S (E, F, G, H) and control *i.e.* glass coverslips (I, J, K, L) at 6 hours, 1, 2 and 3 days of cell culture respectively. Scale bar denotes 100 µm.

The formation of actin stress fibers was delayed in cells cultured on CDHA compared to TCPS. Noteworthy, V_{CM}/V_B had a strong effect on the cytoskeletal organisation, the cells cultured on CDHA-S presenting a well-defined cytoskeletal organization after 1 day of culture whilst non-maturation of actin stress fibers was observed on CDHA-L throughout the analysed time points (Figures 6.6. and 6.7.). A reduced staining of both FN and pFAK was observed in both CDHA substrates compared to TCPS (Figures 6.7. and 6.7.A). Again, strong differences were found when the V_{CM}/V_B ratio was modified, as whereas in CDHA-S fibronectin production and focal adhesions were clearly observed, they were hardly visible in CDHA-L (Figures 6.7. and 6.7.A and 6.7.D). Moreover, CDHA-L resulted in a significant reduction of cell area after 6h. This trend, instead, was not observed for CDHA-S, where a progressive cell spreading was observed (Figure 6.7.A and 6.7.B).

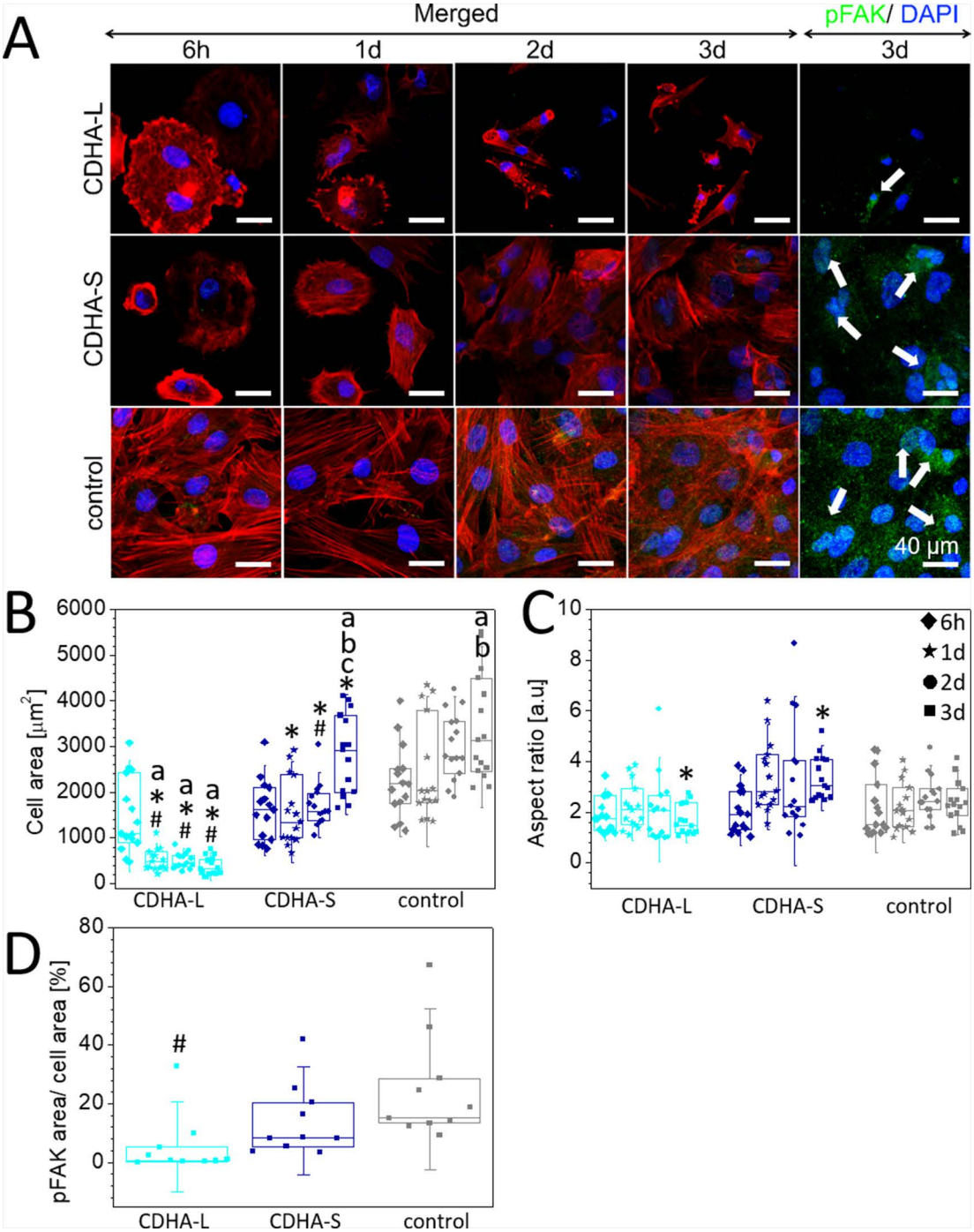

Figure 6.7. A) Merged images of cells stained for F-actin (red), nuclei (blue) and pFAK (green) on CDHA-L, CDHA-S, and control *i.e.* glass coverslips at 6 hours, 1, 2 and 3 days of cell culture. The last column shows the pFAK/ DAPI staining of rMSCs on CDHA-L, CDHA-S and control, at day 3. pFAK was indicated with white arrows. Scale bar denotes 40 µm. The brightness and contrast of images was adjusted using Fiji/Image-J package. **B)** and **C)**, respectively: Evolution of spreading and aspect ratio of cells on CDHA-L and CDHA-S at the different time points; **D)** Area of pFAK at day 3 of cell culture. Symbols represent individual cells (n=15 in B) and C) and n=10 in D), the boxes represent 25th and 75th percentile, the middle line is the median and whiskers are standard deviation. * indicates significant differences ($p < 0.05$) between CDHA substrates at each specific time point. # indicates significant difference ($p < 0.05$) compared with control at each time point. Letters (a,b,c) identify differences ($p < 0.05$) between the time points within the same sample.

6.3.8 Gene expression

The expression of osteoblastic specific markers by rMSCs cultured on the CDHA and β-TCP small discs was performed using RT-qPCR (Figure 6.8.). It was not possible to measure them in large discs due to small cell numbers.

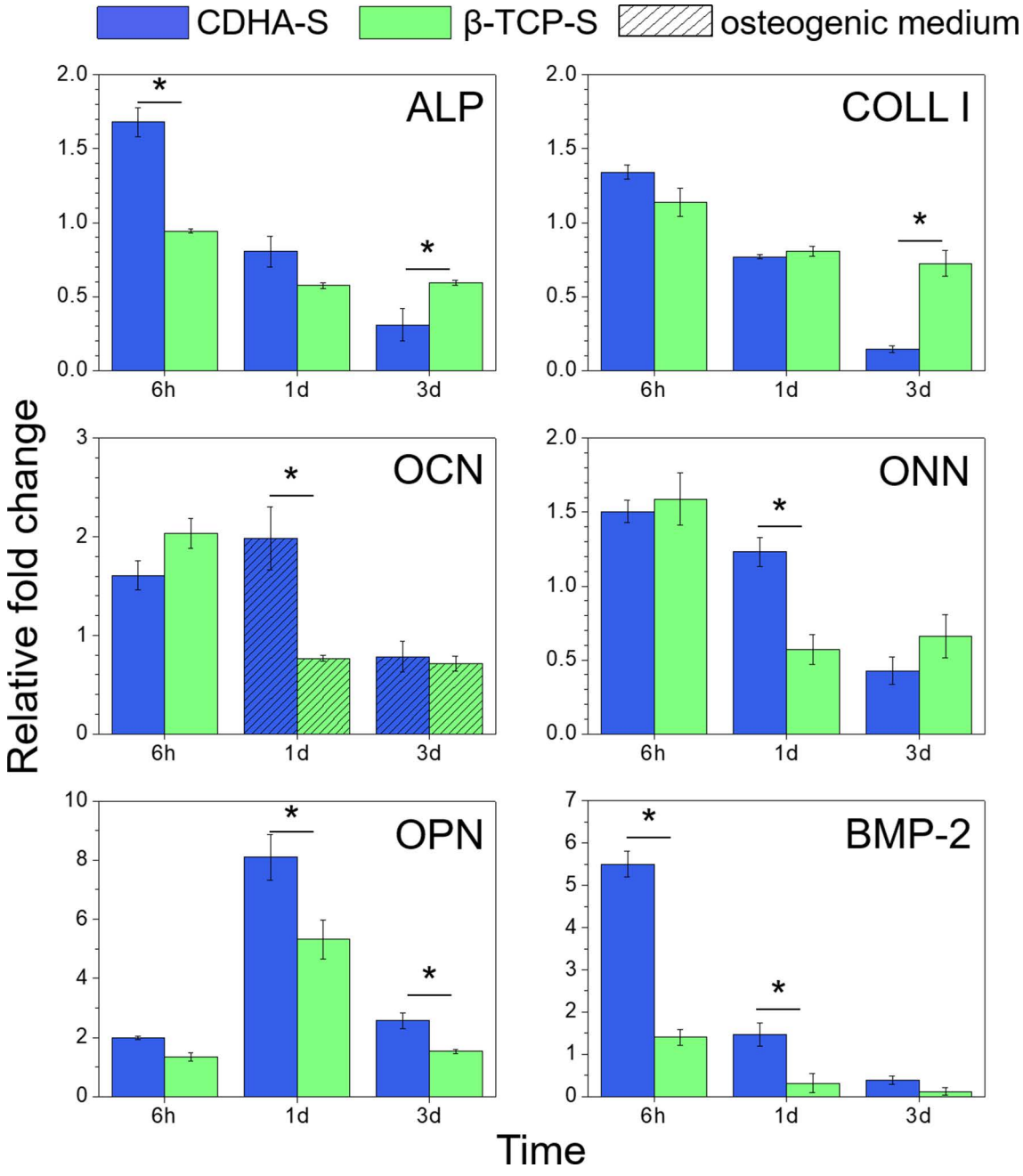

Figure 6.8. ALP, COLL I, OCN, ONN, OPN and BMP-2 gene expression of rMSCs cultured on CDHA-S and β-TCP-S. Expression levels were determined by quantitative real time RT-PCR, normalised versus TCPS at 6 hours and displayed relative to their housekeeping gene. Bars represent mean ± SE of three experiments. * indicates significant difference between substrates at the same time point ($p < 0.05$). The patterned bars indicate the usage of osteogenic medium.

An increase in the ALP and collagen I gene expression was observed on CDHA-S at 6h compared to sintered β-TCP-S (1.78 ± 0.31 and 1.18 ± 0.12-fold upregulation,

respectively). However, the expression of both genes decreased progressively over time on both CDHA-S and β-TCP-S, more markedly for CDHA-S. The expression of late osteogenic markers *i.e.* ONN and OPN was similar on both CDHA-S and β-TCP-S at 6 h. However, CDHA-S showed an up-regulation of both ONN and OPN at 1 day. The relative expression level of ONN and OPN on CDHA-S compared to β-TCP-S was 2.15 ± 0.52 and 1.52 ± 0.44, respectively. Since no expression of OCN was detected at short- term cell culture on CDHA-S, the study was performed replacing basic cell culture medium for osteogenic medium after cell adhesion (6 h). The results for the expression of OCN were similar to those of ONN gene. Whereas at 6 h the expression levels of OCN were lower on CDHA-S than on β-TCP-S (*i.e.* 0.21 ± 0.17-fold lower), a 2.59 ± 1.02-fold up-regulation was observed at day 1 on CDHA-S compared to β-TCP-S. Finally, the expression levels of BMP-2 were higher for CDHA-S at all time points, and more markedly at 6h (3.92 ± 0.66-fold compared to β-TCP-S), although they decreased over time.

6.4 Discussion

Ionic exchange is believed to be one of the mechanisms that play a crucial role in the processes of bone regeneration induced by calcium phosphate biomaterials. Once implanted in the host bone, the degradation of CaPs, mostly mediated by the action of osteoclastic cells, result in the alteration of the ionic concentrations, mainly calcium and phosphate, in the surrounding extracellular fluids. It is generally accepted that both ions, either alone or simultaneously, foster the process of bone formation, by enhancing the activity of bone-forming cells, but also triggering the differentiation of mesenchymal stem cells to the osteogenic lineage.[9,10,27-29]

The extent of this ionic exchange depends on the intrinsic biomaterial properties. For instance, in the case of biomimetic calcium deficient hydroxyapatite, the deficiency in calcium, low crystallinity and SSA lead to a highly reactive material, which can be even more soluble than sintered β-TCP[30] and displays a high bioactivity and osteoinductive properties.[16] These features, which are highly beneficial in the *in vivo* scenario, may however introduce a high level of complexity when looking at the *in vitro* cell response to these materials. The interaction of CDHA with the cell culture medium can cause ionic exchanges that may be detrimental *in vitro*, where cells are cultured in a limited amount of medium, which is periodically renewed. Recently, we demonstrated that CDHA was cytotoxic for rMSCs. However, the specific mechanisms were unknown.[15]

The results obtained in the present study highlight that, unlike in other less reactive CaPs, the outcome of the *in vitro* cell response of biomimetic CDHA is strongly influenced by the ionic exchange with the surrounding medium, which in turn is dependent on cell culture conditions. Specifically, changing the volume ratio between cell culture medium and biomaterial from a low ratio (~5) to a high ratio (~300) allowed

to show separately the effect of the ionic concentration on the cells cultured on substrates with the same chemistry and topography. A significant effect of V_{CM}/V_B was revealed on the proliferation of rMSCs cultured on CDHA, while the differences were irrelevant for the cells cultured on β-TCP (Figure 6.2.A). This behaviour could be clearly correlated with the changes of Ca^{2+} content in the cell culture medium (Figure 6.2.B). The reduction in cell number on the CDHA-L should be attributed to the high decrease of extracellular Ca^{2+}, which was prevented increasing the V_{CM}/V_B, that is, choosing *in vitro* conditions that are closer to the physiological situation (Figure 6.2.B). In contrast, the values of Ca^{2+} and P_i for β-TCP discs remained similar to those of TCPS independently of sample dimensions. Despite β-TCP being more soluble than CDHA, its low SSA resulted in a smaller ionic exchange with the culture medium.[30] Accordingly, cell proliferation was not affected by the dimensions of the specimens (Figure 6.2.A). The still lower proliferation on CDHA-S compared to β-TCP and TCPS might be attributed to the surface chemistry or the topographical features of CDHA as previously reported.[15]

According to these results, a more appropriate evaluation of the cytotoxicity of highly reactive materials like high SSA CDHA should consider using larger cell culture medium volumes to attenuate the effects of strong ionic changes in the cell culture medium. However, this strategy would still have some drawbacks, as it would overlook the potential cytotoxicity associated to undesirable ions/components that could leach out in the case of materials containing toxic contaminants.

The values of calcium and phosphate concentration (Figure 6.2.B) must be analysed with care, since they represent average supernatant concentrations. The reactivity of the CaP triggers the uptake and release of ions by the material, this creating a gradient of ionic concentrations in the surrounding fluid. Therefore, in static conditions the local content of calcium and phosphate in the close proximity of the cells, that is, in the cell-material interphase, might differ from the average measured in the supernatant. ICP and FTIR analyses of the material after soaking in serum-free and cell-free culture conditions proved changes in the composition of CDHA without alteration of the plate-like microstructure. The ICP measurements showed an increase in the average Ca/P ratio, more pronounced in small than in large discs. This in fact indicates that the Ca/P changes are taking place progressively from the surface of the specimens, which is in contact with the cell culture medium. The smaller surface to volume ratio of the small discs explains the higher average Ca/P values in the small than in the large discs. ICP also revealed the incorporation of other ions from the cell culture medium such as Na and Mg. The increase of Ca/P would be consistent with the uptake of calcium from the solution and the maturation of CDHA ($Ca_9(HPO_4)(PO_4)_5OH$) to a more stoichiometric HA ($Ca_{10}(PO_4)6(OH)_2$), but also with carbonate incorporation. In fact, infrared spectroscopy performed in the surface of the samples proved the incorporation of

carbonate ions in B-type positions, which results in an increase of Ca/P since carbonate substitutes phosphate groups. One aspect worth noting is that Ca concentration begins to rise between 7 and 14 d of immersion of the CDHA-L discs (Figure 6.2.B), pointing that the effect of CDHA in the environment is being attenuated. The duration of this transient effect might depend on the conditions of the assay and could be shortened by renewing the medium more frequently.

To assess the repercussion of the culture conditions on the intracellular cytoplasmatic levels of calcium of rMCSs cultured on CDHA, the cells were incubated with Fluo-4, a common intracellular calcium indicator dye (Figure 6.4.) and analysed by flow cytometry.[31] The values of fluorescence per cell were normalized by the cell volume to discard differences in fluorescence associated to cell size. While the cells cultured on small discs (CDHA-S) experienced a notable increase in intracellular calcium, as observed by the higher median fluorescence value (61.87 ± 33.72 % higher than TCPS, Figure 6.4.B and 6.4.D), there were no significant changes in intracellular calcium for the cells cultured on large discs compared to the control cells. One could hypothesize that the extracellular calcium on CDHA-S in the vicinity of the cells, may cause an increased local concentration of calcium in the fluid nearby the CDHA surface, which, by the influx through voltage gated Ca^{2+} channels[32] could lead to the increase of cytosolic Ca^{2+} values detected in the case of CDHA-S. However, for CDHA-L, the lower extracellular calcium concentration did not seem to influence intracellular calcium concentration. This later finding was surprising as we were expecting in fact an efflux of Ca from the cells to counterbalance the lower calcium content in the culture medium.

Both, extra and intracellular calcium are known to play a major role in the regulation of a number of cellular and molecular interactions.[33-35] In particular, the extracellular Ca^{2+} regulates cell spreading by stabilizing integrin structure and modulating integrin-ligand binding.[36,37] For instance, the removal of divalent cations by EDTA (ethylenediaminetetraacetic acid) completely inhibits integrin-ligand binding.[34,38] Herein, we analysed the levels of pFAK as an indicator of the maturation of cellular adhesion complexes (Figure 6.7.). When FAK is phosphorylated, it activates downstream signalling pathways that regulate, thorough polymerization of the actin cytoskeleton, not only cell adhesion and spreading but also cell proliferation, motility and survival.[39] Cells on CDHA-L developed few actin stress fibers and low pFAK levels (Figures 6.7.A and 6.7.D), which can be associated to the decreased extracellular Ca^{2+}, which can be the cause of the dramatic decrease in the number of cells (Figure 6.5.E). Moreover, the reduction of rMSCs number on CDHA-L was accompanied with cell shrinkage (Figures 6.3.B and 6.7.D) and retraction of filopodia (Figures 6.3.A and 6.7.A). This may point to apoptotic condition of rMSCs where general rounding up of cells occurs.[34,40]

For CDHA-S, when the depletion of Ca^{2+} from the cell culture medium was prevented, higher pFAK levels (Figures 6.7.A and 6.7.D) and more extensive cell spreading (Figures 6.3.A and 6.3.B; 6.7.A and 6.7.B) were observed.

In agreement with the previous results, FACS analysis showed that the number of apoptotic cells was higher on CDHA-L (Figure 6.5.). Both immature focal adhesions and decreased intracellular/extracellular Ca^{2+} might be responsible of increased apoptosis on that condition[41], whereas on CDHA-S apoptosis levels were smaller. The involvement of the calcium ion on cellular fate has been extensively studied. For instance, most cell death pathways are triggered either through calcium signalling or through Ca^{2+} alterations at intracellular and extracellular level.[33] According to Zhivotovsky *et al.* the calcium ion regulates both necrosis and apoptosis processes.[34] Whilst necrosis occurs predominantly due to the overload of intracellular calcium, apoptosis can be triggered by more subtle changes. In this regard, apoptotic pathways can be induced either through alterations of calcium homeostasis in intracellular compartments or through Ca^{2+}-mobilised signals that activate apoptotic death effectors-mainly enzymes such as Caspases.[41] The reduced values of extracellular calcium might be one of the possible reasons causing the rMCSs apoptosis due to detachment from CDHA-L substrate (Figure 6.4.A). The FAK localization and phosphorylation in focal adhesions is required for generation of fibrillar adhesions and consequent organization of cell matrix and distribution of actin stress fibers.[42] Here, the little maturation of FAK on CDHA-L, in comparison to TCPS, is likely reflected into insufficient cell adhesion followed by their rounding up, detachment and finally death through apoptosis.

The increased cell survival on CDHA small discs allowed to compare its osteogenic potential with that of β-TCP (Figure 6.8.). Differentiation of rMSCs into the osteoblastic lineage was analysed by RT-qPCR. Alkaline phosphatase (ALP) and collagen I (COLL I) are markers commonly used to evaluate osteoblastic differentiation.[43] ALP expression was higher in CDHA-S compared to β-TCP-S at initial stages of cell culture, whereas COLL I was higher in β-TCP at 3 days. Osteocalcin (OCN), osteonectin (ONN) and osteopontin (OPN) are bone-specific extracellular proteins responsible of the size and quality of mineral growth as well as the regular formation of crystals.[44] Their expression was also higher on CDHA-S compared to β-TCP-S indicating a higher commitment to the osteoblastic lineage. High levels of BMP-2, a growth factor with essential roles in guiding MSCs differentiation and bone regeneration expression were observed also on CDHA-S.[45] Similar trends were observed in other studies on biomimetic calcium phosphates, suggesting a synergistic effect of surface chemistry and topography which fosters the osteogenic differentiation of osteoblasts[46,47] and MSC.[6] Moreover, in line with the increased intracellular calcium found in the cells cultured on CDHA-S, although intracellular calcium is thought to play a more significant role in osteoblast proliferation than in differentiation[32], some studies reported a correlation between

intracellular calcium and the expression of osteogenic genes in osteoblasts[32] and MSCs.[48] Specifically, Barradas *et al.* reported a strong involvement of Ca^{2+} internalization in the overexpression of osteogenesis-related genes, especially BMP-2, but also other calcium-responsive genes such as OPN and OCN.[11]

6.5 Conclusions

The results obtained in this chapter put forward the complexity of performing static cell culture studies on highly reactive materials such as biomimetic CDHA, due to the drastic ionic changes caused in the cell culture, associated to the continuous compositional changes that the apatitic material undergoes with incubation time. The strategy of increasing the medium/biomaterial volume ratio has proved successful in mitigating ionic exchanges and has allowed to decouple the contribution of topography from the material's reactivity on cells and has revealed the effect of ionic exchanges on rMSCs adhesion and proliferation, as well as cell morphology. Nevertheless, further studies are needed to better understand the interaction between the material and the fluid environment, being especially relevant the effect of the cell culture concentration gradients on cell response.

6.6 Bibliography

1. Galván-Chacón, V. P. & Habibovic, P. Deconvoluting the Bioactivity of Calcium Phosphate-Based Bone Graft Substitutes: Strategies to Understand the Role of Individual Material Properties. *Adv. Healthc. Mater.* **6**, 1–15 (2017).
2. Yuan, H. *et al.* A comparison of the osteoinductive potential of two calcium phosphate ceramics implanted intramuscularly in goats. *J. Mater. Sci. Mater. Med.* **13**, 1271–1275 (2002).
3. Wang, C. *et al.* Proliferation and bone-related gene expression of osteoblasts grown on hydroxyapatite ceramics sintered at different temperature. *Biomaterials* **25**, 2949–2956 (2004).
4. Muralithran, G. & Ramesh, S. The effects of sintering temperature on the properties of hydroxyapatite. *Ceram. Int.* **26**, 221–230 (2000).
5. Samavedi, S., Whittington, A. R. & Goldstein, A. S. Calcium phosphate ceramics in bone tissue engineering: a review of properties and their influence on cell behavior. *Acta Biomater.* **9**, 8037–45 (2013).
6. Danoux, C. *et al.* Development of Highly Functional Biomaterials by Decoupling and Recombining Material Properties. *Adv. Mater.* **28**, 1803–1808 (2016).
7. Vallet Regi, M. Calcium phosphates as substitution of bone tissues. *Prog. Solid State Chem.* **32**, 1–31 (2004).
8. LeGeros, R. Z. Calcium phosphate-based osteoinductive materials. *Chem. Rev.* **108**, 4742–53 (2008).
9. Barradas, A., Yuan, H., van Blitterswijk, C. & Habibovic, P. Osteoinductive biomaterials: current knowledge of properties, experimental models and biological mechanisms. *Eur. Cells Mater.* **21**, 407–429 (2011).
10. Danoux, C. B. S. S. *et al.* Elucidating the individual effects of calcium and phosphate ions on hMSCs by using composite materials. *Acta Biomater.* **17**, 1–15 (2015).
11. Barradas, A. M. C. *et al.* A calcium-induced signaling cascade leading to osteogenic differentiation of human bone marrow-derived mesenchymal stromal cells. *Biomaterials* **33**, 3205–15 (2012).
12. Gustavsson, J., Ginebra, M. P. P., Engel, E. & Planell, J. Ion reactivity of calcium-deficient hydroxyapatite in standard cell culture media. *Acta Biomater.* **7**, 4242–52 (2011).
13. Gustavsson, J., Ginebra, M. P., Planell, J. & Engel, E. Osteoblast-like cellular response to dynamic changes in the ionic extracellular environment produced by calcium-deficient hydroxyapatite. *J. Mater. Sci. Mater. Med.* **23**, 2509–20 (2012).
14. Klimek, K. *et al.* 'false' cytotoxicity of ions-adsorbing hydroxyapatite - Corrected method of cytotoxicity evaluation for ceramics of high specific surface area. *Mater. Sci. Eng. C* **65**, 70–79 (2016).
15. Sadowska, J.-M., Guillem-Marti, J., Montufar, E. B., Espanol, M. & Ginebra, M.-P. Biomimetic Versus Sintered Calcium Phosphates: The In Vitro Behavior of Osteoblasts and Mesenchymal Stem Cells. *Tissue Eng. Part A* **23**, 1297–1309 (2017).
16. Barba, A. *et al.* Osteoinduction by Foamed and 3D-Printed Calcium Phosphate Scaffolds: Effect of Nanostructure and Pore Architecture. *ACS Appl. Mater. Interfaces* **9**, 41722–41736 (2017).
17. Ginebra, M. P. *et al.* Setting Reaction and Hardening of an Apatitic Calcium Phosphate *Cement. J. Dent. Res.* **76**, 905–912 (1997).
18. Stern, J. & Lewis, W. H. P. The colorimetric estimation of calcium in serum with o-cresolphthalein complexone. *Clin. Chim. Acta* **2**, 576–580 (1957).
19. Gitelman, J. An Improved Automated Procedure of Calcium in Biological for the Determination Specimens. *Anal. Biochem.* **18**, 521–531 (1967).

20. Pfaffl, M. W. A new mathematical model for relative quantification in real-time RT-PCR. *Nucleic Acids Res.* **29**, 45e–45 (2001).
21. Fleet, M. E. Infrared spectra of carbonate apatites: ν2-Region bands. *Biomaterials* **30**, 1473–1481 (2009).
22. Murugan, R. & Ramakrishna, S. Production of ultra-fine bioresorbable carbonated hydroxyapatite. *Acta Biomater.* **2**, 201–206 (2006).
23. Bonfield, W. & Gibson, I. R. Novel synthesis and characterization of an AB-type carbonate-substituted hydroxyapatite. *J. Biomed. Mater. Res.* **59**, 697–708 (2002).
24. Padilla, S., Izquierdo-Barba, I. & Vallet-Regi, M. High specific surface area in nanometric carbonated hydroxyapatite. *Chem. Mater.* **20**, 5942–5944 (2008).
25. Vines, A., McBean, G. J. & Blanco-Fernandez, A. A flow-cytometric method for continuous measurement of intracellular Ca2+ concentration. *Cytom. Part A* **77**, 1091–1097 (2010).
26. Posey, A. D., Kawalekar, O. U. & June, C. H. Measurement of Intracellular Ions by Flow Cytometry. *Curr. Protoc. Cytom.* **72**, 9.8.1-9.8.21 (2015).
27. Yuan, H. *et al.* Osteoinductive ceramics as a synthetic alternative to autologous bone grafting. *Proc. Natl. Acad. Sci. U. S. A.* **107**, 13614–9 (2010).
28. Barradas, A. M. C. *et al.* The influence of genetic factors on the osteoinductive potential of calcium phosphate ceramics in mice. *Biomaterials* **33**, 5696–705 (2012).
29. Liu, Y. K. Y. K. *et al.* The effect of extracellular calcium and inorganic phosphate on the growth and osteogenic differentiation of mesenchymal stem cells in vitro: implication for bone tissue engineering. *Biomed. Mater.* **4**, 25004 (2009).
30. Diez-Escudero, A., Espanol, M., Beats, S. & Ginebra, M.-P. In vitro degradation of calcium phosphates: Effect of multiscale porosity, textural properties and composition. *Acta Biomater.* **60**, 81–92 (2017).
31. Gee, K. R. *et al.* Chemical and physiological characterization of fluo-4 Ca(2+)-indicator dyes. *Cell Calcium* **27**, 97–106 (2000).
32. Zayzafoon, M. Calcium/calmodulin signaling controls osteoblast growth and differentiation. *J. Cell. Biochem.* **97**, 56–70 (2006).
33. Berridge, M. J., Lipp, P. & Bootman, M. D. The versatility and universality of calcium signalling. *Nat. Rev. Mol. Cell Biol.* **1**, 11–21 (2000).
34. Zhivotovsky, B. & Orrenius, S. Calcium and cell death mechanisms: A perspective from the cell death community. *Cell Calcium* **50**, 211–221 (2011).
35. Sun, S., Liu, Y., Lipsky, S. & Cho, M. Physical manipulation of calcium oscillations facilitates osteodifferentiation of human mesenchymal stem cells. *FASEB J.* **21**, 1472–80 (2007).
36. Werth, D. K. & Pastan, I. Vinculin phosphorylation in response to calcium and phorbol esters in intact cells. *J. Biol. Chem.* **259**, 5264–5270 (1984).
37. Perez-Moreno, M., Avila, A., Islas, S., Sanchez, S. & González-Mariscal, L. Vinculin but not alpha-actinin is a target of PKC phosphorylation during junctional assembly induced by calcium. *J. Cell Sci.* **111** (Pt 2, 3563–71 (1998).
38. Sjaastad, M. D. & Nelson, W. J. Integrin-mediated calcium signaling and regulation of cell adhesion by intracellular calcium. *BioEssays* **19**, 47–55 (1997).
39. Parsons, J. T. Focal adhesion kinase: the first ten years. *J. Cell Sci.* **116**, 1409–1416 (2003).
40. Kroemer, G. *et al.* Classification of cell death: recommendations of the Nomenclature Committee on Cell Death 2009. *Cell Death Differ.* **16**, 3–11 (2009).
41. Orrenius, S., Zhivotovsky, B. & Nicotera, P. Calcium: Regulation of cell death: the calcium–apoptosis link. *Nat. Rev. Mol. Cell Biol.* **4**, 552–565 (2003).
42. Ilić, D. *et al.* FAK promotes organization of fibronectin matrix and fibrillar adhesions. *J. Cell Sci.* **117**, 177–187 (2004).

43. Golub, E. E., Harrison, G., Taylor, a G., Camper, S. & Shapiro, I. M. The role of alkaline phosphatase in cartilage mineralization. *Bone Miner.* **17**, 273–278 (1992).
44. Roach, H. I. Why does bone matrix contain non-collagenous proteins? The possible roles of osteocalcin, osteonectin, osteopontin and bone sialoprotein in bone mineralisation and resorption. *Cell biology international* **18**, 617–628 (1994).
45. Rosen, V. BMP2 signaling in bone development and repair. *Cytokine Growth Factor Rev.* **20**, 475–480 (2009).
46. Shu, R., McMullen, R., Baumann, M. J. & McCabe, L. R. Hydroxyapatite accelerates differentiation and suppresses growth of MC3T3-E1 osteoblasts. *J. Biomed. Mater. Res. A* **67**, 1196–1204 (2003).
47. Sethuraman, S. *et al.* Novel low temperature setting nanocrystalline calcium phosphate cements for bone repair: Osteoblast cellular response and gene expression studies. *J. Biomed. Mater. Res. Part A* **82A**, 884–891 (2007).
48. Petecchia, L. *et al.* Electro-magnetic field promotes osteogenic differentiation of BM-hMSCs through a selective action on Ca2+ -related mechanisms. *Sci. Rep.* **5**, 1–13 (2015).

6.7 Supplementary information

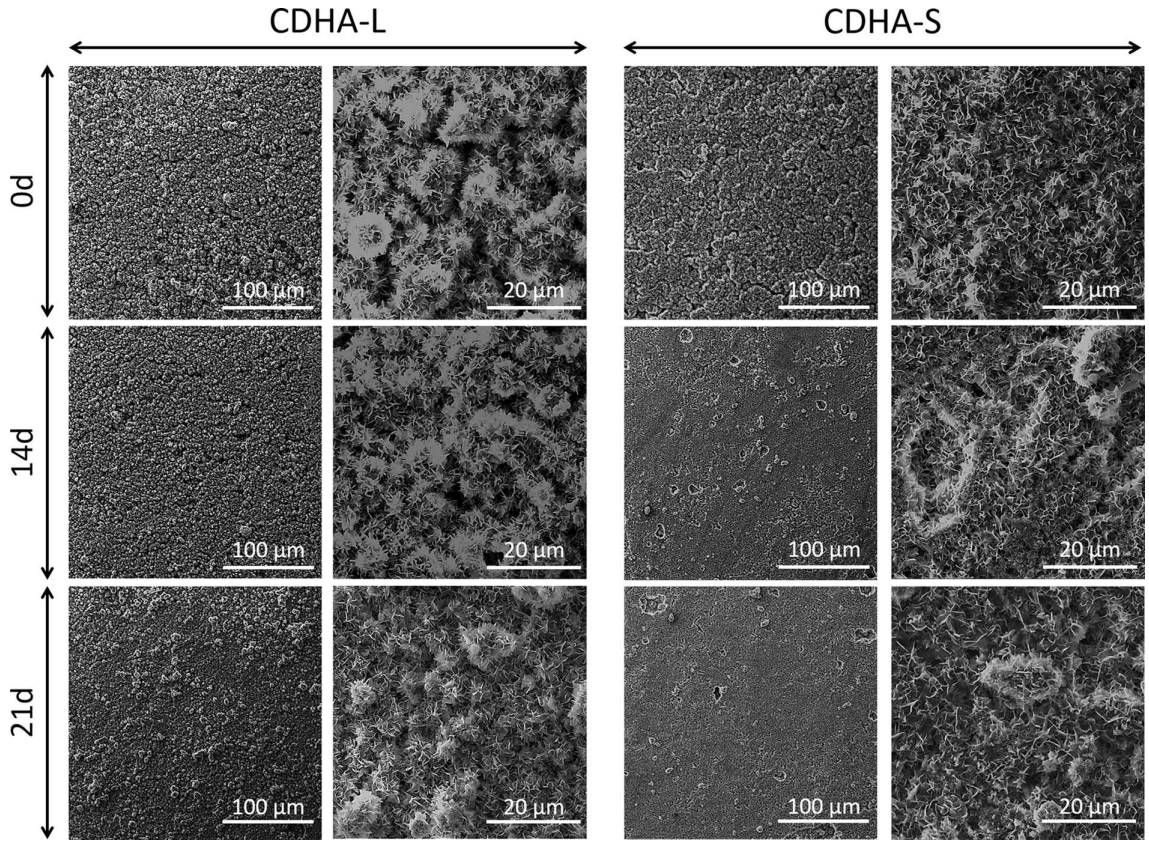

Supplementary Figure 6.1. The effect of cell culture medium on surface topography of CDHA. The evaluation was performed without presence of cells in culture medium. The samples were incubated with FBS- free advDMEM. After exposure to culture medium, the surface of CDHA-L and CDHA-S was observed through SEM. The substrates exposed to cell culture medium for 14 and 21 days exhibited similar plate- like morphology compared to pristine CDHA.

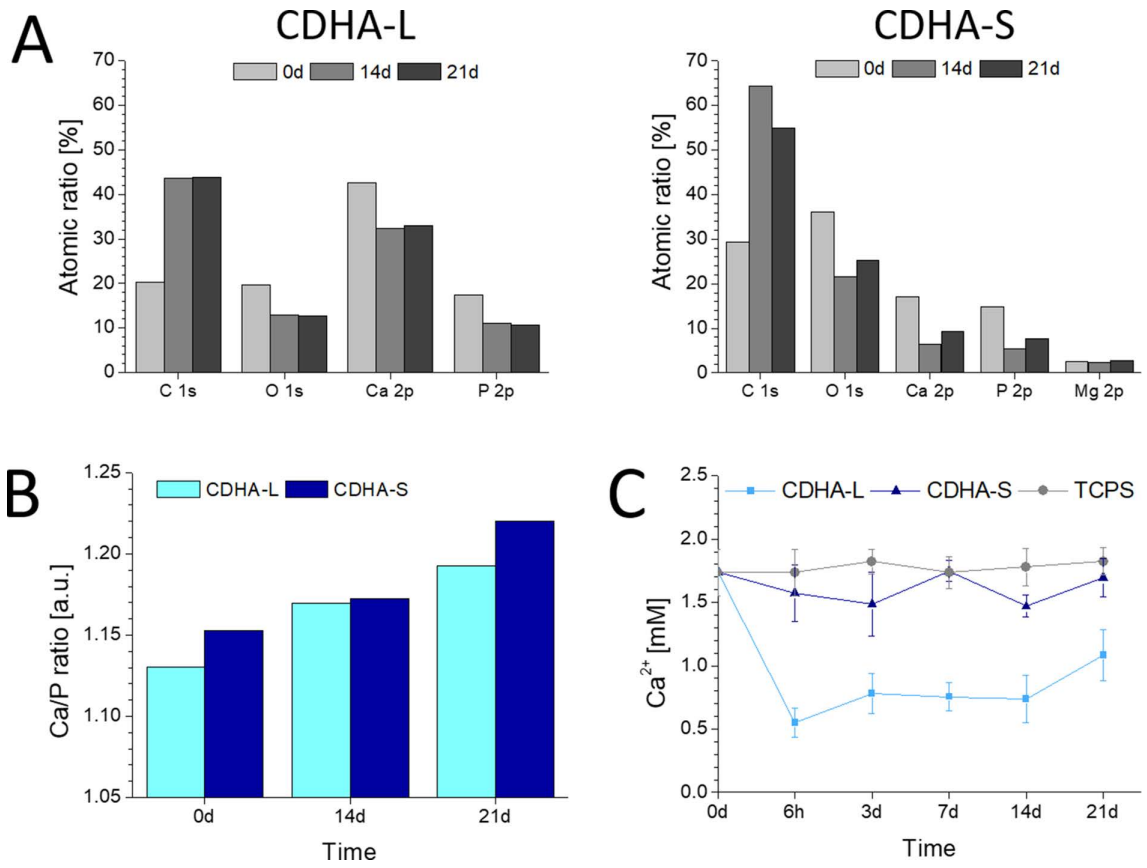

Supplementary Figure 6.2. The effect of cell culture medium on surface composition of CDHA. The evaluation was performed without presence of cells in culture medium. The samples were incubated with FBS- free advDMEM. The surface chemistry of CDHA-L and CDHA-S was determined through X-ray photoelectron spectroscopy (XPS). The spectra were acquired in ultrahigh vacuum (5×10^{-9} mbar) with an XR50 Mg anode source operating at 150 W and a Phoibos 150 MCD-9 detector (D8 advance, SPECS Surface Nano Analysis GmbH, Germany). The spectra for C 1s, O 1s, Ca 2p, P 2p and Mg 2p were recorded at pass energy of 25 eV with step size of 0.1 eV. The CasaXPS software (Casa Software Ltd, UK) was used for the determination of atomic elemental composition using C 1s peak as a reference. **A)** XPS spectra of CDHA-L (left) and CDHA-S (right) after 0, 14 and 21 days of incubation with cell culture media. **B)** The superficial Ca/P ratio of CDHA-L and CDHA-S discs after 0, 14 and 21 days of incubation with culture media. The superficial Ca/P ratio of CDHA-L and CDHA-A increased after exposure to cell culture media. **C)** Concentration of Ca^{2+} in the supernatants at 6 hours, 3, 7 and 14 and 21 day evaluated through o-cresolphthalein complexone method. The CDHA-S maintained similar calcium levels to those observed in TCPS. The depletion of Ca^{2+} for CDHA-L substrate was more pronounced in FBS-free advDMEM than the decrease of calcium observed for CDHA-L incubated with cells and complete advDMEM (Figure 6.2.B).

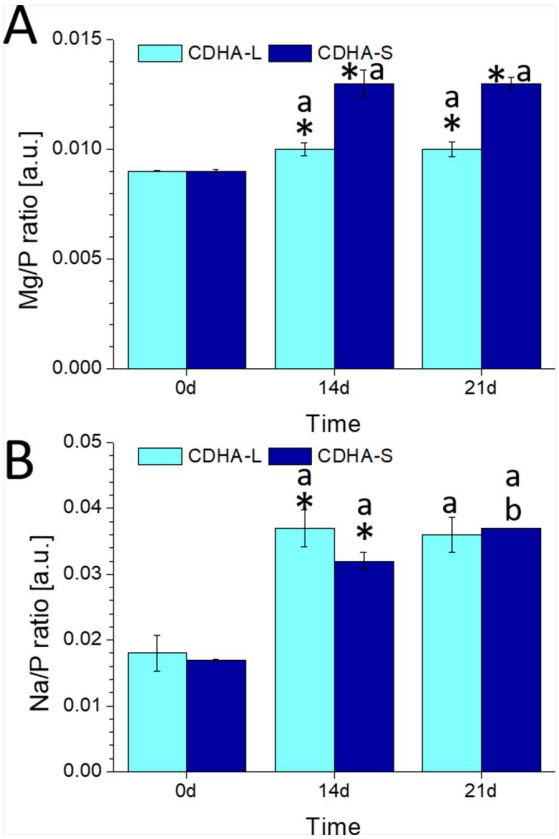

Supplementary Figure 3. The Mg/P ratio **(A)** and Na/P ratio **(B)** of CDHA-L and CDHA-S discs after 0, 14 and 21 days of incubation with culture media evaluated through ICP-MS. The evaluation was performed without presence of cells in culture medium. The samples were incubated with FBS-free advDMEM. The incubation with cell culture medium led to an increase of the Mg/P and Na/P ratio for both CDHA-L and CDHA-S. Overall, CDHA substrates showed similar Mg/P and Na/P ratios at 14 and 21 day of incubation except for CDHA-S where Na/P ratio increased between 14 and 21 day. * indicates significant differences ($p < 0.05$) between CDHA-L and CDHA-S at each time point. Letters (a,b) identify differences ($p < 0.05$) between the time points within the same sample.

Chapter 7

General conclusions and future perspectives

GENERAL CONCLUSIONS

Chapter 2: Effect of nano and microstructural properties of biomimetic hydroxyapatite on osteoimmunomodulation

- The immune response of murine RAW 264.7 macrophages cultured on biomimetic CDHA substrates was guided by combined effects of surface topography, porosity and ionic exchange. The expression of pro- and anti-inflammatory cytokines cannot be directly linked to the surface topography or porosity of substrate.
- The presence of multinucleated RAW cells, the higher values of calcium concentration in the cell culture medium in presence of the cells and the visualisation of degraded crystals of CDHA in the material-cell interphase confirmed osteoclastic-like activity of macrophages on CDHA substrates.
- The results showed that the interaction of macrophages with needle-like CDHA with low L/P ratio created the osteoimmune environment that stimulated osteogenic differentiation of osteoblast-like SaOS-2 cells, resulting in enhanced expression of osteogenic markers (COLL I, BMP-2, BSP) and protein secretion (Runx2, ALP).
- The evaluation of macrophage behaviour under inflammatory conditions revealed that porosity is a key factor in modulating anti-inflammatory potential of CDHA. Overall, CDHA with low L/P ratio decreased the pro-inflammatory gene expression and cytokine release to greater extent than their high L/P counterparts which had the same surface structure but larger porosity.

Chapter 3: The impact of chemistry and surface topography of calcium phosphates on macrophage response under inflammatory environment: osteoimmunomodulatory implications

- The *in vitro* culture of murine RAW 264.7 macrophages under inflammatory environment revealed the anti-inflammatory effect of CaPs, more pronounced for sintered β-TCP than for biomimetic CDHA. The incubation with β-TCP resulted in greater reduction of expression of pro-inflammatory molecules such as IL-1β, IL-6, TNFα and iNOS compared to CDHA.
- Due to the short time of cell culture, there were little signs of osteoclastic-like behaviour of RAW cells on CaPs substrates.
- The interaction of macrophages with CDHA led to the release of inflammatory, osteogenic/osteoclastogenic molecules from RAW which created more favourable osteoimmune environment that stimulated osteogenic differentiation of bone cells.
- BMSCs were more sensitive to changes in the osteoimmune milieu than osteoblast-like SaOS-2 cells, showing a clear upregulation of osteogenic genes

(Runx2, ALP, COLL I, BSP, OCN, BMP-2) when incubated with RAW-CDHA extracts. In contrast, the impact of the osteoimmune environment on SaOS-2 osteogenic differentiation was mainly observed in protein secretion (COLL I, Runx2 and ALP).

Chapter 4: The influence of physicochemical properties of biomimetic hydroxyapatite on endothelial progenitor cells and their interaction with mesenchymal stem cells *in vitro*

- The monocultures of EPCs and MSCs, as well as the coculture of EPCs:MSCs on CaPs showed different proliferative behaviour. The cellular proliferation was more affected for the monocultured MSCs and EPCs:MSCs coculture than for EPCs. This was associated to the higher ionic exchange from CaP substrates, especially highly reactive biomimetic CDHA. In case of β-TCP, where little ionic exchange were observed, the coculturing of ECPs and MSCs foster the proliferation rate of MSCs compared to MCSs cultured alone.
- In general, EPCs presented little proliferative potential in coculture what was demonstrated through reduced number of PECAM-1 positively stained cells. This scenario was likely induced through two different parameters. In case of CDHA, the increased release of phosphate might have contributed to apoptosis of EPCs. In case of β-TCP the enhanced proliferation rate of MSCs in coculture might have curtailed the ability of grow of EPCs.
- A high upregulation of the angiogenic genes was observed when EPCs were cultured on needle-like CDHA substrates, in contrast to plate-like CDHA or β-TCP. Similar PECAM-1 secretion was observed for all CaP substrates.
- The cellular crosstalk between EPCs and MSCs on CaP substrates was not reflected in enhanced production of gap junctional protein but through the upregulation of osteogenesis- related genes. This behaviour was mainly observed when cells were cocultured on needle- like CDHA. From various osteogenesis inducers i.e. BMP-2, EDH 1 or DJ 1 only upregulation of DJ 1 was observed in coculture condition on needle- like CDHA what might suggest the involvement of DJ 1 in stimulating osteogenic gene expression.

Chapter 5: Biomimetic versus sintered calcium phosphates: the *in vitro* behaviour of osteoblasts and mesenchymal stem cells

- The chemical composition as well as textural properties of CaPs strongly affected their reactivity with cell culture media. The ionic exchange was more pronounced for CDHA compared to sintered ceramics due to its low crystallinity and high SSA.
- The cellular response of rMSCs and SaOS-2 cells in terms of proliferation and differentiation depended on three main factors: the physicochemical features of

CaPs, the microenvironment created due to the immersion of CaPs in cell culture media and the cell type.

- The usage of glass coverslips for indirect cell cultures was an effective and simple method to evaluate separately the effect of ionic fluctuations and the topography of CaPs substrates.
- The MSCs were more prone to microenvironmental ionic fluctuations in terms of undergo apoptosis compared to SaOS-2 cells.
- The direct contact with CaPs was found to be a key factor for osteogenic differentiation of both rMSCs and SaOS-2 cells.
- The modification of the ionic concentration of the cell culture medium caused by the immersion of highly reactive CaPs in a limited volume of liquid is far from representing the *in vivo* situation. Thus the need of being cautious when interpreting the *in vitro* results obtained.

Chapter 6: *In vitro* response of mesenchymal stem cells to biomimetic hydroxyapatite substrates: a new strategy to assess the effect of ion exchange

- The volume ratio between cell culture medium and biomaterial (V_{CM}/V_B) is a critical parameter that affects the response of rMSCs to highly reactive CaPs. Whereas in sintered β-TCP the cell response was not affected by changing the V_{CM}/V_B, a significant effect on cell adhesion, proliferation and viability was found for the more reactive CDHA.
- The ionic fluctuations, produced by CDHA at low V_{CM}/V_B led to reduced number of focal adhesions and cell shrinkage, leading to MCSs apoptosis. These effects were mitigated at high V_{CM}/V_B, where the calcium and phosphate fluctuations in the cell culture medium were significantly reduced, resulting in MSCs spreading and a viability over time.
- The immersion of CDHA in cell culture medium led to compositional changes of the substrate over time, like the incorporation of carbonate, magnesium and sodium ions.
- MSCs showed an earlier expression of osteogenic genes *i.e.* ALP, BMP-2 and OPN on CDHA compared to sintered β-TCP suggesting greater osteogenic potential of biomimetic CDHA.

FUTURE PERSPECTIVES

The present thesis shed light on the influence of physicochemical properties of biomimetic CDHA and sintered calcium phosphates on the behaviour of cells involved in the bone healing process. The results demonstrated that the modulation of chemical and textural features of CaPs is an interesting tool for designing smart biomaterials that trigger specific cellular responses (**Chapter 2-5**). Moreover, the thesis suggests awareness on cautious evaluation of highly reactive CaPs as the fluid-mediated effects might have crucial impact on cellular behaviour (**Chapter 6**).

Considering the results obtained concerning the osteoimmunomodulatory effects of CaPs (**Chapter 2** and **Chapter 3**) it might be interesting to evaluate in greater depth the signalling pathways involved in the activation of osteogenesis. For instance, the expression and secretion of SMAD proteins from bone forming cells that are exposed to macrophage-CaPs extracts is an interesting pathway that should be explored. Moreover, the osteoclastic-like behaviour of macrophages cultured on CDHA substrates observed in the present thesis requires further investigation. For instance, cell cultures should be performed over longer time periods in order to monitor the resorption activity of immune cells on CDHA substrate. The other characteristics of osteoclastic-like behaviour of immune cells should be cautiously studied like secretion of TRAP or integrins typical for mature osteoclasts such as $\alpha 2\beta 1$ or $\alpha V\beta 3$. Finally, since bone forming cells are recognised to actively participate in osteoclastogenesis, the expression of osteoclastic factors involved in RANKL/RANK/OPG pathway from mesenchymal or osteoclastic cells exposed to macrophage-CaPs extracts should be also evaluated.

Regarding the angiogenic properties of biomimetic hydroxyapatite (**Chapter 4**), it would be interesting to study the capillary-like structure formation from ECs by performing experiments on three-dimensional samples like macroporous foams or 3D-printed scaffolds. Alternatively, an analysis of a wider range of factors involved in endothelization, like adhesion molecules (Intercellular adhesion molecule; ICAM-1, vascular adhesion molecule; VCAM-1) or pro-thrombogenic (von Willebrand Factor; vWF) and anti-trombogenic (Endothelial Nitric oxide-synthetase; eNOS, Plasminogen activator; tPA) might provide new insights on the angiogenic effects of CDHA.

Regarding the fluid-mediated effects on cellular response discussed in **Chapter 6**, dynamic cell culture conditions should be performed in order to attenuate the high reactivity of CDHA and to mimic to a greater extent the conditions encountered *in vivo*.

ANNEX I

Glossary of terms

Glossary of terms

Full name	Abbreviaiton	Description
Amorphous calcium phosphate	ACP	Low temperature calcium phosphate with chemical formula $Ca_3(P0_4)_2 \cdot nH_2O$ (n = 3-4.5; 15-20 % H_2O) and Ca/P ratio ranging from ~1.18 to ~1.53; frequently a transient phase during formation of other calcium phosphates on aqueous environment; similar in composition to precipitated hydroxyapatite.
Alkaline phosphatase	ALP	Enzyme; an early marker of osteogenic differentiation. Being byproduct of osteoblast activity increases local concentration of phosphate ions initiating mineral growth
Alpha- tricalcium phosphate	α-TCP	High temperature calcium phosphate with chemical formula α-$Ca_3(PO_4)_2$ and Ca/P ratio ~1.50; obtained by thermal treatment above ~1125ºC; starting material for precipitation of calcium deficient hydroxyapatite.
Biphasic calcium phosphates	BCP	Ceramic derived from mixture of two calcium phosphates usually β-TCP + HA or α-TCP + HA.
Bioglass	BG	Biomaterial that usually contains in its matrix silica, calcium and phosphate elements; due to its biocompatibility frequently used in bone grafting.
Bone morphogenic protein 2	BMP-2	Growth factor; chemoattractant for neighbouring endothelial cells; secreted by immature osteoblasts; may trigger a variety of autocrine/paracrine pathways; potent effector in stimulating osteogenic differentiation.
Bone morphogenic protein 4	BMP-4	Growth factor; secreted, among others, by osteoblasts and endothelial cells; fulfil similar functions to BMP-2 regulating processes of differentiation of mesenchymal stem cells during osteogenesis; affects endothelial cell proliferation and blood vessel formation.
Bone morphogenic protein 7	BMP-7	Growth factor; regulates bone and cartilage development.
Bone marrow stromal cells	BMSCs	Progenitor cells of skeletal tissue; posses multi lineage differentiation potential, among others they can differentiate into osteoblasts, chondrocytes or adipocytes.
Basic molecular unit	BMU	A temporary anatomic structure accomplished by assembly of osteoblastic and osteoclastic cells during bone remodelling process.
Bone sialoprotien	BSP	ECM protein; Binds to Ca^{2+} via free hydroxyl groups and promotes nucleation of mineral.
Beta- tricalcium phosphate	β-TCP	High temperature calcium phosphate with chemical formula β-$Ca_3(PO_4)_2$ and Ca/P ratio ~1.50; obtained through heating treatment above ~650 ºC; frequently used as a bone graft either pure or combined with hydroxyapatite forming biphasic calcium phosphate.
Calcium phosphates	CaPs	Chemical compounds typically occurred in nature and human body with chemical formula containing calcium, phosphate and oxygen ions.

C-C chemokine receptor type 7	CCR7	Marker of pro-inflammatory macrophage M1 phenotype; induces chemotaxis of M1 and M2 macrogphages.
Calcium-deficient hydroxyapatite	CDHA	Low temperature calcium phosphate with chemical formula $Ca_{10-x}(HPO_4)_x(PO_4)_{6-x}(OH)_{2-x}$ ($0 < x < 1$) with Ca/P ratio from ~1.50 to < 1.67.
Integrin subunit alpha X	CD11c (ITGAX)	Transmembrane glycoprotein of pro-inflammatory macrophage M1 phenotype; participates in phagocytosis.
Cluster of differentiation 163	CD163	Plasma membrane glycoprotein scavenger receptor; anti-inflammatory M2 phenotype-specific.
Cluster of differentiation 206	CD206	Plasma membrane mannose scavenger receptor; anti-inflammatory M2 phenotype-specific.
Collagen type I	COLL I	Extracellular matrix protein; an early marker of osteoblastic differentiation; serves as a supportive material for mineral nucleation.
Calcium phosphate cements	CPC	Self-setting grafting material obtained through mixing liquid phase with solid phase composed of calcium orthophosphate; their end product is either apatite or brushite depending of pH conditions.
Dicalcium phosphate dehydrate	DCPD	Low temperature calcium phosphate with chemical formula $CaHPO_4 \cdot 2H2O$ and C/P ratio 1.00; known as brushite; crystallized at pH below 6.5; metastable- converts to other calcium phosphates.
Dicalcium phosphate anhydrous	DCPA	Low temperature calcium phosphate with chemical formula $CaHPO_4$ and C/P ratio 1.00; known as monetite; frequently used as a solid phase of calcium phosphate cements.
Endothelial cells	ECs	Cells from endothelium- a selectively permeable barrier between blood and the rest of the body; involved in formation and development of bone vessels.
Extracellular matrix	ECM	Self-assembled complex of macromolecules secreted by cells; mainly composed of collagen, non-collagenous proteins, proteoglycans and hyaluronan.
Endothelin 1	EDH 1	Endothelium derived factor; participate in angiogenesis and osteogenesis through paracrine/autocrine signalling.
Endothelial progenitor cells	EPCs	Bone marrow- derived cells that are recruited to peripheral blood system; participate in blood vessel formation either through activation of endothelial cells or through differentiation into endothelial cells and subsequent integration to blood vessel.
Fibroblast growth factor	FGF	Potent angiogenic inducer; stimulate migration and proliferation of endothelial cells.
Fibronectin	FN	Glycoprotein; component of extracellular matrix; participates in wide range of cell interaction among others cell adhesion and migration.
Hydroxyapatite	HA	Calcium phosphate with chemical formula $Ca_{10}(PO_4)_6(OH)_2$ obtained either at high temperature through solid-state reaction or at low temperature through precipitation (so called: precipitated hydroxyapatite; pHA); principal component of mineral phase of bone.

Human fibroblasts	HF	Main cells of connective tissue; primary source of extracellular matrix proteins and collagen with critical role in inflammatory stage of wound healing process.
Hypoxia inducible factors	HIFs	Transcription factors; activated through decrease of oxygen in cellular environment; involved in angiogenesis and osteogenesis processes.
Human umbilical vein endothelial cell	HUVEC	Cell line derived from the endothelium of umbilical cord; laboratory model of endothelial cells.
Interferon gamma	IFNγ	Pro-inflammatory cytokine; might inhibit the proliferation and osteogenic differentiation of mesenchymal stem cells.
Insulin-like growth factors	IGF	Protein with similar sequence to insulin; in bone environment acts as a potent mitogen.
Interleukin 1 beta	IL-1β	Pro-inflammatory cytokine; Inhibits osteogenic differentiation of mesenchymal cell through downregulation of early osteogenic genes.
Interleukin 4	IL-4	Ani-inflammatory cytokine; stimulus for macrophages polarization into M2; involved in macrophages fusion and subsequent formation of foreign body giant cells.
Interleukin 6	IL-6	Pro-inflammatory cytokine; involved in osteoclastogenesis; stimulates formation of osteoclastic precursors.
Interleukin 10	IL-10	Ani-inflammatory cytokine; in bone biology acts as an inhibitor of osteoclastogenesis stimulating osteoblasts' activity.
Interleukin 13	IL-13	Ani-inflammatory cytokine; stimulus for macrophages polarization into M2 phenotype; supresses tumour necrosis factor alpha.
Interleukin 23	IL-23	Pro-inflammatory cytokine; involved in osteoclastogenesis via stimulation of RANKL expression; activate immune cells to release other cytokines such as interleukin 1 or tumour necrosis factor alpha.
Lipopolysaccharide	LPS	Endotoxin found in outer membrane of gram- negative bacteria; in laboratory conditions used to activate macrophages into pro-inflammatory M1 phenotype.
Non-collagenous proteins	NCP	Fraction of extracellular matrix; in bone tissue they are products of osteoblastic cells, the major ones are: osteocalcin, osteonectin, osteopontin and bone sialoprotein.
Macrophage-colony stimulating factor	M-CSF	Inflammatory cytokine; involved in osteoclastogenesis; together with RANKL stimulates the maturation of osteoclastic precursors.
Monocalcium phosphate anhydrous	MCPA	High temperature calcium phosphate with chemical formula $Ca(H_2PO_4)_2$ and Ca/P ratio 0.5; obtained through thermal treatment above 100^{o}C; rarely used in bone regeneration.
Monocalcium phosphate monohydrate	MCPM	Low temperature calcium phosphate with chemical formula $Ca(H_2PO_4)_2 \cdot H_2O$ and Ca/P ratio 0.5; non biocompatible with bone as a pure phase; as biomaterial for bone regeneration- used in combination with other calcium phosphate or as a component of calcium phosphate cements.
	MG63	Cell line derived from human osteosarcoma; laboratory model of osteoblastic cells.

Mesenchymal stem cells	MSCs	Cells with capacity to self-renewal and capacity to differentiate into various cell types; can be isolated from various tissues, among others: umbilical cord, adipose tissue or bone marrow (so called: BMSCs).
Osteocalcin	OCN	ECM protein; regulates mineral growth, direction, size and quantity during late stages of differentiation. Considered to be late indicator of osteogenic differentiation.
Octacalcium phosphate	OCP	Low temperature calcium phosphate with chemical formula $Ca_8H_2(PO_4)_6 \cdot 5H_2O$ and Ca/P ratio 1.33; metastable phase during precipitation of hydroxyapatite.
Osteonectin	ONN	ECM protein; Regulates mineral growth, direction, size and quantity during late stages of differentiation. Considered to be late indicator of osteogenic differentiation.
Oncostatin M	OSM	An inflammatory cytokine; Regulator of osteoclastogenesis and osteogenesis.
Osteoprotegerin	OPG	An inhibitor of osteoclastogenesis; Serves as a decoy receptor for RANKL.
Osteopontin	OPN	Extracellular matrix protein; inhibits irregular formation of mineral crystals.
Osterix	Osx	Transcription factor; Acts downstream of Runx2 and promotes osteogenesis, while inhibiting chondrogenesis.
Platelet- derived growth factor	PDGF	Pro-angiogenic growth factor; Chemoattractant and mitogenic stimulation for endothelial cells and osteoblasts.
Platelet and endothelial cell adhesion molecule 1	PECAM-1	Transmembrane protein expressed in platelets, endothelial cells, monocytes and neutrophils; involved in cell migration and regulation of permeability of endothelium.
Precipitated hydroxyapatite	pHA	Low temperature calcium phosphate with chemical formula $Ca_{10-x}(HPO_4)_x (PO_4)_{6-x}(OH)_{2-x}$ with Ca/P ratio ranging from ~1.50 to 1.67; in contrast to stoichiometric hydroxyapatite is poorly crystalline.
Polylactic acid	PLA	Biodegradable and bioactive polymer; used, among others, for bone grafting.
Polymorphonuclear leukocytes	PMNs	Type of white blood cells; actively participate on inflammatory stage of bone healing process.
Parathyroid hormone	PTH	Hormone involved in osteoblastogenesis and osteoclastogenesis.
Receptor activator of nuclear factor kappa-B	RANK	Receptor of RANKL; involved in osteoclastogenesis through RANK/RANKL/OPG signalling pathway.
Receptor activator of nuclear factor kappa-B ligand	RANKL	An osteoclastogenic factor; Binds to RANK and enhances osteoclastogenesis through activator protein (AP-1) and nuclear factor of activated T cells 2 (NFAT2) signalling.
Reactive oxygen species	ROS	By-product of cellular metabolism; generated mainly in mitochondria.

Runt-related transcription factor 2	Runx2	Transcription factor; Involved in the differentiation of MSCs into immature osteoblasts.
	SaOS-2	Cell line derived from human osteosarcoma; laboratory model of osteoblastic cells.
Specific surface area	SSA	Total area of material per unit of mass.
Transforming growth factor beta	TGF-β	Inflammatory cytokine; presents three isoforms TGF-β1, TGF-β2, TGF-β3; fibrous agent; expressed, among others, by M2 in response to prolonged pathological inflammation.
Transforming growth factor beta 1	TGF-β1	Inflammatory cytokine; isoform of TGF-β; fibrous agent; expressed, among others, by M2 in response to prolonged pathological inflammation; modulate the expression of interferon gamma and tumour necrosis factor alpha.
Transforming growth factor beta 3	TGF-β3	Inflammatory cytokine; isoform of TGF-β; fibrous agent; expressed, among others, by M2 in response to prolonged pathological inflammation; involved in embryogenesis, cell differentiation and wound healing process.
Tumour necrosis factor alpha	TNFα	Pro-inflammatory cytokine; expressed by M1 macrophages; involved in osteogenesis through stimulation of alkaline phosphatase activity and mineralization of mesenchymal stem cells.
Tetracalcium phosphate	TTCP	High temperature calcium phosphate with chemical formula $Ca_4(PO_4)_2O$ and Ca/P ratio 2.0; obtained through solid-state reaction at 1400^{o}C; solid component of several calcium phosphate cements.
Vascular endothelial growth factor	VEGF	Pro-angiogenic growth factor; critical for survival of endothelial cells.
Vascular endothelial growth factor receptor 1	VEGFR-1	Transmembrane binding site for VEGF; also known as receptor tyrosine kinase.
Vascular endothelial growth factor receptor 2	VEGFR-2	Transmembrane binding site for VEGF; also known as kinase domain region; the main mediator of mitogenic and angiogenic stimulatory effect of VEGF.

ANNEX II

Publications, conference contributions, scholarships and awards

Publications

Barba, A., Diez-Escudero A., Maazouz Y., Rappe K., Espanol M., Montufar E.B., Bonany M., **Sadowska J.M.**, Guillem-Marti J., Öhman-Mägi C., Persson C., Manzanares M.C., Franch J., Ginebra M.P., Osteoinduction by Foamed and 3D-Printed Calcium Phosphate Scaffolds: Effect of Nanostructure and Pore Architecture. *ACS Appl. Mater. Interfaces* **9**, 41722–41736 (2017).

Sadowska, J.-M., Guillem-Marti, J., Montufar, E. B., Espanol, M. & Ginebra, M.-P. Biomimetic Versus Sintered Calcium Phosphates: The In Vitro Behavior of Osteoblasts and Mesenchymal Stem Cells. *Tissue Eng. Part A* **23**, 1297–1309 (2017).

Sadowska J.M., Guillem-Marti J., Espanol M., Stähli C., Döbelin N., Ginebra M.P., *In vitro* response of mesenchymal stem cells to biomimetic hydroxyapatite substrates: a new strategy to assess the effect of ion exchange. (submitted)

Sadowska J.M., Wei F., Guo J., Guillem-Marti J, Ginebra M.P., Xiao Y., Effect of nano-structural properties of biomimetic hydroxyapatite on osteoimmunomodulation. (submitted)

Sadowska J.M., Guillem-Marti J, Ginebra M.P., The influence of physicochemical cues of biomimetic hydroxyapatite on endothelial progenitor cells behavior and their interaction with mesenchymal stem cells in vitro. (under preparation)

Sadowska J.M., Wei F., Guo J., Guillem-Marti J, Ginebra M.P., Xiao Y., The influence of chemistry and surface topography of calcium phosphates on macrophage response under inflammatory environment. (under preparation)

Conference contributions

Sadowska J.M., Wei F., Guo J., Guillem-Marti J., Ginebra M.P., Xiao Y., *Modulation of microstructural features of calcium phosphates for triggering specific osteoimmune response*, 29th European Conference on Biomaterials ESB2018, Maastricht, Netherlands, 9-13th September 2018, Poster presentation

Sadowska J.M., Guillem-Marti J., Ginebra M.P., *Interaction between endothelial progenitor cells and mesenchymal stem cells cultured on biomimetic hydroxyapatite*, 29th Symposium and Annual Meeting of the International Society for Ceramics in Medicine Bioceramics27, Toulouse, France, 25-27th October 2017, Poster presentation

Sadowska J.M., Guillem-Marti J., Ginebra M.P., *Ionic exchanges modulate the in vitro response of mesenchymal stem cells to biomimetic hydroxyapatite*, Tissue Engineering and Regenerative Medicine International Society Meeting TERMIS EU 2016, Uppsala, Sweden, 28th June – 1st July 2016, Poster presentation

Sadowska J.M., Guillem-Marti J., Ginebra M.P., *Effect of physicochemical features of biomimetic hydroxyapatite on endothelial cell behaviour*, Tissue Engineering and Regenerative Medicine International Society Meeting TERMIS EU 2016, Uppsala, Sweden, 28th June – 1st July 2016, Poster presentation

Sadowska J.M., Guillem-Marti J., Ginebra M.P, *La reactividad de fosfatos de calcio en medio de cultivo: el efecto iónico sobre la respuesta celular in vitro*, XXXVIII Congreso de la Sociedad Ibérica de Biomecánica y Biomateriales, SIBB2015, Barcelona, Spain, 6-7th November 2015, Oral presentation

Sadowska J.M., Guillem-Marti J., Ginebra M.P., *In vitro performance of biomimetic hydroxyapatite: unravelling the effect of ionic exchange*, 27th European Conference on Biomaterials ESB2015, Krakow, Poland, 30th August - 3rd September 2015, Poster presentation

Sadowska J.M., Guillem-Marti J., Ginebra M.P., *Interaction of biomimetic ceramics with cell culture medium: effect on in vitro cell response*, 27th Symposium and Annual Meeting of the International Society for Ceramics in Medicine Bioceramics27, Bali, Indonesia, 27-29th October 2015, Oral communication.

Sadowska J., Montufar E., Guillem-Marti J., Espanol M, Ginebra M.P., *Cell behavior of biomimetic versus sintered calcium phosphates*, Tissue Engineering and Regenerative Medicine International Society Meeting TERMIS EU 2014, Genova, Italy, 10-13th June 2014, Oral communication

Scholarships and awards

Winner of the UPC institutional final of the contest “Thesis in 4 minutes”, May 2018

Mobility grant EEBB-I-17-12142, Founding entity: Spanish Ministry of Economics and Competitiveness, August- December 2017

Mobility grant STINT GAIG 2011-2017, Founding entity: Swedish Foundation for International Cooperation in Research and Higher Education, October- December 2016

Mobility grant Erasmus+ ACCIÒ (KA103) Teaching Mobility 2015/2016, Founding entity: European Commission. May 2016

Pre-doctoral grant FPI-MINECO: BES-2013-063131, MAT2012-38438-C03-01, Founding entity: Spanish Ministry of Economics and Competitiveness. January 2014-January 2018